Nidogens are therapeutic targets for the prevention of tetanus

Kinga Bercsenyi

University College London
and
Cancer Research UK London Research Institute
PhD Supervisor: Giampietro Schiavo

A thesis submitted for the degree of
Doctor of Philosophy
University College London
January 2015

Declaration

I, Kinga Bercsenyi, confirm that the work presented in this thesis is my own. Where information has been derived from other sources, I confirm that this has been indicated in the thesis.

Abstract

Tetanus neurotoxin (TeNT) is among the most poisonous substances on Earth and a major cause of neonatal death in non-vaccinated areas. There are approximately 300,000 cases reported worldwide each year, and the mortality rate is between 10-20%.

In this work, I identified an extracellular matrix protein receptor for TeNT at the neuromuscular junction (NMJ) and developed a peptide inhibitor, which prevents tetanic paralysis *in vivo* in mice. TeNT binds to the NMJ with an extremely high affinity, yet the nature of its receptor complex was poorly understood. I showed that the presence of nidogens (also known as entactins) at the NMJ is the main determinant for TeNT binding. Nidogens are extracellular matrix (ECM) proteins, which are taken up into the endosomal carriers containing tetanus toxin binding fragment (H_CT) in motor neurons. Inhibition of the H_CT-nidogen interaction using a peptide originating from nidogen-1 abolishes H_CT binding on these cells.

TeNT causes slowly progressing local tetanus when it is injected intramuscularly into the *triceps surae muscle* in a low dose. When preincubated with the peptide originating from nidogen-1, TeNT injection does not alter the coordination of mice and the muscle force remains largely unchanged. Genetic ablation of nidogens prevented the binding of TeNT to neurons and the intact NMJ and protected mice from TeNT induced spastic paralysis.

In my thesis I demonstrated for the first time, that an ECM protein accumulates and presents a neurotropic pathogen to the presynapse. This study follows recent studies showing that growth factors trigger downstream signalling more efficiently if they bind to certain ECM components – a new and rising concept in neuroscience.

Acknowledgement

Firstly, I have to thank my supervisor, Giampietro Schiavo, for giving me the opportunity to work in his laboratory and for believing that I could tackle a risky but potentially amazing project and giving me the support I needed to go all the way. I would also like to thank Guillermo Menendez, who took me under his wings, taught me how to prepare primary motor neurons from embryos and how to design and use microfluidic chambers.

A big thank you to all the past and present members of the MNP lab, who have always been there for me, both in the good times and in not so good times. I would not be the person I am today without their guidance and I was lucky to work in a friendly environment, where I always had someone to rely on. Special thanks to Matthew Golding and Claire Thomas, who were there for scientific support and who taught me how to be more diplomatic and handle difficult situations with grace and care. Big thank you to my fellow students, Martin (my ever-so-messy benchmate), Nathalie (my Cosy Science partner) and Katherine (the forever focused hard-worker). The wise postdocs and past students, Olga, Solene, Mike and Marco, for always knowing which control I missed and what I should try next. I also want to thank our sister labs, Sharon Tooze's SPW lab and Linda Greensmith's lab for the questions and suggestions during super group meetings. Special thanks to J. Barney Bryson, whose contribution gave the project the final push it needed to make it a big hit, his efficiency and deep knowledge in physiology truly amazed me and I learned a lot in the short time we worked together.

This work would not have been possible without help from the amazing facilities at the London Research Institute. The peptide synthesis facility provided me with all the peptides, tested them for purity and stability and even prepared peptide arrays for me, all of these were completed within a short time frame and I cannot be thankful enough for that. The Biological Resources Unit took good care of my mice both in Clare Hall and the LRI and Julie, Claire and Ian were always there for me when I needed assistance. The Electron Microscopy Unit took images of my newly made microfluidic chambers, a big thank you to both Lucy and Anne for that.

A big thank you goes to my collaborators, Giuseppe Zanotti for biomolecular modelling, Paola Caccin for the hemidiaphragm assay and Roswitha Nischt for providing the nidogen knockout mice.

I would also like to thank my Cosy Science friends, Nathalie, Olga, Mario, Mike, Ale, Mariana and Micka (in chronological order), I still cannot believe what we have achieved together and how big a difference a group of determined and open minded scientists can make to the public engagement scene in London – all you need is a ‘can do’ attitude and a GREAT TEAM!

Finally, I would like to thank my family and friends, for making me believe that the limit was the sky, for encouraging me to be the best in everything I do, whether it's studying, swimming, or changing the world by doing science.
My wonderful husband, Dezsi and my little baby boy, Oliver have always been there for me and I see all my success through their eyes – we are doing all right! They are my everything and my greatest pride! It means a lot to me that even though we live far from our families, we have great support from Oliver’s three aunties: Auntie Ale, Auntie Mariana and Auntie Nathalie!

Table of Contents

Table of figures

List of tables

List of movies

Abbreviations

AChR	acetylcholine receptor
Akt	protein kinase B
ANOVA	analysis of variance
APP	amyloid precursor protein
APR	arrays of presynaptic receptors
BACE1	beta-site APP-cleaving enzyme 1
BAR	bin–amphiphysin-rvs
BDNF	brain-derived neurotrophic factor
BiCD-1	bicaudal D homologue-1
BL	basal lamina
BoNT	botulinum toxin
BS3	bis(sulfosuccinimidyl) suberate
BSA	bovine serum albumin
BSOCOES	bis[2-(succinimidooxycarbonyloxy)ethyl] sulfone
CCV	clathrin-coated vesicle
cDNA	complementary DNA
ChAT	choline-acetyltransferase
CNS	central nervous system
CNT	clostridial neurotoxins
CNTF	ciliary neurotrophic factor
CP	cerebral palsy
CTB	cholera toxin subunit B
DIV	days *in vitro*
DKO	dual knock out
DLAR	*D. melanogaster* LAR homologue
DNA	deoxyribonucleic acid
DRG	dorsal root ganglia
Dvl	Dishevelled
EB	embryoid body
EC	extracellular domain
ECL	enhanced chemiluminescence

EDL	*extensor digitorum longus* muscle
EDTA	ethylenediaminetetraacetic acid
ELISA	enzyme-linked immunosorbent assay
ERK 1/2	extracellular signal-regulated kinase 1/2
ES cell	embryonic stem cell
FGF-2	fibroblast growth factor-2
Fyn	proto-oncogene tyrosine-protein kinase
GD1b	Galβ3NAcGalβ4(NAcNeuα8NAcNeuα3)Galβ4GlcβCer
GDNF	glial cell line-derived neurotrophic factor
GM1	Galβ3NAcGalβ4(NAcNeuα3)GAlβ4GlcβCer
GPI	glycosylphosphatidylinositol
GQ1b	NAcNeuα8NAcNeuα3Galβ3GalNAcβ4(NAcNeuα8NAcNeuα3) Galβ4GlcβCer
GST	gluthatione-S-transferase
GT1b	NAcNeuα3Galβ3GalNAcβ4(NAcNeuα8NAcNeuα3)Galβ4GlcβCer
HA	hemagglutinine
HBSS	Hank's balanced salt solution
H_CA	botulinum toxin A binding fragment
H_CT	tetanus toxin binding fragment
HEPES	4-(2-hydroxyethyl)-1-piperazinethansulfonic acid
HPLC	high-performance liquid chromatography
HRP	horse radish peroxidase
HSPG	heparane sulphate proteoglycans
IF	immunofluorescence
IgG	immunoglobulin G
IHC	immunohistochemistry
IP	immunoprecipitation
ITC	isothermal calorimetry
Ka	association constant
Kd	dissociation constant
KO	knock out
LAL	levator auris muscle
LAR	leukocyte antigen-related protein phosphatase

LB	Luria-Bertani medium
LRP4	Low-density lipoprotein receptor-related protein
MAPK	mitogen- activated protein kinase
MF	microfluidic chamber
MG	myashenia gravis
MSC	congenital myasthenic syndromes
MT	microtubules
MuSK	transmembrane muscle-specific kinase
NMJ	neuromuscular junction
NRG-1	neuregulin-1
OPD	ortho-phenylenediamine
P150	p150 Glued subunit
$p75^{NTR}$	p75 neurotrophin receptor
PAGE	polyacrylamid gel electrophoresis
PBS	phosphate buffered saline
PC12	pheochromocytoma 12 cell line
PCR	polymerase chain reaction
PDMS	polydimethylsiloxane
PFA	paraformaldehyde
PI3K	phosphoinositide 3-kinase
PIP2	phosphatidylinositol(4,5)bisphosphate
PKC	protein kinase C
PLCγ1	phospholipase Cγ1
PM	plasma membrane
PMD	proximal transmembrane domain
PNS	peripheral nervous system
PTK	Src family protein tyrosine kinases
PTP3	*C. elegans* LAR homologue
PVDF	polyvinylidene fluoride
RA	retinoic acid
Rab	rat sarcoma proteins in brain
Ras	rat sarcoma proteins
RIM	regulating synaptic membrane exocytosis protein

SD	standard deviation
SDS	sodium dodecyl sulfate
SEM	scanning electron microscopy
SEM	standard error of the mean
ShAg	smoothened agonist
Shp-2	Src-homology 2 phosphatase
SMI 31	phophorylated neurofilament antigen
SNAP-25	synaptosome associated protein of 25 kDa
SNARE	soluble NSF attachment protein receptors
SV	synaptic vesicle
SV2	synaptic vesicle protein 2
TA	*tibialis anterior* muscle
TBE	Tris-borate-EDTA buffer
TBS	Tris-buffered saline
TCEP	tris(2-carboxyethyl)phosphine hydrochloride
TIG	tetanus toxin immunoglobulin
TeNT	tetanus toxin
tPA	tissue plasmin activator
TRIO	triple functional domain protein
Tris	2-amino-2-(hydroxymethyl)-1,3-propandiol
TrkB	tropomyosin-like kinase B
TS	*triceps surae* muscle
VSVG	vesicular stomatitis virus glycoprotein
WB	western blot
WHO	World Health Organisation
Wnt	Wingless-related integration site protein family

Publications

1. Tetanus toxin entry. Nidogens are therapeutic targets for the prevention of tetanus.

   Kinga Bercsenyi, Nathalie Schmieg, J. Barney Bryson, Paola Caccin, Matthew Golding, Giuseppe Zanotti, Linda Greensmith, Roswitha Nischt and Giampietro Schiavo

   Science. 2014 Nov 28;346(6213):1118-23. doi: 10.1126/science.1258138.

   PMID: 25430769

2. The elusive compass of clostridial neurotoxins: deciding when and where to go?

   Bercsenyi K, Giribaldi F, Schiavo G.

   Curr Top Microbiol Immunol. 2013;364:91-113. doi: 10.1007/978-3-642-33570-9_5. Review.

   PMID:23239350

3. Botulinum neurotoxins A and E undergo retrograde axonal transport in primary motor neurons.

   Restani L, Giribaldi F, Manich M, **Bercsenyi K**, Menendez G, Rossetto O, Caleo M, Schiavo G.

   PLoS Pathog. 2012 Dec;8(12):e1003087. doi:10.1371/journal.ppat.1003087. Epub 2012 Dec 27.

   PMID: 23300443

4. **Uptake and transport of Clostridial Neurotoxins**

   In press

   Nathalie Schmieg*, **Kinga Bercsenyi*** and Giampietro Schiavo‡

   THE COMPREHENSIVE SOURCEBOOK OF BACTERIAL PROTEIN TOXINS (4TH ED. 2014)

   * Equal contribution

Chapter 1. Introduction

1.1 The pathomechanism of tetanus

Tetanus is an acute disease characterised by muscle spasms. It is caused by tetanus toxin (TeNT), which is released upon infection with an anaerobic, gram-positive bacterium, Clostridium tetani. The endospores of C. tetani are ubiquitously present in the soil and in the feces of livestock, such as cattle and sheep. Minor injury sites can get contaminated with the spores and if the wound is deep, anaerobic conditions allow the spores to germinate. TeNT is then released into the circulation and targets skeletal muscles (Wells and Wilkins, 1996). The incubation period ranges from 8 days to up to 4 months. The main form of tetanic intoxication is generalised tetanus (80% of the cases), which presents in a descending pattern, first affecting the mandibular muscles and causing *trismus*, or 'lockjaw'. This is usually followed by stiffness in the neck muscles, difficulty in swallowing and spasms of the abdominal muscles (Centers for Disease, 2012). Tetanus is most common in newborn babies ('neonatal tetanus'), the infection occurs in those who do not have passive immunity against TeNT, due to the lack of maternal vaccination (Vandelaer et al., 2003). The chances of contracting tetanus are highest if the umbilical stump is cut with non-sterile instrument (UNICEF, 2000). If medical care is available, the wound is cleaned and the patients receive tetanus toxin immunoglobulin (TIG) to eliminate TeNT from the cardiovascular system. Mechanical ventilation is required for up to 3-4 weeks, while complete recovery takes months. The most common cause of death is respiratory failure (Centers for Disease, 2012). There are approximately 300,000 tetanus cases each year, and the mortality rate is around 20%. Tetanus is common in countries where the vaccine is not readily available and despite the decrease in the number of these countries, tetanus still claims the lives of 59,000 people per year. Due to the high number of tetanus related fatalities, the World Health Organisation (WHO) named maternal-neonatal tetanus as the 'silent killer' (WHO, 2014).

1.2 Clostridial neurotoxins (CNT)

The CNT family comprises of TeNT and several related botulinum neurotoxins (BoNTs, serotypes A to H) (Swaminathan, 2011, Bercsenyi et al., 2013). BoNT/H has recently been described, but it is currently unclear whether it is a new form of BoNT, or a variation of the already existing serotypes (Dover et al., 2014).

CNT display similar structural organisation, they have the same intracellular targets and primarily bind to motor neurons (Schiavo et al., 2000). However, once internalised, BoNTs and TeNT are sorted to fundamentally different intracellular pathways (Figure 1-1). BoNTs mostly stay in the neuromuscular junction (NMJ), with only a minor fraction of toxin transported back to the motor neuron cell body (Restani et al., 2012a). In contrast, TeNT is efficiently transported in a retrograde fashion within the motor neuron and it is synaptically transferred to inhibitory interneurons in the spinal cord (Figure 1-1) (Schwab and Thoenen, 1976, Lalli et al., 2003a, Bercsenyi et al., 2013). Since CNT cleave SNARE (soluble NSF attachment protein receptor) proteins, which are essential for synaptic vesicle release, the direct consequence of their biological activity is the complete silencing of their target neuron (Binz, 2013).

Due to their fundamentally different intracellular targeting, BoNTs and TeNT lead to pathologies characterised by opposing symptoms. Botulism, which is caused by BoNTs, leads to flaccid paralysis (silencing the motor neuron), whilst tetanus, caused by TeNT, leads to spastic paralysis (silencing the inhibitory interneuron resulting in constant activity of the motor neuron).

BoNTs are extensively used as cosmetic agents and as therapeutics against pathologies caused by synaptic hyper-activity (Davletov et al., 2005, Sanford, 2014, Carod-Artal, 2014). With the improvement of food safety standards, botulism became rare disease. However, in 2006 there was a botulism outbreak due to the consumption of contaminated home-canned bamboo shoots. A total of 209 people were affected, of whom 42 required mechanical ventilation (Thailand, 2006). The WHO identified the outbreak as a public health emergency, and later concluded that the international response and the availability of anti-toxin agents were insufficient.

The study of CNT is very important, both to decrease the mortality rate of tetanus and to overcome the side effects of BoNT treatment.

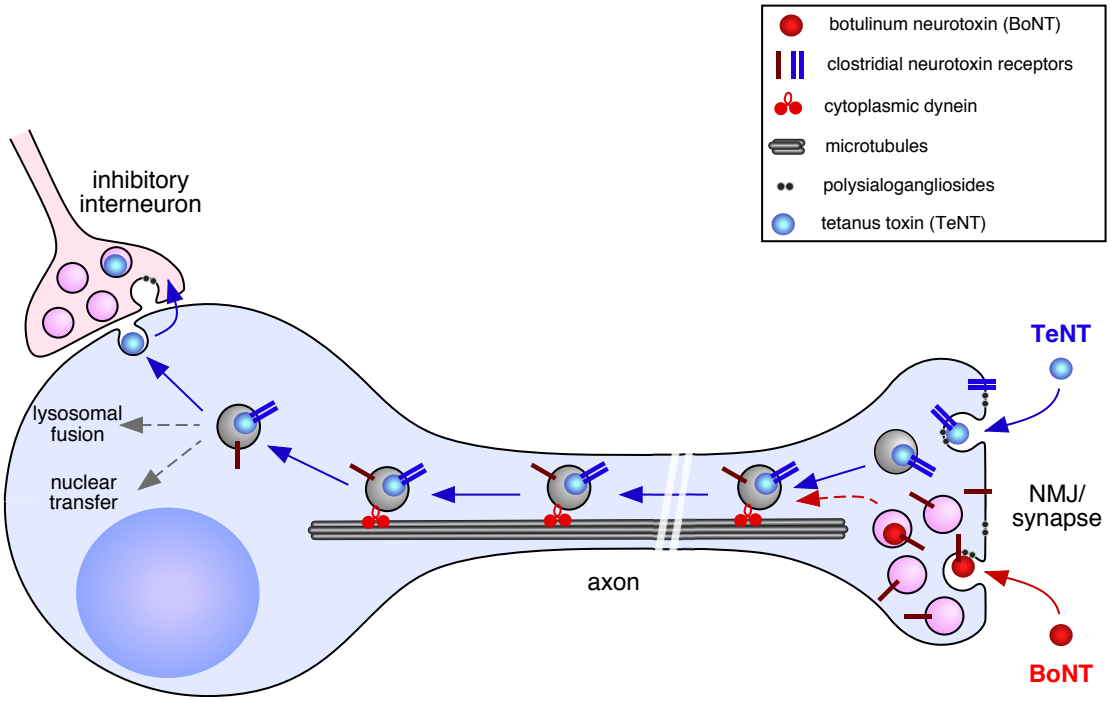

Figure 1-1. TeNT and BoNTs are sorted to different intracellular routes

TeNT and BoNTs bind to the motor neuron end plate (blue cell) at the NMJ, using polysialogangliosides (dots) and protein receptors (sticks). However, TeNT (blue sphere) is sorted into signalling endosomes (grey vesicles) and is retrogradely transported back to the cell body (blue arrows), while BoNTs (red sphere) enter recycling synaptic vesicles (pink vesicles) and mostly stay at the synapse. BoNT/A and BoNT/E were reported to undergo long-range axonal transport (dashed red arrow) (Restani et al., 2012a). Once transcytosed and synaptically transferred into inhibitory interneurons (pink cell), TeNT is likely to enter the synaptic vesicle recycling pathway and cleave synaptobrevin in these cells, leading to the loss of inhibition on the motor neuron. Reprinted with permission from John Wiley and Sons (Bercsenyi et al., 2013).

1.2.1 The structure of CNT

TeNT and BoNTs are synthesised as single chain proteins (150 kDa), which are cleaved by bacterial and extracellular matrix proteases when they are released during bacterial autolysis. This results in a 50 kDa light chain (L) and a 100 kDa heavy chain (H), which are linked via a disulphide bridge and non-covalent interactions (Figure 1-2 B). The carboxyl-terminus of H mediates neuronal binding (H_C), while the amino-terminus (H_N) is required for the pore formation and

subsequent translocation of the L chain through the endosomal membrane into the cytosol (Montal, 2010). The L chain is a metalloprotease (Schiavo et al., 2000) and contains the active site of the toxin. All three domains were investigated in detail by crystallisation and biochemical studies. The structure of L chain and H_C of TeNT (Breidenbach and Brunger, 2005a, Chen et al., 2008) (Figure 1-2 A) and full-length BoNT/A (Stevens et al., 1991, Lacy et al., 1998, Garcia-Rodriguez et al., 2007) (PDB ID: 3BTA, Figure 1-2 C), as well as other BoNTs were determined in high resolution. BoNT/A is an elongated molecule, which suggests that the different domains are unlikely to cause any interference to each other's actions. However, not all BoNTs are hypothesised to have the same 3D structure as BoNT/A. The 3D structure of BoNT/E was calculated by random conical tilt reconstruction. Based on this model, the H_N and the L chain are tightly coupled and a conformation change is required to separate these two domains prior to pore formation and translocation through the endosomal membrane (Fischer et al., 2008).

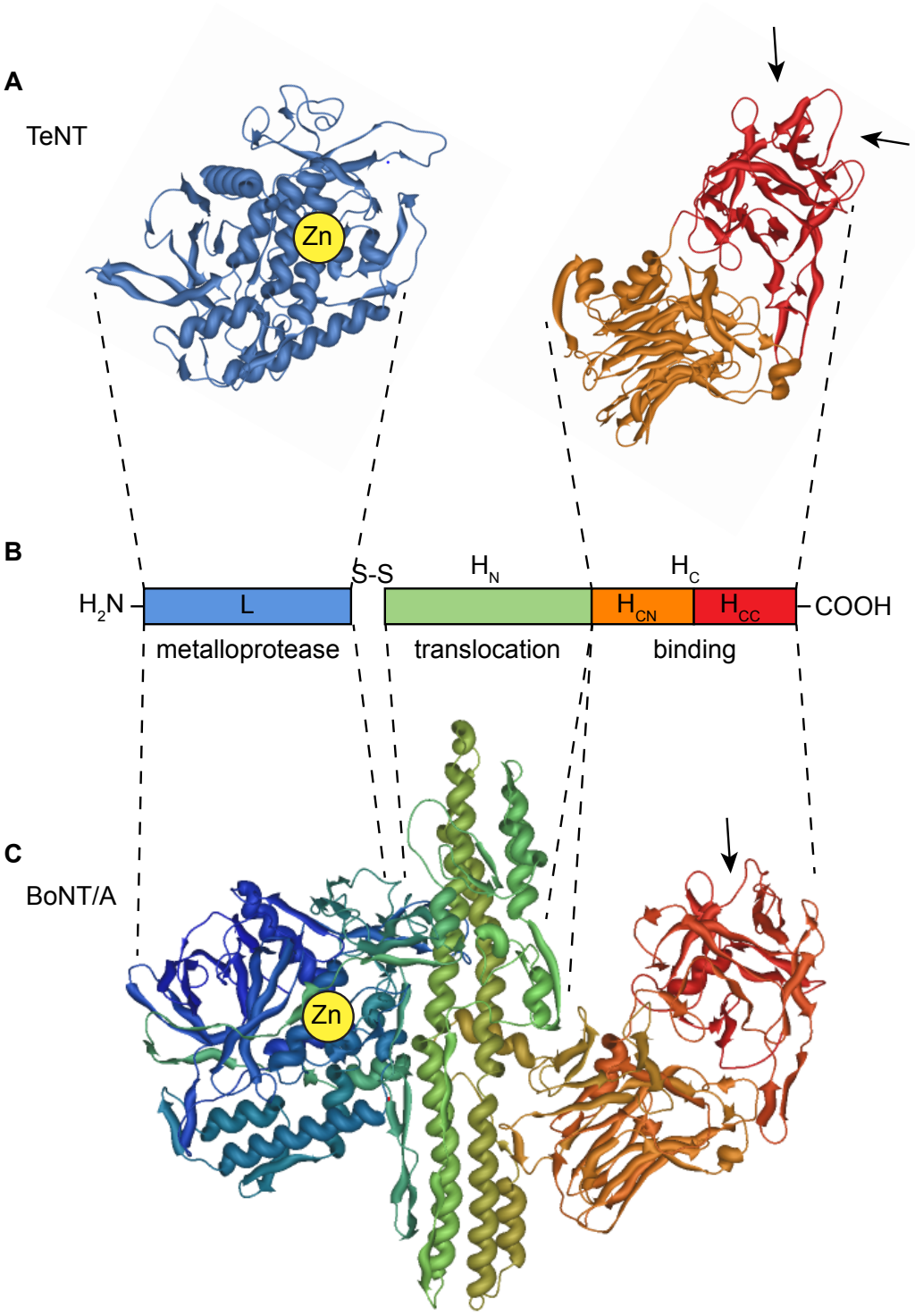

Figure 1-2. The structure of CNT show high similarity

(A) The crystal structure of the L chain and H_C of TeNT were solved at a resolution of 2.3 Å (1Z7H) and 2.0 Å (3HMY), respectively (Breidenbach and Brunger, 2005a) (Chen et al., 2009) **(B)** The two polypeptide chains (L and H_C) are connected via a disulphide bridge. **(C)** The crystal structure of full-length BoNT/A was determined at a resolution of 2.6 Å (2NYY) (Garcia-Rodriguez et al., 2007). The arrows point at the known receptor binding sites. Reprinted with permission from Elsevier (Schmieg, 2015).

1.2.1.1 The binding fragment (H_C)

The H_C domain of CNT mediates their neuron-specific binding (Bizzini et al., 1977, Halpern and Neale, 1995, Herreros et al., 2000b). It contains two subdomains, the amino-terminal subdomain (H_{CN}) and the carboxy-terminal subdomain (H_{CC}). The structure of the H_{CN} is similar to the structure of the carbohydrate-binding domain of oligosaccharide-binding proteins (Chen et al., 2008). The H_{CC} is a β-trefoil domain, which is present in proteins, which are required for binding and cell recognition, such as trypsin inhibitors (Molnar et al., 2013).

The H_C domain is relatively isolated from the rest of the molecule, and this leaves all of the potential binding sites easily accessible (Chen et al., 2008). There are two main binding loops within the H_C domain of TeNT (H_CT), a lactose site ('L') and a sialic acid site ('R'). The sequence is less conserved in these regions between different CNT, suggesting that they have different affinities to certain binding partners (Figueiredo et al., 1997, Lacy and Stevens, 1999, Rummel et al., 2003). Both sites can be occupied simultaneously, suggesting that two receptors might be required for CNT binding and uptake (dual receptor hypothesis) (Montecucco, 1986, Rummel et al., 2007). The deletion of a number of residues within the H_{CC} domain significantly decreases binding, indicating the importance of this fragment in cell recognition (Halpern and Loftus, 1993, Rummel et al., 2003).

1.2.1.2 The translocation domain (H_N)

The pH-dependent membrane-penetration and translocation of the catalytic domain of CNT requires the translocation fragment (H_N). In BoNT/A, it is composed of two long α-helices and a β-strand as the main structural units. The β-strand lies against the two main α-helices and upon acidification it changes its conformation, exposing hydrophobic residues (Donovan and Middlebrook, 1986, Shone et al., 1987, Oblatt-Montal et al., 1995, Puhar et al., 2004). This change enables the H_N domain to insert into the membrane and form a pore. The L chain gets unfolded and migrates through the newly formed pore (Fischer et al., 2009, Montal, 2009). The disulphide bridge between a loop of H_N and L chain is reduced in the cytosol

(Fischer and Montal, 2007, Pirazzini et al., 2013a, Pirazzini et al., 2013b) and the L chain is released (Oblatt-Montal et al., 1995).

1.2.1.3 The metalloprotease domain

The catalytic domain of CNT is a metalloprotease, targeting proteins essential for synaptic vesicle release (Penner et al., 1986, Poulain et al., 1988, Ahnert-Hilger et al., 1989, Bittner et al., 1989, Mochida et al., 1989, Weller et al., 1991). The catalytic zinc atom is essential for the endopeptidase activity, there is one in the L chain of TeNT, BoNT/A, B and F (Schiavo et al., 1992a, Schiavo et al., 1992b, Schiavo et al., 1993a, Stura et al., 2012), whilst BoNT/C binds two zinc atoms with different affinities (Schiavo et al., 1995, Breidenbach and Brunger, 2005b, Garcia-Rodriguez et al., 2007). If the zinc atom is removed with heavy metal chelators, the toxins lose their activity (Bhattacharyya and Sugiyama, 1989, Schiavo et al., 1992a). CNT cleave SNARE proteins, which are essential for the fusion of synaptic vesicles with the plasma membrane (PM) (Montecucco et al., 2005, Binz, 2013). These include synaptobrevin, syntaxin and SNAP-25 (Table 1) (Schiavo et al., 1992, Schiavo et al., 1993, Schiavo et al., 1993a, Blasi et al., 1993a, Blasi et al., 1993b, Rickman et al., 2004, Breidenbach and Brunger, 2004).

Table 1. Intracellular targets of CNT

Synaptobrevin	Syntaxin	SNAP-25
BoNT/B, D, F, G; TeNT	BoNT/C	BoNT/A, C, E

1.2.2 Neuron-specific binding of CNTs

CNT binding has been examined in many different cell lines, including primary motor neurons, as well as in various membrane preparations (Halpern and Neale, 1995, Schiavo et al., 2000). *In vitro*, CNT bind to a large variety of non-neuronal cells, but only at very high concentrations (Montesano et al., 1982). In contrast, *in vivo* binding of CNT is absolutely neuron specific and only requires concentrations in the sub-nanomolar range (Halpern and Neale, 1995, Simpson, 2000). Addition of the H_C fragment alone is sufficient for the entry into neurons, and preincubation with recombinant H_C fragments can inhibit the uptake of the parental

neurotoxin, indicating that this fragment is absolutely essential for neuron-specific binding (Lalli et al., 1999).

1.2.2.1 Polysialogangliosides, as cell surface receptors for CNT

CNT bind the G1b series of polysialogangliosides (GD1b, GT1b and GQ1b) (Montecucco, 1986, Halpern and Neale, 1995). The interaction between polysialogangliosides and CNT is crucial during intoxication; when residues within the carbohydrate-binding pocket of CNT are mutated, the toxicity of the mutant neurotoxins is significantly impaired (Louch et al., 2002, Rummel et al., 2003, Rummel et al., 2004b, Rummel et al., 2009, Strotmeier et al., 2010). However, these sites might participate in protein binding and the drop in toxicity might also be due to the inhibition of this process. Accordingly, lack of polysialoganglioside biosynthesis only partially protects mice from tetanus (Kitamura et al., 1999, Williamson et al., 1999, Kitamura et al., 2005). Also, neuraminidase treatment and the reduction of polysialogangliosides on the PM decreases but does not abolish CNT activity (Bigalke et al., 1986). In addition, CNT binding is sensitive to prior protease treatment (Dolly et al., 1982, Pierce et al., 1986). These results combined with the abundance of polysialogangliosides on all cell types and their low binding affinity to CNT suggest that there are additional protein receptors for CNT. A high-affinity interaction is required to account for the extremely low doses of CNT causing clinical symptoms *in vivo.* Although BoNT/E was shown to partially compete with TeNT for binding to neurons (Herreros et al., 2001) there is no robust competition between TeNT and BoNTs for neuronal binding, which would be expected if they shared their receptors on the PM.

1.2.2.2 Presynaptic receptor arrays for CNT binding

Based on the structural properties of H_CT, both ‘L’ and ‘R’ receptor-binding sites can be occupied simultaneously. Both sites were shown to bind polysialogangliosides, but the binding of a glycoprotein to the ‘R’ site was previously hypothesised (Montecucco, 1986, Rummel et al., 2003, Jayaraman et al., 2005).

Arrays of presynaptic receptors (APRs) could form to bind CNT on the neuronal PM (Montecucco et al., 2004). APRs are very similar to lipid rafts; they are dynamic, and highly concentrated at the NMJ. In this model, polysialogangliosides would serve as the first line of capture, acting as 'antennas' on the presynaptic membrane and allowing CNT to bind to other membrane components. The second binding complex is likely to contain proteins (Dual Receptor Hypothesis), since protease treatment inhibits CNT binding to neurons (Montecucco, 1986, Montecucco et al., 2004, Rummel et al., 2007). Accordingly, specific protein co-receptors have been identified for most CNT.

Most probably, BoNTs bind to APRs, which are different in their composition from those serving as a binding platform for TeNT (Figure 1-1). One or more key components might be responsible for the subsequent differences in the sorting of these toxins.

1.2.2.3 Protein receptors of BoNTs

Both binding and uptake of BoNTs is dependent on synaptic activity (Keller et al., 2004, Baldwin and Barbieri, 2007). Generally, a high rate of neuroexocytosis correlates with a high rate of synaptic vesicle (SV) recycling via endocytosis (Murthy and De Camilli, 2003). Since BoNTs enter the lumen of SV, it is not surprising that they are taken up faster and in higher quantities upon neural stimulation (Matteoli et al., 1992, Kraszewski et al., 1995). Since the intraluminal leaflet of SV gets exposed during neuroexocytosis and a significant proportion of SV proteins are localised on the PM transiently, they can serve as protein receptors for BoNTs.

Accordingly, most of the protein receptors found for BoNTs are SV proteins. BoNT/A, /B, /E and /G interact with synaptotagmins I and II (Nishiki et al., 1994, Nishiki et al., 1996, Yowler et al., 2002, Dong et al., 2003, Rummel et al., 2004a). In addition, synaptic vesicle protein 2 (SV2) serves as a protein receptor for BoNT/A, /C and /F (Mahrhold et al., 2006, Dong et al., 2006, Dong et al., 2007, Peng et al., 2011).

However, our laboratory recently demonstrated that BoNT/A is able to bind to neurons in absence of any synaptic activity (due to previous BoNT/D treatment) (Restani et al., 2012a). In lack of neuroexocytosis, SV proteins are not readily

accessible on the PM, therefore in these conditions BoNT/A must utilise an alternative entry route. If it can enter similar intracellular compartments as TeNT, it should be retrogradely transported within neurons. Accordingly, several research groups have demonstrated that BoNT/A is retrogradely transported in different neuronal types, such as hippocampal, tectal and motor neurons (Restani et al., 2012a, Antonucci et al., 2008). BoNT/A retains its activity during transport and undergoes transcytosis in the visual system (Restani et al., 2011, Restani et al., 2012b).

Recently, FGFR3 was identified as a new protein receptor for BoNT/A in resting conditions (Jacky et al., 2013). FGFR3 undergoes ligand-mediated endocytosis followed by retrograde transport (Haugsten et al., 2011, Garay, 2013), so it is able to mediate the uptake, sorting and transport of BoNT/A along this trafficking route. However, BoNT/A could also exploit the protein receptor of TeNT on motor neurons and get transported in shared organelles.

1.2.2.4 Protein receptors of TeNT

TeNT binds to two different types of neurons: first it binds to peripheral motor neurons and after synaptic transfer, it binds to inhibitory interneurons within the spinal cord. Since it is sorted to different intracellular pathways after internalisation in these cells, it probably associates with distinct receptors. TeNT possesses two polysialoganglioside-binding sites, so it might only need polysialogangliosides for its cell specific entry (Niemann, 1991, Binz and Rummel, 2009, Chen et al., 2009). A strong argument supporting this hypothesis came from the observation that immobilised polysialogangliosides have a high affinity towards TeNT, due to the cis-interactions occurring in this assay (Rinaldi et al., 2009). However, polysialogangliosides are not uniquely localised to the motor neuron end terminals and GD1b is not internalised when bound to H_CT (Deinhardt et al., 2006a), indicating that TeNT definitely requires additional factors to aid its uptake into neurons.

TeNT is unlikely to exploit the SV-recycling pathway in motor neurons, since it does not block synaptic transmission at the NMJ at physiological concentrations causing tetanus. However, when used at extremely high doses, it causes botulism-like symptoms (Matsuda et al., 1982), suggesting that TeNT might be able to

exploit a similar entry path to BoNTs at the NMJ when its preferred route of internalisation is overloaded.

SV2 emerged as a receptor for TeNT in central neurons (Yeh et al., 2010), but these findings were not confirmed by independent experiments (Blum et al., 2012).

There are several considerations suggesting that TeNT preferentially follows an alternative entry route to that of BoNTs in motor neurons:

1. If the TeNT receptor is exposed during neuroexocytosis to allow TeNT to bind and then be endocytosed, an increase in synaptic activity should also increase the accessible binding sites at the NMJ. However, high frequency stimulation does not enhance the binding of TeNT to the NMJ (Schmitt et al., 1981).
2. TeNT is taken up in NMJs where neurotransmitter release is completely blocked by the addition of BoNT/A (Schiavo et al., 2000, Koriazova and Montal, 2003, Deinhardt et al., 2006a).
3. Our laboratory has previously shown that H_CT is transported away from the site of injection *in vivo* (Bilsland et al., 2010). I also observed that the vast majority of H_CT is retrogradely transported; only a minor fraction is retained at the NMJ after 2 hours of incubation.

A potential membrane receptor was identified for TeNT in differentiated pheochromocytoma (PC12) cells. Thy-1, an abundant GPI-anchored protein (Herreros et al., 2000a, Herreros et al., 2000b) was shown to bind H_CT. However, Thy-1 knockout mice do not show a decreased sensitivity to TeNT (Herreros et al., 2001) and this result excludes the possibility of Thy-1 acting as a primary protein receptor on motor neurons.

1.2.3 Internalisation of CNT

BoNT and TeNT bind to distinct receptors on the PM of motor neurons, and this leads to two distinct internalisation pathways: BoNTs are taken up via synaptic vesicle recycling, whereas TeNT undergoes clathrin-dependent endocytosis into signalling endosomes (Deinhardt et al., 2006a, Montal, 2010, Blum et al., 2012).

1.2.3.1 Internalisation of TeNT

The first step of clathrin dependent endocytosis is the recruitment of specific clathrin adaptors to the PM. These proteins recruit bin–amphiphysin-rvs (BAR) domain proteins, which promote the initial curvature of the membrane at the internalisation site (Qualmann et al., 2011). Specific lipids accumulate in the PM, such as phosphatidylinositol(4,5)bisphosphate (PIP_2), which in turn recruits AP2, a major clathrin adaptor complex (Haucke, 2005). TeNT uptake requires AP2, but the overexpression of a mutant form of epsin-1, which is unable to bind to PIP_2, does not affect TeNT binding (Deinhardt et al., 2006a). Epsins lack the BAR domain, they insert an amphipathic helix into the inner leaflet of the membrane and this further curves the membrane (Ford et al., 2002, Hinrichsen et al., 2006). These proteins are involved in the targeting of ubiquitinated receptors for lysosomal degradation (Le Roy and Wrana, 2005). By taking an entry route independent of epsin, TeNT may avoid the carriers destined for acidification, which is crucial to prevent the premature release of the L chain into the cytosol within the motor neuron.

When the recruitment of clathrin scaffold is complete, dynamin binds to the neck of the curved pit and mediates the fission of the clathrin-coated vesicle (CCV) from the PM. Inhibition of dynamin, or overexpression of dynamin mutants inhibits the uptake of both TeNT and BoNTs (Deinhardt et al., 2006a, Harper et al., 2011).

1.2.4 Axonal retrograde transport of CNT

The longest axons in the human body might reach 1 m in length. A very efficient and tightly regulated axonal transport system has evolved to maintain precise and timely communication between the neuronal cell bodies and axon terminals in the periphery (Goldstein and Yang, 2000). Three classes of molecular

motors are required for efficient long-range transport: myosins, kinesins and cytoplasmic dynein. Kinesins are plus-end motors, carrying their cargo towards the growing end of microtubules (MT), which are found at the distal terminal in axons. In contrast, cytoplasmic dynein moves its cargo retrogradely towards the minus ends of microtubules in the cell body (Vale, 2003, Hirokawa et al., 2010). Myosin is an actin-based motor (Vale, 2003) and despite the fact that neuronal traffic is mainly MT-based (Goldstein and Yang, 2000), actin-dependent motors also play a role in neuronal transport.

1.2.4.1 Axonal transport of TeNT

TeNT is retrogradely transported from the motor neuron endplate to the cell body (Stöckel et al., 1975). Cytoplasmic dynein is essential in the axonal retrograde transport of TeNT, as was demonstrated both *in vitro* and *in vivo* (Lalli et al., 2003b, Hafezparast et al., 2003). Interestingly, myosin Va loss of function mutation and a potent kinesin inhibitor also reduced the speed of retrograde transport of H_CT carriers (Lalli et al., 2003b). Interfering with the normal function of these motors disturbs the balance and tight regulation of the axonal transport system, and this might explain why they indirectly affect the retrograde transport of TeNT.

Numerous motor protein adaptors are recruited to the signalling endosomes, such as Bicaudal D homologue 1 (BICD1). The reduction of the expression of BICD1 affects both TeNT and $p75^{NTR}$ trafficking, but does not alter the speed of retrograde transport in general (Terenzio et al., 2014b, Schmieg et al., 2014).

Two small GTPases are required for the axonal transport and sorting of H_CT: Rab5 and Rab7 (Deinhardt et al., 2006b). The former is required for the early steps after internalisation, while the latter is essential for sustained axonal retrograde transport (Deinhardt et al., 2006b, Salinas et al., 2009).

H_CT transport is considerably slower in primary motor neuron cultures than *in vivo* (Herreros et al., 2000b, Hafezparast et al., 2003, Bilsland et al., 2010). This difference might be due to the myelination of motor neuron axons within the sciatic nerve. Alternatively, the different developmental state of the observed neurons might be the reason for the slower transport observed in primary motor neuron cultures; these are derived from embryos, while the *in vivo* experiments were performed on adult mice (Bohnert and Schiavo, 2005, Bilsland et al., 2010).

The moving transport organelles have a neutral pH, which is essential to prevent pore formation and the release of the L chain into the cytosol (Montecucco et al., 1994, Williamson and Neale, 1994). However, the stationary organelles containing H_CT are more acidic, which is dependent on the presence of the vacuolar (H^+) ATPase. By targeting organelles, which do not contain this enzyme, H_CT avoids its premature release from axonal transport carriers (Bohnert and Schiavo, 2005).

1.2.4.2 Axonal transport of BoNTs

BoNTs are preferentially sorted into synaptic vesicles, which stay in close vicinity to the presynaptic membrane (Colasante et al., 2013, Holtje et al., 2013). However, BoNT/A was shown to have central effects after injection, which can only occur if it undergoes long range axonal transport within neurons (Antonucci et al., 2008, Caleo and Schiavo, 2009). Recent studies conducted in our laboratory have shown that both BoNT/A and /E undergo retrograde transport in motor neurons (Restani et al., 2012a). The speed profile of BoNT/A positive organelles is similar to the ones containing H_CT, while BoNT/E-positive carriers displayed slower retrograde transport with more pauses and a higher incidence of reversals (Restani et al., 2012a). This result suggests that BoNT/E exploits a less efficient axonal transport pathway, while BoNT/A targets a common or very similar pathway to the one used by TeNT. This finding may explain why BoNT/E does not display any central nervous system effects, in spite of having the same intracellular target as BoNT/A.

1.2.5 Synaptic transfer of TeNT

TeNT is transcytosed in the motor neuron and stays hidden within vesicles characterised by neutral pH (Lalli et al., 2003a). It is retrogradely transported together with neurotrophin receptors (i.e. $p75^{NTR}$) and reaches the cell body (Figure 1-3 A-C), where it is sorted to the trans-synaptic transfer route. The molecular mechanism of the targeting is unclear, but it is re-exposed on the PM of motor neuron cell bodies and gets selectively taken up by inhibitory interneurons (Figure 1-3 D) (Schwab and Thoenen, 1976).

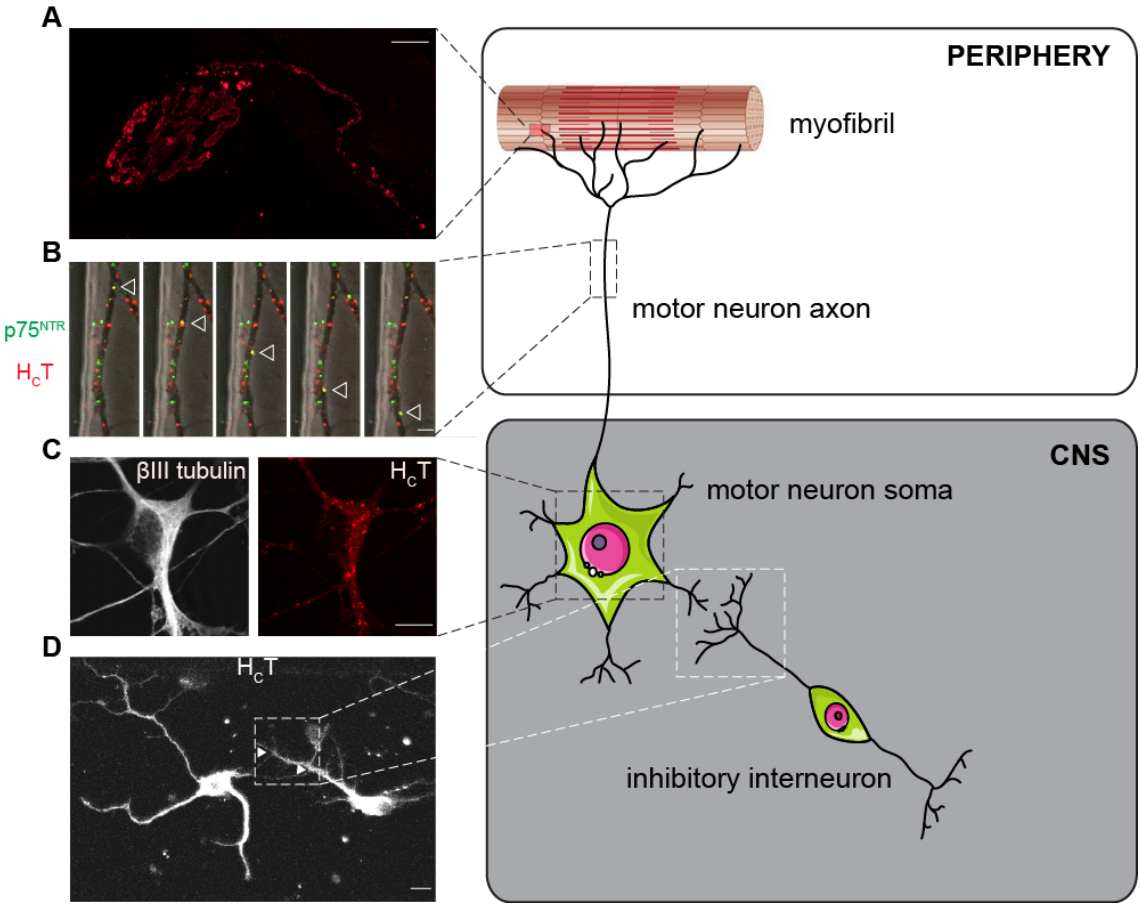

Figure 1-3. TeNT is taken up, transported and synaptically transferred by motor neurons

(A) TeNT is taken up by motor neurons the NMJ, as shown by the red labelling of the presynaptic membrane (AlexaFluor555-H_CT was injected intramuscularly). It then enters the motor nerve (red puncta within the motor neuron axon). **(B)** AlexaFluor555-H_CT (red) is retrogradely transported together with neurotrophin receptors, such as $p75^{NTR}$ (green). The white arrowheads track the journey of a single signalling endosome towards the cell body. **(C)** AlexaFluor555-H_CT (red) accumulates in the cell body (βIII tubulin, white) before its targeting to the PM. **(D)** AlexaFluor555-H_CT (pseudocolored white) is synaptically transferred between motor neurons and inhibitory interneurons in microfluidic chambers (Chapter 5).

1.2.6 Pore formation and translocation into the cytosol

In recent years, the molecular mechanism of pore formation and subsequent translocation of the L chain has been studied in detail and led to the proposal of a new model (Montal, 2010, Fischer, 2013, Burns and Baldwin, 2014). During synaptic vesicle (SV) recycling the vesicular ATPase (vATPase) proton pump accumulates H^+ ions in the SV lumen, resulting in the drop of the intraluminal pH.

This is required for the re-loading of neurotransmitters into the SV after neuroexocytosis (Ahnert-Hilger et al., 2003). When the vATPase is blocked with chemical inhibitors, BoNTs still enter neurons but loose their ability to block SV release, indicating that the activity of this enzyme plays a crucial role in the translocation of the L chain (Simpson et al., 1994, Williamson and Neale, 1994, Sun et al., 2011, Sun et al., 2012, Colasante et al., 2013). Patch clamp experiments were carried out on Neuro2A and PC12 cells, and it became evident, that when the pH drops on the cis side of the membrane (the luminal leaflet), the L chain of BoNT/A and /E1 cross the pore formed by the H_N domain (15-20 Å in diameter) (Sheridan, 1998). There are several amino acids, which change protonation state when the pH drops, since the substitution of three different carboxylate residues to the corresponding amides in BoNT/B1 bypassed the need for the pH drop for membrane translocation (Pirazzini et al., 2013b).

This channel is not big enough for the fully folded L chain to cross; it must unfold prior to translocation (Bade et al., 2004, Fischer et al., 2008). Once the L chain has reached the cytosol, the disulphide bridge linking the L chain and H chain is reduced and the metalloprotease is released into the cytosol. It is crucial that the disulphide bridge remains intact during translocation, since BoNTs with a reduced disulphide bridge do not form channels and display reduced toxicity (Schiavo et al., 1990a, Fischer and Montal, 2007).

According to a study, where the translocation of TeNT, BoNT/C and /D was forced through the PM, the translocation process takes only minutes and requires a pH range of 4.5-6 (Pirazzini et al., 2013c).

1.2.7 Substrate recognition and cleavage

To date, the synaptic SNARE proteins: syntaxin-1, SNAP25 (synaptosomal associated protein of 25 kDa) and VAMP/synaptobrevin are the only identified substrates of CNT. Cleavage of the cytosolic fragments of synaptic SNARE proteins yields the persistent blockade of neurotransmitter release (Schiavo et al., 1992, Schiavo et al., 1993, Schiavo et al., 1993a, Blasi et al., 1993a, Blasi et al., 1993b, Yamasaki et al., 1994, Rickman et al., 2004, Breidenbach and Brunger, 2004). A peptide belt occupies the long channel of the active site, which is removed

upon the unfolding event prior to translocation (Rossetto et al., 2014). The substrate recognition site binds to the substrate with high specificity, but the efficiency of the metalloprotease cleavage varies between subtypes and this is likely to cause the different onset, duration and toxicity (Whitemarsh et al., 2013, Wang et al., 2013).

1.3 TeNT uptake and neurotrophin signalling

Since large distances separate the motor neuron end terminal and the soma, efficient neurotrophin trafficking and signalling is essential to maintain the communication with the distal synapses. Signalling endosomes carry receptor-ligand complexes from the periphery towards the soma within the spinal cord through long-range axonal transport (Hoeller et al., 2005, Howe, 2005). These carriers are unidirectional and undergo fast retrograde transport, presenting a more efficient alternative to signalling pathways relying on diffusion. One of the best-known complexes within signalling endosomes are neurotrophins and their receptors (Schecterson and Bothwell, 2010).

1.3.1 Neurotrophin signalling in motor neurons

1.3.1.1 Tropomyosin-receptor-kinase B (TrkB) and brain derived neurotrophic factor (BDNF)

Motor neurons mainly express TrkB and $p75^{NTR}$. Trks were initially described as oncogenic proteins (Barbacid et al., 1991). They are receptor tyrosine kinases; possess a ligand binding extracellular domain (EC), a single transmembrane domain and a tyrosine kinase intracellular domain (Figure 1-4). The EC domain contains three N-terminal leucine-rich motifs and two IgG-like domains. Neurotrophins bind to two sites: the third leucine-rich domain and the second cysteine cluster form one binding site, and the second IgG domain is the second binding site. Ligand binding triggers the dimerisation and auto-phosphorylation of the receptors at specific tyrosine residues in the intracellular domain. The phosphorylated tyrosine residues bind to a variety of effector proteins, and activate several pro-survival and growth signalling cascades, such as the phospholipase Cγ1 (PLCγ1), phosphoinositide 3-kinase (PI3K) and the mitogen-

activated protein kinase (MAPK) pathways. The primary ligand of TrkB is BDNF (Klein et al., 1991, Garcia et al., 2010), which is essential for motor neuron survival.

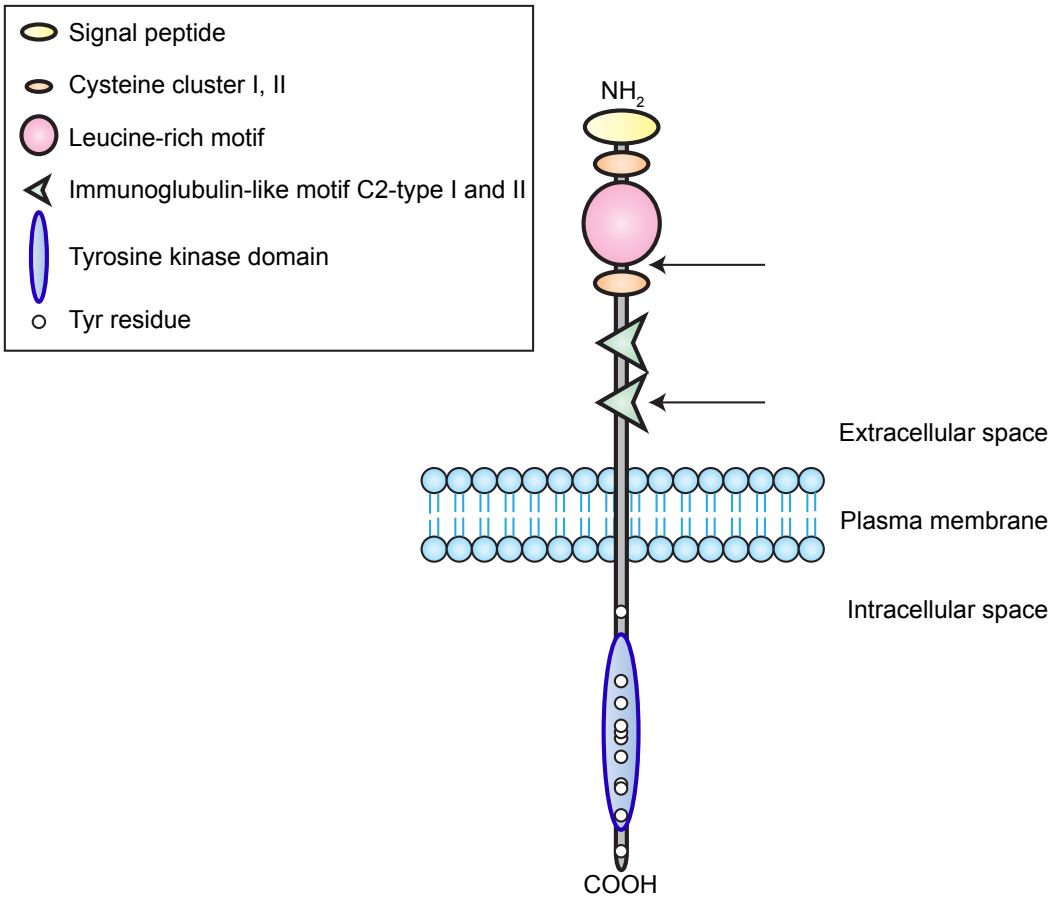

Figure 1-4. The domain structure of TrkB

The two neurotrophin binding sites are indicated with arrows (amino acid residues 103-181 and amino acid residues 342-394). Both of these sites are able to bind BDNF independently (Haniu et al., 1997). There are 10 important Y residues within the intracellular domain, which can be modified by the addition of a phosphate group. Upon ligand binding, the receptor dimerises and autophosphorylates the Y residues; this step is crucial for the opening of the activation loop and the subsequent activation of the tyrosine kinase domain (Minichiello, 2009).

BDNF is secreted in its precursor form (proBDNF) and this molecule has an opposing function compared to the mature form. It preferentially binds to $p75^{NTR}$ and sortilin and activates a pro-apoptotic signalling pathway (Teng et al., 2005). However, a group of extracellular matrix proteases, tPA matrix metalloproteases (tissue plasmin activator), including plasmin, cleave the pro-domain and produce the mature form of the neurotrophin (Lu et al., 2005, Gray and Ellis, 2008, Teng et

al., 2010). Once cleaved, BDNF forms dimers and binds to heterodimers of TrkB and $p75^{NTR}$, and activates survival and growth promoting downstream signalling pathways described above.

Our laboratory previously demonstrated that TeNT shares its transport compartment with BDNF, $p75^{NTR}$ and TrkB both in dorsal root ganglia and primary motor neurons (Figure 1-1-5) (Deinhardt et al., 2006b, Terenzio et al., 2014b). This pathway has a functional relevance to tetanus intoxication, since mature BDNF increases the efficiency and speed of H_CT internalisation at the NMJ in a dose dependent manner (Roux et al., 2006). Moreover, H_CT promotes TrkB signalling in the absence of BDNF; both extracellular signal-regulated kinase 1/2 (ERK1/2), protein kinase B (Akt), protein kinase C (PKC) and PLCγ1 are activated upon the addition of H_CT to neurons (Gil et al., 1998, Gil et al., 2000, Gil et al., 2001, Gil et al., 2003).

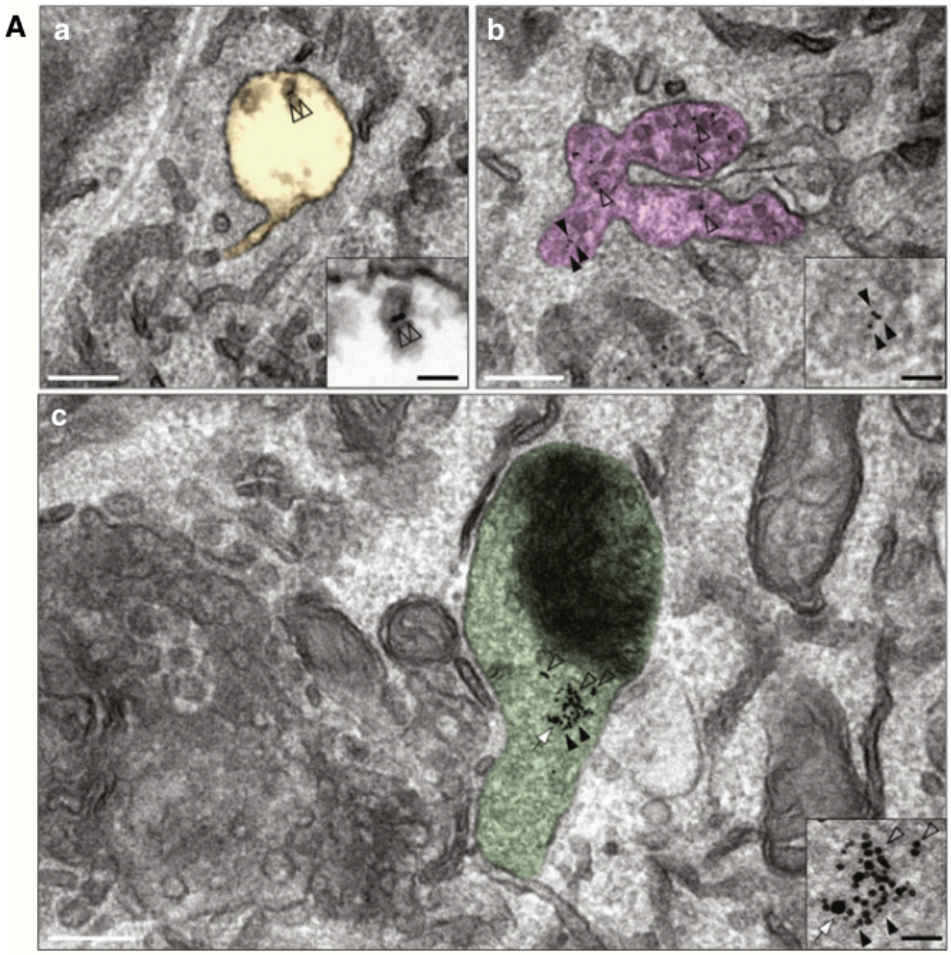

Figure 1-1-5. H_CT accumulates in signalling endosomes with TrkB and $p75^{NTR}$
Primary motor neurons were incubated with colloidal gold-labelled H_CT (10nm, empty arrowheads), α-TrkB (20 nm, white arrowheads) and α-$p75^{NTR}$ (5nm, black arrowheads) for 2 h at 37 °C to allow internalisation. The probes were taken up into endosomes, which were pseudocoloured according to the number of probes that they contain: yellow (a), pink (b) and green (c) representing single, double and triple labelled compartments, respectively. Scale bars: 200 nm (main panels), 50 nm (insets). Reprinted with permission from John Wiley and Sons (Terenzio et al., 2014a).

1.3.1.2 Leukocyte common antigen-related (LAR) phosphatase

A co-regulator of the neurotrophin-signalling pathway, the leukocyte common antigen-related (LAR) phosphatase binds to TrkB in a BNDF dependent manner (Yang et al., 2006) and it promotes neurite outgrowth (Yang et al., 2005). In LAR KO cells, phosphorylation of Y515 in TrkB is decreased, and this leads to a

decrease in the activity of the downstream signalling pathway. These results suggest that LAR facilitates pro-survival and growth signalling through TrkB. There are two possible mechanisms to serve as a molecular background for this hypothesis:

1. By recruiting and dephosphorylating and activating a tyrosine kinase, which then phosphorylates Y515 on TrkB. Src family protein tyrosine kinases (PTK) are excellent candidates for this, as LAR directly binds to them and dephosphorylates their negative regulatory C-terminal domain (Tsujikawa et al., 2002). Fyn, a PTK associates with the intracellular domain of TrkB in a BDNF dependent manner (Iwasaki et al., 1998). Furthermore, adenosine activation of Fyn causes direct phosphorylation and activation of Trks in PC12 cells (Rajagopal and Chao, 2006).
2. By dephosphorylating and thus inactivating a phosphatase, which in turn cannot dephosphorylate Y515 on TrkB. Shp-2 (Src homology 2 phosphatase) would be good candidate, as it was shown to dephosphorylate Y515 (Minichiello, 2009, Gupta et al., 2012), but it is currently unknown whether it is a substrate for LAR.

LAR has three extracellular IgG domains and eight fibronectin domains (Pot et al., 1991, Cho et al., 1992, Streuli et al., 1992). It has two phosphatase domains, one is active, while the other is inactive and it binds to various intracellular effector proteins, such as TRIO (triple functional domain protein), β-catenin, liprin-α and enabled (Figure 1-6) (Debant et al., 1996, Kypta et al., 1996, Serra-Pages et al., 1998, Wills et al., 1999, Haapasalo et al., 2007). Its expression is restricted to the presynaptic membrane, where it binds to the laminin-nidogen complex among other extracellular matrix proteins, such as syndecan and dallylike (heparane sulphate proteoglycans, HSPG) (O'Grady et al., 1998, Johnson et al., 2006).

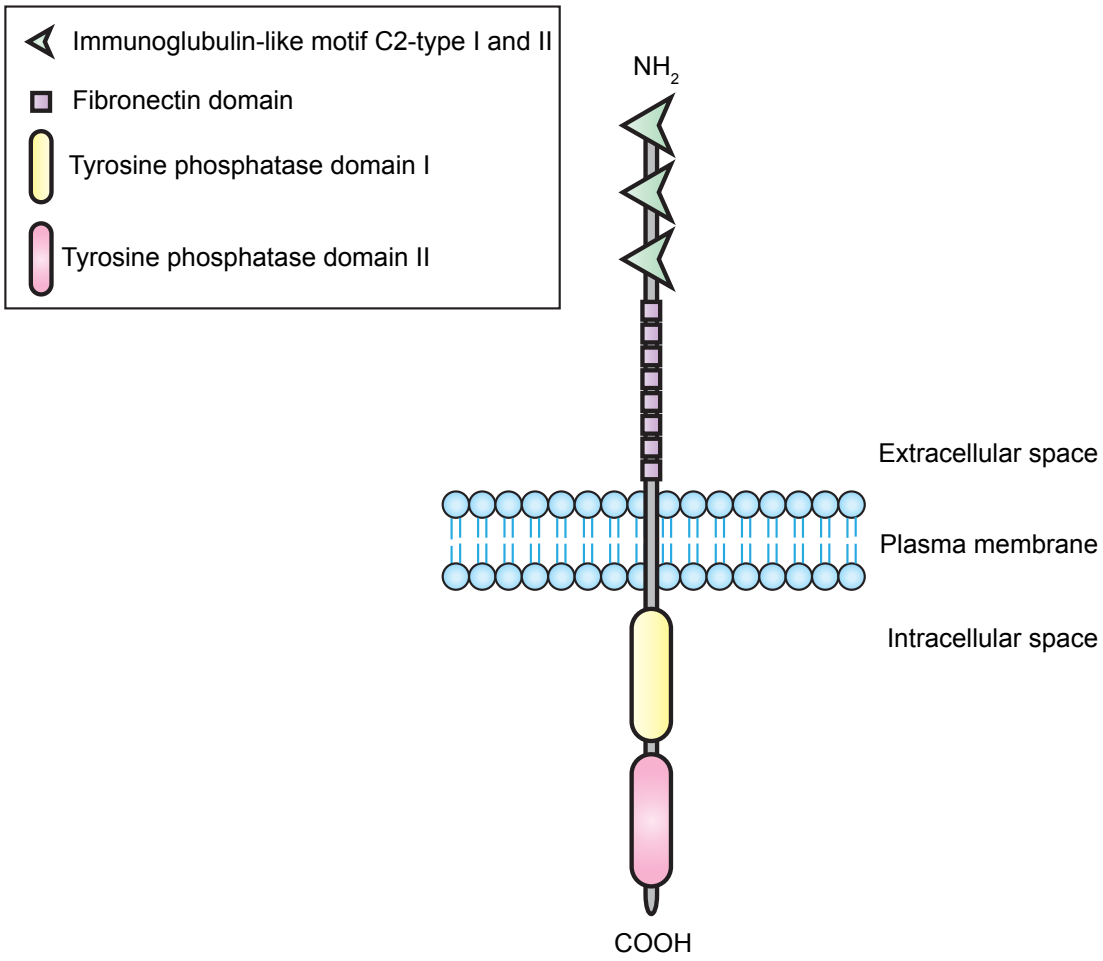

Figure 1-6. The domain structure of LAR

There are 3 IgG and 8 fibronectin domains in the extracellular part of LAR, while it contains two tyrosine phosphatase domains in its intracellular part. The first tyrosine phosphatase domain is inactive and serves as a binding site for intracellular effectors, such as liprin-α. The other tyrosine phosphatase domain dephosphorylates the substrates of LAR, such as ephrin A2 (Lee and Bennett, 2013) and Src-PTK, such as Fyn (Tsujikawa et al., 2001).

The loss of function mutation of PTP3 and DLAR, the *Caenorhabditis elegans* and *Drosophila melanogaster* isoforms of LAR, respectively, resulted in the impairment of presynaptic terminal size regulation; the active zones are enlarged within the NMJs of knock out animals.

There are two PTP3 isoforms; PTP3A is the full-length isoform, while PTP3B lacks the extracellular IgG domains and the first four fibronectin domains. The former regulates synapse formation, while the latter plays a role in axonal guidance. PTP3A binds to nidogen-1 (a heavily glycosylated extracellular matrix protein) and this interaction is crucial for its accumulation around the perimeter of

the presynaptic terminal and the recruitment of the synapse size regulator, RIM (regulating synaptic membrane exocytosis protein). If either of the two proteins is lost, active zones in the en-passant NMJs become enlarged, indicating that these proteins act as synaptic gatekeepers (Ackley et al., 2003, Ackley et al., 2005).

In *D. melanogaster*, when the expression of DLAR, or its downstream effector, Dliprin-α is reduced, NMJs are enlarged by three fold and there is a dramatic reduction in the quantal content of each terminal. This result suggests that the disruption of the regulation of the presynaptic terminal boundaries lead to the increased size of the active zone and with the SV content remaining the same, but spread to a larger area, the quantal content is decreased (Kaufmann et al., 2002).

The observation that both mutations lead to similar phenotypes and that the function of PTP3 depends on the presence of nidogen-1 suggests that nidogens and LAR are components of a signalling pathway, which is crucial for presynapse specification and maintenance. The role of this protein complex in the mammalian nervous system was not investigated, it would be very interesting to test whether the complex is conserved through evolution and how it affects the downstream signalling of BDNF and TrkB.

1.3.2 Nidogens are specialised extracellular matrix (ECM) proteins

Nidogens (entactins) are heavily glycosylated ECM proteins and their main function is believed to be formation of a bridge between collagen IV and laminin (Ho et al., 2008). Both isoforms have a similar secondary structure; they consist of three globular domains with a rod-like and link-like connecting region (Kohfeldt et al., 1998, Fox et al., 1991). They are present in epithelial basal lamina (BL) in high quantities. The bridge between collagen IV and laminin is predicted to be crucial for ECM stability; however, genetic ablation of single nidogens does not cause any major disruption in the BL of epithelial cells (Murshed et al., 2000, Schymeinsky et al., 2002, Gersdorff et al., 2007). These results combined with the observed increase in nidogen-2 expression in nidogen-1 KO mice (Miosge et al., 2002) lead to the suggestion that the two isoforms have overlapping functions. The loss of nidogen-1 causes neurological phenotypes, such epilepsy and progressive hindlimb paralysis, while nidogen-2 knockout mice are healthy (Dong et al., 2002).

Mice lacking both nidogen isoforms die shortly after birth, have abnormal BL in both the lung and the heart, and present with syndactyly (due to the lack of finger separation) (Bader et al., 2005, Bose et al., 2006).

Nidogens are subject to metalloprotease cleavage, but are largely protected when bound to laminin (Mayer et al., 1995). There are numerous target sites within the proteins, including a site for plasmin, which was also implicated in the cleavage of the pro-domain of BDNF (Mayer et al., 1993, Mayer et al., 1995, Lu et al., 2005, Gray and Ellis, 2008). Plasmin cleaves nidogen in the link domain (Lys_{203}-Ser_{204}), separating the G1 domain from the rest of the molecule. This is predicted to release nidogens from the extracellular matrix and make them more accessible to bind to soluble ligands.

1.3.3 Signalling endosomes as H_CT carriers

Several lines of evidence indicate that TeNT and H_CT enter axonal signalling endosomes in motor neurons (Bercsenyi et al., 2013, Schmieg et al., 2014), therefore suggesting that the TeNT receptor complex is a constituent of these axonal organelles (Figure 1-7). The Molecular Neuropathobiology Laboratory was in a unique position to identify this complex based on the available protocols for the isolation of axonal signalling endosomes, which allowed their proteomic mapping (Deinhardt et al., 2006b, Wade et al., 2012). Finding the protein receptor of TeNT might not only shed light on tetanus intoxication, but also increase our understanding on the targeting of extracellular ligands for retrograde transport.

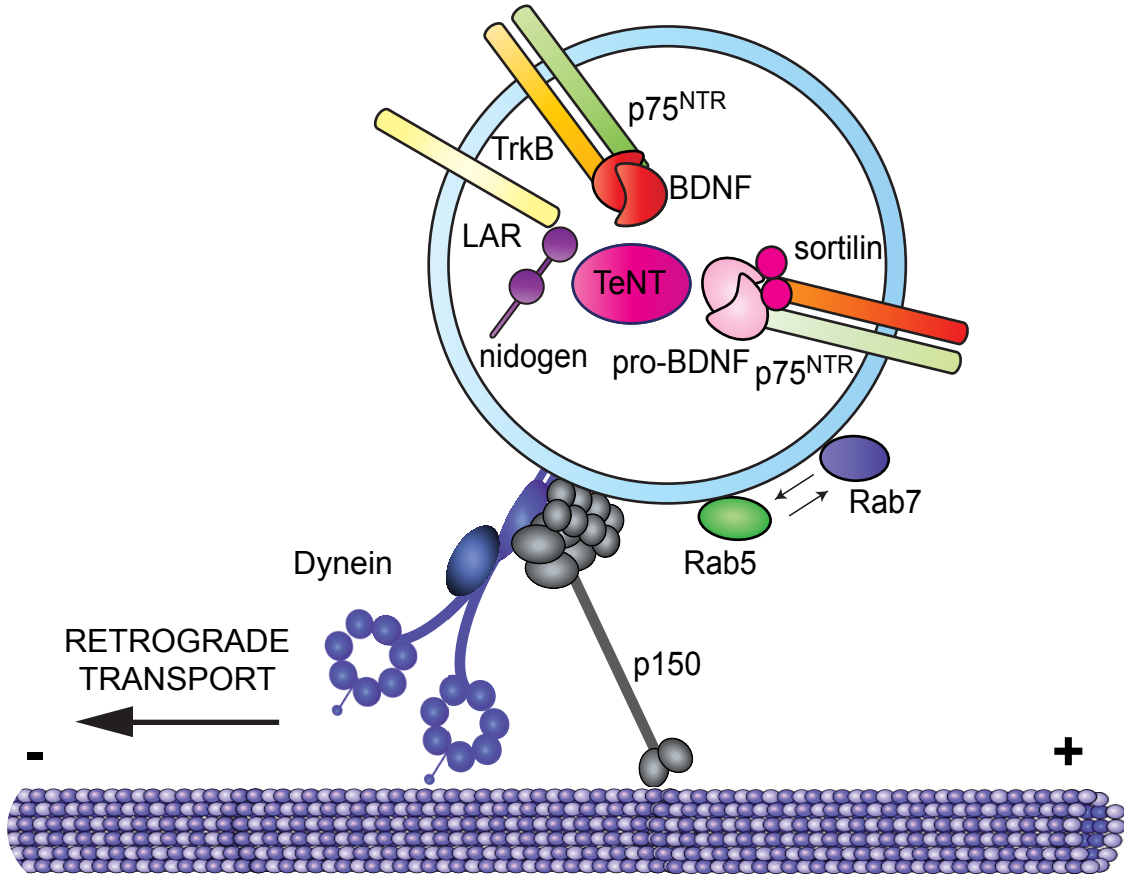

Figure 1-7. Proposed model of TeNT transport in signalling endosomes

Signalling endosomes containing neurotrophin receptors (TrkB, $p75^{NTR}$ and their binding partners, sortilin and LAR) and extracellular matrix components, such as nidogens are formed after ligand-mediated endocytosis (BDNF and pro-BDNF). After binding to the motor neuron membrane, TeNT enters these endosomes. Following initial sorting, Rab5, and then Rab7 is recruited and the endosome is transported towards the minus end of the MT, which is located in the cell body. Created based on the scheme in (Schmieg et al., 2014).

Chapter 2. Materials and Methods

2.1 Ethics statement

All experiments were carried out following the guidelines of the Cancer Research UK and UCL-Institute of Neurology genetic manipulation and Ethic Committees and in accordance with the European Community Council Directive of November 24th, 1986 (86/609/EEC). Animal work was carried out under license from the UK Home Office in accordance with the Animals (Scientific Procedures) Act 1986 (Amended Regulations 2012).

2.2 Materials

2.2.1 Reagents and media

Standard reagents were obtained from Sigma-Aldrich, unless stated otherwise. Recombinant nidogens were purchased from R&D Systems. Phosphate buffered saline (PBS), 0.5 M EDTA pH 8.0, glutamine Luria Bertani (LB) medium, and SOC medium and penicillin/streptomycin were provided by Cancer Research UK Laboratory Services.

2.2.2 Animals

All animals were kept on the C57/Bl6 background. Wild type pregnant females were purchased from Charles River. Nidogen-1 and -2 knock out (KO) lines were provided by R. Nischt (University of Cologne).

2.2.3 Bacterial Strains

E.coli strain XL1Blue was used for DNA amplification, and the TG1 strain was used for protein expression.

2.2.4 Antibodies

AlexaFluor-maleimide and AlexaFluor-conjugated secondary antibodies were purchased from Life Technologies and used at 1:500. HRP (horse radish

peroxidase)-conjugated secondary antibodies were obtained from Amersham Bioscience and used at 1:2000. The source and dilution of primary antibodies are shown in Table 2.

Table 2. Primary Antibodies

Antigen	Host	Provider	Dilution/Application
VSVG	Mouse	CRUK (P5D4)	1:500 (IP,WB)
βIII tubulin	Mouse	Covance (MMS-435P)	1:1000 (WB, IF)
βIII tubulin	Rabbit	Covance (PRB-435P)	1:1000 (IF)
HA	Mouse	CRUK (12CA5)	2 µg/10 µl beads (IP)
HA	Rat	Roche (3F10)	1:1000 (WB, IF)
nidogen-1	Rabbit	Abcam (ab14511)	1:500 (WB)
nidogen-2	Rabbit	Abcam (ab14513)	1:500 (WB, IF)
His	Mouse	Qiagen (34698)	1:300 (IF)
LAR PMD	Mouse	F.M. Longo	1:500 (WB, IF)
TrKB	Rabbit	Millipore (07-225)	1:500 (WB, IF)
SV2C	Rabbit	T. Sudhof	1:100 (IF)
SV2A	Rabbit	Synaptic System (SYSY119002)	1:500 (IF)
ChAT	Goat	Millipore (AB144P)	1:100 (IF)
GST	Rabbit	Abcam (ab9085)	1:100 (IF)
SMI31	Mouse	Covance	1:1000 (IF)

IHC: immunohistochemistry, IF: immunofluorescence, WB: western blot, IP: immunoprecipitation

The following probes were used in addition to the antibodies described above:

Name	Provider	Dilution
α-Bungarotoxin, Alexa Fluor® 555 conjugate	Molecular Probes (B35451)	1:1000 (IHC)
AlexaFluor488-Cholera Toxin Subunit B	Molecular Probes (C-347775)	1:500 (IF)

2.2.5 Primers

2.2.5.1 List of primers for genotyping

The primers used for genotyping nidogen-1 and -2 KO mice are shown in Table 3. The genotyping primer sequences for nidogen-1 were kindly provided by I. Koxholt (University of Cologne). I designed the genotyping primers for the detection of nidogen-2 wt gene using the Sigma-Aldrich online tool, while the primers detecting the Neo cassette were kindly provided by M. Golding (Molecular Neuropathobiology laboratory, Cancer Research UK).

Table 3. Genotyping primers

PCR	Sequence 5´-3´	Product (bp)
Nidogen-1	FW-CCTCATTTGACCTACATGTAGC RW-CTTCAAACTCAGAGGACACAG RW-GAGAAAGAGTGGGACGATAG	900-wt 350-mu
Nidogen-2 wt	FW-GGCAGATGCAGCTCTCCTAA RP-GTCAGGAGGCTCCAAGAAGAAC	1000
Nidogen-2 (Neo casette)	FW-CGCCAAGCTCTTCAGCAATATCACGGGTAG RW-TGCTCCTGCCGAGAAAGTATCCATCATGGC	380

2.2.5.2 List of primers for site directed mutagenesis of H_CT

The primers for site directed mutagenesis were designed by M. Wallace (Molecular Neuropathobiology laboratory, Cancer Research UK and UCL-Institute of Neurology). The target sites on H_CT and primer sequences are shown in Table 4.

Table 4. Primers used for site directed mutagenesis

Mutant	Direction	Sequence
Y1229A	Forward	5'-CTAAGAGTAGGTGCTAATGCCCCAGGTATCCC-'3
Y1229A	Reverse	5'-GGGATACCTGGGGATTAGCACCTACTCTTAG-3'
T1146A	Forward	5'-GTTCAATTGAAAAATATAGCAGATTATATGTATTTGAC-3'
T1146A	Reverse	5'-GTCAAATACATATAATCTGCTATATTTTTCAAATTGAAC-3'
P1212W	Forward	5'-GAGCACATTGTAGGTTATTGGAAAGATGGAAATGCC-3'
P1212W	Reverse	5'-GGCATTTCCATCTTTCCAATAACCTACAATGTGCTC-3'
G1215F	Forward	5'-GCACATTGTAGGTTATCCGAAAGATTTCAATGCCTTTAATAATC-3'
G1215F	Reverse	5'-GATTATTAAAGGCATTGAAATCTTTCGGATAACCTACAATGTGC-3'
R1226F	Forward	5'-CTTGATAGAATTCTATTCGTAGGTTATAATGCCCCAGG-3'
R1226F	Reverse	5'-CCTGGGGCATTATAACCTACGAATAGAATTCTATCAAG-3'

2.2.6 Preparation of AlexaFluor555-H_CT

H_CT (441 residues) with an improved cysteine-rich tag was prepared by F. Giribaldi (Molecular Neuropathobiology laboratory, Cancer Research UK) as previously described (Restani et al., 2012a). I labelled H_CT with AlexaFluor555-maleimide. 750 µg of purified H_CT was mixed with 85 µl 2.5x buffer (50 mM HEPES NaOH, pH 7.4, 250 mM NaCl) and 29 µl of 10 mM TCEP (tris(2-carboxyethyl)phosphine hydrochloride). dH_2O was added to reach a final volume of 375 µl. 0.5 mg AlexaFluor maleimide was dissolved in dimethyl sulfoxide (DMSO) and was then added drop-by-drop under continuous mixing. The reaction mixture was incubated overnight at 4°C, on a rotating wheel. The reaction was stopped the following day by adding 80 µl of STOP solution (50 mM Tris pH 8.0, 25 mM reduced glutathione). To separate the unbound dye from AlexaFluor555-H_CT, the reaction mix was applied on a PD-10 desalting column (GE Healthcare) and the

presence of H_CT was tested with a dot blot. The fractions containing AlexaFluor555-H_CT were combined and dialysed against the storage buffer (10 mM HEPES-NaOH pH 7.4, 150 mM NaCl) at 4°C for three days. The storage buffer was exchanged every day. After three days, the labelled H_CT solution was aliquoted, frozen in liquid N_2 and stored at -80°C. The protein concentration and labelling efficiency were determined using a NanoDrop spectrophotometer.

2.3 Methods

2.3.1 Statistical analyses

To test for statistical significance, all results were plotted in Graphpad Prism. Data was tested for normality using three tests:

1. D'Agostino&Pearson omnibus normality test
2. Shapiro-Wilk normality test
3. KS normality test

If any of the three tests confirmed that the data is normally distributed, Student's t-test or analysis of variance (ANOVA) was used depending on the number of groups to compare (<2 – Student's t-test; >2 - ANOVA). To compare individual groups within these samples, I used Dunnett's multiple comparison test.

If none of the tests confirmed that the data is normally distributed, Mann-Whitney or Kruskal Wallis test was used depending on the number of groups to compare (<2 – Mann-Whitney test; >2 – Kruskal Wallis test). When the observations were paired, Friedman test was used. To compare individual groups within these samples, I used Dunn's multiple comparison test.

Significance was determined using the confidence interval of 95% ($p<0.05$ *). Additional * were give if the p value fell below 0.01 (**), 0.005 (***) and 0.001 (****). The test used is indicated within the description of each method.

Error bars indicate standard deviation (SD) unless stated otherwise.

2.3.2 Genotyping

2.3.2.1 Extraction of genomic DNA

Mice earsnips were lysed overnight in 120 **µ**l of DirectPCR Lysis Reagent (Viagen Biotech) with 0.1 mg/ml Proteinase K at 55 °C with gentle shaking. The reaction was then inactivated at 85°C for 30 min.

During preparation of primary neuronal cultures, the rapid lysis method was used to extract genomic DNA quickly. A piece of embryo tail was incubated in 50 **µ**l of Rapid Lysis Buffer (10 mM Tris-HCl pH8.3, 50 mM KCl, 0.1 mg/ml gelatin, 0.45% NP-40, 0.45% Tween 20) with 0.4mg/ml Proteinase K, and incubated at 55°C for 10 min, then at 95°C for 5 min.

2.3.2.2 Genotyping PCR

Genotyping PCR was carried out using the Megamix-Blue (Microzone Ltd.), a PCR master-mix containing recombinant Taq polymerase. 15 µl of Megamix-Blue, 0.125 µl of sequencing primers (forward and reverse), and 1 µl of fresh genomic DNA were mixed for a PCR reaction. The programme used for the PCR is shown in

Table 5. Genotyping PCR programmes

	Nidogen-1	**Nidogen-2 wt**	**Nidogen-2 mutant (Neo)**
1. Melting	94°C, 2 min	95°C, 4 min	95°C, 2 min
2. Melting	94°C, 30 sec	95°C, 30 sec	95°C, 30 sec
3. Primer annealing	55°C, 1 min	61°C, 30 sec	69°C, 30 sec
4. Elongation	68°C, 2 min	72°C, 1 min;	72°C, 30 sec
5. Elongation	68°C, 5 min	72°C, 5 min	72°C, 5 min
Number of cycles (2-4)	34	29	30

2.3.2.3 Agarose Gel Electrophoresis

DNA amplified by PCR was subjected to agarose gel electrophoresis. Agarose gels were prepared by dissolving 2% agarose in TBE (90 mM Tris-HCl, 90 mM boric acid, 2 mM EDTA pH 8.0), with ethidium bromide (0.5 µg/ml) and after loading 10 µl of PCR products, the gel was electrophoresed at 150 V in TBE buffer.

2.3.3 In vitro assays

2.3.3.1 H_CT mutagenesis

M. Wallace (Molecular Neuropathobiology laboratory, UCL-Institute of Neurology) performed the site directed mutagenesis of the H_CT fragment. Based on the biomolecular model (Figure 4-6), the following H_CT sites were selected for mutagenesis: H_CT^{T1146A}, H_CT^{P1212W}, H_CT^{G1215F}, H_CT^{R1226F}, H_CT^{Y1229A}. The mutations were generated using PfuTurbo® DNA polymerase, according to the manufacturer's instructions using the primers listed in Table 4. Briefly, each 50 µl reaction comprised 50 ng of plasmid template: pGEX-4T3-H_CT441 (24), 5 µl 10× reaction buffer, 125 ng each of the forward and reverse primers, 150 µM of each dNTP and 1 µl PfuTurbo® DNA polymerase (2.5 U/µl). PCR conditions were as follows: 95 °C for 2 min, followed by 16 cycles of 95 °C for 30 s, 55 °C for 1 min, and 68 °C for 8 min. After digestion with Dpn1, 2 µl of each PCR reaction were transformed in E. coli XL-1 Blue and grown overnight at 37 °C. DNA was purified using the QIAprep Spin Miniprep Kit (Qiagen, UK), and mutations were verified by direct sequencing. Once the sequences were verified, G. Schiavo (Molecular Neuropathobiology laboratory, UCL-Institute of Neurology) expressed the proteins as previously described (Restani et al., 2012a).

2.3.3.2 Fluorescent binding assay

2.3.3.2.1 Peptide Screen and Alanine scanning

To test the peptides for H_CT binding, I dried 10 ng of biotin-labelled peptides and their alanine mutants on a 96-well plate overnight and incubated the wells with Tris-buffered saline (TBS) containing 0.05% Tween-20 and 1% bovine serum albumin (BSA) for 1 h to block unspecific interactions. Plates were then washed

with TBS containing 0.05% Tween-20 (TBST) three times before adding 40 nM AlexaFluor555-H_CT in TBS and incubating it overnight at 4°C. Plates were then extensively washed with TBS and the fluorescent signal was measured using an EnVision® Multilabel Plate Reader. The highest fluorescence intensity for each plate was set at 100% for all three independent experiments. The results were plotted and tested for significance using Friedman test (**, $p<0.01$) followed by Dunn's multiple comparisons test against TBS (Figure 3-2). One-way ANOVA was used for the analysis in Figure 3-7 (****, $p<0.001$) followed by Dunnett's multiple comparisons test against N1 (B), or N2 (C) (Table 12).

2.3.3.2.2 Competition binding assay

To get an estimate on the dissociation constant (Kd) of the interaction between the N1 peptide and H_CT, I prepared 96-well plates with the N1, $N1_{AA}$ and other YEW-like peptides as described above, and following blocking, AlexaFluor555-H_CT was added at increasing concentrations (3.75, 37.5, 75 and 150 nM). To test whether the interaction was stable at pH 5; the same concentrations of AlexaFluor555-H_CT were added to the N1 peptide in TBS adjusted to pH 5 by the addition of HCl.

2.3.3.3 Classic ELISA

For classic ELISA, 96-well plates were prepared as described above, washed with TBST three times before adding 4 nM VSVG-H_CT (Herreros et al., 2001),or 80 nM HA-H_CT (wild type and point mutants) in TBS and then incubated overnight at 4 °C (VSVG-H_CT, Figure 3-4) or 1 h at room temperature (HA-H_CT, Figure 4-7). Wells were extensively washed with TBS and incubated with a monoclonal mouse antibody against the VSVG or HA epitopes for 2 h at room temperature. Following washes with TBST, an HRP conjugated goat anti-mouse secondary antibody was added for 1 h at room temperature. Wells were then washed with TBST and blocked with TBST, 1% BSA before adding ortho-phenylenediamine (OPD) substrate for colorimetric detection. The reaction was quenched with 2 M HCl and the absorbance measured at 490 nm. For the peptide screen (Figure 3-4), the results were normalised to samples where H_CT was omitted and analysed using paired Student's *t* test. For the mutant H_CT ELISA

(Figure 4-8), the mean values of triplicates from one assay were determined and the results of four independent experiments were tested for significance using paired Student's *t* test comparing the mutants to wild type H_CT.

2.3.3.4 SDS-PAGE

Protein samples were mixed in 5% Laemmli sample buffer (20% glycerol, 5% β-mercaptoethanol, 10% sodium dodecyl sulfate (SDS), 120 mM Tris-HCl pH 6.8, bromophenol blue) (Laemmli, 1970), and denatured for 10 min at 65°C. Samples were then loaded on pre-cast 4-12% NuPAGE® polyacrylamide gels (Invitrogen). Gels were ran at 200V for 60 min in 3-(N-morpholino)propanesulfonic acid (MOPS) buffer (Invitrogen).

2.3.3.5 Western-blotting

Proteins were transferred from the NuPAGE® gels to methanol-activated polyvinylidene fluoride (PVDF) membrane in transfer buffer (20 mM Tris-OH, 150 mM glycine and 20% methanol). The membranes were stained with Ponceau S to monitor the efficiency of transfer, and blocked in 5% skimmed milk in PBST (blocking buffer, Marvel) for 1 h at room temperature. Membranes were then incubated with primary antibodies diluted in blocking buffer at room temperature for 1 h, or alternatively overnight at 4 °C. Membranes were washed five times with PBST, and then incubated with HRP-conjugated secondary antibody diluted in blocking buffer for 1 h at room temperature. After washing in PBST and in dH_2O, immunoreactivity was detected using enhanced chemiluminescence (ECL, GE Healthcare) according to manufacturer's instructions.

2.3.3.6 Immunoprecipitation

2.3.3.6.1 *In vitro* peptide pull down

For the in vitro pull down assay, biotin-tagged peptides (20 nM) were bound to streptavidin-coated agarose beads, and used to quantify the binding between the peptides and VSVG-H_CT: 1 µg of VSVG-H_CT was added to the beads, and after extensive washes in TBS, samples were analysed by SDS-PAGE and western blotting using the P5D4 antibody. The intensity of the bands was measured using

Image J and the results analysed by paired Student's *t* test comparing the peptide-bound beads to the empty bead control.

2.3.3.6.2 Direct binding assay

For the in vitro immunoprecipitation, we bound HA-H_CT (1 µg) to anti-HA antibodies (2 µg) coupled magnetic Dynabeads® (10 µl; Life Technologies). After blocking with 0.1 mg/ml BSA in PBS for 1 h, samples were incubated with peptides (24 µM) or DMSO for 1 h at room temperature, washed and recombinant nidogens (0.5 µg of human nidogen-1; 2570-ND-050; or 1 µg of human nidogen-2; 3385-ND-050; both from R&D Systems) were added to the samples and incubated overnight at 4 °C. Beads were then washed with PBS and bound proteins were analysed by SDS-PAGE and western blotting using rabbit anti-nidogen-1 and anti-nidogen-2 and rat anti-HA antibodies.

2.3.3.6.3 Immunoprecipitation of endogenous proteins

For the immunoprecipitation of endogenous H_CT receptor complexes, HA-H_CT (80 nM) was added to primary motor neurons for 5 min at 37 °C to allow endocytosis. The cells were immediately cooled on ice, washed with ice-cold Hank's buffer and proteins were cross-linked using bis[2-(succinimidooxycarbonyloxy)ethyl] sulfone (BSOCOES; 1 mM; Thermo Scientific) in PBS for 30 min at 4 °C. The reaction was stopped by the addition of 50 mM (final concentration) Tris-HCl, pH 7.5. Following washes with PBS, cells were lysed on ice using IP lysis buffer (20 mM Tris-HCl pH 8, 137 mM NaCl, 1 mM EDTA, 10% glycerol, 0.5% NP40, HALT protease/phosphatase inhibitors; Thermo Scientific). The lysates were cleared by centrifugation at 14,000 *g* for 10 min and proteins binding non-specifically to empty beads were cleared by incubating the samples with pre-washed Dynabeads for 30 min at room temperature. Monoclonal mouse anti-HA antibody (12CA5; 2 µg) was cross-linked to Dynabeads (20 µl) using 5 mM bis(sulfosuccinimidyl) suberate (BS3; Thermo Scientific) in 20 mM sodium phosphate, 150 mM NaCl, (pH 8). After 30 min incubation at room temperature on a rotating wheel, the reaction was terminated by addition of 50 mM Tris-HCl pH 7.5 and further incubation for 15 min at room temperature. Beads were then added to lysates on a rotating wheel for 2 h at 4 °C, captured proteins magnetically isolated

as described above, washed and analysed by SDS-PAGE and immunoblotting using rabbit anti-nidogen-2 and rat anti-HA antibodies.

2.3.3.7 Motor neuron lysates

Following washes with PBS, motor neurons (DIV7-14) were lysed on ice using IP lysis buffer (20 mM Tris-HCl pH 8, 137 mM NaCl, 1 mM EDTA, 10% glycerol, 0.5% NP40, HALT protease/phosphatase inhibitors). The lysates were cleared by centrifugation at 14,000 *g* for 10 min and the supernatants were transferred to new tubes. The protein concentration was determined by Bradford assay (Bradford, 1976) and the lysates were denatured by adding 5x Laemmli sample buffer and heated for 10 min at 65°C. The lysates were either used for SDS PAGE or stored at -20°C for future experiments.

2.3.3.8 Molecular modelling of the nidogen-1/N1 peptide-H_CT interaction

G. Zanotti (University of Padua) performed this analysis. The crystal structure of H_CT with the bound tri-peptide YEW (PDB ID 1YXW) (Jayaraman et al., 2005) was used as a template. The N1 peptide (THIYQWRQT) was constructed using Coot software (Emsley and Cowtan, 2004)replacing the glutamic acid with a glutamine within the YEW peptide. The remaining residues (THI---RQT) were manually constructed and adjusted inside the crevice of H_CT. The structure was optimised by several runs of energy minimisation with CNS software (Brunger, 2007).

A model of the human nidogen-1 fragment (amino acids 389 to 661), was built by homology modelling using the Swiss-Model web server (Arnold et al., 2006) based on the crystal structure of mouse nidogen-1 G2/perlecan Ig3 complex as a template (PDB code 1GL4) (Hopf et al., 2001). The human and mouse proteins display 85% sequence identity (Figure 4-6).

The peptide 604-612 of human nidogen-1 was manually superimposed to the N1 peptide in the nidogen-1-H_CT complex using Coot (Emsley and Cowtan, 2004) (Figure 3-7). The model of the two proteins was optimised by energy minimisation and subjected to molecular dynamics with CNS software. Several steps of dynamics at room temperature were performed, keeping the structure of

nidogen-1 fixed. The Cα atoms of H_CT were harmonically restrained during the dynamics, with the exception of residues 1142-1149 and 1212-1227 in the interaction region of the two proteins, which were left free to move.

2.3.3.9 Isothermal calorimetry (ITC)

To assess the association constant (Ka) of the interaction between the N1 peptide and H_CT, I used isothermal titration calorimetry under the supervision of J. Lally (Cancer Research UK, London Research Institute). To ensure that the H_CT sample did not contain any protein multimers, we used dynamic light scattering; which confirmed that the vast majority (81.6%) of the proteins were present as monomers (estimated diameter 6.52 nm≃60 kDa). 15 μM of H_CT in storage buffer (20 mM HEPES-NaOH pH 7.4, 150 mM NaCl) was added to the sample cell, and 300 μM of N1 peptide dissolved in the same buffer was loaded into the injector. The temperature of the reference cell and sample cell were set at 20°C and the ligand (N1) was titrated into the sample cell (containing H_CT) in precise aliquots (0.4 μl at the first injection, 2 μl for the rest of the experiment) every 2 min. The temperature of the sample cell increased compared to the temperature of the reference cell when the N1 peptide was injected, due to the heat release during binding between the peptide and H_CT (exothermic reaction). The input of power required to keep the temperature equal between the sample and reference cell was recorded. The pattern of the changes in the feedback power were plotted as a function of the molar ratio in Figure 3-8. Enthalpy changes (ΔH) and (Ka) can be directly calculated using the equation below (where ΔG is change in Gibbs free energy, R is the gas constant, T is absolute temperature, ln is natural logarithm and ΔS is change in entropy):

$$\Delta G = -RTlnKa = \Delta H - T\Delta S$$

The dissociation constant (Kd) is the inverted association constant (Ka):

$$C \leftrightarrow R + L$$

$$Kd = \frac{1}{Ka} = \frac{[R][L]}{[C]}$$

Where C stands for complex, R for receptor and L for ligand.

2.3.4 Primary motor neuron mass cultures and immunofluorescent assays

2.3.4.1 Preparation of primary motor neuron cultures

Spinal cord motor neurons were prepared from E13.5 old mouse embryos (C57/Bl6, Charles River) and plated onto glass coverslips, plastic bottom culture dishes and microfluidic chambers. Coverslips and culture dishes were coated with a solution of 15 µg/ml poly-ornithine (Sigma, P-8638) in PBS over night at room temperature. Coverslips and tissue culture dishes were then dried and 0.33 µg/ml laminin (Sigma, L-2020) was added in Neurobasal medium for 2 h at 37 °C. Cells were plated after two washes with Neurobasal. Microfluidic dishes were coated following a special protocol, described in **2.3.7**.

Following Schedule 1 termination of the pregnant mouse, the uterus was extracted and the embryos were kept on ice during the dissection to maintain tissue preservation. The head and tail of the embryo were removed using two straight no.5 jeweller forceps (Sigh Ltd, OS.56/5) and the back of the embryo was opened with one sharp incision in the midline. Since the roof plate of the developing spinal cord is very thin and lies directly beneath the skin, it was cut through during the incision. The opened spinal cord was gently removed from the embryo, the meninges were peeled off and the dorsal horn was cut off with a scalpel. The ventral horn was triturated with a scalpel and added to a 15 ml Falcon tube with 1 ml PBS. For wild type embryo dissections, isolated ventral horns from several embryos were pooled together, while for nidogen-1 and -2 KO motor neuron dissections, samples of tails were saved for genotyping and ventral horns were processed individually. The tissue was digested with 0.025% trypsin (Sigma, T-1426) for 10 min in a water bath at 37°C. For further digestion, two 15 ml Falcon tubes were prepared containing DNAse (Sigma, DN-25) in decreasing concentration (100 ng-10 ng DNAse in 1 ml L-15 medium containing 100 µl 4% BSA). The trypsin-digested samples were gently triturated and transferred to the first 15 ml Falcon tube containing 100 ng/ml DNAse. Following further trituration, the undigested fragments were allowed to settle and the supernatant was transferred to the second 15 ml Falcon tube containing 10 ng/ml DNAse and gently mixed to ensure that there were no undigested spinal cord fragments left. A cushion of 4% BSA was applied to the bottom of the tube and cells were

centrifuged at 370 *g* for 5 min at room temperature. The supernatant was discarded and the cells were resuspended in complete motor neuron medium (Table 6), which contain essential neurotrophins, ciliary neurotrophic factor (CNTF), glial cell line-derived neurotrophic factor (GDNF) and brain-derived neurotrophic factor (BDNF). The typical yield of the preparation was 1-2x10^6 cells per spinal cord. Cells were kept at 37 °C in a 7.5% CO_2 incubator.

Table 6. Composition of complete motor neuron medium (50 ml)

Ingredients	Required volume (ml)
Neurobasal	46.25
B27 supplement (50x)	1
Heat inactivated horse serum (2%)	1
L-Glutamine (430x dil.)	0.104
β-mercaptoethanol (1 mM)	1.25
CNTF (100 µg/ml)	0.005
GDNF (100 ng/ml)	0.05
BDNF (25 µg/ml)	0.002
Penicillin/Streptomycin (250x)	0.25

2.3.4.2 H_CT binding assays

2.3.4.2.1 Testing the effect of peptides on H_CT binding

For the initial H_CT binding studies, wild type motor neurons were cooled on ice prior to incubation with AlexaFluor555-H_CT (20 nM), which was pre-treated with either DMSO, or the D/J/O/N1/N2/N3/$N1_{AA}$ peptides (20 µM). Cells were incubated with the mixture for 45 min at 37 °C to allow internalisation. Following washes with Hanks' buffer (HBSS, 20 mM HEPES-NaOH pH 7.4, 0.44 mM KH_2PO_4 0.42 mM NaH_2PO_4, 5.36 mM KCl, 136 mM NaCl, 0.81 mM $MgSO_4$, 1.26 mM $CaCl_2$, 6.1 mM glucose), the cells were fixed with 4% paraformaldehyde (PFA) in PBS, pH 7.4 for 15 min at room temperature. The coverslips were mounted with Mowiol and imaged on a Zeiss LSM510 confocal microscope equipped with a Zeiss 40x objective.

2.3.4.2.2 Testing the effect of exogenous nidogens on H_CT binding

To assess the effect of recombinant nidogens on H_CT binding, cells were preincubated with H_CT (20 nM), which was pre-treated with either DMSO, the N1/$N1_{AA}$ peptides, recombinant nidogens (1 nM), or a combination of the above for 1 h at room temperature at a molar ratio of 1:20:20,000 (recombinant nidogens:H_CT:N1/$N1_{AA}$ peptide, respectively). Cells were incubated with AlexaFluor555-H_CT for 10 min before washing with ice-cold HBSS and fixing with 4% PFA in PBS for 15 min at room temperature. To obtain a mask for fluorescence intensity quantification, I stained the cells with a mouse monoclonal antibody against βIII tubulin and an AlexaFluor488-conjugated goat anti-mouse secondary antibody. Twenty images were acquired for each condition using a Zeiss LSM510 confocal microscope equipped with a Zeiss 40x objective and acquired images were analysed for H_CT binding using Cell Profiler. The mean fluorescence intensity was plotted for each condition and statistical significance was analysed using Kruskal-Wallis test (****, $p<0.001$) followed by Dunn's multiple comparisons test.

To confirm that His_9-tagged recombinant nidogen-1 binds to motor neurons, the cells were not tested for βIII tubulin, but probed with mouse anti-His antibody instead, followed by an AlexaFluor488-conjugated goat anti-mouse secondary antibody.

2.3.4.2.3 Time competition between H_CT and the N1 peptide

To assess the ability of the N1 peptide to block H_CT accumulation when applied after H_CT, wild type motor neurons were incubated with AlexaFluor555-H_CT together with either the vehicle control (DMSO) or the N1/$N1_{AA}$ peptide, with the latter being added either together with or 10 min after the application of AlexaFluor555-H_CT. The cells were allowed to internalise H_CT for 45 min at 37 °C before cooling on ice, acid washing for 2 min (100 mM citrate-NaOH, 140 mM NaCl, pH 2.0) to remove the surface-bound probes, and fixation with 4% PFA in PBS (as above). The cells were subjected to the same immunofluorescence protocol against βIII tubulin as described above, and 4x4 tile scan images were taken using a Zeiss LSM780 confocal microscope equipped with a 63x objective. Images of H_CT binding were analysed using Cell Profiler. The mean intensity of H_CT alone (DMSO) was set at 100% for both the 0 and 10 min samples and the effects of

N1/N1$_{AA}$ addition were analysed using one-way ANOVA (***, p<0.005) followed by Dunnett's multiple comparisons test.

2.3.4.2.4 H_CT binding to primary motor neurons lacking nidogens

To assess the ability of nidogen-1 and -2 KO primary motor neurons to bind H_CT, I isolated motor neurons from nidogen-1 and -2 KO and wild type E13.5 embryos as described above and cultured them for 7-10 days (DIV 7-10). Cells were cooled on ice, and incubated with HA-H_CT (40 or 10 nM) for 10 min. Following a wash with ice-cold Hanks' buffer, the cells were fixed with 4% PFA in PBS for 15 min at room temperature and immunostained with a rat anti-HA and mouse anti-βIII tubulin antibodies. Primary antibodies were detected using AlexaFluor555-conjugated goat anti-rat and AlexaFluor488-conjugated goat anti-mouse secondary antibodies (dilution 1:500) to reveal H_CT binding and the neural network, respectively. Ten images were acquired for each condition using a Zeiss LSM510 confocal microscope equipped with a Zeiss 40x objective. Images were analysed for H_CT binding using Cell Profiler. Image acquisition parameters were adjusted by setting the signal detection threshold to 0 for the sample where H_CT was omitted and the mean fluorescence intensity was plotted for each genotype. Statistical significance was analysed using unpaired Student's *t* test.

2.3.4.3 Colocalisation between H_CT and other proteins

- Nidogen-2

Motor neurons were incubated with AlexaFluor555-H_CT (40 nM) together with rabbit polyclonal antibody against nidogen-2 at 37 °C for 45 min, then cooled on ice and subjected to an acid wash before fixation with 4% PFA in PBS for 15 min at room temperature. Cells were permeabilised using 0.1% Triton X-100 in PBS (PBSTr) for 10 min at room temperature and blocked with 5% BSA in PBS for 1 h. The primary antibody was revealed using an AlexaFluor488-conjugated goat-anti-rabbit secondary antibody. The cells were washed and the coverslips were mounted using Mowiol. Samples were imaged using a Zeiss 63x, Plan Apochromat oil-immersion objective of a LSM780 confocal microscope. The microscope was optimised for co-localisation analysis. The sampling was set to maximum and the

level of co-localisation was quantified using ImageJ. Mander's coefficient was determined on randomly chosen fields.

- Nidogen-2 and LAR

The experiment was performed as above, but after permeabilisation, a mouse anti-LAR PMD antibody (Yang et al., 2006) was added to the cells for 1 h at room temperature. AlexaFluor488-conjugated goat-anti-rabbit secondary antibody was added to reveal internalised nidogen-2, and AlexaFluor647-conjugated goat anti-mouse antibody was added to reveal the localisation of LAR. The cells were washed and the coverslips were mounted using Mowiol. Samples were imaged using a Zeiss 63x, Plan Apochromat oil-immersion objective of the Zeiss LSM510 confocal microscope.

- TrkB

AlexaFluor555-H_CT was added to primary motor neurons for 45 min at 37 °C to allow internalisation. The cells were cooled on ice, acid washed as before, fixed with 4% PFA for 15 min at room temperature before permeabilising using 0.1% Triton X-100 in PBS for 10 min at room temperature and blocking with 5% BSA in PBS for 1 h. A rabbit anti-TrkB antibody was added to the cells for 1 h at room temperature. The cells were then washed and an AlexaFluor488-conjugated goat anti-rabbit secondary antibody was added for 1 h at room temperature to detect the presence of TrkB. The cells were washed with PBS and the coverslips were mounted with Mowiol before imaging with a Zeiss LSM510 confocal microscope.

For the competition experiments, the motor neurons were cooled on ice, and either the mouse anti-TrkB antibody or AlexaFluor555-H_CT was added first to the cells for 10 min. The excess probes were washed off and AlexaFluor555-H_CT or mouse anti-TrkB antibody was then added. Coverslips were washed with ice-cold HBSS, cells were fixed and the immunofluorescence protocol using the AlexaFluor488-conjugated anti-rabbit antibody was performed as above. Samples were imaged using a Zeiss 63x, Plan Apochromat oil-immersion objective on a Zeiss LSM510 confocal microscope.

- SV2

For the SV2 co-localisation studies, motor neurons were incubated either with fluorescent H_CT alone (40 nM), or together with recombinant nidogen-1 (1.6 nM) for 45 min at 37 °C. Cells were then acid washed, fixed, permeabilised and

blocked using a special blocking buffer (2% BSA and 10% foetal bovine serum (FBS) in PBS) prior to staining with a rabbit polyclonal antibody against SV2A (SYSY119002; Synaptic System; 1:500) or SV2C (a kind gift from T. Südhof; 1:100) and a mouse monoclonal antibody against βIII tubulin. Primary antibodies were detected using AlexaFluor488-conjugated anti-rabbit antibody and AlexaFluor647-conjugated anti-mouse antibody. The cells were washed and the coverslips were mounted with Mowiol. Samples were imaged using a Zeiss 63x, Plan Apochromat oil-immersion objective on a Zeiss LSM510 confocal microscope. The microscope was optimised for co-localisation analysis. The sampling was set to maximum and the level of co-localisation was quantified using ImageJ. Mander's coefficient was determined on randomly chosen fields. Statistical significance was assessed using unpaired Student's *t* test with Welch's correction.

2.3.4.4 Nidogen-2 uptake in primary motor neurons

Primary motor neuron cultures were left untreated, or were treated with either BDNF (100 ng/ml), H_CT (40 nM), or incubated in Neurobasal medium for 2 h (starved). Rabbit anti-nidogen-2 antibody was added to the culture for 30 min at 37°C; this allowed internalisation of the probe before acid washing to remove surface bound antibodies. The cells were fixed, permeabilised and blocked as before and stained with goat AlexaFluor488-conjugated anti-rabbit antibody to reveal the internalised pool of nidogen-2 and a mouse anti-βIII tubulin antibody followed by AlexaFluor647-conjugated anti-mouse antibody to stain the neuronal network. The cells were washed and the coverslips were mounted with Mowiol. Samples were imaged using a Zeiss 63x, Plan Apochromat oil-immersion objective on a Zeiss LSM510 confocal microscope.

2.3.5 Differentiation of motor neurons from embryonic stem (ES) cells

2.3.5.1 Maintenance of pluripotency

Low passage (up to 4) embryonic stem (ES) cells were defrosted in a water bath at 37 °C. The cells were spun down at 1,000 rpm (rotation per min) for 3 min. The pellet was resuspended in ES growth medium (Table 7) and plated in a fish skin gelatin-coated T25 flask. The cells were never allowed to reach full confluency, as it promotes differentiation. The cells were detached from the surface of the flask

by Accutase (Life Technologies, according to manufacturer's instructions) treatment for 5 min and vigorous shaking. Once in suspension, they were spun down at 1,000 rpm for 3 min, the pellet was resuspended in 1 ml of ES growth medium and split in 3 to decrease cell density. The cells were plated in a gelatinised T25 flask and kept at 37° C in 5 % CO_2.

Table 7. Composition of the ES growth medium (125 ml)

Ingredient	Required volume (ml)
Glasgow Minimal Essential Medium (GMEM, Gibco)	110
ES cell tested foetal bovine serum (FBS)	6.25
Knockout serum replacement	6.25
Glutamax	1.25
B-Mercaptoethanol (1:1400 stock in GMEM)	1.25
Leukaemia inhibitory factor (LIF, 107 units/ml ESGRO stock; Millipore)	0.0125

2.3.5.2 Differentiation

The ES cell cultures were washed with warm PBS before adding Trypsine-Versene (Life Technologies, 0.125%) for 1 min at room temperature. The flask was shaken vigorously to detach the cells. 4 ml ES growth medium was added to the cell suspension before centrifuging at 1,000 rpm for 3 min. The cell pellet was resuspended in ES growth medium and the cells were counted. $2x10^5$ cells were carried forward for 'small' (5 ml) differentiation, while $2x10^6$ were carried forward for 'big' (10 ml) differentiation. 5 ml DNFK medium (Table 8) was added to the cell suspension before centrifuging at 1000 rpm for 3 min. The supernatant was removed and the appropriate volume of DNFK medium was added to the pellet. The ES cells were plated into uncoated Petri dishes (Sterilin) and kept at 37 °C in 5 % CO_2. The medium was changed every day, with additional retinoic acid (RA; 1:10,000) and Smoothened agonist (SAG, Enzo Life Sciences, 1:6,000) present from day 2. The embryoid bodies (EB) were allowed to grow until day 5.

On day 5 of the differentiation protocol, EB were disaggregated following the same protocol as the primary motor neuron disaggregation. Motor neurons were plated on poly-ornithine/laminin coated coverslips, or BSA/poly-ornithine/laminin-coated microfluidic chambers.

Table 8. Composition of the DNFK medium (50 ml)

Ingredient	Required volume (ml)
DMEM supplemented with F12	62.25
Neurobasal	62.25
GLUTAMAX	0.6
KO serum replacement	13
β-Mercaptoethanol	0.0014

2.3.6 Design and preparation of microfluidic chambers

Microfluidic chamber templates were already present in the laboratory; however, these did not favour the crossing of motor neuron axons. To overcome this, I designed new chambers with shorter microgrooves (500 μm) using the software Canvas (ADC Systems), under the guidance of G. Menendez (Molecular Neuropathobiology laboratory, Cancer Research UK). The height of the grooves was set at 1-2 μm to maintain the microfluidic isolation between the somal and axonal compartments. The photo masks were custom-made microLIQUID (Mondragón, Spain). The final design was replicated onto SU9 silicone wafers using photolithography and I used these wafers to make the initial Polydimethylsiloxane (PDMS, also known as Sylgard 184; Dow Corning) replicas, which can be mounted on plastic or glass bottom dishes and used as a microfluidic chamber. PDMS is a polymer, which is a liquid in its unpolymerised form, and turns into a semi-flexible material when polymerised. Polymerised PDMS pieces were produced by mixing the base component of PDMS with a curing agent (mixed 10:1, according to manufacturer instructions). This liquid mixture was put under vacuum

to eliminate bubbles for approximately 30 minutes and then poured into the SU9 wafers. These were put in an oven at 65°C to polymerise the PDMS. PDMS devices were then peeled from the wafers. To avoid any damage to the original wafer, I refrained from using them for repetitive chamber preparation. I used the first PDMS insets to create identical epoxy resins and I used these as templates for the chamber preparations. To make the resin replicas, all components of the epoxy resin (Table 9) were mixed and air bubbles were removed under vacuum for 60 min. This was poured into a tin cup and a PDMS microfluidic chamber copied from the model SU9 silicon wafer was used as a mould. The PDMS device was set to float on the liquid mix of epoxy resin with the pattern facing downwards. The epoxy resin was polymerised at 65°C overnight. The PDMS mould was then peeled from the hardened epoxy block. A first PDMS device produced by replica moulding from these new masters was inspected with a scanning electron microscope to confirm that all dimensions of the original design were copied with high fidelity.

Table 9. Ingredients for EPON resin preparation (final weight 20 g)

Ingredient	Required weight (g)
Taab 812 resin	9.6
MNA (g)	6.6
DDSA (g)	3.8
Accelerator DMP-30	0.4

The PDMS pieces were cut to shape using a 28 mm diameter Wad Punch (Roebuck). Finally four wells were cut, one at each end of each of the two lateral compartments. These wells were cut with a 5 mm borer.

I used 50 mm diameter glass bottom dishes (IntraCel, UK) for live cell imaging and immunofluorescence applications. PDMS insets were irreversibly attached to the dish using plasma cleaner. Plasma cleaner creates temporarily reactive chemical groups on the surface of the glass and PDMS that can form irreversible bonds if put in contact immediately after treatment. Complete microfluidic chambers were incubated at 65°C for 5 minutes to complete the

binding reaction. The plasma treatment sterilises microfluidic devices, but it renders the surface of PDMS hydrophobic. Therefore, coating must be applied immediately after chamber assembly.

First, the hydrophobic surface must be neutralised and made more hydrophilic by the addition of 0.8% BSA in L-15 medium at 37°C over night. A higher volume of coating media was added to the future somatic side of the chambers, and they were tipped towards the axonal side to aid the coating for the microgrooves. The following day this media was removed and the chambers were coated with poly-L-ornithine and laminin following the protocol described above for coating coverslips. A higher volume of coating reagent was added to the somatic side and the chambers were incubated tipped towards the axonal side.

2.3.7 Scanning Electron Microscopy

Microfluidic chambers were observed under a JEOL 6700 Field Emission Scanning Electron Microscope to assess that the size of all features corresponded to our design. For this purpose, microfluidic PDMS devices were cut, mounted on a cylinder stub and attached with a piece of carbon tab. The exposed surface was covered with a film of platinum in a sputter coater. The analysis was performed by A. Weston (Cancer Research UK London Research Institute).

2.3.8 Plating primary or ES derived motor neurons in microfluidic chambers

Primary motor neurons or ES derived embryoid bodies were disaggregated as explained before. The cells were resuspended in a low volume of complete motor neuron medium and counted using a Neubauer chamber. Briefly, I performed a 1:10 dilution of the cell suspension and 10 µl was loaded into the chamber. Cells were counted in 3 big squares along the diagonal angle. Since the volume of 1 big square is 1 µl and there is a pre-dilution factor of 10, the concentration of the suspension is as follows:

$$Concentration = \frac{Numer\ of\ cells \times 100{,}000}{3}$$

A high cell density is required to encourage motor neuron axons to cross. 50.000 cells were plated from primary motor neuron dissections, while 100.000

cells were required from ES derived motor neurons due to the higher mortality of cells after *in vitro* differentiation.

2.3.9 Immunofluorescence assays in microfluidic chambers

Since there is microfluidic isolation between the two compartments; the antibodies cannot penetrate into the microgrooves. Antibodies were always added to both compartments at the same dilution to ensure that both the axons and cell bodies are stained to an equal level.

2.3.9.1 βIII tubulin and SMI31 staining in microfluidic chambers

To test whether motor neurons were able to cross the short microgrooves (500 µm), I plated ES derived motor neurons into the somatic compartment of microfluidic chambers. The ES line express GFP under the motor neuron specific HB9 promoter (HB9::GFP) and GFP is present throughout the cytosol of every motor neuron in the culture. 4 days after plating, the level of crossing was determined under a light microscope, and both the somatic and axonal compartments were fixed with 4% PFA in PBS for 15 min at room temperature. To fix the axons within the isolated microgrooves, a higher volume (200 µl) was applied to the axonal compartment compared to the somatic compartment (100 µl) and the chambers were tipped towards the lower liquid column, this promotes liquid flow within the microgrooves. The cells were permeabilised and blocked as before and both compartments were stained with rabbit anti-βIII tubulin and mouse anti-SMI31 antibodies for 1 h at room temperature. βIII tubulin labels all neuronal cells, while SMI31 specifically recognises a heavily phosphorylated form of neurofilament, which is highly enriched in axons. The primary antibodies were washed off with PBS and AlexaFluor647-conjugated goat anti-rabbit and AlexaFluor555-conjugated goat anti-mouse secondary antibodies were added for 1 h at room temperature to both sides. Following several washes with PBS, the compartments were post-fixed with 4% PFA in PBS for 15 min at room temperature. The fixing solution was replaced with PBS and the axonal side of the chambers was imaged with a Zeiss LSM 510 confocal microscope in a custom-design chamber holder.

2.3.9.2 H_CT transport in microfluidic chambers

To test if H_CT is taken up at the axonal compartment and transported to the somal compartment, I plated primary motor neurons into microfluidic chambers, and once the axons crossed the microgrooves (DIV 7), I added a higher volume of motor neuron medium to the somatic side (200 µl) and a lower volume of the same medium (100 µl) containing AlexaFluor555-H_CT (40 nM) to the axonal side. The neurons were left to internalise H_CT for 2 h at 37 °C before washing the axonal compartment with HBSS. Both compartments were processed the same way as previously described, but the SMI31 antibody was omitted. Both sides of the chamber were imaged as before.

2.3.9.3 Uptake and differential sorting of H_CT and cholera toxin B (CTB)

To show that H_CT undergoes synaptic transfer in motor neuron cultures, I plated primary motor neurons in microfluidic chambers and let them extend their axons through the microgrooves (DIV 7). I added a higher volume of motor neuron medium to the somatic side (200 µl) and a lower volume of the same medium (100 µl) containing AlexaFluor555-H_CT (40 nM) and AlexaFluor488-CTB to the axonal side and left the cells to internalise and transport the probes for 2 h at 37 °C. Both sides of the chambers were stained for βIII tubulin and imaged as before. Every axon in the axonal compartment contained both CTB and H_CT, but there were a few cell bodies in the somatic side, which contained H_CT but not CTB.

2.3.9.4 Transcytosis of H_CT and nidogen-2

To test whether nidogen-2 was re-exposed together with H_CT on the surface of motor neurons after axonal retrograde transport, we added AlexaFluor555-HA-H_CT (40 nM) together with a rabbit polyclonal antibody against nidogen-2 to the axonal side of the chamber and incubated it for 2 h at 37 °C. Cells were prepared for immunofluorescence as before and the somatic compartment was stained with a rat monoclonal anti-HA antibody in detergent-free conditions. After removing the unbound antibody with three PBS washes, the somatic compartment was stained with AlexaFluor647-conjugated goat anti-rabbit and AlexaFluor488-conjugated goat

anti-rat secondary antibodies to reveal the transcytosed pool of nidogen-2 and H_CT, respectively. The chambers were post-fixed and imaged as before.

2.3.10 Immunofluorescence assays on neuromuscular junctions and hindbrains

2.3.10.1 Colocalisation between choline-acetlytransferase, nidogen-2 and H_CT at the NMJ

To determine whether nidogen-2 and H_CT colocalise to presynaptic sites at the NMJ, we injected the tibialis anterior (TA) muscle of age and sex matched C57/Bl6 mice (n = 3) with HA-H_CT (14 µg, 4 µl total volume) using a 10 µl Hamilton syringe under brief isoflurane-induced anaesthesia. After 60 min animals were terminally anaesthetised and transcardially perfused with saline followed by 4% PFA in 0.05 M (pH 7.8) TBS. Both the TA and extensor digitorum longus (EDL) muscles were dissected, post-fixed for 1 h in 4% PFA in TBS and cryoprotected in 20% sucrose in TBS overnight at 4 °C. Muscles were mounted in O.C.T. (Tissue-Tek) and frozen on dry-ice before being sectioned on a cryostat (20 µm thickness) and collected onto poly-lysine coated slides. Sections were air-dried for 1 h prior to staining according to standard immunofluorescence staining protocols. Briefly, sections were washed three times with TBS, blocked with 5% normal goat serum (NGS) in TBS, 0.1% Triton X-100 before application of primary antibodies: rat anti-HA antibody rabbit anti-nidogen-2, goat anti-choline acetyltransferase (blocked and diluted in donkey serum), which were diluted in TBS, 2% NGS, 0.1% Triton X-100 and incubated overnight at room temperature in a humidified chamber. After three 5 min washes with TBS, appropriate secondary antibodies were applied: AlexaFluor647-conjugated goat anti-rat; AlexaFluor488-conjugated goat anti-rabbit or AlexaFluor488-conjugated donkey anti-goat, blocked and diluted in donkey serum. Secondary antibodies were diluted in combination with AlexaFluor555-α-bungarotoxin (α-BTx) and applied to sections for 1 h at room temperature, after which sections were washed three times with TBS. Coverslips were mounted with fluorescence mounting media (Dako) and slides were then imaged using a Zeiss LSM780 confocal microscope equipped with a Zeiss 40x Plan Apochromat oil-immersion objective. The integrated intensity of H_CT and nidogen-2 was tested

using Spearman correlation in Graphpad Prism. The injection and immunohistochemistry was performed by J. B. Bryson (UCL-Institute of Neurology) and I imaged the sections and analysed the colocalisation.

2.3.10.2 The effect of the N1 peptide on H_CT binding at the NMJ

To test whether the N1 peptide is capable of blocking the entry of H_CT at the NMJ, levator auris longus (LAL) muscles were isolated from wild type animals and incubated with H_CT (20 nM), which had been pre-treated with either DMSO, or the N1/$N1_{AA}$ peptide (20 µM) for 1 h at 37 °C. The muscles were washed, fixed in 10% NBF overnight at 4 °C, permeabilised using 0.1% Triton X-100 in PBS for 1 h at room temperature and blocked with 5% BSA in PBS for 1 h. Rat anti-HA antibody was added for 1 h at room temperature. The muscles were washed with PBS before the addition of AlexaFluor555-α-BTx and AlexaFluor488-conjugated goat anti-rat antibody. The samples were mounted with Mowiol and imaged as described above. I used α-BTx staining as a mask to identify NMJs and determined the ratio between H_CT positive and negative NMJs. The results were plotted and tested for significance by Kruskal-Wallis test (**, $p<0.001$) followed by Dunn's multiple comparisons test.

2.3.10.3 H_CT binding to nidogen KO NMJs

Freshly-isolated LAL muscles from adult nidogen-1 and nidogen-2 KO mice were used to assess the requirement of nidogens to internalize H_CT at the NMJ. The muscles were incubated with H_CT (40 or 20 nM) in motor neuron medium for 2 h at 37 °C, then processed and imaged as above. The results were plotted and tested for significance by Kruskal-Wallis test (****, $p<0.001$) followed by Dunn's multiple comparisons test. To test whether exogenous nidogen-1 rescue the phenotype of nidogen-1 KO NMJs and restore H_CT binding, the experiment was performed as above, but His_9-tagged recombinant nidogen-1 (1 nM) was added together with HA-H_CT. The recombinant nidogen-1 was then detected using mouse anti-His_5 antibody and an AlexaFluor647-conjugated goat anti-mouse secondary antibody.

2.3.10.4 Testing synaptic vesicle recycling in nidogen KO NMJs

To test whether nidogen KO NMJs exhibited normal synaptic vesicle recycling, the GST-tagged binding fragment of botulinum neurotoxin A (H_CA; 12 µg in 4 µl) was injected into the TA muscle of wild type, nidogen-1 and nidogen-2 KO mice, as described above, and muscle sections were immunostained with rabbit anti-GST (ab9085, Abcam; 1:100), followed by AlexaFluor488-conjugated goat anti-rabbit antibodies.

2.3.10.5 H_CT binding to nidogen-1 and -2 dual knock out (nidogen DKO) hindbrains

To assess the requirement of nidogens to bind H_CT in vivo, freshly isolated hindbrains of nidogen DKO E11.5 embryos were incubated with AlexaFluor555-H_CT in motor neuron medium for 2 h at 37 °C, followed by 10% NBF fixation overnight at 4 °C. The samples were then immunostained for βIII tubulin as described above, mounted with Mowiol and imaged using a Zeiss LSM780 confocal microscope equipped with a Zeiss 20x Plan Apochromat objective. The mean grey value of the H_CT signal for the entire sample was determined using Image J, plotted and tested for significance using unpaired Student's *t* test with Welch's correction.

2.3.11 The effect of peptides on H_CT binding in a hemidiaphragm assay

Mouse phrenic nerve-hemidiaphragms were dissociated from male Swiss-Webster CD1 mice weighing about 20 g and mounted in 2-4 ml of oxygenated (95% O_2, 5% CO_2) Krebs-Ringer solution of the following composition: 137 mM NaCl, 5 mM KCl, 1.8 mM $CaCl_2$, 1.0 mM $MgCl_2$, 24 mM $NaHCO_3$, 1 mM NaH_2PO_4 and 11 mM glucose, pH 7.4, at 37 °C. Two innervated hemidiaphragm preparations were isolated from each animal; muscles were stretched to the optimal length for twitch response and allowed to equilibrate for at least 20 min at 37 °C before the start of the experiment. The phrenic nerve was stimulated via two ring platinum electrodes with supramaximal stimuli of 10 V amplitude and 0.1 ms pulse duration with a frequency of 0.1 Hz. Muscle contraction was monitored with an isometric transducer (Harvard Apparatus); data was recorded and analysed via an i-WORX 118 system with Labscribe software (Harvard Apparatus). TeNT aliquots (final

concentration 5 nM) were preincubated with vehicle (DMSO) or with the N1 peptide (2.5 µM), corresponding to a molar ratio of 1:500 (TeNT:peptide), for 1 h at room temperature, and then added directly to the tissue bath of two nerve-muscle preparations obtained from a single animal. Muscular twitch was monitored until complete paralysis. Data were expressed as the time required to decrease the twitch to 50% of the initial value (paralysis half-time). The experiment was performed by P.Caccin (University of Padova).

2.3.12 *In vivo* assays

2.3.12.1 The effect of the N1 peptide on local tetanus

2.3.12.1.1 Local tetanus of the *triceps surae* muscle (TS) analysed by a footprint assay

Age- and body weight-matched C57/Bl6 male mice were injected with TeNT (1 or 2 ng/kg, concentration set to have an injection volume of 5,5 µl) preincubated with either DMSO, the N1 or the $N1_{AA}$ peptide at a molar ratio of 1:13,800 (TeNT:peptide) for 1 h at room temperature into the right TS muscle. Mice were monitored for period of 96 h unless they reached the humane endpoint (appearance of moderate symptoms: hunched back and paralysis of rear limbs, or disappearance of the righting reflex for 30 s) earlier.

Footprint assays were performed following the previously described protocol (Carter et al., 1999). Briefly, the non-injected paws were painted black and the paw of the injected hindlimb (right) was painted red. The mice were let to walk on a white stripe of paper. To quantify the extent of paralysis, the distance between the contralateral (injected side) front and hind paw prints was measured. This parameter provides a reliable assessment of normal foot positioning during walking in mice, with increased distance between the front and hind footprints reflecting triceps surae muscle paralysis. Data were analysed using one-way ANOVA (****, $p<0.0001$) followed by Dunnett's multiple comparisons test to compare the groups. Following termination, the triceps surae muscles were isolated and weighed to determine the exact TeNT dose/mg TS muscle (Table 10). The body weight

correlates well with the weight of the TS muscle, but for future experiments I used weight-matched mice.

Table 10. Determination of TeNT dosage in the TS muscle

1 ng/kg	Body weight (g)	Inj. vol.(µl)	Weight TS (mg)	Dose (pg/mg TS)
TeNT alone	23.5	5.6	123	0.19
	21.2	5.1	117	0.18
TeNT+N1$_{AA}$	23.3	5.6	138	0.17
	23	5.5	120	0.19
TeNT+N1	23	5.5	142	0.16
	23	5.5	112	0.21

2 ng/kg	Body weight (g)	Inj. vol.(µl)	Weight TS (mg)	Dose (pg/mg TS)
TeNT alone	22.8	5.5	132	0.35
	23	5.5	128	0.36
TeNT+N1$_{AA}$	22.7	5.4	127	0.36
	22.4	5.4	111	0.41
TeNT+N1	22.3	5.4	110	0.41
	22.4	5.4	117	0.39

2.3.12.1.2 Local tetanus analysed by isometric muscle tension physiology

8-week old female C57Bl6 mice received unilateral intramuscular injection of TeNT into the *tibialis anterior* (TA) muscle (0.125 ng/kg, 4 µl injected volume per 20 g body mass), after preincubation with vehicle (DMSO), N1 or N1$_{AA}$ peptides at a molar ratio of 1:13,800 (TeNT:peptide) for 1 h at room temperature. After 24 h, isometric muscle tension force was recorded under terminal anaesthesia from the distal TA tendon following electrical stimulation (40-100 Hz, 0.02 ms square-wave pulses, for 450 ms) of the exposed sciatic nerve to induce maximal tetanic muscle contraction, as previously described (37). Contractile force of injected muscles was compared to contralateral (non-injected) TA muscle, as an internal control, and average changes within each group were analysed using unpaired Student's *t* test.

The experiment was performed by J. B. Bryson (UCL-Institute of Neurology) and I analysed the results for significance.

2.3.12.2 The effect of exogenous nidogen-1 on local tetanus

The right TS muscle of weight matched C57/Bl6 mice was injected with 1 ng/kg of TeNT, following preincubation with DMSO as a vehicle control, nidogen-1 alone or the N1 peptide followed by nidogen-1 (molar ratio; TeNT:N1:nidogen-1 = 1:13,800:0.25). Mice were closely monitored and scored blind according to the scoring system shown in Table 11. Before injection, and 45 and 69 h after injection, a footprint analysis was performed as described before and the coordination (distance between the prints on the same side) was measured. I performed the experiment together with N. Schmieg (Molecular Neuropathobiology laboratory, Cancer Research UK) and members of the Molecular Neuropathobiology laboratory assisted with the scoring of the behaviour of the mice. To assess the progression of tetanic paralysis, we distinguished between 6 different stages of progression (scale 5-0, Table 11). The animals' behaviour was assessed at 29, 27, 52 and 73 h after injection. During tetanic paralysis, the toes and the paw show the first signs of paralysis, the paw is touching the floor progressively less (Score 4), then the animal starts walking using its toes only (Score 3). This is followed by the extension of the injected hindlimb when the mouse is lifted up by its tail (Score 2). The TS muscle gets completely paralysed (Score 1), then the animal bends to one side when lifted up by its tail (Score 0). Mice were monitored for period of 96 h unless they reached the humane endpoint (appearance of moderate symptoms: hunched back and paralysis of rear limbs, or disappearance of the righting reflex for 30 s) earlier.

Table 11. Scoring system to assess in vivo local tetanus progression

Scores	Behaviour
5	Normal walking
4	Partial loss of paw print
3	Walking on toes
2	Extended leg
1	Loss of TS movement
0	Stiff back muscles

2.3.12.3 Analysis of TeNT toxicity in nidogen-2 KO mice

Age and body mass-matched wild type and nidogen-2 KO mice were injected intraperitoneally with different doses of TeNT (1.5, 3, 6, or 12 ng/kg). Mice were regularly monitored for up to 96 h after injection. Animals were terminated by Schedule 1 method when mice showed moderate tetanus symptoms (hunched back and paralysis of rear limbs or disappearance of the righting reflex for 30 s). The time of survival prior to termination was plotted against the administered dose of TeNT and data was analysed using Kolmogorov-Smirnov test for each dose. The experiment was performed by N. Schmieg and G. Schiavo (Molecular Neuropathobiology laboratory, Cancer Research UK and UCL-Institute of Neurology) and I analysed the results.

2.4 Supplemental material

2.4.1 Description of movies

2.4.1.1 Movie 1. The N1 peptide prevents TeNT-induced paralysis in vivo

Mice injected in the right *triceps surae* muscle with TeNT showed signs of local paralysis (the affected limb is extended) with no grip reflex. Pre-treatment of TeNT with vehicle control or the $N1_{AA}$ peptide had no effect on the progression of tetanic paralysis. In contrast, when mice were injected with TeNT pre-treated with the N1 peptide, they showed an overall normal posture, strong grip reflex and no gait abnormalities, demonstrating a blockade in TeNT induced paralysis. From (Bercsenyi et al., 2014). Reused with permission from AAAS.

2.4.1.2 Movie 2. Model of the interaction of H_CT and nidogen-1

The crystal structure of HcT (cyan) is shown bound to the N1 peptide or to human nidogen-1 (orange). The model of the molecular complex was built and minimised as described in Figure 3-8 and Figure 4-6. The modeling was performed by G. Zanotti (University of Padova). From (Bercsenyi et al., 2014). Reused with permission from AAAS.

2.4.1.3 Movie 3. Localisation of nidogen-2 and H_CT at the NMJ

3-D rendering of a NMJ from the extensor digitorum longus muscle, fixed 1 h after H_CT injection, compiled from a z-stack of confocal images. Individual channels show fluorescent labeling of α-bungarotoxin (blue), combined with immunolabelling of nidogen-2 (green) and HcT (red). The merged image reveals colocalisation of HcT with nidogen-2 within the NMJ (see also Figure 4-24). The 3-D rending was perfomed by J. B. Bryson (UCL-Institute of Neurology). From (Bercsenyi et al., 2014). Reused with permission from AAAS.

2.4.1.4 Movie 4. Additional nidogen-1 speeds up the progression of tetanic paralysis

The *triceps surae* muscle was injected with lethal dose of TeNT (1.5 ng/kg) intraperitoneally. 24 h post-injection wild type mice were showing typical signs of early general tetanus (stiff muscles, hyperventilation and delay in exploration), while nidogen-2 KO animals have a close to normal posture, breath normally and explore their surrounding without delay (see also Figure 4-13). The video was taken with the help of N. Schmieg (Cancer Research UK, London Research Institute).

Chapter 3. The N1 peptide blocks tetanic paralysis

3.1 YEW peptide screening for TeNT binding

It was proposed that protein receptors play a role in CNT binding at the NMJ alongside polysialogangliosides (Montecucco, 1986, Rummel et al., 2007). There are several arguments indicating that a protein is likely to play part in the process of TeNT binding:

1. Firstly, polysialogangliosides are highly abundant acidic lipids, decorating all neuronal membranes, and binding to these alone cannot provide specificity to the motor neuron membrane.
2. Moreover, the affinity of TeNT to polysialogangliosides is in the nanomolar range, whereas it binds to neuronal membranes at femtomolar concentrations, making it lethal at very low doses (Habermann and Dreyer, 1986).

A tripeptide (YEW) was crystallised in the 'R' site of H_CT, where sialic acid was previously shown to bind (Figure 3-1 A)(Jayaraman et al., 2005). This work brought up the possibility that a protein receptor could engage with this site simultaneously with gangliosides binding to the lactose site, and this dual receptor complex could provide a very efficient, high affinity-binding platform for TeNT at the neuromuscular junction (Rummel et al., 2003, Rummel et al., 2007).

To investigate whether a protein containing the YEW motif, or its variants binds to this site, we queried a list of candidate receptors from an H_CT magnetic pull-down screen performed in our laboratory for the presence of YEW like sequences (Deinhardt et al., 2006b). In the screen, H_CT was conjugated to magnetic beads, allowed to internalise in primary motor neurons and endosomes containing this probe were purified on a magnetic column, lysed and subjected to mass spectrometry analysis to determine their molecular composition (Figure 3-1 B).

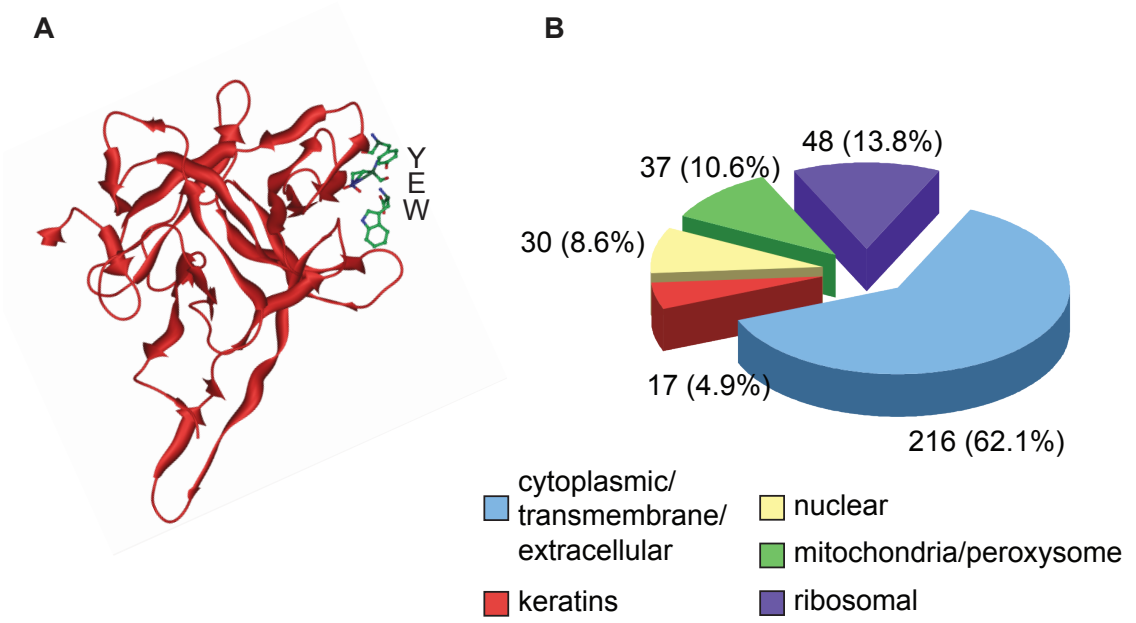

Figure 3-1. The YEW peptide binds to H_CT and the H_CT carriers' main components are transmembrane and extracellular proteins

(A) H_CT was co-crystallised with the tripeptide, YEW bound in the 'R' site (1YXW). The YEW peptide is highlighted with the ball and stick model (Jayaraman et al., 2005). **(B)** The composition of H_CT carriers in motor neurons. H_CT was coupled to magnetic beads and the endosomes containing this probe were purified using a magnet. The composition of the endosomes was determined by mass spectrometry analysis (Deinhardt et al., 2006b, Wade et al., 2012).

Candidates, in which the putative binding motif was found within the luminal part of the endosomes (topologically equivalent to the extracellular side of the PM) were carried forward and subjected to a series of tests for binding to H_CT. The Peptide Synthesis Service, Cancer Research UK London Research Institute synthesised 9mer peptides containing the YEW motif in the middle with biotin tag at their amino terminal and purified these peptides by high-performance liquid chromatography (HPLC) (Table 12). I then performed a fluorescent binding assay, an enzyme-linked immunosorbent assay (ELISA) and an *in vitro* pull-down assay to test these peptides for H_CT binding.

Table 12. Components of signalling endosomes containing variants of the YEW motif

The peptide sequences are shown on the right, while the unique identifiers are shown on the left. Peptides binding to H_CT in any of the *in vitro* assays (Figure 3-2, Figure 3-3 and Figure 3-4) are in bold, and the N1 (nidogen-1) and N2 (nidogen-2) peptides are in red. The YEW-like motif is underlined.

Peptide	Gene name	Sequence
A	Coxsackievirus and adenovirus receptor homolog	PLQFEWQKL
B	glypican-4	DLDFEWNNF
C	neural cell adhesion molecule 1	VAVYTWEGN
D	**nicastrin**	**SRSFFWNVA**
D_A	nicastrin	SRSFFANVA
D_{AA}	nicastrin	SRSAFANVA
D3	nicastrin	LYEYSWVQG
E	Poliovirus receptor-related protein 2/Nectin-2	PTDYDWSTT
F	msn	KIGFPWSEI
G	sodium/potassium-transporting ATPase subunit a1	ILEYTWLEA
H	sodium/potassium-transporting ATPase subunit a3	ILGYTWLEA
I	V-dependent calcium channel subunit a2/d1	NRTYTWTPV
J	**Vdac3 voltage gated anion channel**	**PTIYGWAVL**
J_{AA}	vdac3 voltage gated anion channel	PTIAGAAVL
K	V-dependent anion-selective channel protein 1	ETKYRWTEY
L	V-dependent anion-selective channel protein 2	ETKYKWCEY
N1	**nidogen-1**	**THIYQWRQT**
$N1_{AA}$	nidogen-1	THIAQARQT
N2	**nidogen-2**	**NQTWSYHID**
$N2_{AA}$	nidogen-2	NQTASAHID
N3	**nidogen-1**	**LVGFLWKSN**
$N3_{AA}$	nidogen-1	LVGALAKSN
N_4	nidogen-1	STGYCWCVD
$ND3_{-1}$	nidogen-2	GGLFGWLFA
$ND3_{-2}$	nidogen-2	STGFCWCVD
$ND3_{-3}$	nidogen-2	KSDFCWCVD
$ND3_{-5}$	nidogen-2	KEFYHYRDS
O	**lysosome membrane protein 2**	**GLIFTWLAC**
P	putative phospholipase B-like 2	CPPFQWSKS
R	St13 Hsc70-interacting protein	AQPYKWRGK
SV2A	SV2A	IPHYGWSFQ
SV2B	SV2B	IPHYGWGFS
SV2C	SV2C	IPHYGWSFS

3.1.1 D, N1 and N3 peptides bind H_CT in a fluorescent binding assay

For the fluorescent binding assay, the peptides were immobilised on the surface of a black 96-well plate and AlexaFluor555-H_CT was added to the wells following blocking with 2% bovine serum albumin (BSA) in tris-buffered saline pH 7.4 (TBS). The wells were washed extensively with TBS and fluorescence intensity was determined, which correlates with the amount of AlexaFluor555-H_CT bound to the peptides. The percentage of maximal binding in 3 experiments was pooled together to get a correct representation of the binding intensity. Peptides D, N1 and N3 bound AlexaFluor555-H_CT with N1 being the only one significantly different from the TBS control; the other peptides did not display any binding (Figure 3-2).

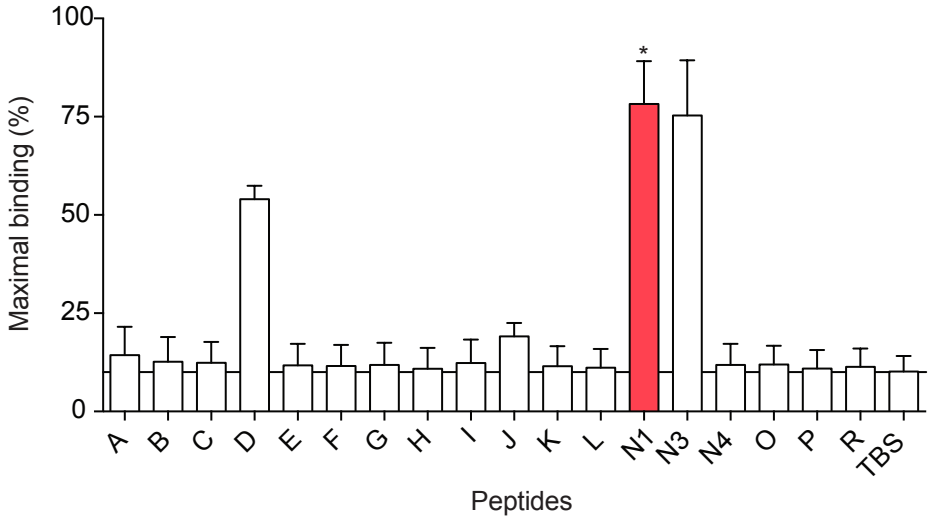

Figure 3-2. Peptides from nicastrin and nidogen-1 bind to H_CT in a fluorescent binding assay

In vitro screen for peptides binding AlexaFluor555-H_CT (see Table 12). In every experiment, the highest value was set at 100% and the results of 3 experiments were pooled together. The data was analysed with Friedman test followed by Dunn's multiple comparisons test against TBS control (n=3; *, $p<0.05$; error bar: SD). Modified from (Bercsenyi et al., 2014). Reprinted with permission from AAAS.

3.1.2 D, J, N1, N3 and O peptides bind H_CT in an *in vitro* pull-down assay

To test whether the peptides can bind H_CT on the surface of beads, we used an *in vitro* pull-down assay. The biotinylated peptides were bound to streptavidin coated agarose bead and blocked with BSA; these were then incubated with VSVG-H_CT (vesicular stomatitis virus glycoprotein tag) on a rotating wheel. Following a series of washes, the beads were lysed and the supernatant was subjected to sodium dodecyl sulphate-polyacrylamide gel electrophoresis (SDS-PAGE) and immunoblotting with anti-VSVG tag antibody (Figure 3-3 A). The intensity of the bands was measured and the percentage of maximal binding in 3 experiments was pooled together to get a correct representation of the binding intensity. The mutant peptide D_A showed equal binding compared to its wild type counterparts, D and D2 (both peptides are the same sequence, for internal control during the screen); while the double alanine substitution of amino acids F and W (D_{AA}) abolished binding. Surprisingly, the J peptide binds VSVG-H_CT the strongest in this assay and the double substitution of amino acids Y and W to A (J_{AA}) blocks this peptide from binding. Both the N1 and N3 peptides bind VSVG-H_CT, but not their double alanine mutants ($N1_{AA}$ and $N3_{AA}$, respectively). The O peptide also emerged as a candidate in this assay, as it pulls down VSVG-H_CT, albeit not significantly more than the empty beads. The peptides from SV2A and SV2C showed a low degree of binding compared with the other peptides (Figure 3-3 B).

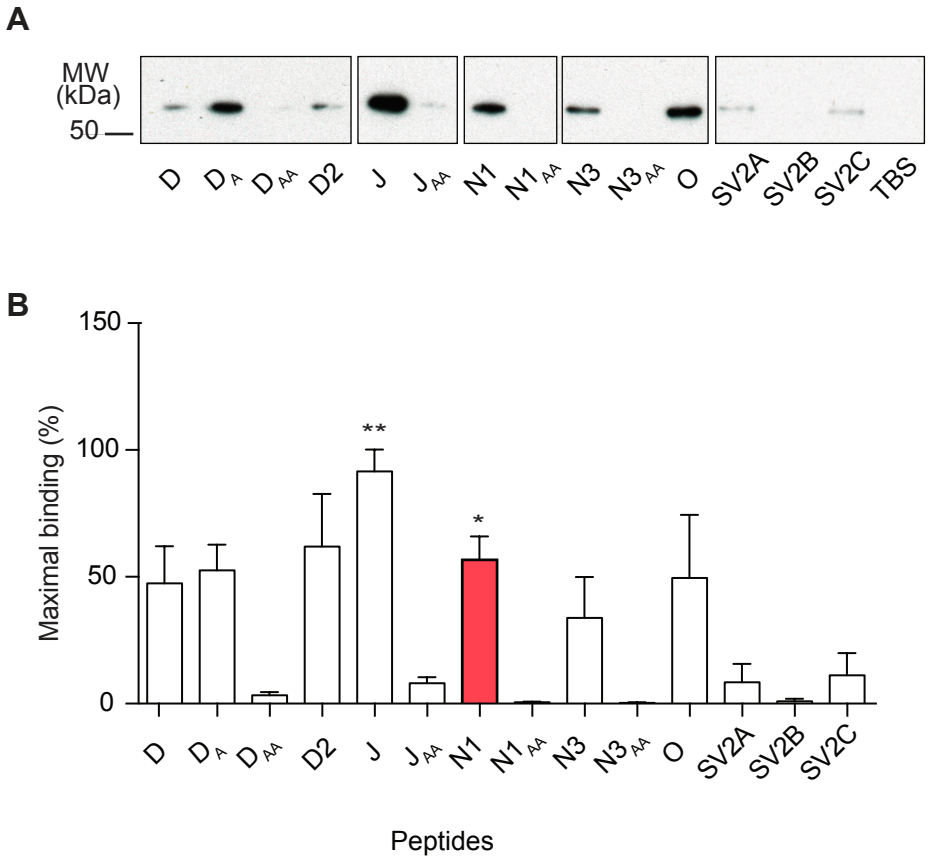

Figure 3-3. The same peptides show strong binding to H_CT in an in vitro pull-down assay as in an the fluorescent binding assay

Selected biotin-tagged peptides containing variants of the YEW motif and their alanine mutants (see Table 12) were bound to streptavidin beads and incubated with recombinant VSVG-tagged H_CT. **(A)** After washing, the captured H_CT was eluted from the beads, subjected to SDS-PAGE and detected by western blotting. One representative experiment is shown. **(B)** Band intensity was determined by densitometry using ImageJ. The results were normalised to empty beads and the maximal value was set at 100% in each experiment. The final results were analysed using paired t-test comparing the peptide bound beads to the empty bead (TBS) control (*n*=3 for wild type peptides, *n*=2 for mutants; *, $p<0.05$, **, $p<0.01$; error bars: SD). Modified from (Bercsenyi et al., 2014). Reprinted with permission from AAAS.

3.1.3 Only the N1 peptide shows specific binding to H_CT in an ELISA

For the ELISA, the peptides were immobilised on the bottom of the wells before adding VSVG-H_CT. Following several washes, VSVG-H_CT was revealed using a mouse antibody against VSVG and an HRP-conjugated goat anti-mouse secondary antibody. I noticed that the anti-VSVG antibody bound unspecifically to some of the peptides, so in control samples VSVG-H_CT was omitted (blank). These

blank values were subtracted from the experimental readings. Among the top candidates, only the N1 peptide showed significant binding to VSVG-H_CT (Figure 3-4).

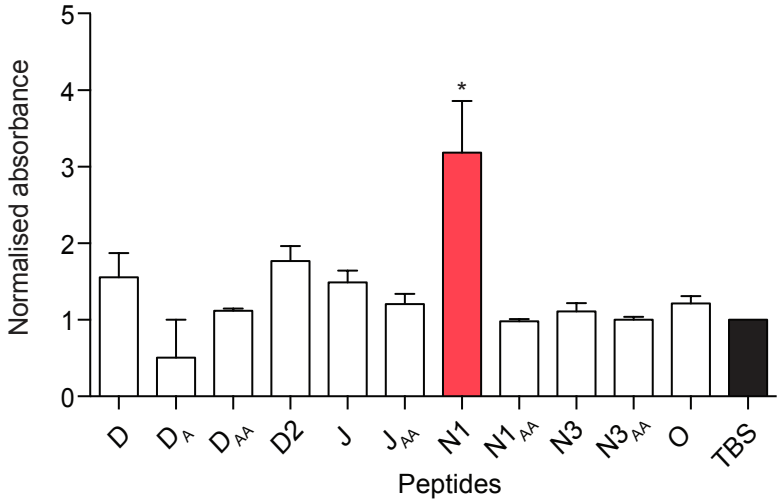

Figure 3-4. The N1 peptide is the top candidate for H_CT binding in ELISA

Selected peptides (see Table 12) were dried on 96-well plates, blocked for non–specific binding and incubated with VSVG-tagged H_CT, which was detected by ELISA at 490 nm using TBS as a control. Results were normalised to samples where H_CT was omitted and analysed for statistical significance using paired t-test (*n*=3; *, $p<0.05$; error bars: SD). Modified from (Bercsenyi et al., 2014). Reprinted with permission from AAAS.

3.2 The N1 and N2 peptides block H_CT binding on primary motor neurons

One of the aims of this study was to find a potential blocking agent to fight tetanus. The N1 peptide originates from nidogen-1 and there are two nidogen isoforms in mammals. There is a very similar peptide to N1 in the corresponding region of nidogen-2, which has an inverted sequence. We included this peptide (N2) in further analyses (Table 12). To determine which peptides were capable of blocking H_CT internalisation in primary motor neurons, the peptides were preincubated with AlexaFluor555-H_CT and the mixture was added to primary motor neuron cultures (DIV 7-10) at 37 °C and after 45 min to allow internalisation. The cells were washed with *Hank's* Balanced Salt Solution (HBSS) then fixed with 4%

paraformaldehyde (PFA) for 15 min at room temperature. The coverslips were mounted in Mowiol and imaged to determine the extent of AlexaFluor555-H_CT internalisation (Figure 3-5). The D peptide caused aggregation of AlexaFluor555-H_CT, while the J and N3 peptides did not have a significant effect on the amount of probe internalised compared to the dimethylsulfoxide (DMSO)-treated control sample. The N1 and N2 peptides both caused a dramatic decrease in the internalised pool of AlexaFluor555-H_CT, while the double alanine mutant of N1 ($N1_{AA}$) did not have any effect. The finding that both peptides from the same regions of nidogens block H_CT internalisation in motor neurons suggests that both nidogen-1 and -2 could potentially act as protein receptors for TeNT at the NMJ.

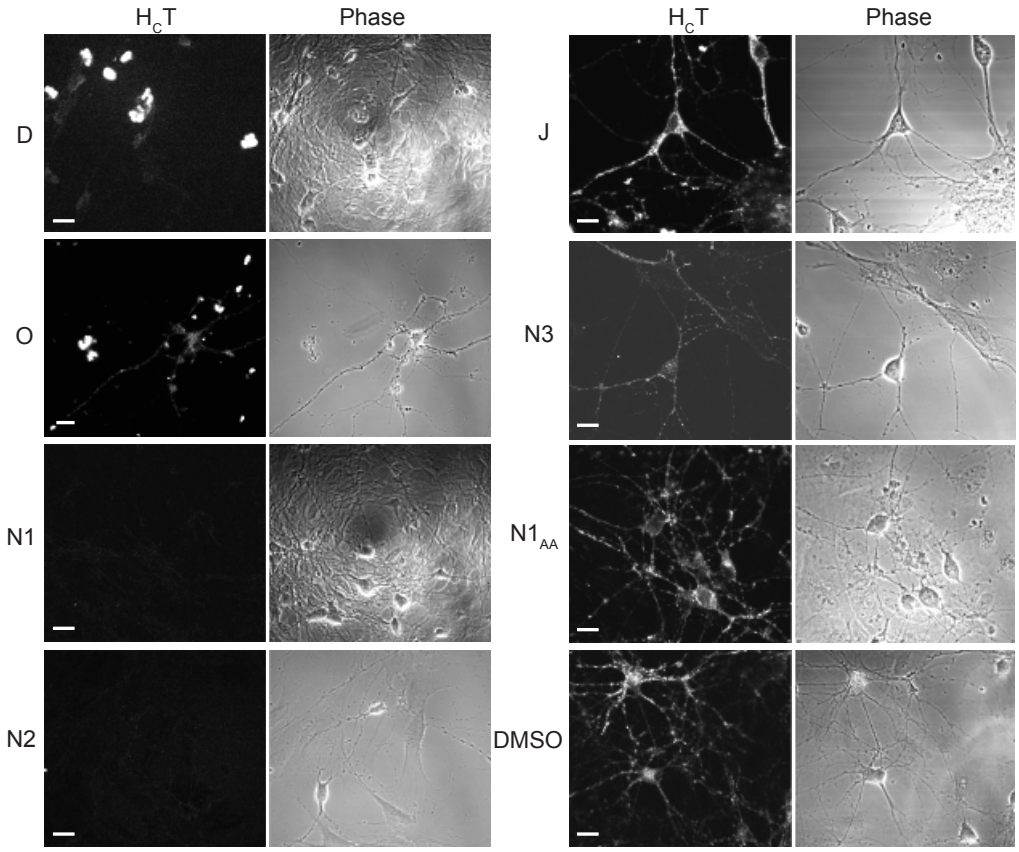

Figure 3-5. The N1 and N2 peptides block H_CT internalisation on primary motor neurons

AlexaFluor555-H_CT was preincubated with peptides D, J, O, N3, N1, $N1_{AA}$ and N2, or vehicle control (DMSO) and it was added to primary motor neurons at 37°C for 45 minutes. The cells were acid washed on ice, then fixed and imaged on a confocal microscope. Scale bar: D, N1, $N1_{AA}$, N2, DMSO: 20 µm; J, O, N3: 10 µm. From (Bercsenyi et al., 2014). Reprinted with permission from AAAS.

3.3 Biomolecular analysis of the interaction between H_CT and the N peptides

3.3.1 Peptide array – an attempt to identify a synthetic peptide with the highest possible affinity for TeNT

To determine the specificity of the nidogen-binding motif, we designed a peptide array, where the four key residues in both the N1 and N2 peptides (YEWR and TWSY, respectively, Table 12) were modified with single substitution to all 20 natural amino acids. Dhira Joshi in the Peptide Synthesis Service, Cancer Research UK London Research Institute prepared the array. I incubated the array with AlexaFluor555-H_CT for 1 h at room temperature. After several washes with TBS, a Typhoon gel reader was used to measure the amount of AlexaFluor555-HCT bound to the peptide spots.

Unfortunately there was a huge variability between the peptide content of each spot and this made the assay non-quantitative and hard to reproduce. Due to these limitations we could only conclude that the R residue within the N1 peptide can solely be replaced by a K and no other amino acids to retain its binding ability (Figure 3-6 C). Since all four residues are highly conserved among all species with known sensitivity to tetanus, we could not contemplate on the potential effect of this substitution *in vivo* (Figure 3-6 A, Table 13).

We also noted that if the W residue in the N2 peptide is replaced with an R or a Q, the peptide loses its binding ability (Figure 3-6 D). When comparing the amino acid sequence of the corresponding region in nidogen-2 in species with known sensitivity to tetanus, we found that in *Rattus norvegicus* (rat) this residue is replaced with an R, making the protein potentially unable to bind TeNT (Figure 3-6 B, Table 14). This could explain why rats are partially insensitive to tetanus intoxication (Rozanova, 1964).

Table 13. Sequence conservation of the N1 peptide region of nidogen-1 among species with known sensitivity to tetanus

The last 6 residues, including the 4 key residues (YQWR) are highly conserved among vertebrates. Substitutions compared to the mouse sequence are highlighted in red.

Mus Musculus	**Mouse**	T	H	I	Y	Q	W	R	Q	T
Rattus norvegicus	**Rat**	T	H	I	Y	Q	W	R	Q	T
Cricetulus griseus	Chinese hamster	T	H	I	Y	Q	W	R	Q	T
Homo sapiens	**Human**	I	Y	T	Y	Q	W	R	Q	T
Pongo abelii	Orangutan	I	Y	T	Y	Q	W	R	Q	T
Pan troglodytes	Chimpanzee	I	Y	T	Y	Q	W	R	Q	T
Callithrix jacchus	Marmoset	I	Y	T	Y	Q	W	R	Q	T
Nomascus leucogenys	Gibbon	V	Y	T	Y	Q	W	R	Q	T
Sus scrofa	Wild Boar	V	H	I	Y	Q	W	R	Q	T
Heterocephalus glaber	Mole rat	T	Y	T	Y	Q	W	R	Q	T
Meleagris gallopavo	Turkey	T	G	A	Y	Q	W	R	Q	T
Canis lupus	Dog	I	Y	T	Y	Q	W	R	Q	T

Table 14. Sequence conservation of the N2 peptide region of nidogen-2 among species with known sensitivity to tetanus

Substitutions are highlighted in red. The 4 middle residues (WSYH) are less conserved among vertebrates than those of nidogen-1. The substitution of W to R or Q (highlighted in blue) lead to a potential loss of binding between nidogen-2 and TeNT and this might explain the low sensitivity of these species to tetanus intoxication.

Mus Musculus	**Mouse**	N	Q	T	W	S	Y	H	I	D	Q
Rattus norvegicus	**Rat**	N	Q	T	**R**	S	Y	R	I	D	Q
Cricetulus griseus	Chinese hamster	N	Q	T	W	S	Y	H	I	D	Q
Homo sapiens	**Human**	N	Q	T	W	S	Y	H	I	H	Q
Pongo abelii	Orangutan	N	Q	T	W	S	Y	H	I	H	Q
Pan troglodytes	Chimpanzee	N	Q	T	W	S	Y	H	I	H	Q
Callithrix jacchus	Marmoset	N	Q	T	W	S	Y	R	V	H	Q
Nomascus leucogenys	Gibbon	N	Q	T	W	S	Y	R	I	H	Q
Bos taurus	Bull	N	Q	T	**Q**	T	Y	R	I	H	Q
Sus scrofa	Wild boar	N	Q	T	R	S	Y	S	I	H	Q
Heterocephalus glaber	Mole rat	N	Q	T	G	S	Y	R	V	H	Q
Meleagris gallopavo	Turkey	N	Q	T	L	S	Y	R	L	H	Q
Canis lupus	Dog	N	Q	T	R	S	Y	R	I	Y	Q

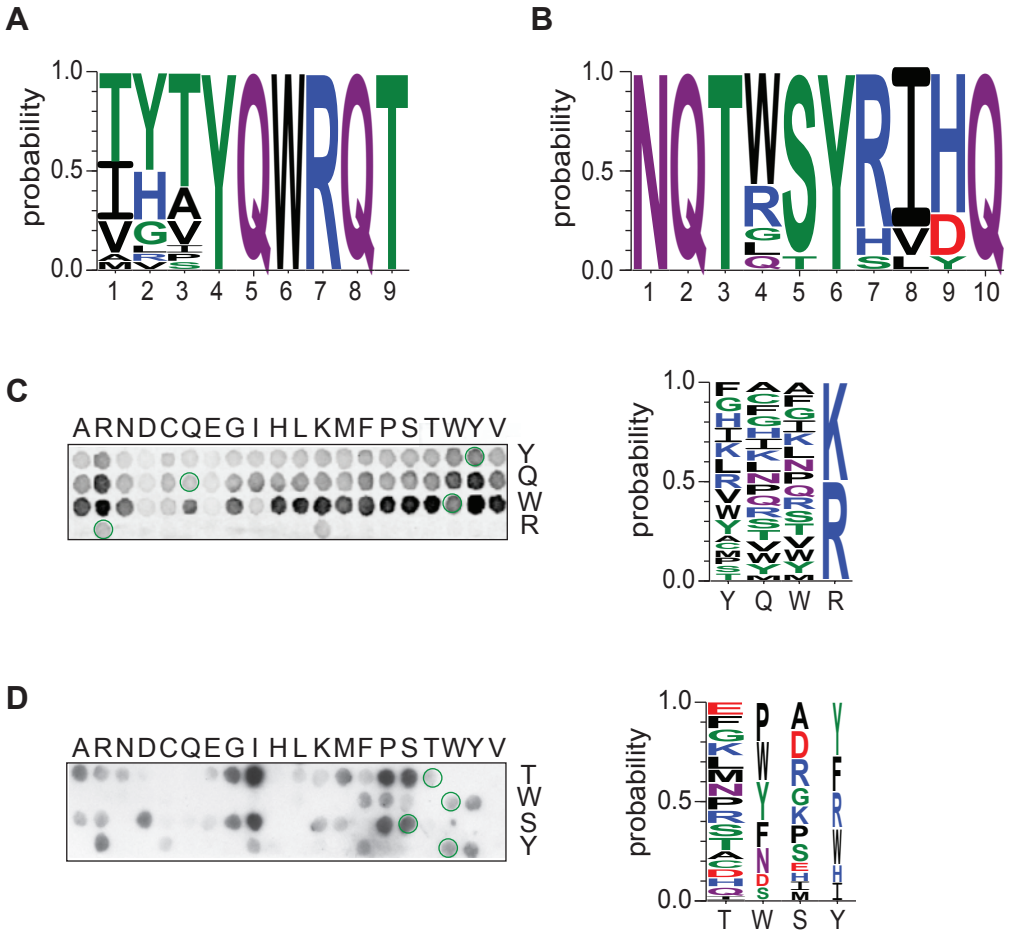

Figure 3-6. Peptide array to refine the binding motif of the N1 and N2 peptides

(A,B) We analysed the sequence of the corresponding region of nidogen-1 in a variety of species. **(A)** The last six amino acids, including the three key residues of the N1 peptide (YQW) are conserved from fish to humans. **(B)** Nidogen-2 is less conserved in the putative binding region (TWSY) than nidogen-1, the W is substituted with four different amino acids, S can be replaced with a T and the Y is highly conserved. **(C)** Representative result of a peptide array on the N1 peptide. The weblogo diagram shows the probability of a certain residue to be present at the given position and still bind H_CT. R in position 7 can only be substituted with a K, this residue must play a key role in H_CT binding (n=3 experiments, all the positive peptides were represented in the weblogo diagram). The double alanine mutant (AQAR) does not bind H_CT in this assay (data not shown), which is expected based on the results of the previous binding assays. **(D)** Representative result of a peptide array on the N2 peptide. Due to the variability between experiments, none of the residues appear to be irreplaceable without affecting H_CT binding. However, W cannot be replaced by a Q or R, which are present in this position in nidogen-2 in cows and rats.

Despite the high conservation within this region of nidogens, there are subtle differences between the human and murine sequences, so we also tested if the human peptides bind H_CT. Based on the fluorescent binding assay, the human

versions of both N1 and N2 (hN1 and hN2, respectively) bind H_CT, but significantly less than their murine counterparts (Figure 3-7)

To further elucidate the importance of each residue within the murine peptides in a more quantitative manner, single alanine mutants of the 3 residues forming the YEW-like motif and the flanking residues, R (N1) and H (N2) were synthesised. Binding was assessed using the fluorescent binding assay as before (Figure 3-2). The double alanine mutants of both the N1 and N2 peptides ($N1_{AA}$, $N2_{AA}$, respectively) show no binding to H_CT. Single alanine substitution of the W in both peptides (N1WA, N2WA) completely abolished H_CT binding, while alanine substitution of the other residues caused a smaller, yet significant decrease (Figure 3-7 B). The effect of alanine substitution of W is in agreement with the peptide array for N2, but it is different for N1.

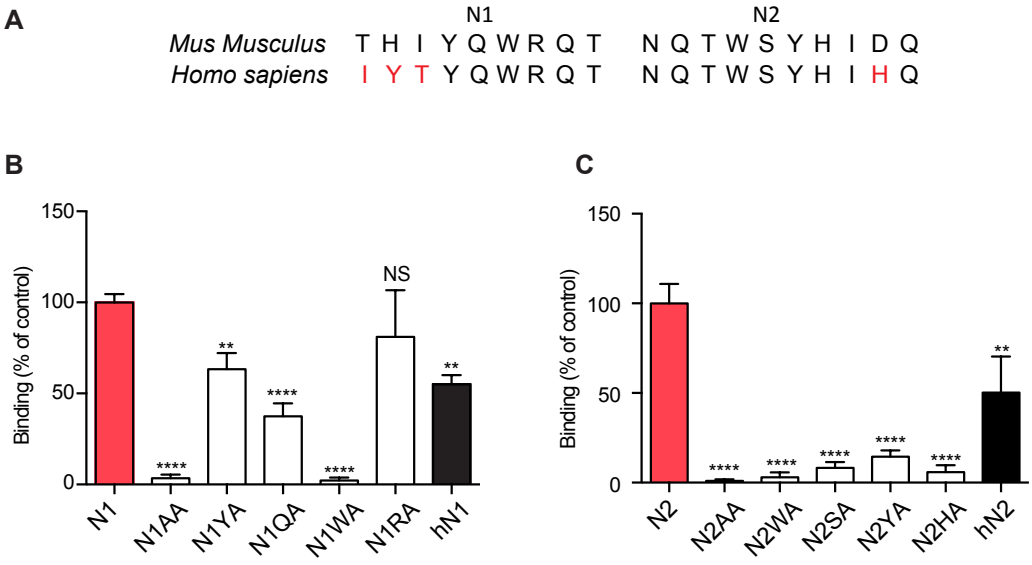

Figure 3-7. Single alanine mutants of the N1 and N2 peptides bind H_CT less than their wild type counterparts

(A) There is a high level of conservation between human and murine nidogens, but the first three residues of the N1 peptide are replaced with IYT in humans, while there is a DH substitution in N2, which is predicted to bind H_CT with less efficiency based on Figure 3-6 A. **(B)** The double alanine mutant ($N1_{AA}$) and the single alanine mutant (N1WA) do not bind H_CT, while other alanine substitutions show a varied degree of decrease in H_CT binding compared to the N1 peptide. The human N1 peptide (hN1) binds H_CT, but less efficiently than the murine N1 peptide (N1). **(C)** The single alanine mutants of N2 bind significantly less H_CT than N2. The human N2 peptide (hN2) binds H_CT but with a lower affinity than the murine N2. Repeated measures one-way ANOVA (****, $p<0.001$), followed by Dunnett's multiple comparisons test against the wild type murine peptides was used to assess significance (n=2, **, $p<0.01$; ****, $p<0.001$, error bars: SD). From (Bercsenyi et al., 2014). Reprinted with permission from AAAS.

3.3.2 Biomolecular modelling reveals the docking site of the N1 peptide

Next, to test whether it is possible to saturate the interaction between the N1 peptide and H_CT, I performed a titration fluorescent assay, where AlexaFluor555-H_CT was incubated with immobilised peptides at increasing molar ratio (Figure 3-8 A). The YEW peptide, which was previously co-crystallised with H_CT (Jayaraman et al., 2005), was used as a positive control (Figure 3-8 A, blue line). The N1 peptide displayed a stronger binding (Figure 3-8 A, red line) than the YEW peptide, which indicated that its affinity to H_CT must be high enough to allow co-crystallisation. However, the H_CT-YEW co-crystal was obtained at pH 5, hence N1 interaction must be preserved at low pH to allow co-crystallisation. To test this, the incubation was run at pH 5 (Figure 3-8 A, yellow line), which simulated the conditions used for crystallisation. Unfortunately the binding between H_CT and N1 appeared to be highly sensitive to changes in pH. This might be a physiological property of this complex and be required during tetanus intoxication; in particular, the acidic pH triggers the insertion of the N terminal part of the heavy chain into the endosomal membrane and the translocation of the L chain into the cytosol. In contrast to N1, the $N1_{AA}$ peptide does not bind to H_CT in this assay, further proving the importance of the Y and W residues in this interaction (Figure 3-8 A, orange line).

We made a number of attempts at determining the Kd between the N1 peptide and H_CT but the results were inconclusive. In our hands, the most reliable approach was isothermal calorimetry (ITC), in which the N1 peptide solution (150 μM) was injected into a bath of H_CT (15 μM) and the thermal changes occurring during the interaction were measured under these experimental conditions at 37°C (Figure 3-8 D). The reaction was found to be exothermic with an estimated Kd of 7.4±0.11 μM. This is surprisingly low considering the results of previous binding experiments. The H_CT solution was tested for the presence of dimers with dynamic light scattering (DLS, data not shown) and it was mainly monomeric. Based on this analysis there is only one binding site for the N1 peptide on H_CT, which is in agreement with the results of biomolecular modelling.

Following unsuccessful attempts at the crystallisation of the complex, we turned to biomolecular modelling to gain deeper insights on the molecular details of binding. G. Zanotti (University of Padua) performed this analysis, which revealed that the N1 peptide is able to dock to the ‘R’ site of H_CT, where sialic acid,

disialyllactose and the tri-peptide YEW, bind (Jayaraman et al., 2005). The surface concealed by the formation of the N1 peptide-H_CT complex is predicted to be 518 $Å^2$ for the H_CT domain and 592 $Å^2$ for the N1 peptide (Figure 3-8 C). This site is located on the opposite side of the main binding domain for polysialogangliosides, which have an established role as clostridial neurotoxin co-receptors (Binz and Rummel, 2009), thus it should not interfere with ganglioside binding. The molecular surface predicted to be concealed by the N1 peptide-H_CT complex constitutes more than 40% of the total peptide surface (Figure 3-8 C), suggesting that this interaction, which is driven by the potential formation of five hydrogen bonds and other polar interactions (Table 15) is very strong.

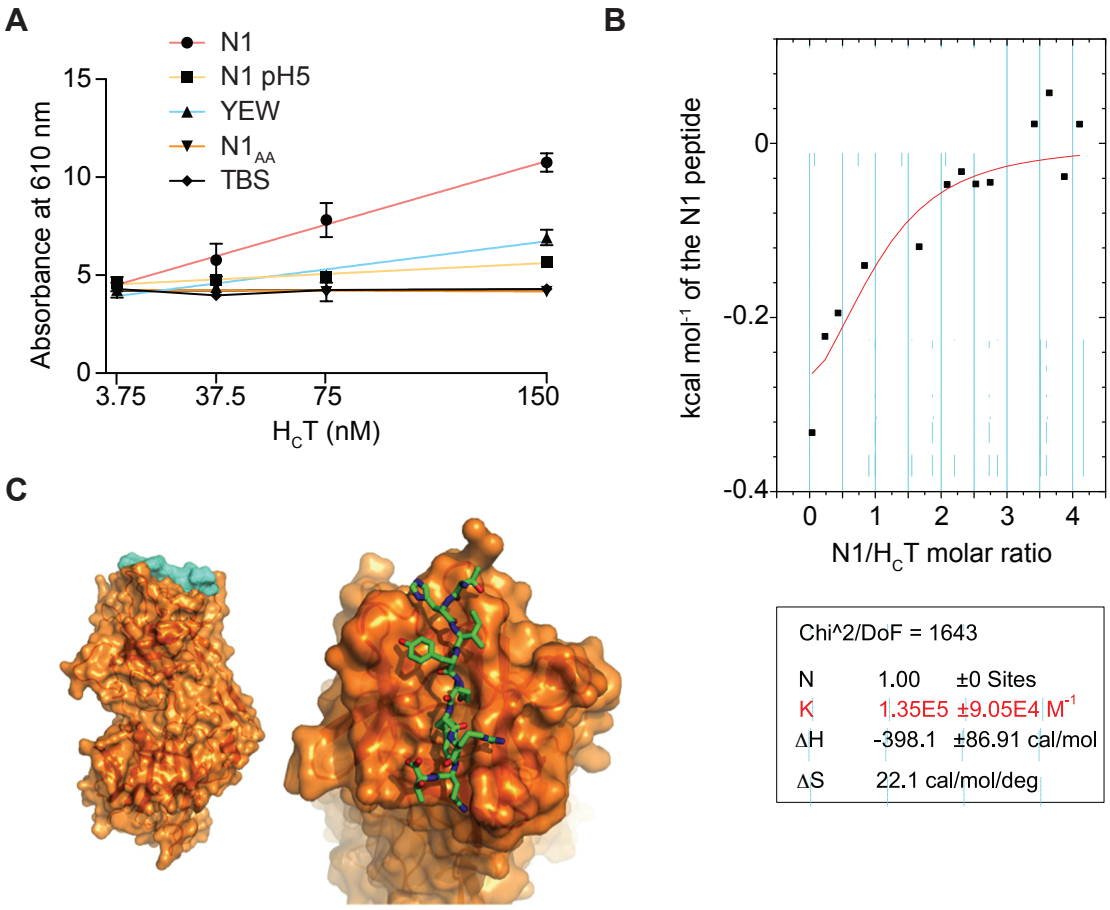

Figure 3-8. Molecular modelling of the interaction between the N1 peptide bound to H_CT

(A) Binding assay of fluorescent H_CT to immobilised peptides. The pH of the incubation buffer was changed to pH 5 (yellow line) to test if the binding between the N1 peptide and H_CT is pH sensitive. **(B)** Polynomial regression analysis on an isothermal calorimetry recording where the N1 peptide was injected into the sample cell containing H_CT. The Kd is estimated to be 7.4±0.11 μM with one binding site on H_CT. **(C)** Details of the crystal structure of H_CT (orange) bound to peptide N1 (green, stick model; PDB code 1XYW (Jayaraman et al., 2005)). The N1 peptide was built using Coot, the glutamic acid of the YEW sequence present in the PDB structure 1XYW (Jayaraman et al., 2005) was replaced with a glutamine; the remaining residues (THI---RQT) were manually built and adjusted inside the crevice of the toxin. The modelling was performed by G. Zanotti (University of Padova). From (Bercsenyi et al., 2014). Reprinted with permission from AAAS.

Table 15. Potential hydrogen bonds and other polar interactions between H_CT (A) and the N1 peptide from nidogen-1 (P)

The predicted distance between the interacting residues is indicated. Distances must be considered as indicative, since they are based on a theoretical model. Contacts and concealed surfaces were calculated with server PISA (http://www.ebi.ac.uk). These calculation are based on the model shown in Figure 3-8 were performed by G. Zanotti (University of Padova). From (Bercsenyi et al., 2014). Reprinted with permission from AAAS.

Bond	H_CT	Distance (Å)	nidogen-1 (N1 peptide)
H-bond			
1	A:ASP1214[OD2]	2.81	P:THR1[OG1]
2	A:ARG1226[NE]	3.47	P:GLN5[OE1]
3	A:LYS1143[NZ]	2.91	P:GLN8[OE1]
4	A:LYS1143[NZ]	3.22	P:GLN8[O]
5	A:ASP1278[OD1]	3.08	P:GLN8[NE2]
Polar			
6	A:ILE1224[O]	Via a water molecule	P:GLN5[OE1]
7	A:LYS1213[O]	Via a water molecule	P:ILE3[O]
8	A:GLY1233[O]	3.15	P:HIS2[ND1]

3.4 The N1 peptide blocks H_CT uptake *in situ*

To test whether the N1 peptide can significantly block H_CT binding, the cells were cooled on ice before adding AlexaFluor555-H_CT for 10 min. Because this temperature does not allow internalisation, AlexaFluor555-H_CT decorates the membrane, but it is not taken up by the neurons. Following washes with HBSS and fixing with 4% paraformaldehyde (PFA) for 15 min at room temperature, the cells were permeabilised using phosphate buffered saline (PBS) containing 0.01% Triton-X for 10 min at room temperature. To avoid non-specific staining from the antibodies, the cells were blocked with 5% bovine serum albumin (BSA) in PBS (immunofluorescence blocking buffer, IFBB) for 1 h at room temperature and stained for βIII tubulin, a specific marker of neuronal microtubules, prior to imaging. A mouse anti-βIII tubulin was added to cells in IFBB for 1 h at room temperature. The excess of primary antibody was washed off with multiple rounds of PBS washes before adding goat AlexaFluor488-anti-mouse secondary antibody to reveal the βIII tubulin staining. Unbound secondary antibody were removed with PBS washes and the coverslips were mounted in Mowiol. βIII tubulin staining was used as a mask in Cell Profiler to identify neurons and the fluorescence intensity of AlexaFluor555-H_CT was measured. The N1 peptide significantly blocked H_CT binding, while its alanine mutant ($N1_{AA}$), did not have a significant effect (Figure 3-9). The N1 peptide does not only bind to H_CT, but it is able to block its interaction with its cell surface receptor(s).

Next, I wanted to test whether the N1 peptide can interfere with H_CT internalisation. AlexaFluor555-H_CT was incubated on primary motor neurons and DMSO, the N1 or the $N1_{AA}$ peptide was added either together with the probe or with a delay of 10 min. The experiment was performed at 37°C for 45 min, which allows the internalisation of H_CT. The presence of the N1 peptide decreases H_CT internalisation in the absence of preincubation (Figure 3-10), and even when it is added with a 10 min delay (Figure 3-11). These results indicate that the peptide successfully competes with the endogenous receptor(s) of H_CT and stops it from entering motor neurons.

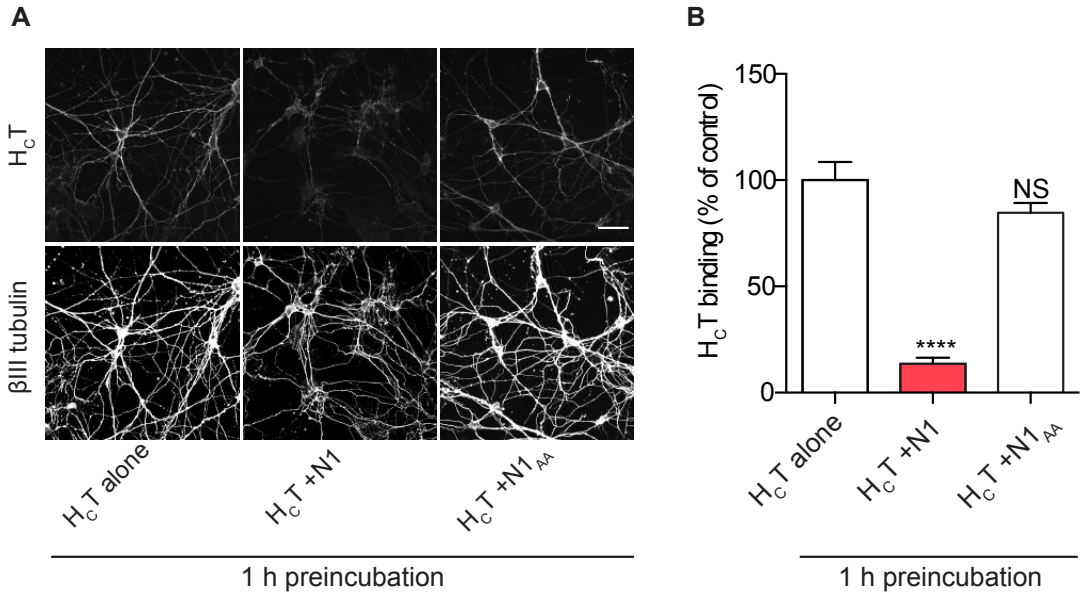

Figure 3-9. The N1 peptide significantly blocks H_CT binding on primary motor neurons

(A) AlexaFluor555-H_CT was preincubated with DMSO (vehicle control, H_CT alone) or wild type and mutant N1 peptides for 1 h at room temperature and added to primary motor neurons on ice before staining for βIII tubulin and confocal imaging. **(B)** Twenty images were taken for each condition and fluorescence intensity of AlexaFluor555-H_CT bound to neurons (βIII tubulin mask) was quantified. Results were tested for statistical significance using one-way ANOVA (****, $p<0.001$) followed by Dunnett's multiple comparisons test (*n*=3; NS, non significant; ****, $p<0.001$; error bar: SEM). Scale bar, 40 µm. Modified from (Bercsenyi et al., 2014). Reprinted with permission from AAAS.

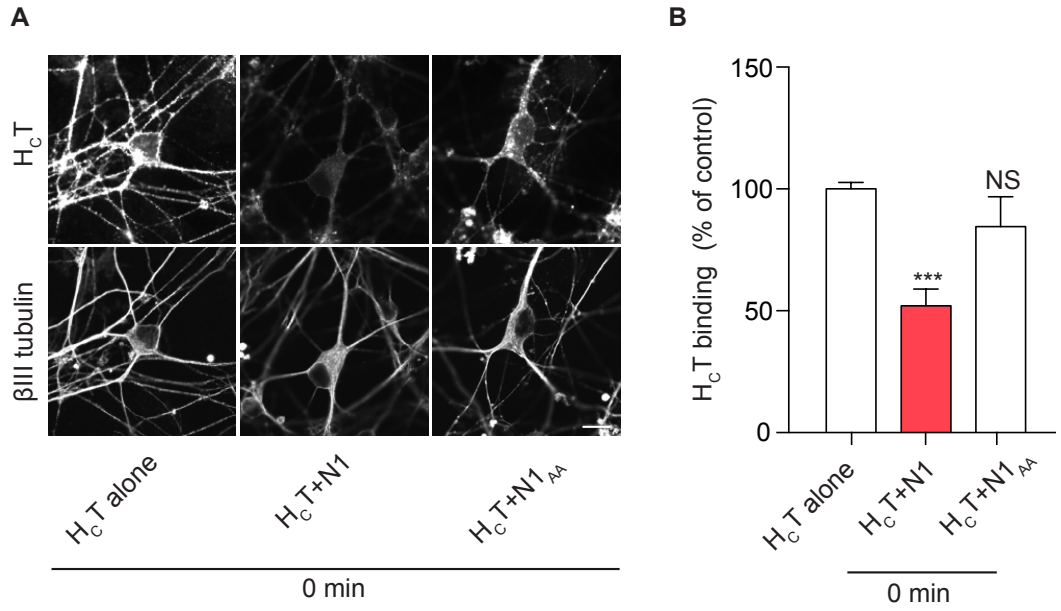

Figure 3-10. The N1 peptide blocks H_CT entry into motor neurons when added simultaneously to the medium

(A) AlexaFluor555-H_CT was added to primary motor neurons before adding DMSO (vehicle control; H_CT alone), N1 or $N1_{AA}$ peptides to the medium for 45 min at 37°C. The cells were then washed and stained for βIII tubulin and imaged on a confocal microscope. **(B)** Three tile scans of 16 images were taken for every condition, and fluorescence intensity of AlexaFluor555-H_CT internalised in neurons (βIII tubulin mask) was quantified. Results were tested for statistical significance using one-way ANOVA (***, $p<0.005$) followed by Dunnett's multiple comparisons test. (*n*=3; NS, non significant; ***, $p<0.005$; error bar: SD). Scale bar, 10 µm. Modified from (Bercsenyi et al., 2014). Reprinted with permission from AAAS.

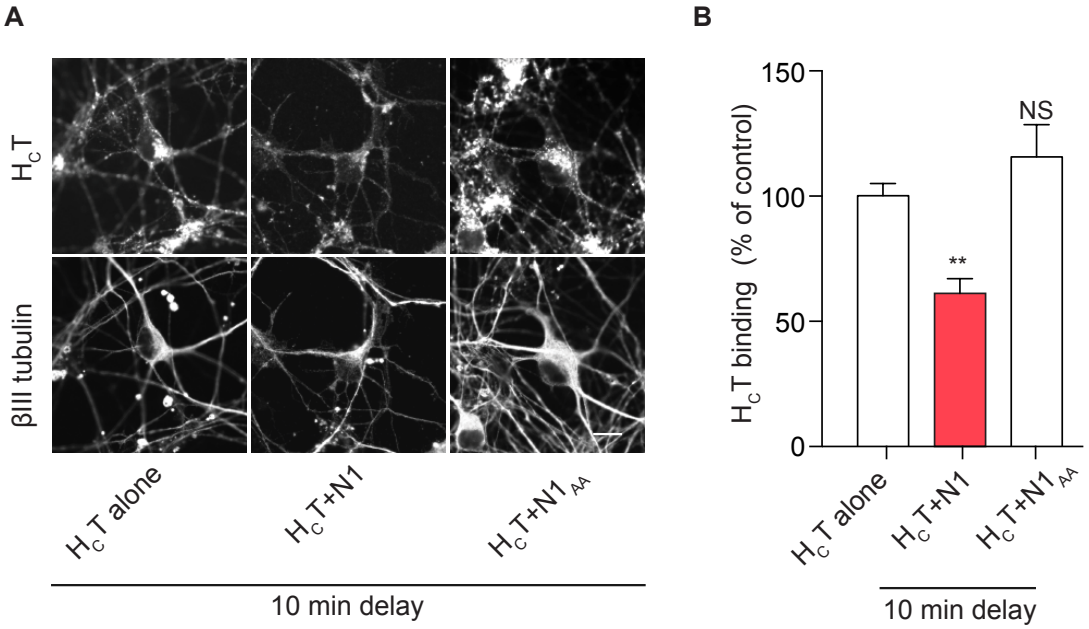

Figure 3-11. The N1 peptide blocks H_CT entry into motor neurons when added to the medium with a 10 min delay

(A) AlexaFluor555-H_CT was added to primary motor neurons before adding vehicle control (H_CT alone), wild type or mutant N1 peptides with a delay of 10 min. The total length of the incubation was 45 min at 37°C. The cells were then washed and stained for βIII tubulin and imaged on a confocal microscope. **(B)** Three tile scans of 16 images were taken for every condition, and fluorescence intensity of AlexaFluor555-H_CT internalised in neurons (βIII tubulin mask) was quantified. Results were tested for statistical significance using one-way ANOVA (***, $p<0.005$) followed by Dunnett's multiple comparisons test. (n=3; NS, non significant; **, $p<0.001$; error bar: SD). Scale bar, 10 µm. Modified from (Bercsenyi et al., 2014). Reprinted with permission from AAAS.

3.5 The N1 peptide is a potent inhibitor of tetanic paralysis *in vivo*

3.5.1 The N1 peptide blocks H_CT binding at the NMJ

Next, I wanted to test if the N1 peptide was capable of blocking H_CT from binding to the NMJ. To do this, I isolated *levator auris longus* (LAL) muscles from wild type adult mice. These muscles are extremely thin (only a couple of cell layers) and can be incubated with H_CT in a motor neuron medium bath without sectioning. However, due to the lack of transcardial perfusion, the strong autofluorescence of haemoglobin makes imaging more challenging (Figure 3-12).

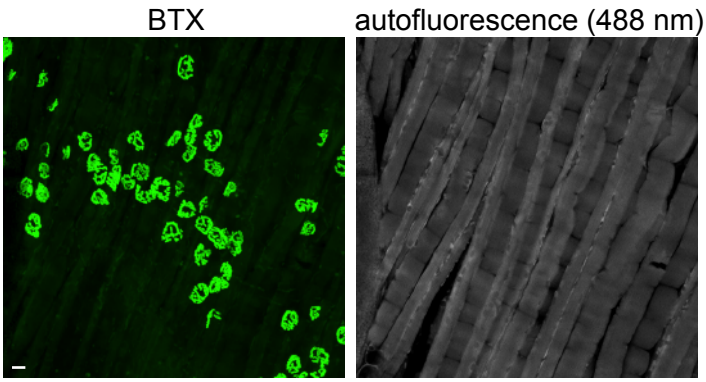

Figure 3-12. BTX labels NMJs in the LAL muscle

Levator auris longus (LAL) muscles of adult mice were dissected, fixed and stained with AlexaFluor555-BTX (pseudocolored in green) to label NMJs. Due to the lack of transcardial perfusion, there is a high background in the 488 channel (autofluorescence). Scale bar: 10 µm.

The muscles were incubated with HA-H_CT, which was preincubated either with DMSO (H_CT alone), N1 or $N1_{AA}$, washed, fixed and stained for HA with a rat anti-HA primary antibody followed by a donkey AlexaFluor488-anti rat secondary antibody and AlexaFluor555-α-Bungarotoxin (BTX) to label the NMJs. There is a big variability among NMJs in their H_CT binding ability (63.6±6.0% SEM bind H_CT), but preincubation with the N1 peptide significantly reduces the ratio of H_CT positive NMJs (14.3±4.7% SEM, Figure 3-13).

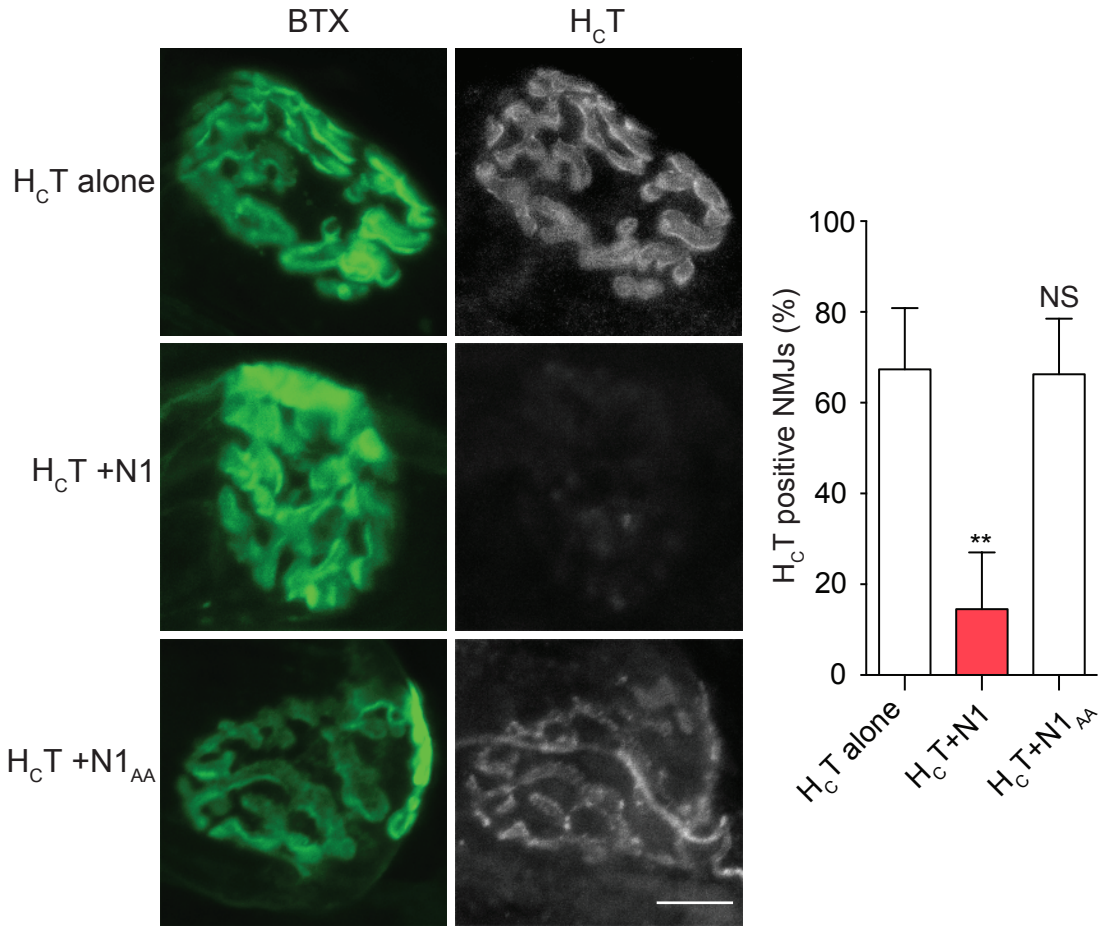

Figure 3-13. The N1 peptide significantly blocks H_CT binding at the NMJ

LAL muscles were incubated with H_CT pretreated with DMSO (H_CT alone), N1 or $N1_{AA}$. Samples were then washed, fixed and counterstained with AlexaFluor555-α-BTX (pseudocolored in green) and a rat monoclonal antibody against HA (pseudocolored in grey). Low magnification images were taken and the number of H_CT positive vs. H_CT negative NMJs was determined. The results were plotted and tested for significance by Kruskal-Wallis test (**, $p<0.001$) followed by Dunn's multiple comparisons test. (NS, non significant; ****, $p<0.001$; n=3 experiments, >100 NMJs per condition). Scale bar: 10 µm. Modified from (Bercsenyi et al., 2014). Reprinted with permission from AAAS.

3.5.2 The N1 peptide blocks tetanic paralysis on hemidiaphragm preparations

Mouse phrenic nerve-hemidiaphragm (HD) preparations were extensively used in the field to test the action of TeNT and BoNTs and it is considered as a reliable alternative to *in vivo* mouse experiments. To test the effect of the N1 peptide preincubation on the toxicity of TeNT, two HD preparations were isolated

from mice; one was submersed in Ringer solution containing TeNT (5 nM) preincubated with DMSO, the other was submersed in Ringer solution containing TeNT preincubated with the N1 or the N2 peptide, which were previously dissolved in DMSO. The phrenic nerve was stimulated with supramaximal stimuli and muscle contraction was monitored with an isometric transducer. Muscular twitch was monitored until complete paralysis and the time required to decrease the twitch to 50% of the initial value (paralytic half-time) was recorded. P. Caccin (University of Padova) performed the experiment. The N1 peptide increased the time for achieving complete paralysis, while the N2 peptide appeared to have the opposite effect (Figure 3-14). These differences were not significant. It has to be noted however, that this is not the most reliable assay to assess TeNT activity, since it is based on local TeNT-mediated paralysis (NMJ based), which occurs independently of the physiologically targeted interneurons. When used at high doses, the normal entry and transport pathway of TeNT is over-saturated and the toxin enters via an alternative route, enabling it to cleave synaptobrevin (VAMP2) at the NMJ. This in turn leads to the silencing of the motor neuron and the subsequent paralysis of the muscle.

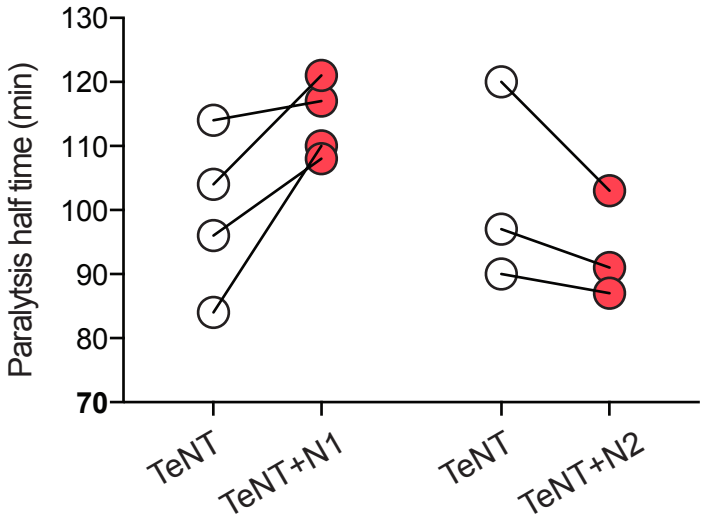

Figure 3-14. The N1 peptide prolongs tetanic paralysis half time, while the N2 peptide has a mild acceleration effect.

TeNT preincubated with vehicle control (DMSO), or the indicated peptides was added to HD preparation in Krebs-Ringer solution at 37°C. Muscle twitch was induced by nerve stimulation and paralysis times were monitored. Data is expressed as paralysis half time and reported as paired observations (*n*=4). Modified from (Bercsenyi et al., 2014). Reprinted with permission from AAAS.

3.5.3 Treatment of native TeNT with the N1 peptide prior injection prevents the appearance of tetanic paralysis in the *triceps surae* muscle

Since the N1 peptide is capable of blocking H_CT binding at the NMJ as well as on primary motor neurons, we wanted to test if the pre-treatment of native TeNT with the N1 peptide was sufficient to block its entry into motor neurons and the following tetanic paralysis. Age- and weight-matched adult C57Bl6 mice were injected with the sub-lethal dose of 1 or 2 ng/kg TeNT (8 µl total volume per 20 g body mass) in the right *triceps surae* muscle. Prior to the injection, TeNT was incubated with DMSO, the N1 or the $N1_{AA}$ peptide. The administration of this dose causes local tetanus, which leads to coordination defects at an early stage of the pathology (Figure 3-15) followed by spastic paralysis of the injected hindlimb (Figure 3-16). To assess the coordination defects of these mice in a quantitative manner, I used the footprint assay (Carter et al., 1999). The experiment was performed with the help of Francesco Giribaldi (Molecular Neuropathobiology Laboratory). The paw of the injected hindlimb was painted red, while all the other paws were painted black. Mice were then allowed to walk along a white stripe of

paper (Figure 3-15 A,B). When mice walk, the hind paw is always placed very close (d≃0.5 cm) to the position of the front paw during the previous step. This distance increases when the mice display coordination defects. The coordination of mice in groups TeNT+DMSO and TeNT+$N1_{AA}$ at 24 h post-injection was significantly worse than the non-injected group (control), when 2 ng/kg dose of TeNT was used. In contrast, the TeNT+N1 peptide group showed no significant change in coordination at this time point (Figure 3-15 C). Pre-treatment of TeNT with the N1 peptide prevented tetanic paralysis at both doses.

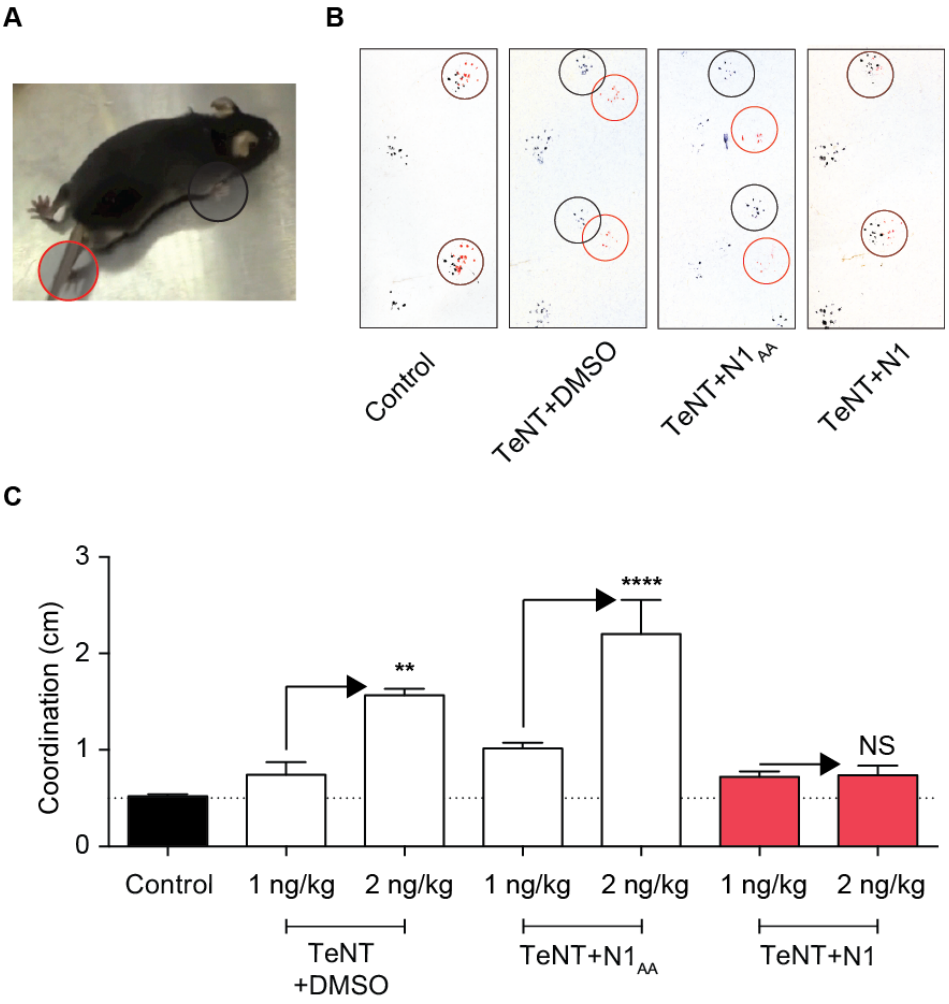

Figure 3-15. Preincubation with the N1 peptide prevents the coordination defects observed in mice injected with TeNT

The right triceps surae muscle was injected with either 1 or 2 ng/kg of TeNT, following preincubation with DMSO as a vehicle control, $N1_{AA}$ or N1 peptide. (A) 24 h after injection, a footprint analysis was performed where the paw of the injected leg was painted red, while all the other paws were painted black. (B) Mice were let to walk on a white stripe of paper, and the coordination (distance between the prints on the same side) was measured (red circle: hind paw, black circle: front paw, only the group, which received a 2ng/kg dose is shown). (C) Data were analysed using one-way ANOVA followed by Dunnett's multiple comparisons test to compare the groups to the control value. Following termination, triceps surae muscles were dissected and weighed to determine whether the administered dose based on total body weight was in accordance with the dose/mg muscle. (*n*=2; NS, non significant; **, $p<0.01$; ****, $p<0.001$; error bar: SD). Modified from (Bercsenyi et al., 2014). Reprinted with permission from AAAS.

Pictures were taken of the mice at 48 h post-injection. Strikingly, the N1 peptide treated group did not show any symptoms of local tetanus. The injected leg of the DMSO and $N1_{AA}$ treated groups was completely paralysed at this time point; they were not able to grip the cage and moved around slowly and with great difficulty. In contrast to the other two groups, these mice were able display the grip-reflex, did not extend their right hindlimb and they showed no delay in exploring the environment once they set free outside the cage (Figure 3-16, Movie 1).

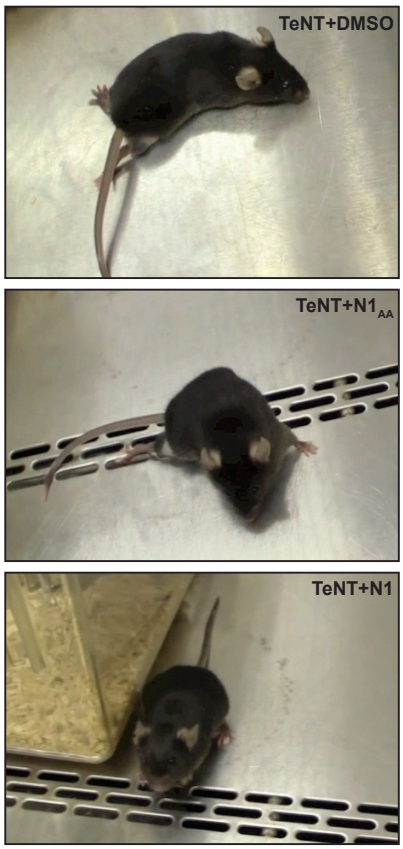

Figure 3-16. Posture of mice injected with TeNT preincubated with DMSO control, $N1_{AA}$ or the N1 peptide

The *triceps surae* muscle was injected with 2 ng/kg TeNT intramuscularly and mice were photographed 48 h later. Both the DMSO and $N1_{AA}$ treated group showed severe local paralysis, while the N1 treated group appeared normal.

3.5.4 Treatment of native TeNT with the N1 peptide prior injection prevents the physiological effects of TeNT in the *tibialis anterior* muscle

Next, I wanted to show using physiological methods that the N1 peptide prevents the appearance of tetanus symptoms by reducing tetanic paralysis of the muscle. To do this, 8-week-old weight matched C57Bl6 mice were injected with the sub-lethal dose of 0.125 ng/kg TeNT (4 µl total volume per 20 g body mass) in the right *tibialis anterior* (TA) muscle after preincubation with DMSO (vehicle control), $N1_{AA}$ or the N1 peptide. After 24 h, the mice were terminally anaesthetised and the isometric muscle tension force was recorded from the distal TA tendon following supramaximal electrical stimulation of the sciatic nerve. The injection and subsequent recordings were performed by J. B. Bryson (UCL-Institute of Neurology). The contractile force of the TeNT-injected muscle was minimal (3.11±0.88% SEM of non-injected control; Figure 3-17 A), as was the case for muscles co-injected with TeNT and the $N1_{AA}$ peptide (2.14±1.44% SEM of non-injected control; Figure 3-17 B). However, co-administration of the N1 peptide significantly reduced the TeNT-mediated decline in contractile force compared to the other two groups (47.46±10.31% SEM of non-injected control; Figure 3-17 C). These results confirmed that the N1 peptide prevents symptoms of clinical tetanus by blocking the effect of TeNT on the muscle contraction.

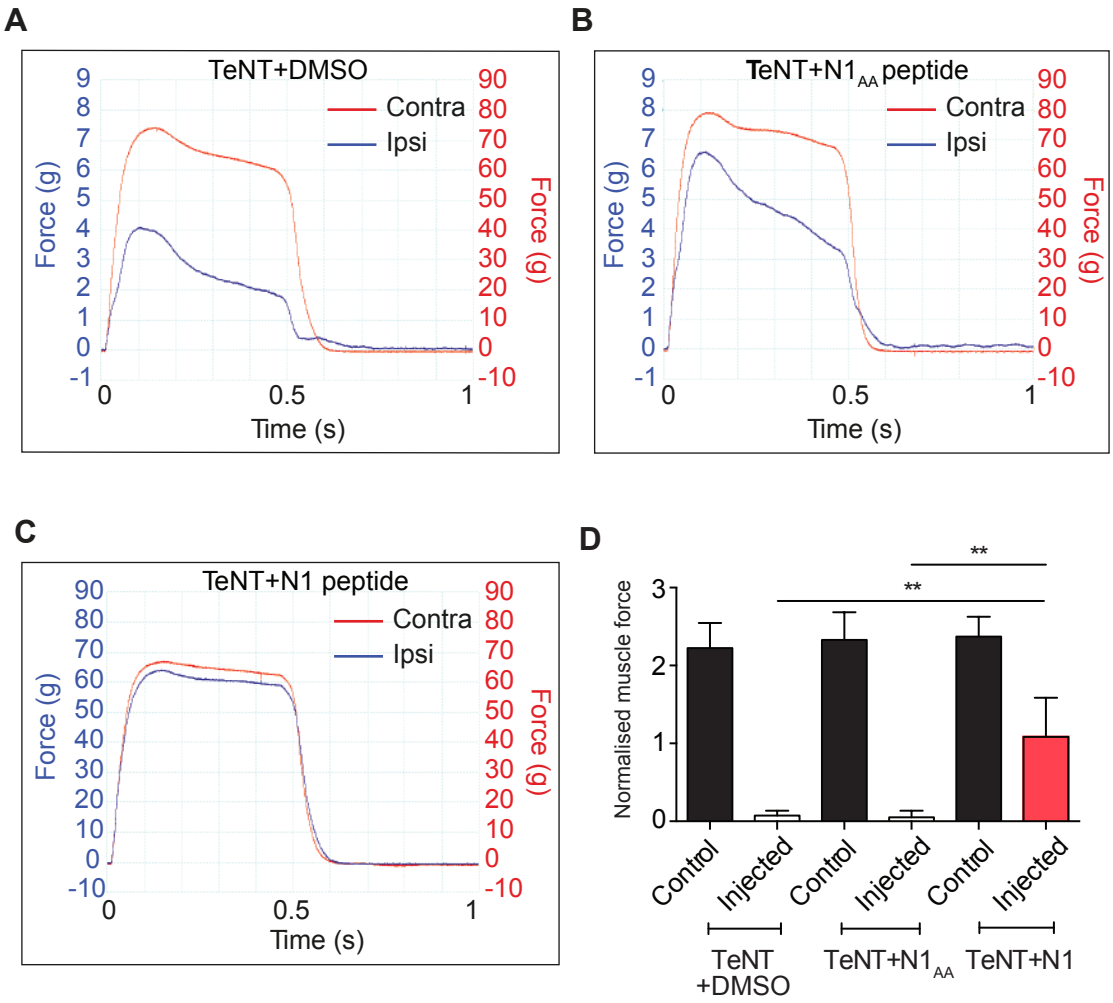

Figure 3-17. Preincubation with the N1 peptide reduces the effect of TeNT on isometric muscle tension force

The *tibialis anterior* (TA) muscle was injected with TeNT preincubated with either DMSO (vehicle control), $N1_{AA}$ or N1 peptides. Following anaesthesia, the tendon of the TA muscle was attached to a tension sensor, the peroneal nerve was stimulated and isometric muscle force was measured. **(A-C)** Representative isometric muscle force recordings obtained from the ipsilateral (ipsi; injected side) and contralateral (contra; non-injected internal control) TA muscles, 24 h after administration of TeNT preincubated with vehicle control (DMSO) **(A),** the $N1_{AA}$ peptide **(B)** or the N1 peptide (**C**). Ten-fold lower scale was applied to ipsilateral and contralateral traces in **(A)** and **(B)**, while the scales are identical for both traces in **(C). (D)** Maximal muscle force was measured, normalised to muscle weight and tested for significance (control vs. injected muscle). The N1-treated group retained a significantly higher muscle force than the vehicle- or $N1_{AA}$-treated groups. Significance was assessed by unpaired t-test comparing the DMSO, or $N1_{AA}$ treated group to the N1 treated group (*n*=6 mice per group; **, p<0.01; error bar: SD). From (Bercsenyi et al., 2014). Reprinted with permission from AAAS.

3.6 Summary

- The N1 peptide emerged as the strongest and most reliable candidate in the initial peptide screen.
- Both the N1 (nidogen-1) and N2 (nidogen-2) peptides block H_CT binding and entry into primary motor neurons.
- Single alanine mutation of the W residue abolished the interaction with H_CT for both the N1 and N2 peptides.
- The correspondent human N1 and N2 peptides bind H_CT, but with lower affinity than the murine peptides.
- The interaction between the N1 peptide and H_CT is pH sensitive, suggesting a possible mechanism of dissociation of the complex in the endosomal lumen.
- Based on biomolecular modelling, the N1 peptide fits into the 'R' pocket of H_CT and over 40% of the surface of the peptide is involved in the interaction.
- The Kd between N1 and H_CT is in the low micromolar range based on isothermal calorimetry data.
- The N1 peptide decreases H_CT entry in primary motor neurons when added simultaneously, or even with a 10 min delay.
- 65% of the NMJs of LAL muscle binds H_CT. This is decreased to 18% when H_CT is preincubated with the N1 peptide
- The N1 peptide blocks the tetanic paralysis in the nerve-hemidiaphragm preparation.
- The N1 peptide blocks tetanic paralysis *in vivo*.

Chapter 4. Nidogens are the protein receptors for tetanus toxin

4.1 The N1 peptide is derived from an extracellular protein, nidogen-1

The N1 peptide is present within the second globular domain (G2) of nidogen-1 (Figure 4-1 A). This domain has a β-barrel structure and both the Y and W of the N1 peptide face the inner cavity of the barrel (

Figure 4-1 B, Table 12) (Hopf et al., 2001, Kvansakul et al., 2001). When nidogen-1 is in its intact form, these residues are not accessible to H_CT. However, some of the metalloprotease cleavage products might have their YQWR motif exposed and available for H_CT binding.

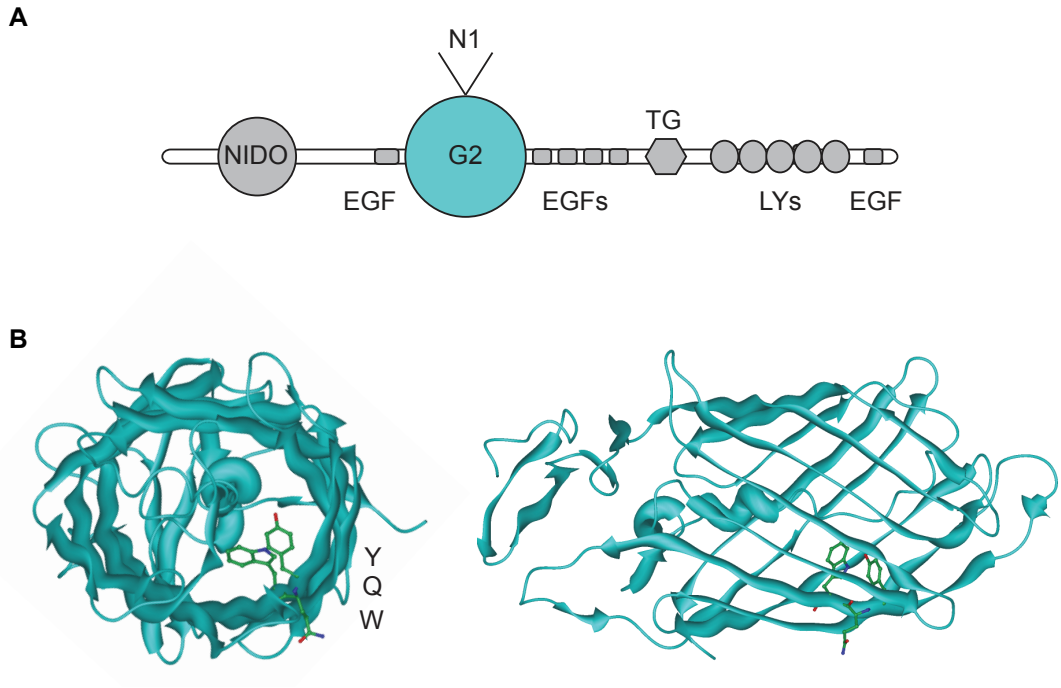

Figure 4-1. Nidogen-1 contains a YEW-like domain

(A) Module structure of nidogen-1 showing the position of the N1 peptide within the β-barrel G2 domain (cyan; top). In addition to the G2 domain, nidogen-1 contains a nidogen domain (NIDO), six EGF-like domains (EGFs), a thyroglobulin type 1 domain (TG) and five low-density lipoprotein receptor (LY) domains. **(B)** Top and lateral view of the crystallised G2 domain of human nidogen-1 (1GL4). The YQW sequence is highlighted with the ball and stick model (Kvansakul et al., 2001).

4.2 The basal lamina (BL) of the NMJ

Skeletal muscle is made up of multinucleated myofibrils that are innervated by motor neurons. The cell bodies of these neurons are located either in the brainstem or in the ventral horn of the spinal cord. Motor units are made up of the collection of myofibrils innervated by branches of one motor neuron axon. Each axonal branch innervates a particular patch on the muscle; these are called neuromuscular junctions (NMJs). The NMJ is a specialised synapse, with three major structural elements: the presynaptic membrane (the motor neuron end terminal), the synaptic cleft and the postsynaptic surface. All three compartments contain molecules, which are not found outside of the synapse. The synaptic cleft is filled with specialised extracellular matrix (sECM), which contains a thin acellular layer; the basal lamina (BL) (Hughes et al., 2006). The BL lies on the basal side of every epithelial cell, including cells derived from the neuroepithelium. It provides mechanical support for tissues, but it also acts as an important regulator of cell behaviour (Kalluri, 2003). The individual components of the BL regulate many different biological processes, such as cell division, migration, differentiation, shape maintenance and growth via cell surface receptors (Erickson and Couchman, 2000). The BL also binds and modulates the local concentration of cytokines, growth factors and neurotrophins (Hari et al., 2004, Clark, 2008, Hynes, 2009, di Summa et al., 2013).

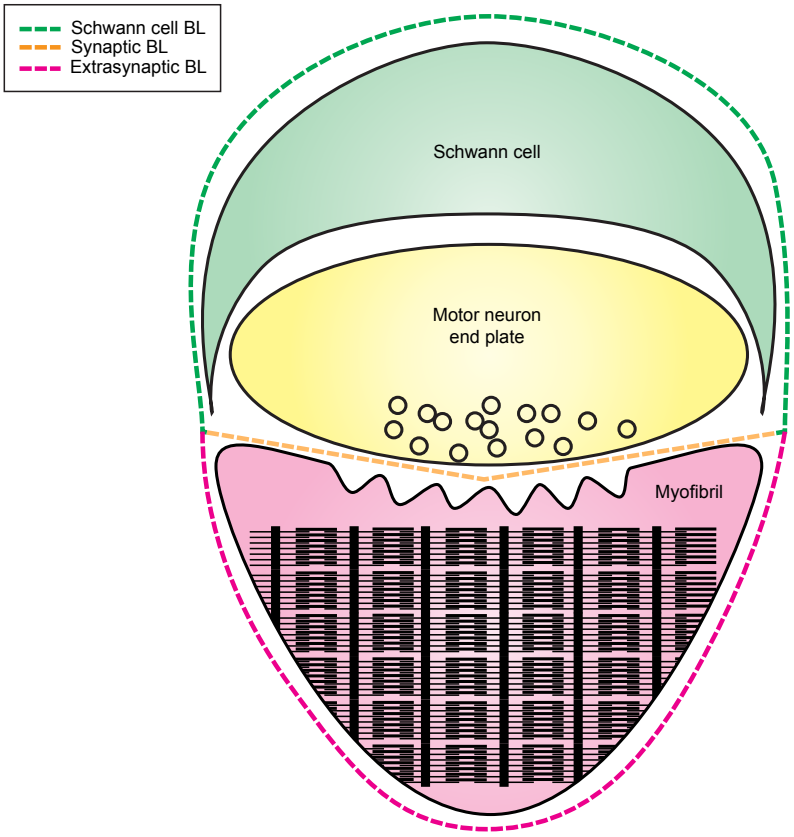

Figure 4-2. Schematic representation of the basal lamina at the NMJ

The NMJ is made up of three components: the presynaptic membrane, the synaptic cleft and the postsynaptic membrane. Schwann cells shield the NMJ on both sides, and their BL (green dashed line) appears to be anatomically continuous with the synaptic BL (orange dashed line), but their composition is dramatically different. The glial cells produce their own BL, while the motor neuron and the muscle release the components of the synaptic BL. The extrasynaptic BL (pink dashed line) is produced solely by the muscle and lacks some of the synaptic BL components (see Table 16). Recreated based on (Fox et al., 2008).

There are four main ECM components: laminins, type IV collagens, HSPGs, such as syndecan and dallylike and nidogens. The BL at the NMJ contains a highly specialised combination of these four main proteins (Table 16).

Table 16. Specialised ECM components at the NMJ basal lamina (Chiu and Ko, 1994, Fox et al., 2008)

Laminin	Collagen	HSPG	Nidogens
α2β2γ1	IV α3α4α5	syndecan-2	nidogen-2
α4β2γ1	IV $(\alpha5)_2\alpha6$	dallylike (Dlp)	nidogen-1 (9H6)
α5β2γ1	XIII	agrin z8	

4.3 Nidogen-2 is internalised together with H_CT in primary motor neurons

4.3.1 Both nidogen-1 and -2 are expressed in primary motor neuron cultures

First, I wanted to test if nidogens are expressed in primary motor neuron cultures (Figure 4-3). Both antibodies appeared to be very specific for nidogen-1 and -2, respectively. Immunoblotting for nidogen-1 revealed a band slightly higher than the predicted molecular weight (136 kDa). This might be due to glycosylation of the protein in primary motor neuron cultures. Immunoblotting for nidogen-2 gives two bands, one at 153 kDa (expected molecular weight) and one slightly above that. Since both bands were present in a recombinant nidogen-2 sample purified from chinese hamster ovary cells, they might be different glycosylation variants. Both nidogen-1 and -2 are present in motor neuron cultures, but nidogen-1 is expressed at much higher quantities than nidogen-2. It is currently unknown which cell type is the source of nidogens in the spinal cord.

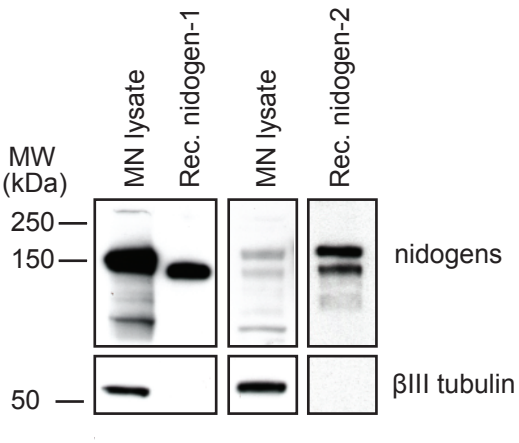

Figure 4-3. Both nidogen-1 and nidogen-2 are expressed in primary motor neurons

Primary motor neurons (DIV 7) were lysed in IP lysis buffer (2.3.3.7), the protein concentration was determined with a Bradford assay and 40 µg of protein was subjected to SDS-PAGE followed by immunoblotting with rabbit anti-nidogen-1 and -2 antibodies. βIII tubulin was used as a loading control. To estimate the abundance of nidogens in the primary motor neuron culture, 100 ng of recombinant nidogen-1 and -2 were loaded in separate lanes.

4.3.2 Nidogen-2 is taken up together with H_CT in primary motor neurons

Unfortunately the antibody against nidogen-1 was not suitable for immunofluorescence assays. I used the nidogen-2 antibody to assess whether nidogen-2 binds to motor neurons and is internalised together with H_CT.

Anti-nidogen-2 and AlexaFluor555-H_CT were added together to primary motor neurons, and left to internalise for 45 min at 37°C. The cells were cooled down and acid washed to remove any probes still bound to the surface. Following PFA fixation and permeabilisation, the cells were blocked with IFBB. AlexaFluor488-conjugated anti-rabbit antibody was added to detect internalised anti-nidogen-2. Unbound antibodies were removed with a series of washes before post-fixing and mounting. There is 65% colocalisation between the two probes, indicating that the vast majority of H_CT is taken up together with nidogen-2 in motor neurons (Figure 4-4).

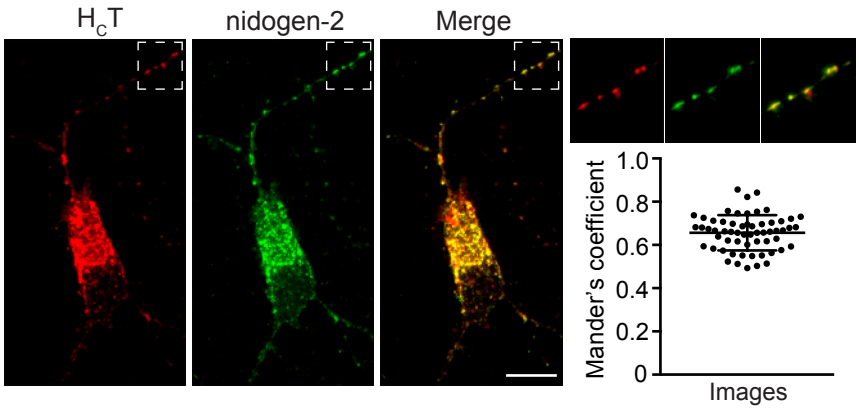

Figure 4-4. Nidogen-2 is taken up together with H_CT in primary motor neurons

Primary motor neurons were incubated with AlexaFluor555-H_CT and rabbit anti-nidogen-2 at 37°C for 45 min before acid washing, fixing and immunostaining with AlexaFluor488 anti-rabbit antibody. 20 images were taken of single cells and the colocalisation was measured in ImageJ using the JACoP plugin. Mander's coefficient showing the portion of H_CT colocalising with nidogen-2 was plotted for all 3 experiments. Scale bar: 10 µm. Modified from (Bercsenyi et al., 2014). Reprinted with permission from AAAS.

Next, I wanted to test if nidogen-2 and H_CT can be co-immunoprecipitated from primary motor neuron cultures. To do this, motor neurons were incubated with hemagglutinin tagged H_CT (H_CT-HA) for 5 minutes to allow for binding and

endocytosis to occur. Since the interaction between H_CT and polysialogangliosides is detergent-sensitive, it is not possible to efficiently immunoprecipitate this probe in complex with its protein receptors on the motor neuron surface. Once H_CT enters early endosomes, the disruption of its interaction with polysialogangliosides does not lead to its release into the medium and does not affect its recovery during immunoprecipitation. Following the 5 min incubation at 37°C the cells were cooled on ice, the proteins were cross-linked with bis[2-(sulfosuccinimidooxycarbonyloxy)ethyl] sulfone (BSOCOES) and lysed with an IP buffer containing 0.5% NP40. It was previously demonstrated in our laboratory, that the immunoprecipitation of proteins bound to H_CT is more efficient following crosslinking (Herreros et al., 2000a, Herreros et al., 2001) and I opted for this method after several failed attempts at immunoprecipitating the two proteins without crosslinking. The lysates were cleared by centrifugation and proteins binding to empty beads were excluded from the lysate. Mouse anti-HA antibody was crosslinked to magnetic Dynabeads using BS3, and these were used to immunoprecipitate H_CT and its interacting partners. To test whether nidogen-2 is bound to H_CT, the eluate from the beads was subjected to SDS-PAGE followed by immunoblotting with rabbit anti-nidogen-2 and rat anti-HA. There were several nidogen-2 bands present in the eluate, including a strong band at 250 kDa (Figure 4-5), which is present in motor neuron lysates, but at much lower quantities than the native form of nidogen-2 (running at 153 kDa, Figure 4-3).

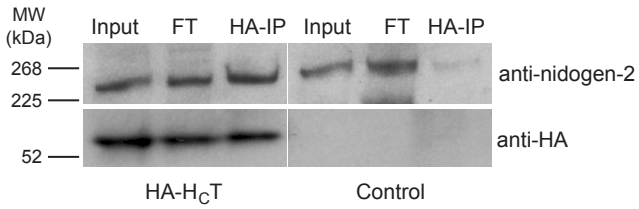

Figure 4-5. Nidogen-2 and HCT are co-immunoprecipitated from motor neurons

HA-H_CT was allowed to enter early endosomes in primary motor neurons before cross-linking and immunoprecipitation. Immunoprecipitated proteins were subjected to SDS-PAGE followed by Western blotting for nidogen-2 and HA. Modified from (Bercsenyi et al., 2014). Reprinted with permission from AAAS.

4.4 Biomolecular modelling predicts a high affinity interaction between nidogen-1 and H_CT

4.4.1 The G2 domain of nidogen-1 fits into the binding pocket ('R' site) of H_CT

Since our attempts to co-crystallise nidogens with H_CT failed due to the pH sensitivity of the interaction, we turned to biomolecular modelling to gain a molecular understanding of the potential binding site between the two proteins. G. Zanotti (University of Padua) performed the analysis. A model of the human nidogen-1 fragment, amino acids from 389 to 661, was built by homology modelling with the webserver Swiss-Model (Arnold et al., 2006) using the crystal structure of the nidogen-1 G2/perlecan Ig3 complex from Mus musculus as a template (PDB code 1GL4) (Hopf et al., 2001). The latter presents an overall 85% sequence identity with the human orthologue of nidogen-1. The model shows that nidogen-1 nicely fits into a large crevice of H_CT (the 'R' site, where sialic acid and the YEW peptide were previously shown to bind), with only minor adjustments of the loop 1144-1147 and of area 1211-1223 (Figure 4-6 A, Movie 2). The contact surface is quite extended, since the solvent-accessible area concealed by the complex is 1114 $Å^2$ and 1106 $Å^2$ for H_CT and nidogen-1, respectively. The area of nidogen-1 involved in the interaction includes four antiparallel β-strands (residues 517-523, 571-576, 580-586, 608-614) whilst the surface of the neurotoxin corresponds to the large crevice where also the YEW-like peptide binds. The latter includes four loops and some extended conformations, residues 1144-1147, 1211-1226, 1230-1235, 1273-1280. The electrostatic surfaces are also complementary: the interacting surface of nidogen-1 is negatively charged in the central area and positively at the border (Figure 4-6 B), while the centre of the crevice in H_CT is slightly positively charged, and the two borders are mostly negative (Figure 4-6 C).

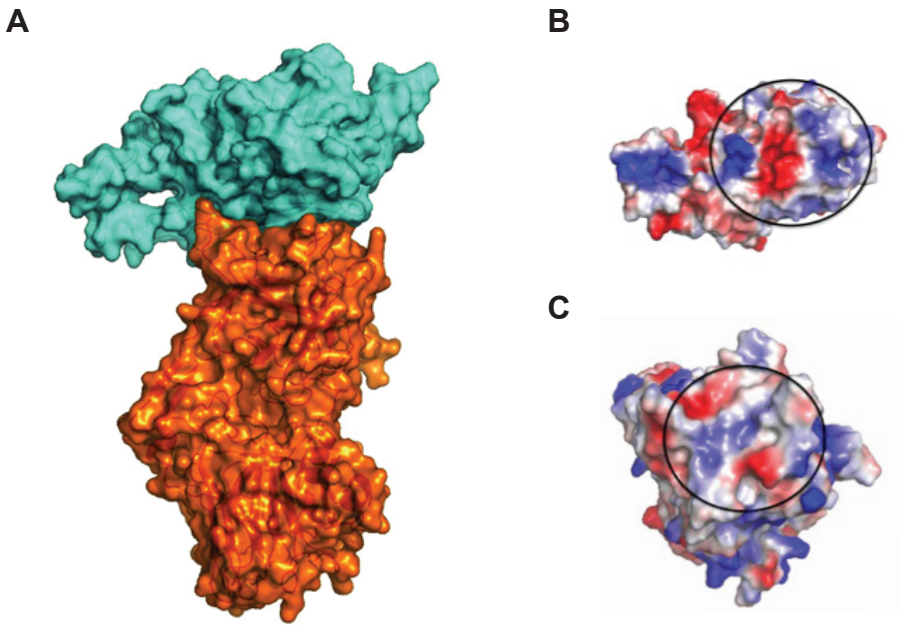

Figure 4-6. Nidogen-1 fits into the 'R' pocket of H_CT

(A) The G2 domain of nidogen-1 can potentially form a strong interaction covering a long surface area within the 'R' pocket of H_CT. **(B)** The electrostatic surface of the G2 domain of nidogen-1 is negatively charged in the middle, and positive on the two sides. **(C)** The binding area of H_CT is positively charged in the centre and is surrounded by negative borders. Modified from (Bercsenyi et al., 2014). Reprinted with permission from AAAS.

Fifteen potential H-bonds can be formed between H_CT and nidogen-1 (Table 17). These interactions together with the electrostatic complementarity suggest that the binding between the two proteins is very strong, but it may be highly sensitive to changes in pH. I observed that the interaction between the N1 peptide and H_CT is disrupted at pH 5 (Figure 3-8 B), and based on this model (Figure 4-6, Table 17), the interaction between nidogen-1 and H_CT is likely to be pH-sensitive too. This might be important for the release of TeNT from its receptor binding complex after the acidification of the endosome in the somatodendritic compartment of motor neurons, which is indispensable for the release of TeNT from these cells and its entry into spinal cord interneurons, where the cleavage of its intracellular target, VAMP/Synaptobrevin takes place (Schiavo et al., 1992, Bercsenyi et al., 2013).

Table 17. Potential hydrogen bonds between H_CT and the nidogen-1 G2 domain.

The predicted distance between the interacting residues of H_CT (A) and the intact G2 domain of nidogen-1 (D) is indicated. Distances must be considered as indicative, since they are based on a theoretical model. Contacts and concealed surfaces were calculated with server PISA (http://www.ebi.ac.uk). The effects of mutating the highlighted residues (T1146 and Y1229) on the binding to the N1 and N2 peptides are shown in Figure 4-7. From (Bercsenyi et al., 2014). Reprinted with permission from AAAS.

Bond	H_CT	Distance (Å)	nidogen-1 (G2 domain)
1	A:ASN1144[ND2]	2.64	D:HIS 575[O]
2	A:ASN1144[ND2]	2.85	D:VAL 580[O]
3	A:THR1146[OG1]	3.48	D:THR 582[O]
4	A:ASN1216[ND2]	3.67	D:GLU 521[OE2]
5	A:TYR1229[OH]	2.91	D:SER 584[OG]
6	A:ASN1277[N]	2.63	D:THR 614[OG1]
7	A:ASN1277[ND2]	3.83	D:THR 614[O]
8	A:ILE1145[O]	3.85	D:THR 582[OG1]
9	A:LYS1213[O]	3.88	D:THR 586[OG1]
10	A:ASP1214[O]	2.82	D:ARG 610[NH1]
11	A:GLY1215[O]	2.71	D:ARG 610[NH2]
12	A:GLY1215[O]	3.56	D:THR 523[OG1]
13	A:ALA1217[O]	3.06	D:ASN 530[ND2]
14	A:TYR1229[OH]	3.74	D:THR 586[N]
15	A:TYR1229[OH]	2.94	D:GLN 608[NE2]

4.4.2 Single point mutations in the 'R' pocket significantly reduce binding between H_CT and the N peptides

To test the accuracy of the model, we mutated selected residues (some are highlighted in Table 17) and tested the binding between mutant H_CT and the N peptides in an ELISA following the same protocol as before. The site-directed mutagenesis was performed by M. Wallace (Molecular Neuropathobiology laboratory, UCL-Institute of Neurology) and the recombinant proteins were expressed in E.coli and purified by G. Schiavo (Molecular Neuropathobiology laboratory, UCL-Institute of Neurology) (Figure 4-7 A). All point mutants showed significantly reduced binding to both N1 and N2 when compared to the wild type control (Figure 4-7 B,C). The R1226F mutation, which replaces a positively charged amino acid with a bulky hydrophobic residue, proved to be the most disturbing for the binding. Interestingly when this mutation is grafted into full-length TeNT, the mutant toxin displayed dramatic loss in toxicity in the mouse phrenic nerve assay (1.4% of wild type; MPN assay) (Rummel et al., 2003). G1215F also binds less to both N1 and N2 peptides. This mutant has a loss of toxicity of 15% in the MPN assay, which is less dramatic than that of R1226F (Rummel et al., 2003). This correlates with the binding affinity of these mutants to the N peptides, implicating that the loss of toxicity might be a result of the decreased affinity of these mutants to nidogens.

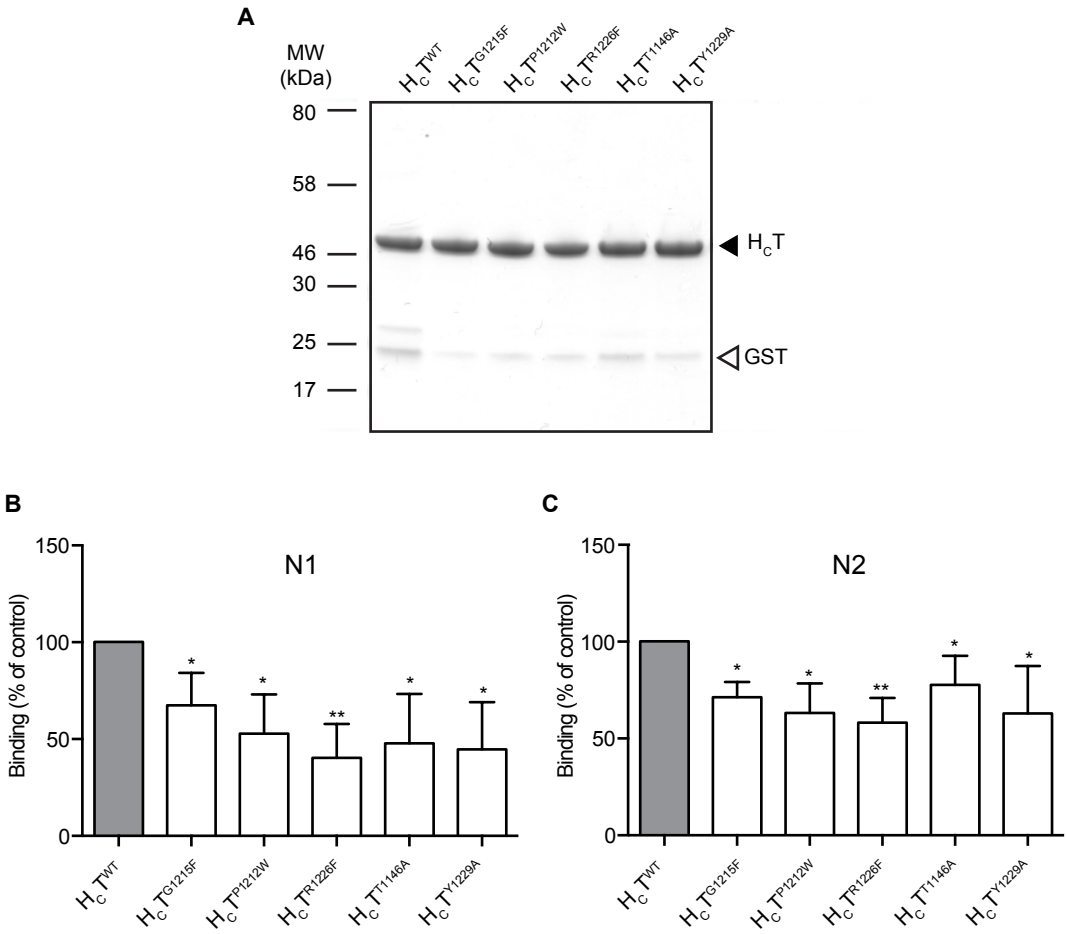

Figure 4-7. The binding of H_CT to the N1 and N2 peptides is significantly reduced by point mutations in the 'R' site of H_CT.

(A) Single point mutants of the 'R' site of H_CT were generated, expressed as glutathione s-transferase (GST) fusion proteins, and after purification and GST cleavage, subjected to SDS-PAGE to assess purity. The position of HA-H_CT (filled triangle) and a small amount of GST contaminant (empty triangle) are shown. **(B,C)** H_CT 'R' site mutants display impaired binding to the N1 **(B)** and N2 **(C)** peptides. These peptides were immobilised on the surface of 96-well plates, blocked for non–specific binding and incubated with wild type HA-H_CT (H_CT^{WT}) or the indicated mutants. Binding was detected by ELISA using TBS as a control. Averages of triplicates within one assay were determined and the results of four independent experiments were analysed for significance using paired t-test comparing the mutants to wild type H_CT. (n=4; *, $p<0.05$; **, $p<0.01$; error bars: SD). From (Bercsenyi et al., 2014). Reprinted with permission from AAAS.

4.5 The N peptides block the direct interaction between recombinant nidogens and H_CT

The biomolecular modelling suggested a strong interaction between nidogen-1 and H_CT, which is dependent on the N1 peptide region within the G2 domain of nidogen-1. To test this prediction and to get further insights into the molecular interactions of the H_CT/nidogen complex, I sought to test if both nidogens bind H_CT in isolation and if the N peptides can block this binding.

I incubated full-length nidogen-1 or 2 in the presence or absence of the N1 and N2 peptides with HA-H_CT immobilised on Protein G-Dynabeads for 2 h at 4°C. The beads were washed with TBS before lysing with Laemmli sample buffer (LSB) for 15 min at 65°C. The lysates were subjected to SDS-PAGE followed by immunoblotting for nidogens and H_CT. This experiment demonstrated that both nidogens bind HA-H_CT directly under these experimental conditions (Figure 4-8 A). The N1 and N2 peptides play a key role in this interaction since pre-incubating H_CT with an excess of these peptides, but not the $N1_{AA}$ or $N2_{AA}$ mutants, abolished binding (Figure 4-8). On average, 10% and 7.5% of the total amount of nidogen-1 and nidogen-2 were recovered with the H_CT immunoprecipitate. However, analysis of the amount of H_CT associated to the anti-HA beads revealed that only a small percentage of H_CT added to the samples was recovered in the pellet under our experimental conditions used to test the binding (5-7.5%). This corresponds to a molar ratio between nidogen-1/H_CT of 1, and nidogen-2/H_CT of 0.5, which suggests that there is a stoichiometric interaction between H_CT and nidogens.

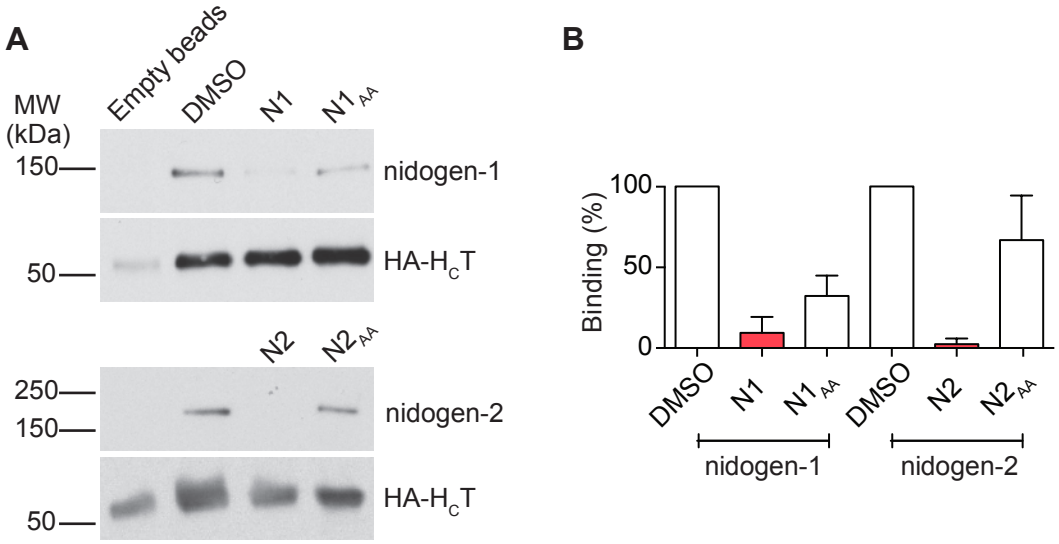

Figure 4-8. Nidogens bind directly to H_CT and the N peptides can block this interaction

(A) In vitro pull down of HA-H_CT preincubated with full length nidogen-1 (upper panel) or nidogen-2 (lower panel) with a mouse monoclonal anti-HA antibody followed by SDS-PAGE and western blotting with rabbit anti-nidogen-1, rabbit anti-nidogen-2 or rat anti-HA antibodies. 'Empty beads' corresponds to samples in which HA-H_CT was omitted, and DMSO to samples treated with vehicle control. Both nidogen-1 and -2 bind directly to HA-H_CT, and pre-treatment with the N1 or N2 peptide blocks this interaction. In contrast, mutant peptides in which both the Y and W residues have been replaced by alanines ($N1_{AA}$ and $N2_{AA}$, respectively) are ineffective. The heavy chain of the capture antibody runs at 50 kDa (empty beads). **(B)** The mean grey value of each band has been determined using ImageJ, the results were normalised to the mean grey value of the HA-H_CT pull down and expressed as percentage of DMSO control (*n*=2 for both proteins).

4.6 Increase in soluble nidogen-1 to motor neurons enhances H_CT binding and uptake

4.6.1 Exogenous nidogen-1 increases the amount of H_CT bound and internalised in primary motor neurons

The N1 peptide blocks H_CT binding and internalisation in primary motor neurons (Figure 3-5, Figure 3-9). This effect is most probably due to its high affinity binding to an important receptor-binding site on H_CT. Based on the results of the *in vitro* IP, the N peptides can block the interaction between H_CT and nidogens (Figure 4-8). However, this does not exclude the possibility that there is another

crucial receptor, whose binding is inhibited by the N peptides leading to the block of H_CT binding to motor neurons.

To show that the blocking effect of the N peptides is due to the inhibition of the interaction between H_CT and nidogen-1, I sought to test H_CT binding and internalisation following preincubation of cells with recombinant full-length nidogens and block their effect using the N peptides.

Firstly, to determine the effect of exogenous nidogens on H_CT binding and internalisation, the proteins (H_CT+ nidogen-1, H_CT+nidogen-2, H_CT+mix of both nidogens) were incubated for 1 h at room temperature and added to motor neurons either on ice to assess binding, or at 37°C to test internalisation. The internalised samples were acid washed and cells were fixed and stained for βIII tubulin to reveal the neuronal network. There was a robust increase in both H_CT binding and internalisation when additional nidogen-1 was present (H_CT+nidogen-1 and H_CT+mix of both nidogens) and this increase was significant compared to the H_CT alone control (Figure 4-9). However, when nidogen-2 was added alone, there was only a small increase, which was significant for internalisation, but not for binding (Figure 4-9).

The expected effect of adding an excess of exogenous receptor to a binding assay is a decrease in the binding and uptake of the ligand, since the exogenous receptor would act as a sink, sequestering the ligand without promoting its internalisation. But nidogens are extracellular proteins, linking laminin and collagen, and they are tightly packed in the basal lamina. Thus it is likely that some of the nidogen binding sites are not accessible for H_CT for binding in normal conditions. By adding soluble exogenous nidogen-1, there is an increase in the pool available for H_CT capture, and this in turn leads to a significant increase in both binding and internalisation of H_CT. Since exogenous nidogen-2 has a much smaller effect on H_CT binding and internalisation, nidogen-1 is likely to play a greater role in H_CT binding than nidogen-2 in primary motor neuron cultures.

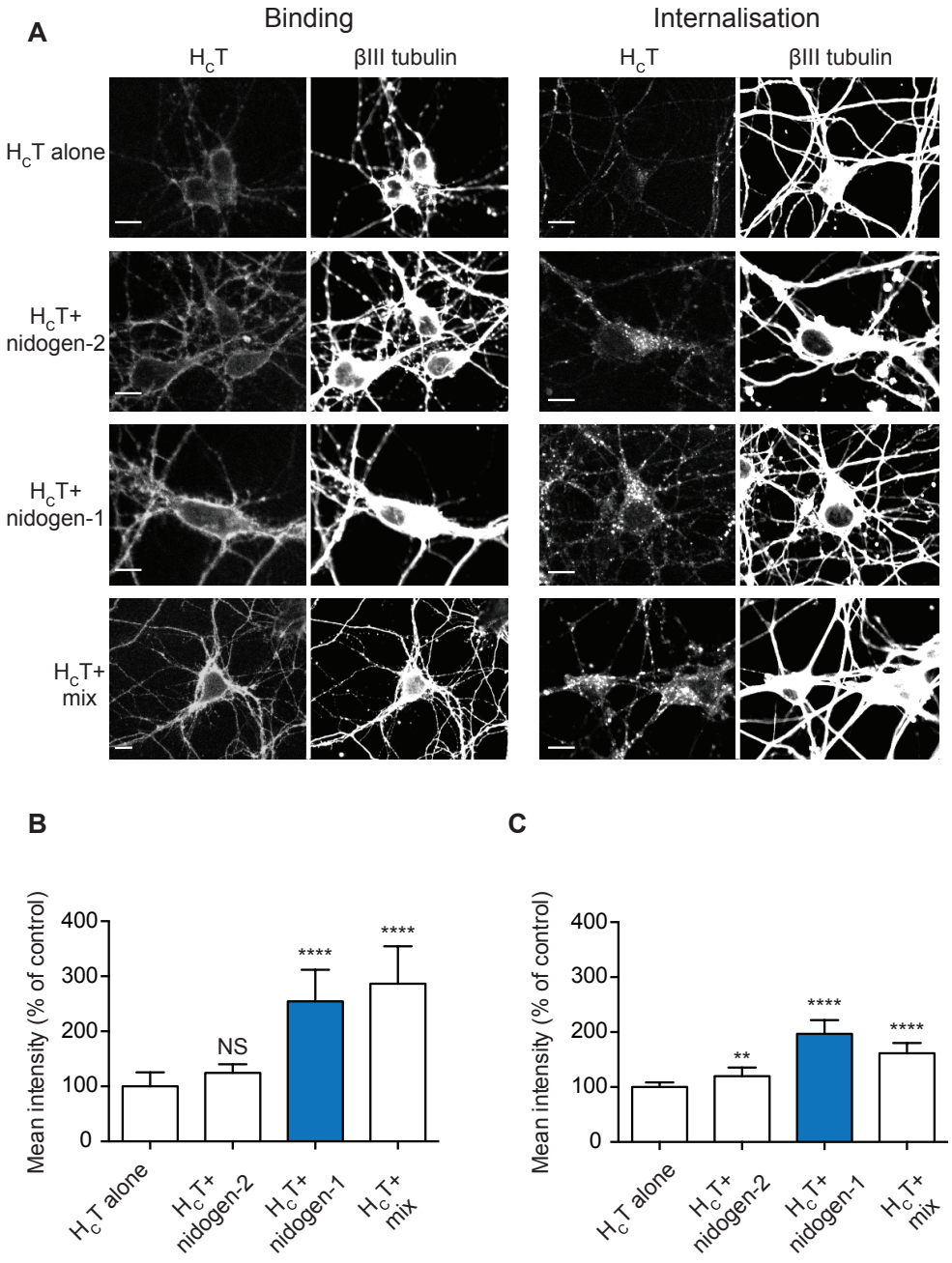

Figure 4-9. Recombinant nidogen-1 increases H_CT binding to primary motor neurons

(A) AlexaFluor555-H_CT was preincubated with full-length recombinant nidogen-1, -2 or the mixture of these two proteins prior to addition to primary motor neurons. The cells were incubated with the protein mixture either on ice (Binding) or at 37°C (Internalisation). **(B,C)** The fluorescence intensity of AlexaFluor555-H_CT (pseudocolored grey) was quantified using βIII tubulin (pseudocolored grey) as a mask. The results of 20 images per condition were plotted and analysed for significance using one-way ANOVA followed by Dunnett's multiple comparisons test, **** $p<0.001$ (** $p<0.01$; **** $p<0.001$; NS non significant; n=3 experiments). Scale bars: 10 µm.

To test if recombinant nidogen-1 enhances H_CT uptake by binding to primary motor neurons and bringing H_CT to close proximity of the PM, we exploited the His_9-tag of the recombinant protein. H_CT was added to motor neurons together with recombinant nidogen-1 on ice, allowing only binding to occur. After washing and fixing, the cells were counterstained with mouse anti-His antibody to reveal surface bound nidogen-1. The His antibody binds to neuronal cell bodies unspecifically (Figure 4-10; H_CT alone condition, middle panel), but there is a clear difference between the samples where nidogen-1 was omitted, or added to the motor neuron medium. It binds to cell bodies as well as the axonal network (Figure 4-10).

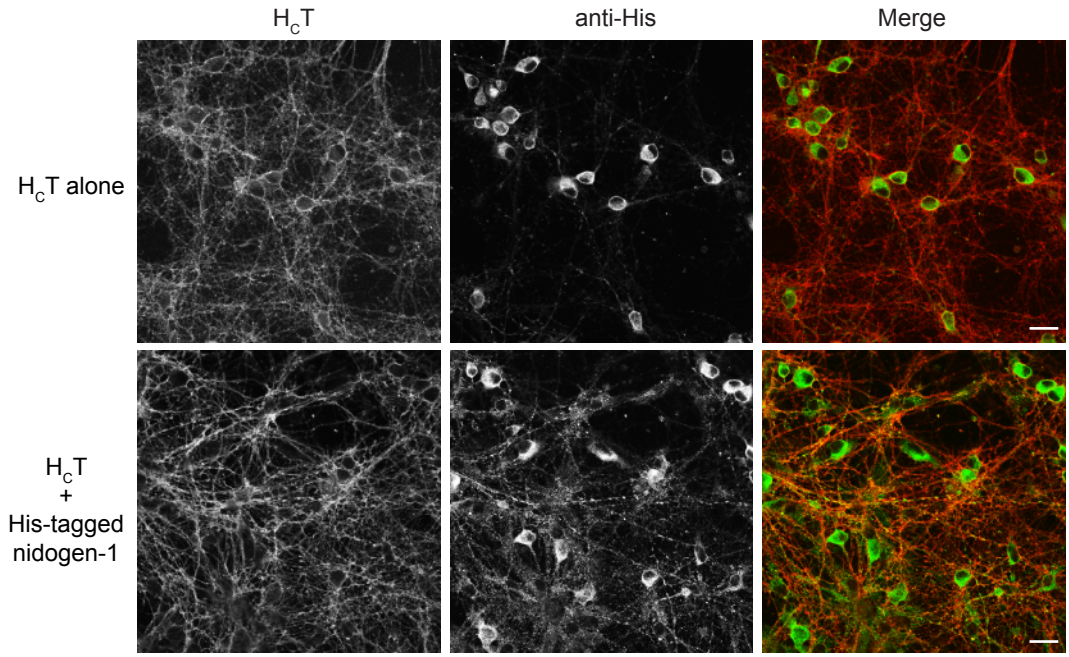

Figure 4-10. Recombinant nidogen-1 binds to primary motor neurons together with H_CT

Primary motor neurons were cooled on ice, before the addition of AlexaFluor555-H_CT (pseudocolored grey, red in merge) alone or preincubated with recombinant His_9-tagged nidogen-1 for 10 min. Following a high-volume wash with ice-cold HBSS buffer, the cells were fixed with PFA, blocked and stained with a mouse anti-His antibody (pseudocolored grey, green in merge). Note the unspecific staining of the His antibody in motor neuron cell bodies. Nidogen-1 binds to the motor neuron network together with H_CT. Scale bar: 20 µm. From (Bercsenyi et al., 2014). Reprinted with permission from AAAS.

4.6.2 Preincubation with the N1 peptide blocks H_CT binding even in the presence of soluble nidogen-1

To test if the N1 peptide can block the interaction between H_CT and both endogenous and exogenous nidogen-1 on primary motor neurons, we preincubated AlexaFluor555-H_CT with DMSO (vehicle control), the N1 or $N1_{AA}$ peptide prior to addition to the motor neuron medium already containing recombinant nidogen-1. The experiment was performed on ice, to allow binding but not internalisation.

Preincubation with the N1 peptide completely blocked H_CT binding both in the absence and presence of recombinant nidogen-1, but the $N1_{AA}$ peptide did not have any effect (Figure 4-11). This result shows that the N1 peptide is able to block the interaction between both endogenous and exogenous nidogen-1 and H_CT on primary motor neurons when H_CT is preincubated with it and this is sufficient to abolish H_CT binding.

This result does not exclude the possibility that the N1 peptide also blocks other potentially important receptors from binding to H_CT, but clearly highlights the importance of the interaction between nidogen-1 and H_CT for its entry in primary motor neurons.

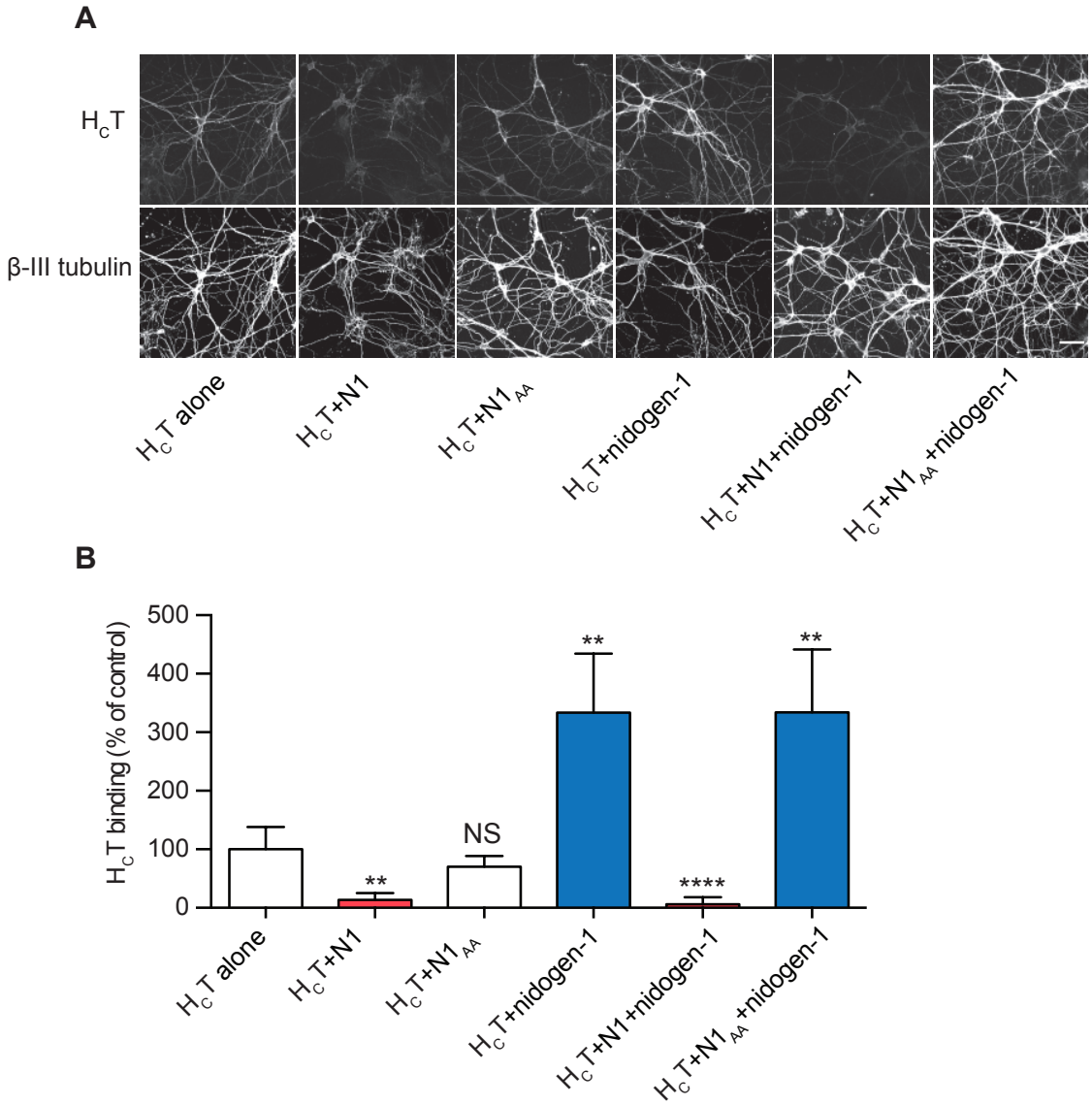

Figure 4-11. The N1 peptide blocks the effect of nidogen-1 on H_CT binding to primary motor neurons

(A) Motor neurons were incubated with AlexaFluor555-H_CT on ice, following preincubation with vehicle control (DMSO, 'H_CT alone') or wild type and mutant versions of the N1 peptide in the absence or the presence of exogenous nidogen-1 before staining for βIII tubulin and confocal imaging. Scale bar, 50 μm. **(B)** Twenty images were taken for each condition and fluorescence intensity of AlexaFluor555-H_CT bound to neurons (βIII tubulin mask) was quantified. Results were tested for statistical significance using Kruskal Wallis test followed by Dunn's Multiple Comparisons Test (*n*=3; NS, non significant; **, p<0.01; ****, p<0.001; error bar: SD). Modified from (Bercsenyi et al., 2014). Reprinted with permission from AAAS.

4.7 The progression of tetanic paralysis accelerates when soluble nidogen-1 is present

Since the addition of nidogen-1 caused a significant increase in H_CT binding and internalisation in motor neurons, I wanted to assess its effect on TeNT intoxication *in vivo*. To do this, the *triceps surae* muscle of wild type adult mice was injected with 1 ng/kg TeNT, preincubated with vehicle control (DMSO) or nidogen-1 (9 nM) in the presence or absence of the N1 peptide (50 mM). The preincubation was performed at a molar ratio of TeNT:N1:nidogen-1 1:13,800:0.125. The mice were kept under observation for 96 h in total, or until the loss of righting reflex. The experiment was performed with the help of N. Schmieg (Molecular Neuropathobiology laboratory, UCL-Institute of Neurology).

The intramuscular administration of this dose causes local tetanus, first affecting the coordination by causing mild local paralysis, then progressing to general spastic paralysis of the injected hindlimb and subsequent stiffness of the back muscles.

The mice injected with TeNT preincubated with nidogen-1 in the absence of the N1 peptide showed an earlier onset and faster progression of paralysis than the other two groups (Figure 4-12, Figure 4-13). At later stages of disease all three groups progressed at a similar rate. Preincubation of TeNT with the N1 peptide partially blocks the early effect of added nidogen-1, however at the concentrations used in this assay it did not entirely block tetanic paralysis. We used the footprint assay described before (Figure 3-15) to assess the coordination defects in a quantitative manner (Figure 4-12), and set up a scoring system, which allowed us to follow both the early and later stages of the disease (Figure 4-13). Mice injected with nidogen-1 in the absence of N1 start to show defects in coordination at an earlier stage than the other two groups, and at 69 h the injected hindlimb is hardly functional for walking (Figure 4-12).

The scoring system is a decreasing scale from 5 to 0, where 5 corresponds to normal walking and muscle movement, and 0 corresponds to completely paralysed injected hindlimb and stiff back muscles. When mice were terminated early, they were given a score of -1. The affected hindlimb of mice injected with nidogen-1 in the absence of N1 is stiff, but still functional 29 h after injection. The triceps surae muscle gets completely paralysed by 52 h and 2 out of 3 mice

reached the humane endpoint of the experiment at 73 h (-1 score). The remaining mouse showed the first signs of paralysis in the back muscles at 73 h (Figure 4-13). In contrast, the other two groups progressed at a much slower rate at the early stages of intoxication and the injected leg was completely paralysed only at 73 h (Figure 4-12). Various members of the Molecular Neuropathobiology laboratory scored the animals without information on the grouping (blind).

The results of this experiments recapitulated the observations made earlier in primary motor neurons (Figure 4-9); the addition of recombinant nidogen-1 increases the binding and internalisation of TeNT in motor neurons and this in turn leads to a faster progression of tetanic paralysis.

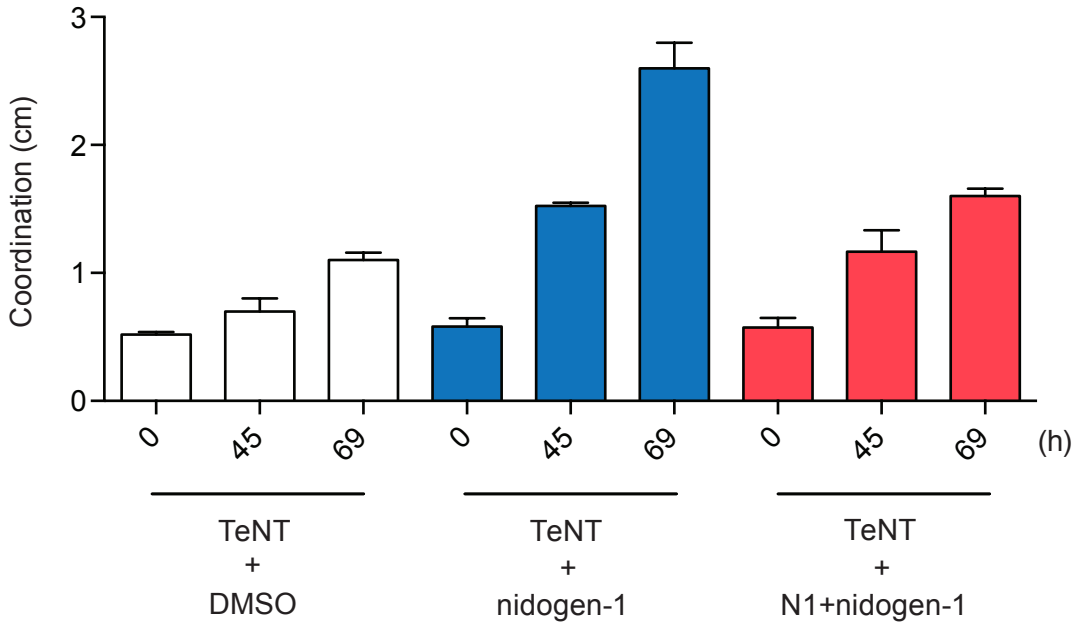

Figure 4-12. Recombinant full-length nidogen-1 makes coordination defects worse after TeNT injection

The right *triceps surae* muscle was injected with 1 ng/kg of TeNT, following preincubation with DMSO as a vehicle control, nidogen-1 alone or the N1 peptide followed by nidogen-1. Before injection, and 45 and 69 h after injection, a footprint analysis was performed as before (Figure 3-15) and the coordination (distance between the prints on the same side) was measured.

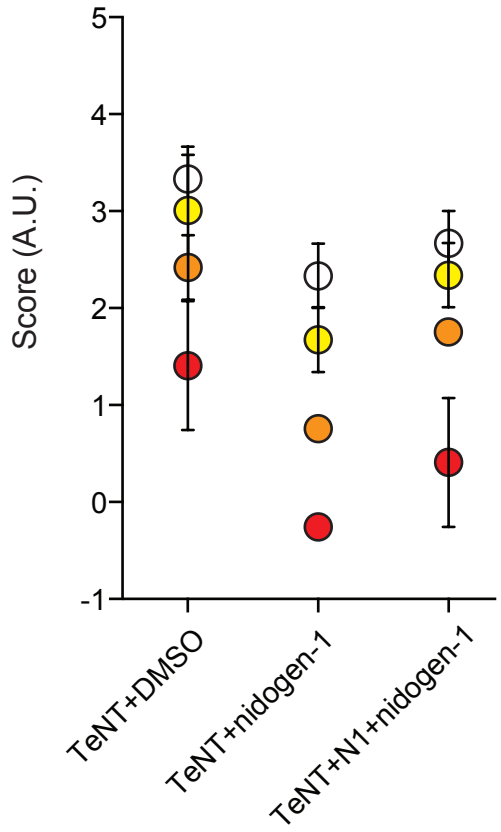

Figure 4-13. Additional nidogen-1 increases the progression of tetanic paralysis

The right *triceps surae* muscle was injected with 1 ng/kg TeNT, following preincubation with DMSO as a vehicle control, nidogen-1 alone or the N1 peptide followed by nidogen-1. Animals were scored according to the scoring system explained in Table 11 at 29 (empty circles), 47 (yellow circles), 52 (orange circles) and 73 (red circles) h and the results were plotted for the 3 different groups.

4.8 The cell entry route for the H_CT-nidogen complex

4.8.1 Both nidogen-2 and H_CT colocalise with LAR after uptake in primary motor neurons

The complex of H_CT bound to nidogens must engage with a transmembrane protein to ensure its uptake into signalling endosomes. It was previously published that nidogen and laminin bind to LAR (O'Grady et al., 1998). Furthermore, LAR was present in the endosomal carriers of H_CT in the magnetic pull down experiment performed by S. Debaisieux (Molecular Neuropathobiology laboratory, Cancer Research UK and UCL-Institute of Neurology). To test whether LAR is involved in

H_CT internalisation, AlexaFluor555-H_CT and anti nidogen-2 were internalised together for 45 min at 37°C. The cells were acid washed, fixed, permeabilised and blocked before staining with mouse anti-LAR PMD primary antibody (proximal transmembrane domain, kind gift from Frank M. Longo, Stanford University). Unbound antibodies were washed away before staining with goat AlexaFluor488-anti-rabbit and goat AlexaFluor647-anti-mouse antibodies. The mouse anti-LAR PMD antibody recognises a single band at 90 kDa in primary motor neurons, which corresponds to the molecular weight of the intracellular fragment of LAR (Figure 4-14 A) (Yang et al., 2006). There is a strong overlap between H_CT, nidogen-2 and LAR staining in the axonal network (Figure 4-14 A). This result suggests that LAR might be a component of the H_CT binding complex.

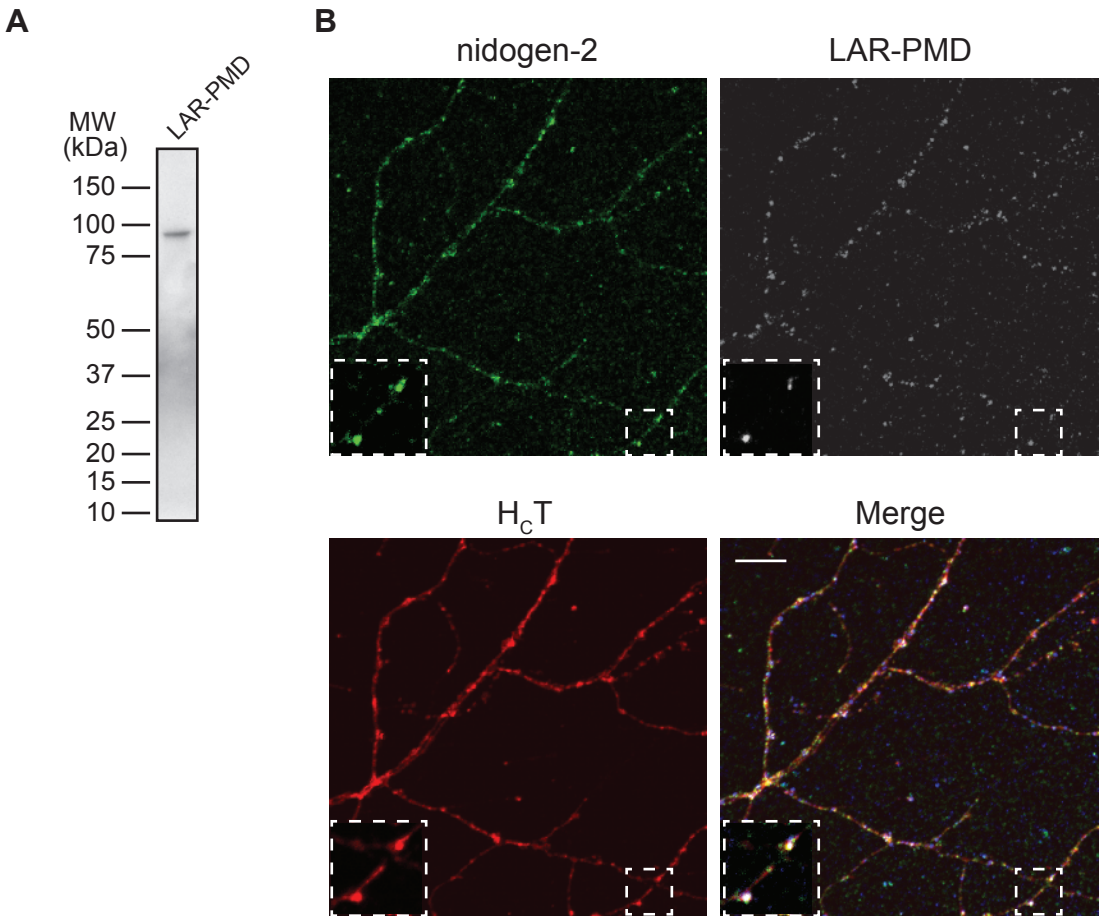

Figure 4-14. LAR is taken up together with nidogen-2 and H_CT in primary motor neurons

(A) Primary motor neuron lysate was subjected to SDS-PAGE followed by immunoblotting for LAR-PMD. There is one band at 90 kDa recognised by the antibody, which corresponds to the estimated molecular weight of the PMD fragment. **(B)** Anti-nidogen-2 and AlexaFluor555-H_CT (red) were added to primary motor neuron cultures and allowed to internalise for 45 min at 37°C. The cells were washed, then stained for the rabbit anti-nidogen-2 antibody (green) and anti-LAR-PMD (pseudocolored grey). The axonal network was imaged. Scale bar: 10 µm.

4.8.2 H_CT colocalises with TrkB

TrkB is the main neurotrophin receptor present on motor neurons. Its ligand, BDNF was previously shown to enhance binding and internalisation of H_CT (Roux et al., 2006). Furthermore, H_CT is known to trigger the downstream signalling pathway of TrkB even in the absence of BDNF (Gil et al., 2000, Gil et al., 2003). LAR was previously shown to bind TrkB in a BDNF dependent manner (Yang et al.,

2006). Since nidogens are likely promote the uptake of H_CT via LAR, its BDNF dependent interaction with TrkB could explain the enhancing effect of BDNF on H_CT binding and internalisation. Furthermore, TrkB was present alongside nidogen-1 in the proteomic screen of H_CT containing endosomes (Deinhardt et al., 2006b).

First, I wanted to test if TrkB colocalises with H_CT after uptake. To do this, I added AlexaFluor555-H_CT to primary motor neurons and left it to internalise for 45 min at 37°C. The cells were cooled on ice and acid washed to remove surface bound probes before fixing, permeabilising and blocking. The determine the extent of colocalisation between internalised H_CT and TrkB, the cells were stained with a rabbit anti-TrkB antibody followed by donkey AlexaFluor488-anti-rabbit secondary antibody.

The rabbit anti-TrkB antibody recognises a singe band at 90 kDa in primary motor neurons, which corresponds to the molecular weight of TrkB (Figure 4-15 A). The colocalisation between H_CT and TrkB is very high, confirming the mass spectrometry data and suggesting that TrkB might be involved in the binding complex of H_CT.

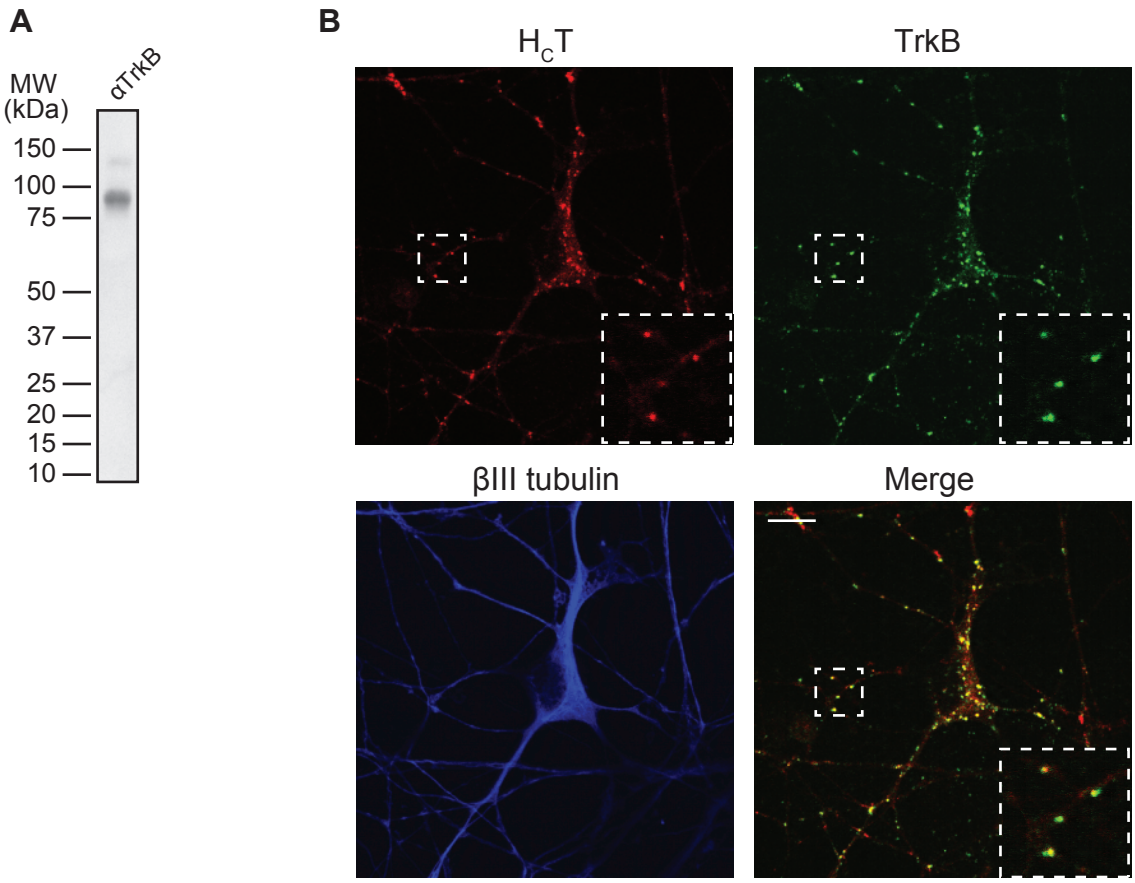

Figure 4-15. TrkB is taken up together with H_CT in primary motor neurons

(A) Primary motor neuron lysate was subjected to SDS-PAGE followed by immunoblotting for TrkB. There is one band at 90 kDa recognised by the antibody, which corresponds to the estimated molecular weight of TrkB. **(B)** AlexaFluor555-H_CT (red) were added to primary motor neuron cultures and allowed to internalise for 45 min at 37°C. The cells were washed, then stained with an anti-TrkB antibody (green) and βIII tubulin (blue). Scale bar: 10 μm.

4.8.3 Addition of anti-TrkB antibody prior to H_CT impairs H_CT binding and vice versa

Following the extensive colocalisation observed in Figure 4-15, I wanted to show that TrkB is taken up together with H_CT in primary motor neurons. To do that, the rabbit anti-TrkB antibody was added to motor neuron cultures together with H_CT for 45 min at 37°C. I observed that both the TrkB and H_CT staining were less intense then in the previous experiment suggesting that there is a competition between the antibody and H_CT for binding sites on the motor neuron surface.

To test this hypothesis, the cells were cooled down on ice, before adding either anti-TrkB (top panel, Figure 4-16) or AlexaFluor555-H_CT (bottom panel, Figure 4-16) alone for 10 min. The unbound probes were washed away before adding AlexaFluor555-H_CT (top panel, Figure 4-16) or anti-TrkB (bottom panel, Figure 4-16) for another 10 min. The cells were washed extensively, fixed and stained with donkey AlexaFluor488-conjugated anti-rabbit antibody to reveal surface-bound anti-TrkB. It appears that there is a two-sided competition, depending on which probe is added first, the other one cannot access its binding site on the motor neuron surface. This is most probably due to steric hindrance. If the initial hypothesis is correct, and H_CT-nidogen-2-LAR-TrkB form a complex, the presence of the polyclonal antibody might block the entry of TrkB into the complex. However, if H_CT is added to the cells first, it triggers the formation of the complex and recruits TrkB, making it inaccessible for the anti-TrkB antibody. Future experiments would be required to test this hypothesis in more detail.

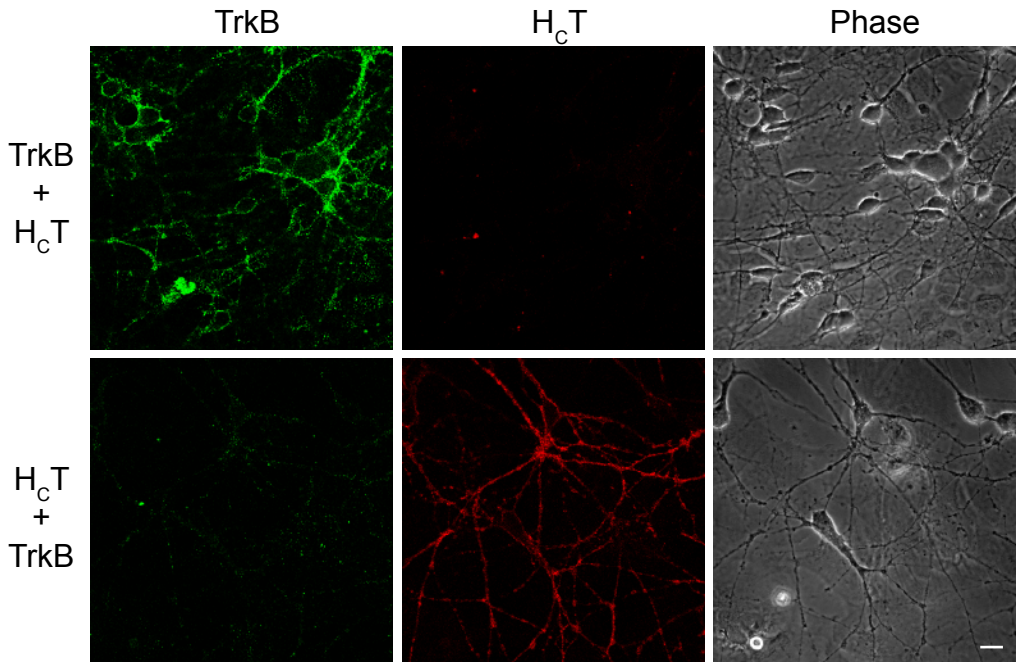

Figure 4-16. The anti-TrkB antibody blocks H_CT binding and vice versa

Primary motor neurons were incubated on ice either with anti-TrkB (top panel), or AlexaFluor555-H_CT (bottom panel) first, before washing with ice-cold HBSS and addition of AlexaFluor555-H_CT(top panel), or anti-TrkB (bottom panel). Anti-TrkB binding (green) is inhibited if H_CT is bound first, while H_CT binding (red) is blocked by the presence of anti-TrkB. Scale bar: 10 µm.

4.8.4 Both starvation, BDNF and H_CT increase the uptake of nidogen-2 in primary motor neurons

ECM components are generally thought to be stable, with a slow turnover, since they are integrated into the matrix. To test whether nidogen-2 is taken up during general maintenance in motor neuron cultures, the anti-nidogen-2 antibody was added to motor neurons under resting conditions. In the absence of H_CT, there is very little uptake in glial cells, and almost no uptake in motor neurons (Figure 4-17). When cultures were treated with BDNF (50 ng/ml, 10 min) without prior starvation, the glial uptake of nidogen-2 increased. When H_CT was added together with nidogen-2, motor neurons internalised the antibody together with H_CT. However, the most striking change in nidogen-2 uptake was observed under starvation conditions, which trigger massive internalisation of nidogen-2 in both neurons and glial cells (Figure 4-17).

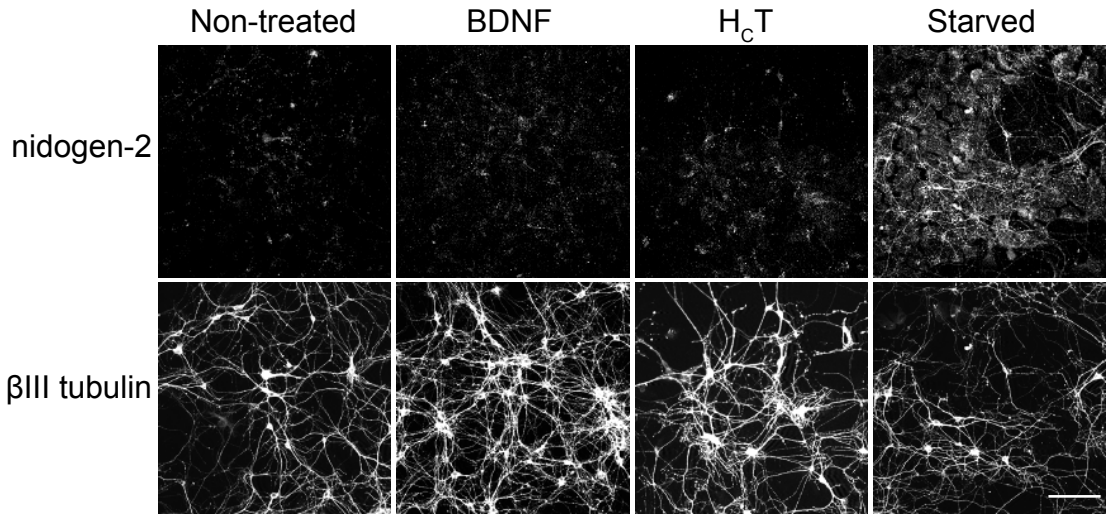

Figure 4-17. Nidogen-2 is taken up in a BDNF- and H_CT-dependent manner

Primary motor neuron cultures were non-treated, or treated with either BDNF (100 ng/ml), H_CT (40 nM), or incubated in neurobasal medium for 2 h (Starved). Anti-nidogen-2 antibody was added to the culture for 30 min at 37°C; this allowed internalisation of the probe before acid washing to remove surface bound antibodies. The cells were fixed, permeabilised, blocked and stained with donkey AlexaFluor488-anti-rabbit antibody to reveal the internalised pool of nidogen-2 (pseudocolored grey, top panel) and anti-βIII tubulin antibody to stain the neuronal network (pseudocolored grey, middle panel). Scale bar: 50 µm.

4.8.5 The colocalisation between SV2A and H_CT is blocked by the addition of soluble nidogen-1

Synaptic vesicle protein A and C (SV2A-C) have been implicated in BoNT binding to motor neurons (Dong et al., 2006, Peng et al., 2011, Benoit et al., 2014), and TeNT binding to central neurons (Yeh et al., 2010), but their role in binding and internalisation of TeNT into motor neurons remains to be elucidated. First, I wanted to test if H_CT colocalised with either SV2A or SV2C after uptake in motor neurons and if this was affected by the presence of nidogen-1. Primary motor neurons were incubated with either AlexaFluor555-H_CT alone, or with additional soluble nidogen-1 for 45 min at 37°C. The cells were acid washed, fixed, permeabilised, blocked and stained for SV2C (Figure 4-18 A) or SV2A (Figure 4-19 A). SV2C showed very little colocalisation with H_CT, and the addition of soluble nidogen did not have any effect (Mander's coefficient 0.1, Figure 4-18 B). However, around 50% of H_CT resides in SV2A positive vesicles when it is used at relatively high concentration (40nM in this assay, Figure 4-19 B). When additional soluble nidogen-1 is applied together with H_CT, they are increasingly taken up into different compartments, which are targeted to the retrograde transport pathway and accumulate in close vicinity of the nucleus (white arrowheads, Figure 4-19 A). These vesicles do not contain SV2A and this leads to a significant drop in the colocalisation to around 20% (Figure 4-19 B). This result is very important as it showed that H_CT is able to enter motor neurons via synaptic vesicle recycling (as shown by the high colocalisation with SV2A), but prefers an alternative way of entry when sufficient number nidogen-1 binding sites are available. Its preferred entry route is dependent on nidogen-1 and leads to its retrograde transport and accumulation in the motor neuron cell body.

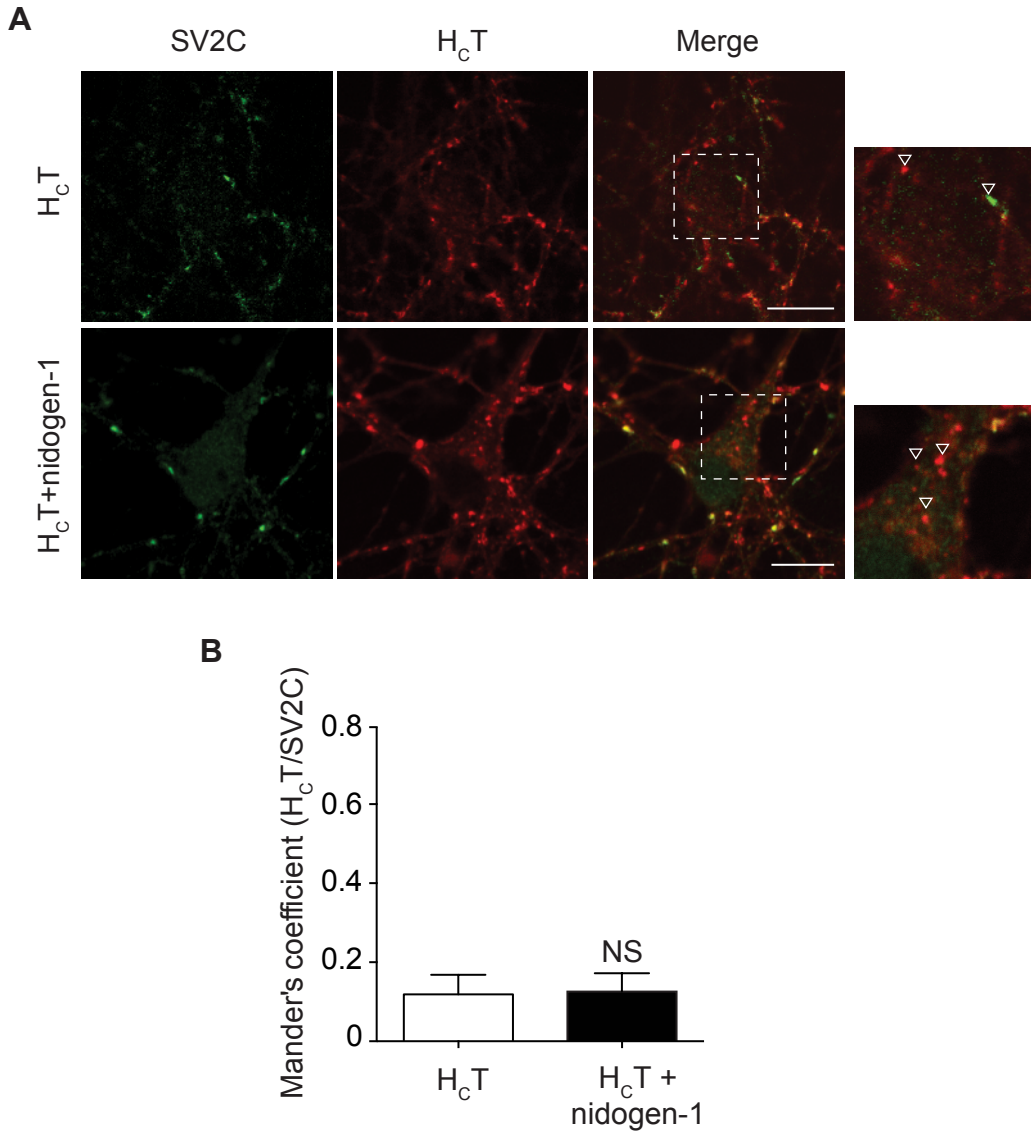

Figure 4-18. SV2C does not colocalise with H_CT in primary motor neurons

(A) Wild type primary motor neurons were incubated either with AlexaFluor555-H_CT (shown in red; 40 nM) alone, or in the presence of full-length recombinant nidogen-1 (1.6 nM) for 45 min at 37°C. Cells were fixed and immunostained for SV2C (in green). **(B)** Mander's coefficient was used as an indicator of co-localisation. Significance was assessed using unpaired with Welch's correction (n=3, 10 images per condition; NS, non significant; error bar: SD). Scale bar, 10 µm. Modified from (Bercsenyi et al., 2014). Reprinted with permission from AAAS.

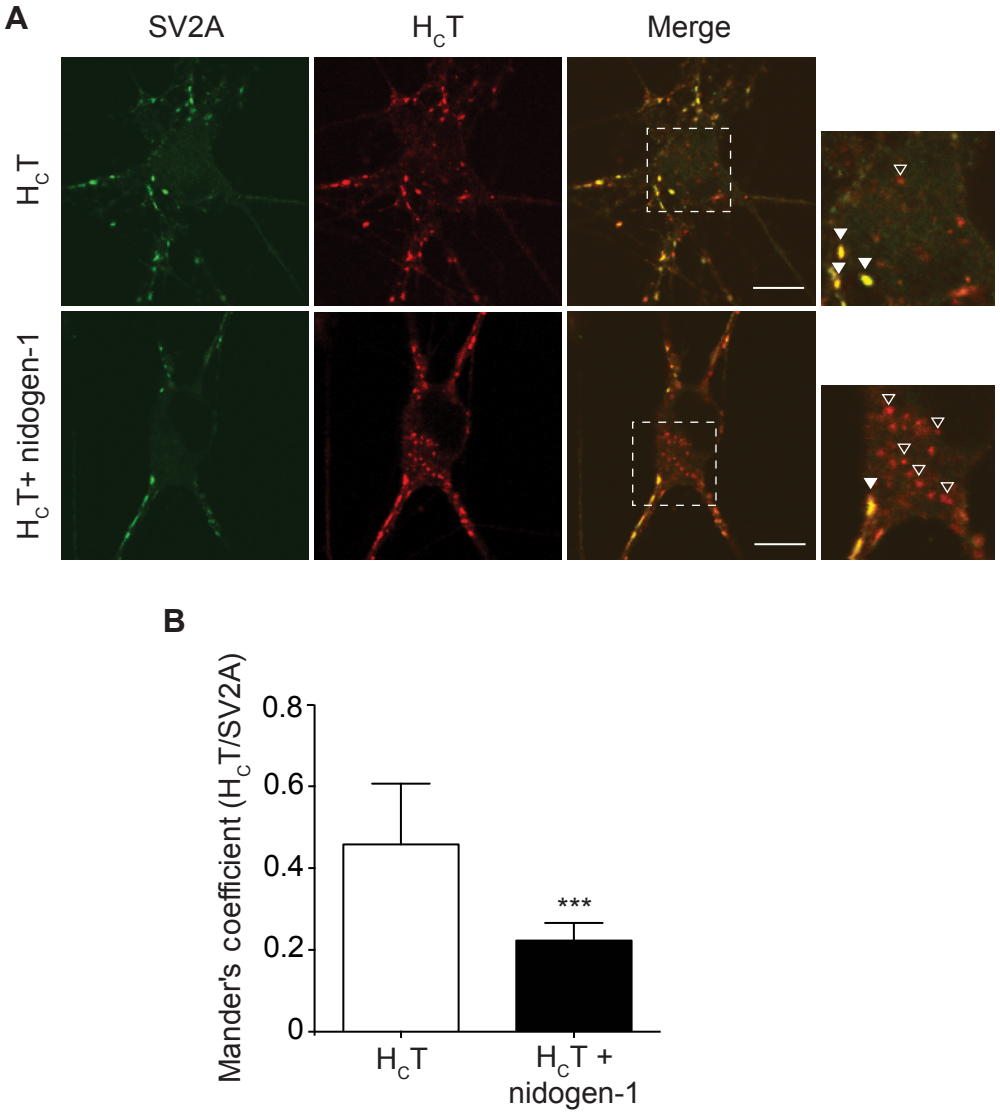

Figure 4-19. The colocalisation between SV2A and H_CT is decreased upon addition of soluble nidogen-1

(A) Wild type primary motor neurons were incubated either with AlexaFluor555-H_CT (shown in red; 40 nM) alone, or in the presence of full-length recombinant nidogen-1 (1.6 nM) for 45 min at 37°C. Cells were fixed and immunostained for SV2A (in green). The inset shows that there is an increase in the cell body pool of H_CT upon the addition of soluble nidogen-1 and this area contains no SV2A. **(B)** Mander's coefficient was used as an indicator of co-localisation. Significance was assessed using unpaired t test with Welch's correction (n=3, 10 images per condition; ***, $p<0.005$; error bar: SD). Scale bar, 10 µm. Modified from (Bercsenyi et al., 2014). Reprinted with permission from AAAS.

4.9 Nidogen-2 KO motor neurons show decreased H_CT binding

Single nidogen knock out (KO) mice are viable, but nidogen-1 KO animals display an ascending paralysis that worsens with age and females are not able to give birth (Dong et al., 2002). Both mutant lines were kindly provided by R. Nischt (University of Cologne).

I obtained primary motor neuron cultures from E13,5 nidogen-1 and nidogen-2 KO embryos and tested them for H_CT binding. When AlexaFluor555-H_CT was added to cells at a concentration of 40 nM for 45 min at 37°C, there was no striking difference between wild type cells and neurons lacking nidogen-1, or -2 (nidogen-1 KO: Figure 4-20, nidogen-2 KO: Figure 4-21). However, when H_CT-HA was added to nidogen-2 KO motor neurons at 10 nM on ice, I detected a small, but significant drop in H_CT binding in the KO cells (Figure 4-22). Since both nidogens are involved in the binding and subsequent uptake of H_CT in motor neurons, it is not surprising that the single KO cells did not display a major deficit in H_CT binding and internalisation. Both nidogen isoforms were shown to fulfil partially overlapping roles, and compensate for each other's loss in the KO animals (Mann et al., 1989, Ho et al., 2008, Kruegel and Miosge, 2010), and this in turn may help to maintain close to normal H_CT internalisation in single KO neurons.

The observation that there is a defect in H_CT binding only when it is used at a lower concentration further suggests that H_CT could use its alternative entry route through SV2A to gain access to the cell in the absence of available nidogen binding sites.

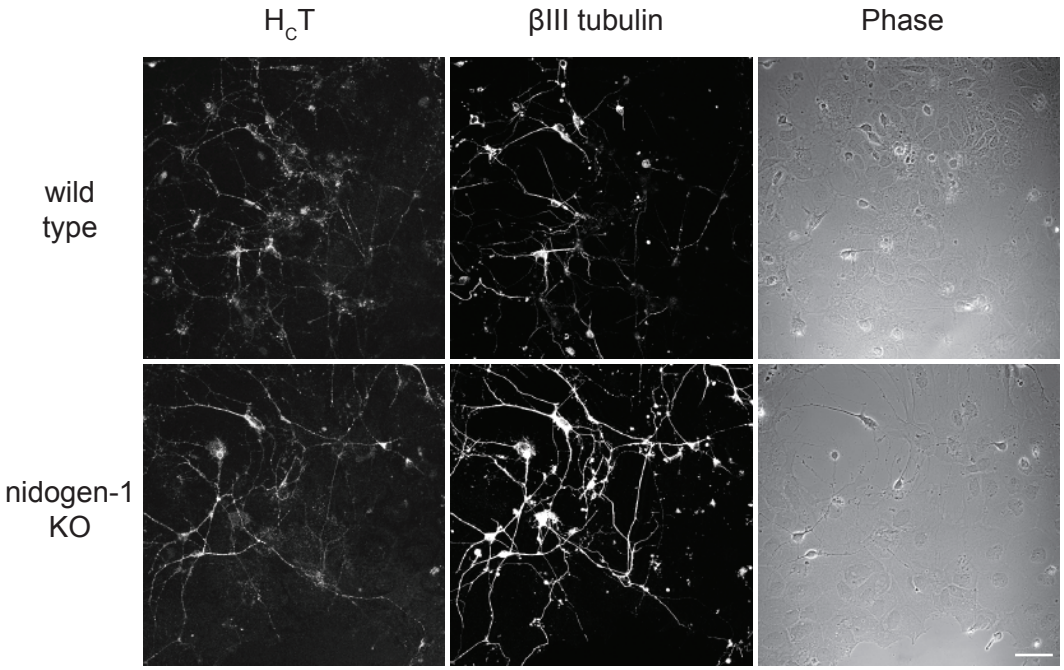

Figure 4-20. Nidogen-1 KO neurons internalise H_CT to a similar extent as wild type cells

Wild type and nidogen-1 KO motor neurons were incubated with 40 nM AlexaFluor555-H_CT for 45 min at 37°C, The cells were washed, fixed, permeabilised, blocked and stained for βIII tubulin to reveal the neuronal network. Scale bar: 50 µm.

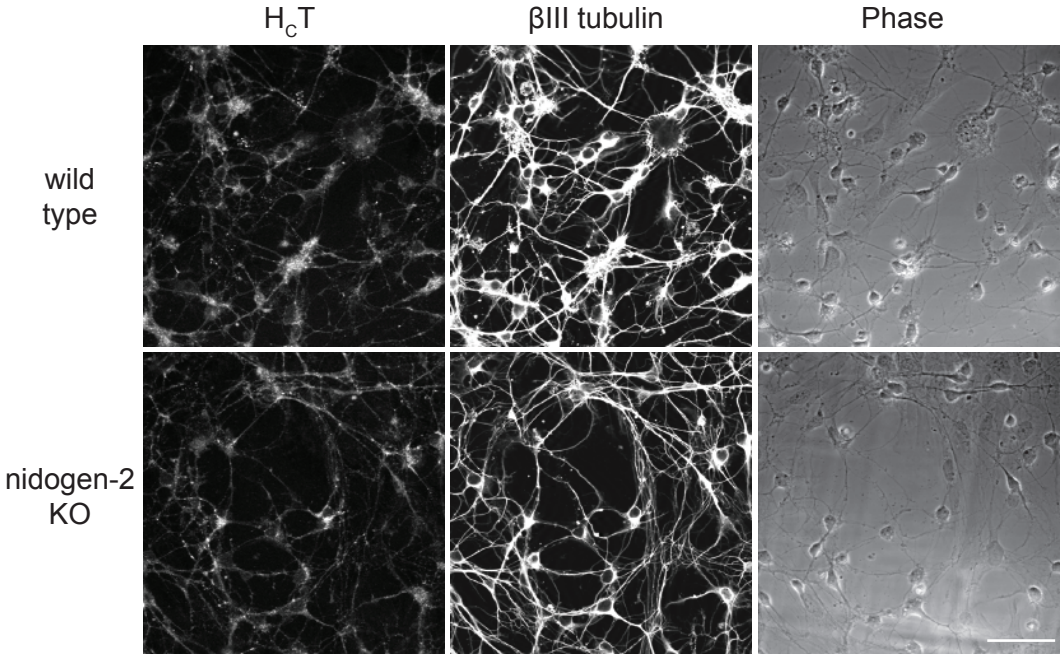

Figure 4-21. Nidogen-2 KO cells internalise H_CT to a similar extent as wild type cells

Wild type and nidogen-2 KO motor neurons were incubated with 40 nM AlexaFluor555-H_CT for 45 min at 37°C, The cells were washed, fixed, permeabilised, blocked and stained for βIII tubulin to reveal the neuronal network. Scale bar: 50 µm.

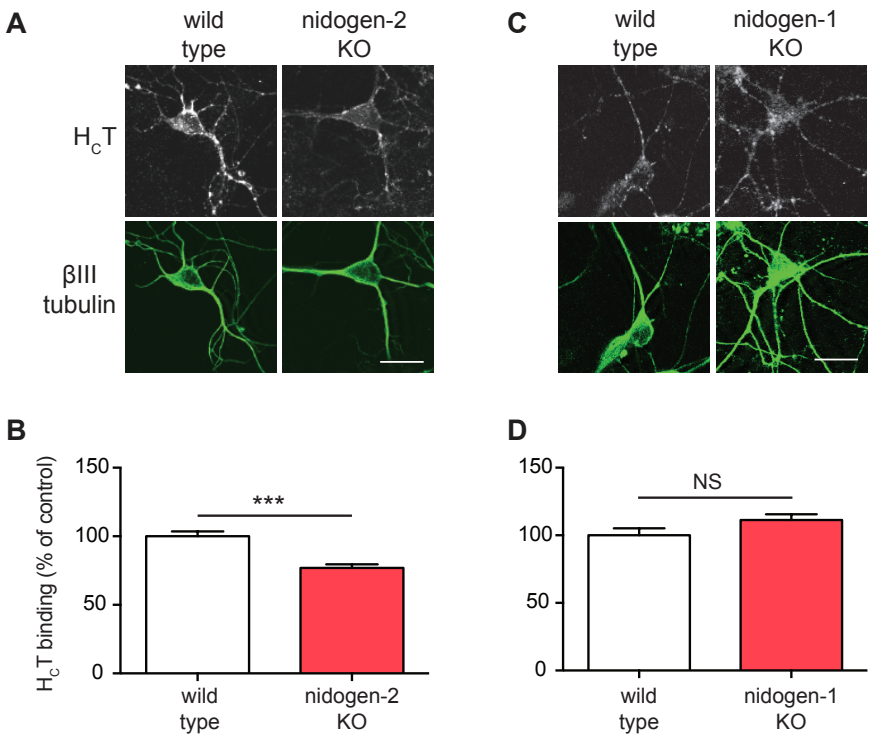

Figure 4-22. There is a significant impairment in H_CT binding of nidogen-2 KO neurons when H_CT is used at a lower concentration

(A,C) Wild type and nidogen-2 KO (A) or nidogen-1 KO (C) motor neurons were incubated with 10 nM H_CT-HA for 10 min on ice. The cells were washed, fixed, permeabilised, blocked and stained for βIII tubulin to reveal the neuronal network. Modified from (Bercsenyi et al., 2014). Reprinted with permission from AAAS.
(B,D) Fluorescence intensity was quantified in 10 images using a βIII tubulin mask (in green). Scale bar, 20 μm. Following setting the level of samples lacking H_CT to zero, the mean fluorescence intensity was plotted for each genotype as percentage of wild type and statistical significance was analysed using unpaired t-test. (n=3; ****, $p<0.001$; error bar: SD). Scale bar: 20 μm.

4.10 The nidogen-2 content of the NMJ is a limiting factor for H_CT binding

4.10.1 H_CT is taken up by the motor neuron endplate at the NMJ

To show that H_CT is taken up by the presynaptic terminal of the motor neuron endplate, the anterior part of the lower hindlimb of a wild type mouse was injected with HA-H_CT and after 60 min the animal was terminally anesthetised and transcardially perfused with saline followed by 4% PFA. The *extensor digitorum longus* (EDL) muscle was dissected, cryoprotected and sectioned (20 µm thickness) on a cryostat. The sections were post-fixed, air dried, blocked and stained with rat anti-HA and goat anti-choline acetyl transferase (ChAT) antibodies over night at room temperature in a wet chamber. Following several washes, AlexaFluor555-BTX, goat AlexaFluor647-conjugated anti-rat and donkey AlexaFluor488-conjugated anti-goat (green) were added for 1 h at room temperature. BTX labels the postsynaptic terminal of the NMJ, while ChAT labels the presynaptic membrane. J. B. Bryson (UCL-Institute of Neurology) performed the experiment and I imaged the slides (Figure 4-23). H_CT localises to the presynaptic side of the NMJ and it is taken up by motor neuron axons innervating the muscle (top right panel).

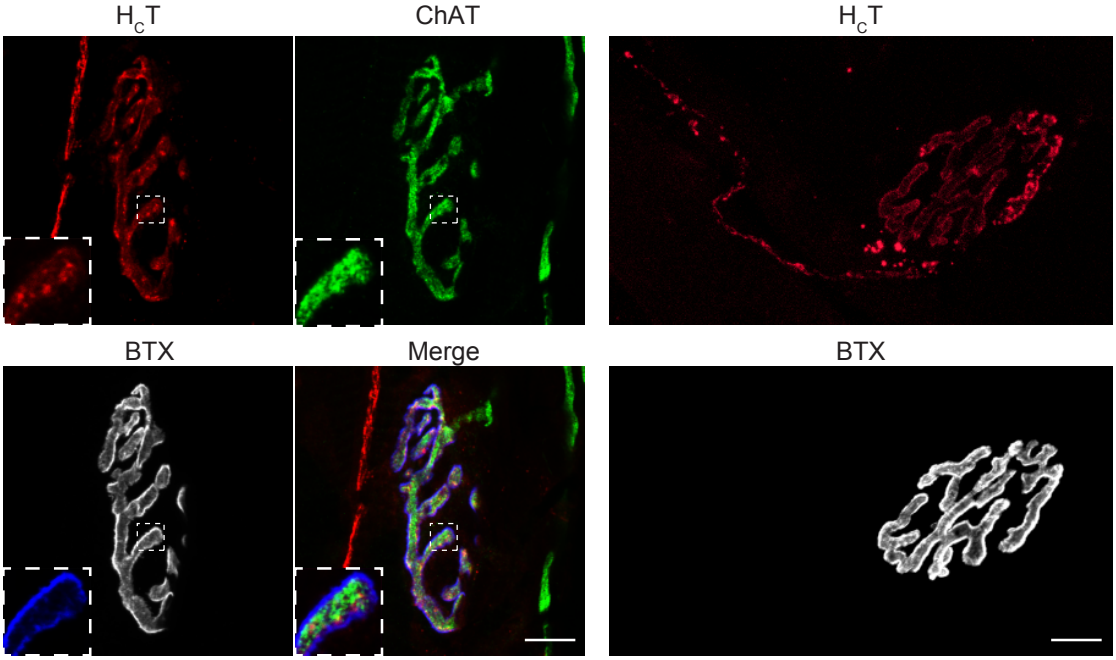

Figure 4-23. H$_C$T is taken up at the presynaptic side of the NMJ

The anterior part of the lower hindlimb of adult mice was injected with HA-H$_C$T. After 60 min, animals were transcardially perfused; the muscles were dissected, post-fixed, sectioned and stained for HA (pseudocolored red), ChAT (green) and AlexaFluor555-α-BTX (pseudocolored grey) to label NMJs. H$_C$T binds to the presynaptic site of the NMJ, where ChAT is localised (inset). H$_C$T is taken up by the motor neuron and it is retrogradely transported in the motor neuron axons (top right panel). Scale bar: 10 μm. Modified from (Bercsenyi et al., 2014). Reprinted with permission from AAAS.

4.10.2 The nidogen-2 content of the NMJ correlates with H$_C$T binding

I sought to test if H$_C$T is taken up together with nidogen-2 at the NMJ. To do this, the lower hindlimb of a wild type mouse was injected with H$_C$T-HA and the mouse was anesthetised after 60 min for transcardial perfusion with saline followed by 4% PFA. The *extensor digitorum longus* (EDL) muscle was dissected, cryoprotected and sectioned (20 μm) on a cryostat. The sections were blocked and stained with rat anti-HA and rabbit anti-nidogen-2 primary antibodies for 1 h at 37°C. Following several washes, AlexaFluor555-BTX, AlexaFluor647-anti-rat and AlexaFluor488-anti-rabbit were added for 1 h at 37°C. The unbound probes were washed off and the sections were mounted for imaging. J. B. Bryson (UCL-Institute of Neurology) performed the injection and processed the tissue; I performed the immunohistochemistry and imaged the slides. Nidogen-2 and H$_C$T localises to the same compartment of the NMJ, but nidogen-2 is only partially taken up into

endosomes together with H_CT (Figure 4-24, Movie 3). It became clear however, that there is a strong correlation between the nidogen-2 content and H_CT binding ability of the NMJ. Some NMJs did not contain nidogen-2 and these did not bind H_CT, whilst others with high nidogen-2 content bound vast amount of H_CT (Figure 4-25). I have observed that not every NMJ in the LAL muscle bind H_CT (Figure 3-13). To assess the level of correlation between nidogen-2 and H_CT content, 50 images of NMJs were taken and the fluorescence intensity of H_CT vs. nidogen-2 staining was compared using Spearman correlation.

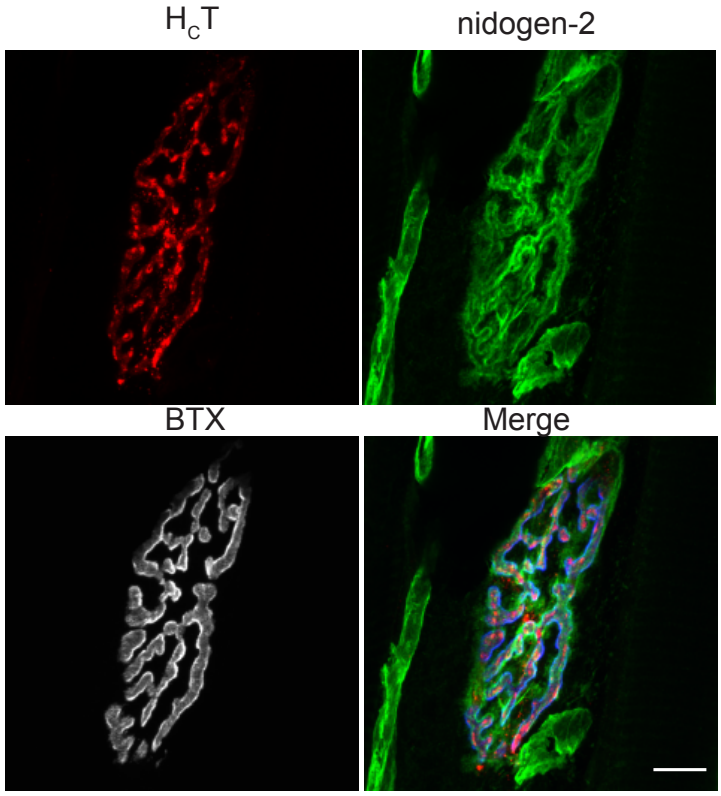

Figure 4-24. Nidogen-2 is present where H_CT is taken up at the NMJ

The anterior part of the lower hindlimb of adult mice was injected with HA-H_CT. After 60 min, animals were transcardially perfused; the muscles were dissected, post-fixed, sectioned and stained for HA (pseudocolored red), nidogen-2 (green) and AlexaFluor555-α-BTX (pseudocolored grey) to label NMJs. Nidogen-2 accumulates in areas where H_CT is taken up with high efficiency (bright red spots). Scale bar: 10 μm. Modified from (Bercsenyi et al., 2014). Reprinted with permission from AAAS.

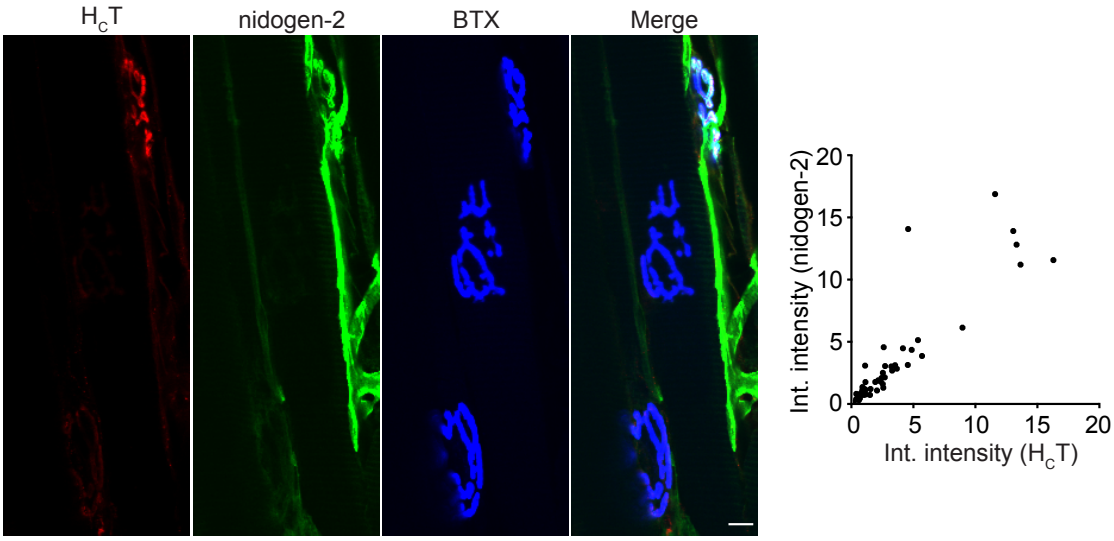

Figure 4-25. Nidogen-2 content of the NMJ correlates with the amount of H_CT binding

The anterior part of the lower hindlimb of adult mice was injected with HA-H_CT. After 30 min, animals were transcardially perfused; the muscles were dissected, post-fixed, sectioned and stained for HA (pseudocolored red), nidogen-2 (green) and AlexaFluor555-α-BTX (pseudocolored blue) to label NMJs. The fluorescence intensity of both H_CT and nidogen-2 intensity were measured under the BTX mask. The results were paired and plotted to analyse for correlation with Spearman test (r=0.9227; ****, p<0.001; n=3; Scale bar: 10 μm). Modified from (Bercsenyi et al., 2014). Reprinted with permission from AAAS.

4.10.3 The single nidogen KO NMJs bind significantly less H_CT than their wild type counterparts

Since the nidogen-2 content of the NMJ is a determinant of H_CT binding, I wanted to test if the NMJs of nidogen KO animals show a greater decrease in H_CT binding than the KO motor neurons (Figure 4-22). To test this, I dissected LAL muscles from wild type, nidogen-1 and nidogen-2 KO animals. H_CT-HA was added to the medium, and it was left to bind and enter in the NMJs for 2 h at 37°C. The muscle preparations were washed thoroughly in HBSS buffer before fixing overnight at 4°C. The samples were permeabilised, blocked and stained the following day with rat anti-HA and goat AlexaFluor488-anti-rat antibodies to reveal bound H_CT, rabbit anti-nidogen-2 and goat AlexaFluor647-anti-rabbit antibodies to detect nidogen-2 and AlexaFluor555-BTX was used to label NMJs. Initially, due to the high background in the 488 channel, a higher concentration of H_CT was used

(60 nM). At this concentration both nidogen-1 and nidogen-2 KO NMJs bind H_CT close to wild type levels (Figure 4-26).

However, when the concentration of H_CT was dropped to 20 nM, the KO NMJs lose their ability to bind and internalise H_CT (Figure 4-27). Note the large error bar in the fluorescence intensity of H_CT staining in wild type NMJs. This is due to H_CT specifically targeting only a subset of NMJs (the ones with high nidogen-2 content) since the imaging was done blind; this resulted in some images where no H_CT was bound to the NMJ.

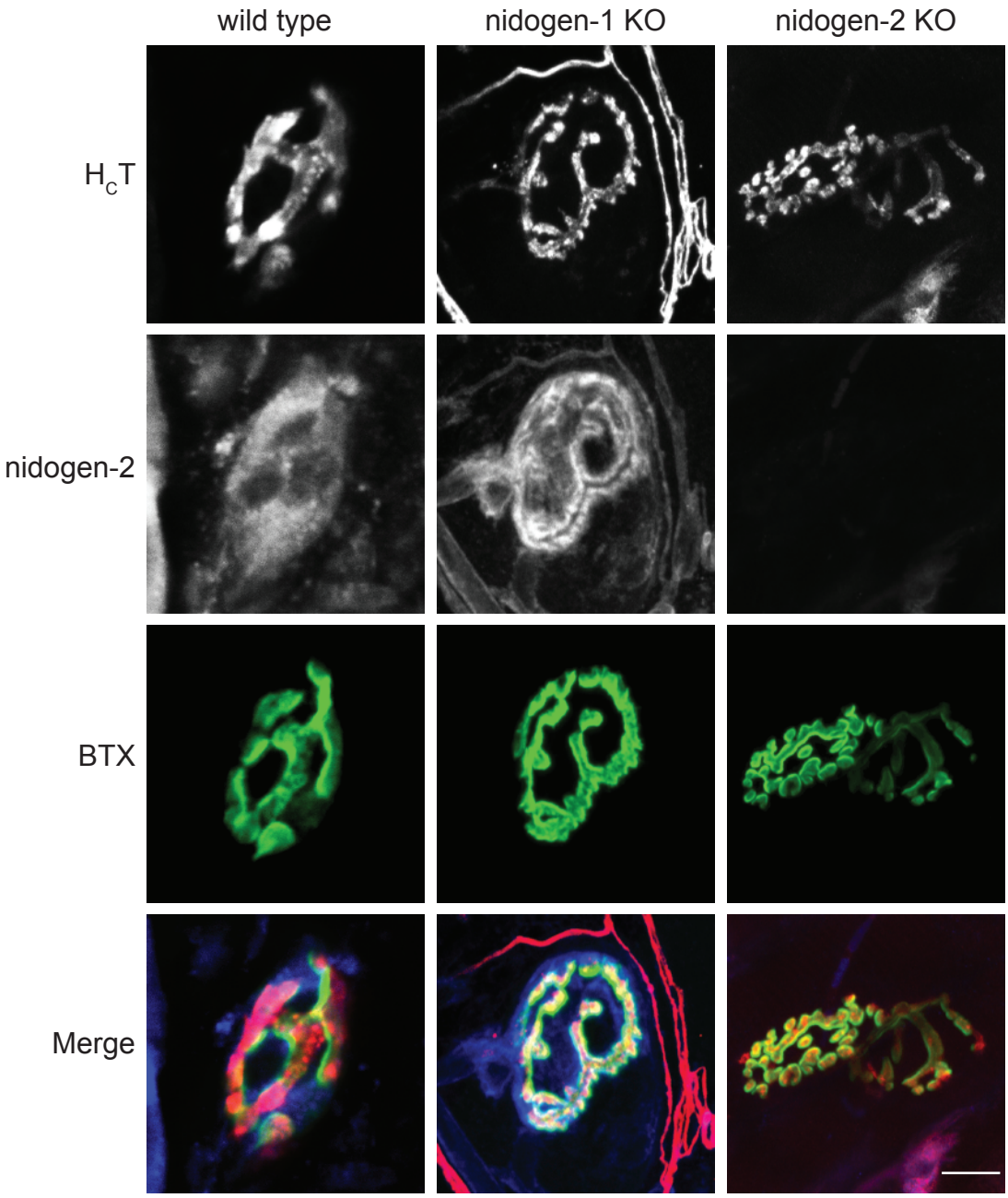

Figure 4-26. H_CT binds to nidogen KO NMJs at 60 nM

LAL muscles of wild type, nidogen-1 and -2 KO animals were incubated with HA-H_CT, fixed and stained for HA (pseudocolored grey, red in merge), nidogen-2 (pseudocolored grey, blue in merge) and AlexaFluor555-BTX (pseudocolored green) to identify NMJs. Scale bar, 10 µm.

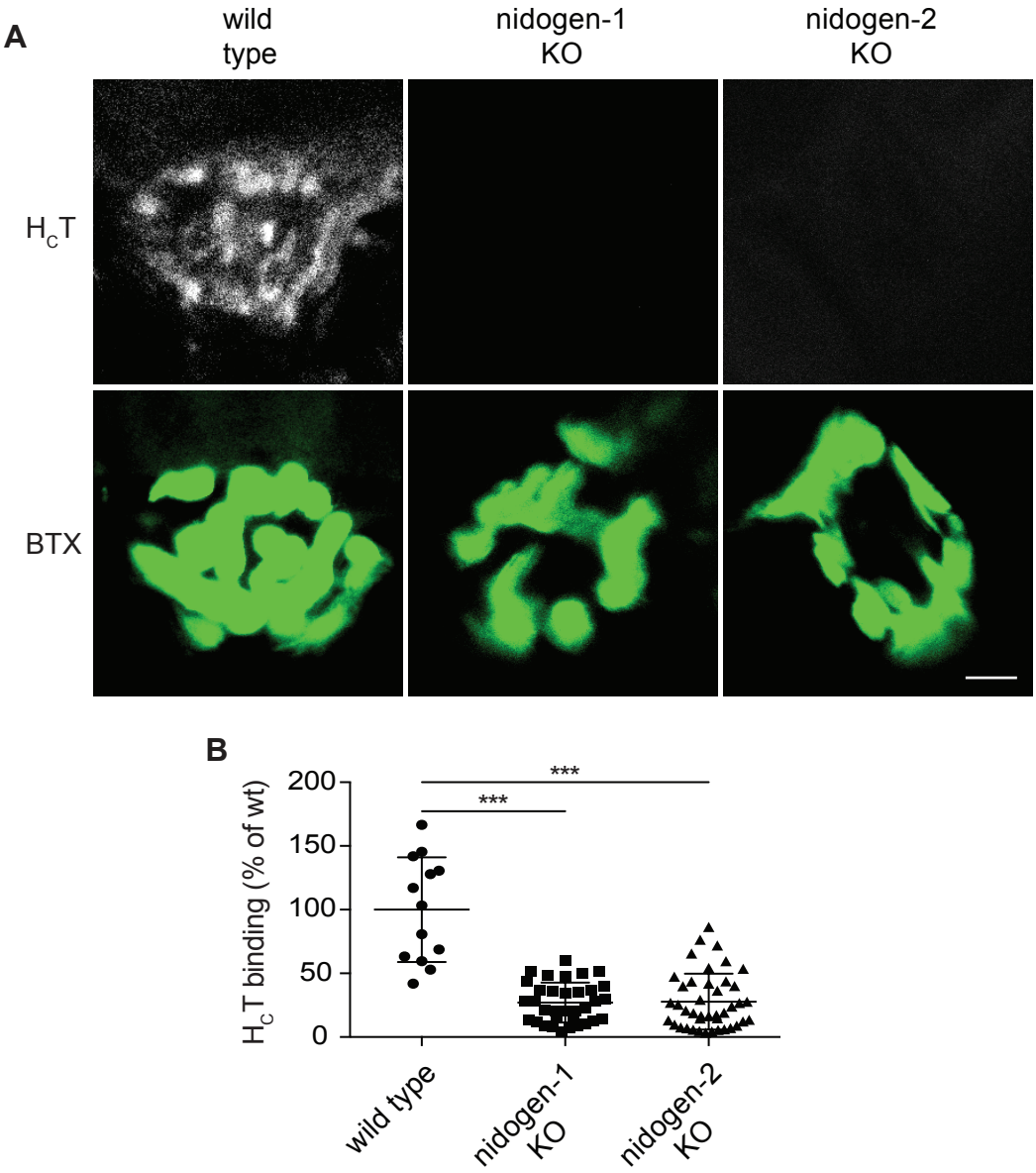

Figure 4-27. H_CT does not bind to nidogen-1 and nidogen-2 KO NMJs at 20 nM

LAL muscles of wild type, nidogen-1 and -2 KO animals were incubated with HA-H_CT, fixed and stained for HA (pseudocolored grey) and AlexaFluor555-BTX (pseudocolored green) to identify NMJs. Scale bar, 5 µm. (**B)** Both nidogen-1 and -2 KO NMJs show a significant decrease in their ability to bind and internalise H_CT. Significance was tested with by Kruskal-Wallis test (****, $p<0.001$) followed by Dunn's multiple comparisons test. (n=3 animals per group, 20 images per animal; ****, $p<0.001$; error bar: SD). Modified from (Bercsenyi et al., 2014). Reprinted with permission from AAAS.

4.10.4 Nidogen-1 and -2 KO NMJs bind BoNT/A at similar levels to wild type NMJs

As disruption of the general structure of the NMJ has been reported in nidogen KO animals (Fox et al., 2008), I wanted to test the functionality of the NMJ in KO animals by testing whether botulinum neurotoxin (BoNT/A) binding is affected by the loss of nidogen expression at the NMJ. BoNTs rely on synaptic vesicle recycling and binding to synaptic vesicle proteins (either SV2A-C or synaptotagmin I/II) for their entry into motor neurons (Mahrhold et al., 2006, Dong et al., 2006, Peng et al., 2011, Benoit et al., 2014). The GST-tagged binding fragment of BoNT/A (H_CA; 12 µg in 4 µl) was injected into the TA muscle of wild type, nidogen-1 and nidogen-2 KO mice, as described above, and muscle sections were labelled with rabbit anti-GST followed by staining with goat AlexaFluor488-anti-rabbit and AlexaFluor555-BTX to label NMJs. J. B. Bryson (UCL-Institute of Neurology) performed the injection and processed the tissue, I performed the immunohistochemistry and imaged the slides.

Both nidogen-1 and nidogen-2 KO NMJs bind H_CA (Figure 4-28). This result confirms that synaptic vesicle recycling and SV2A presentation on the PM of the motor neuron endplate is not impaired in the nidogen KO animals. Hence, the dramatic reduction of H_CT binding is certainly not due to the lack of synaptic vesicle recycling, which would lead to the reduced accessibility of SV2A.

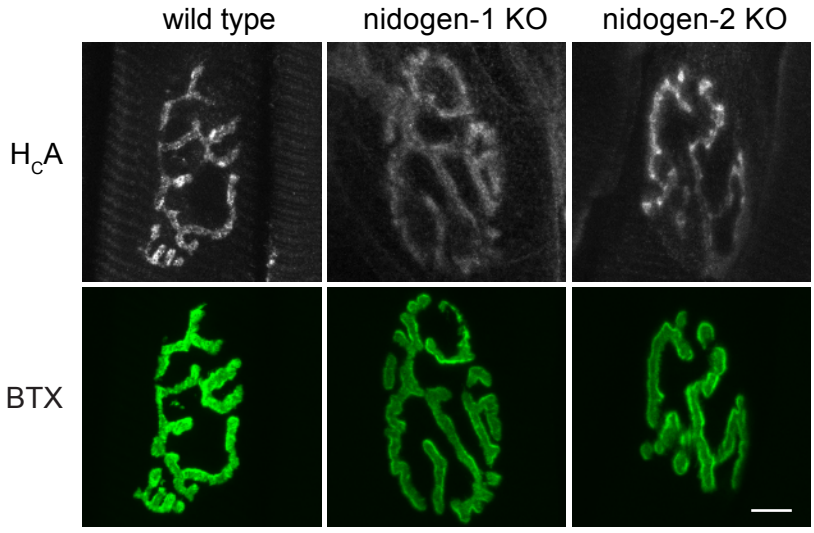

Figure 4-28. Single nidogen KO NMJs bind H_CA at a comparable level to wild type

The *tibialis anterior* (TA) muscle of wild type or nidogen-1 and nidogen-2 KO mice was injected with GST-H_CA. After 30 min, the animals were transcardially perfused, the muscles cryosectioned before staining for GST (pseudocolored grey). NMJs were labeled with AlexaFluor555-BTX (pseudocolored green). Scale bar, 10 µm. Modified from (Bercsenyi et al., 2014). Reprinted with permission from AAAS.

4.10.5 Additional soluble nidogen-1 rescues the H_CT binding defect in nidogen-1 KO NMJs

To prove that the inability of nidogen-1 KO NMJs to bind and internalise H_CT at 20 nM is due to the loss of nidogen-1, I wanted to prove that binding can be rescued by the addition of soluble recombinant nidogen-1 to the medium during H_CT incubation. LAL muscles were isolated from wild type and nidogen-1 KO animals and incubated in motor neuron medium in the presence or absence of full-length recombinant His_9-tagged nidogen-1. 20 nM H_CT-HA was added to the medium for 2 h at 37°C. The muscles were washed and fixed overnight at 4°C. The following day rat anti-HA and mouse anti-His antibodies were added followed by goat AlexaFluor488-anti-rat, goat AlexaFluor647-anti-rabbit and AlexaFluor555-BTX. As expected, nidogen-1 KO NMJs did not bind H_CT in the absence of recombinant nidogen-1 (middle panel, Figure 4-29). However, when recombinant nidogen-1 was present in the medium, the nidogen-1 KO NMJ showed equivalent H_CT binding to the wild type NMJ (Figure 4-29). The anti-His staining revealed that

recombinant nidogen-1 binds to the NMJ, even though its localisation is more disperse in the KO than in the wild type NMJ (right panels, Figure 4-29).

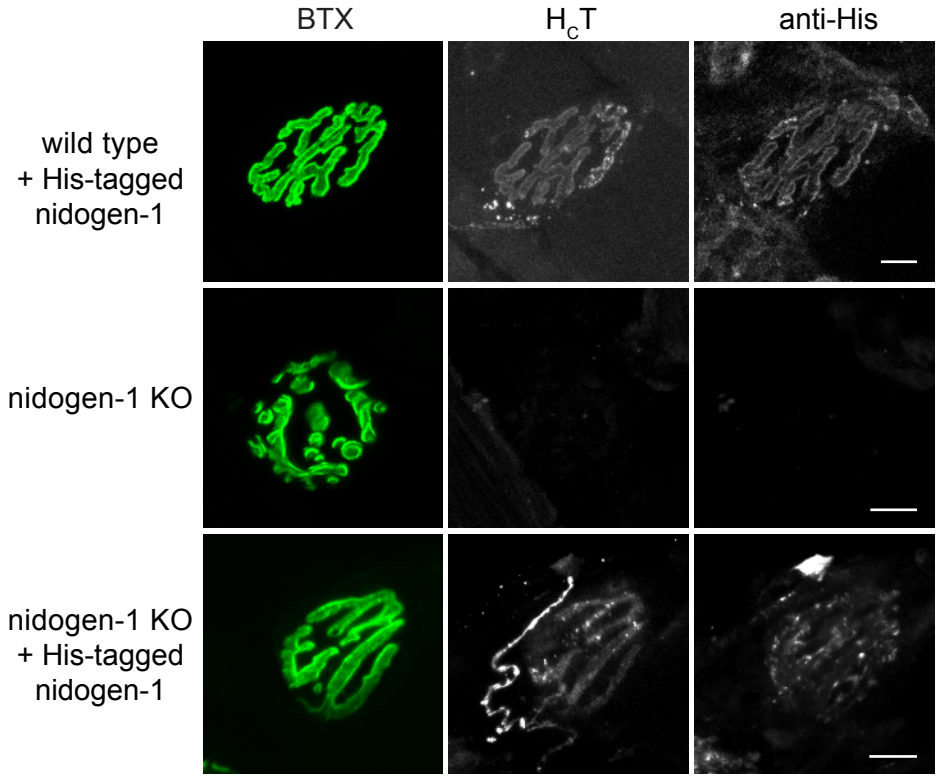

Figure 4-29. Recombinant exogenous nidogen-1 rescues the H_CT binding defect in nidogen-1 KO NMJs

LAL muscles of wild type and nidogen-1 KO animals were incubated with HA-H_CT in the absence or the presence of full-length His_9-tagged recombinant nidogen-1. Muscles were fixed and stained for HA (pseudocolored grey, middle), His (pseudocolored grey, right) and AlexaFluor555-BTX (pseudocolored green, left). Scale bar, 10 µm. Modified from (Bercsenyi et al., 2014). Reprinted with permission from AAAS.

4.11 Double KO hindbrains do not bind H_CT

In our hands, nidogen-1 and -2 double KO mice are not viable beyond E11,5. This prevented me from testing double KO motor neurons for H_CT binding. As an alternative, I dissected the hindbrains of embryos at E11,5 and incubated the samples with 20 nM H_CT-HA for 1 h at 37°C. The hindbrains were washed with HBSS and fixed in 4%PFA in PBS for 2 h at room temperature. Following permeabilisation with PBSTr for 1 h and blocking with IFBB for 1 h, the hindbrains

were stained with rat anti-HA and rabbit anti-βIII tubulin in IFBB for 1 h at room temperature. The unbound antibodies were removed with washes and goat AlexaFluor555-conjugated anti-rat and goat AlexaFluor647-conjugated anti-rabbit secondary antibodies were added for 1 h at room temperature. After three washes for 30 min, the tissue was post-fixed for 10 min and mounted with Mowiol. Imaging was done as before, but to capture the whole sample, 3x9 tiles were taken. The nidogen DKO hindbrains bound significantly less H_CT than their wild type counterparts (Figure 4-30 A,C), however, a subset of cells within the developing mesencephalon bound H_CT with high affinity (Figure 4-30 B). At closer inspection it became clear that this subset of cells is a much smaller population than in the wild type, however I could not investigate the identity of these cells due to the lack of expertise in our laboratory. E11,5 is a very early stage in mesencephalic development, the first neural precursors do not leave the ventricular zone before E12,5. These cells are most probably early precursor cells, which secrete a lot of ECM molecules to prepare the environment for the arrival of the migrating neurons.

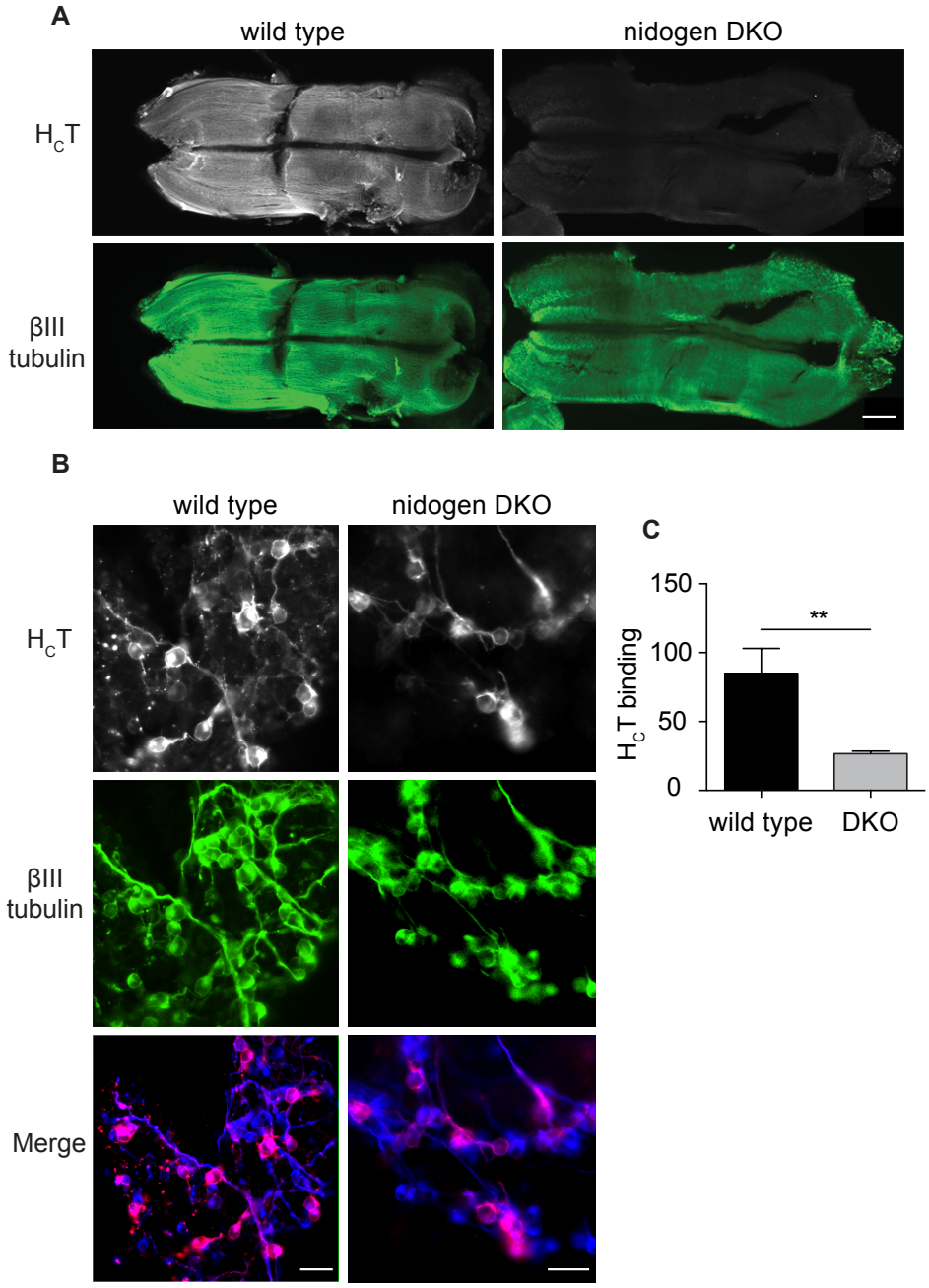

Figure 4-30. Nidogen DKO hindbrains do not bind H_CT, with an exception of a small region within the mesencephalon.

(A) Wild type and nidogen DKO hindbrains were dissected from E11,5 mouse embryos and tested for H_CT-HA binding. 3x9 tiles were taken to observe the whole tissue. Scale bar: 1 mm. **(B)** A small subset of βIII tubulin positive cells within the mesencephalon still bind H_CT even in the absence of both nidogen isoforms, but within this region there are less H_CT positive cells than in the wild type. Scale bar: 20 µm. **(C)** The fluorescence intensity of HA staining was quantified using Image J, the average value for wild type tissue was set at 100% and the results were plotted to test for statistical significance. Unpaired t test was used to assess significance (n=2 animals per group; ** $p<0.01$). Modified from (Bercsenyi et al., 2014). Reprinted with permission from AAAS.

4.12 Mice lacking nidogen-2 are less sensitive to tetanus intoxication

Nidogen-1 KO mice presented with a severe epileptic phenotype alongside ascending progressive paralysis (Kohling et al., 2006). As a result of this, we were not able to use these mice to test the effects of TeNT *in vivo* (Figure 4-31). Nidogen-2 KO mice show no epileptic symptoms and present milder hindlimb paralysis at a later stage in life than nidogen-1 KO mice. We decided to test the sensitivity of nidogen-2 KO mice to general tetanus. To do this, adult weight matched nidogen-2 KO mice were injected with different lethal doses of TeNT intraperitoneally (1.5, 3, 6 and 12 ng/kg). The mice were closely monitored and terminated at the loss of righting reflex. Nidogen-2 KO mice survived significantly longer than their wild type counterparts when injected with a lower (1.5 ng/kg) dose of TeNT (Movie 4). However, when the dosage was increased, there was no difference between the different genotypes (Figure 4-32). This might be due to the alternative entry pathway used by TeNT when it is applied at high concentrations.

Mice injected with high doses of TeNT displayed botulism-like symptoms (Matsuda et al., 1982). Interestingly we found that nidogen-2 KO mice injected with TeNT showed botulism like symptoms: they had a silver crescent in their eyes, which resembled *keratoconjuctivitis sicca* (‘Silver eye syndrome’, Figure 4-32 B). *Keratoconjuctivitis sicca* is due to the block of the lacrimal gland and production of tears, it is one of the characteristic symptoms of botulism in mice (Suwan-apichon et al., 2006). This result further suggests that TeNT has an alternative entry route at the NMJ, which is independent of nidogens, and resembles that used by BoNTs.

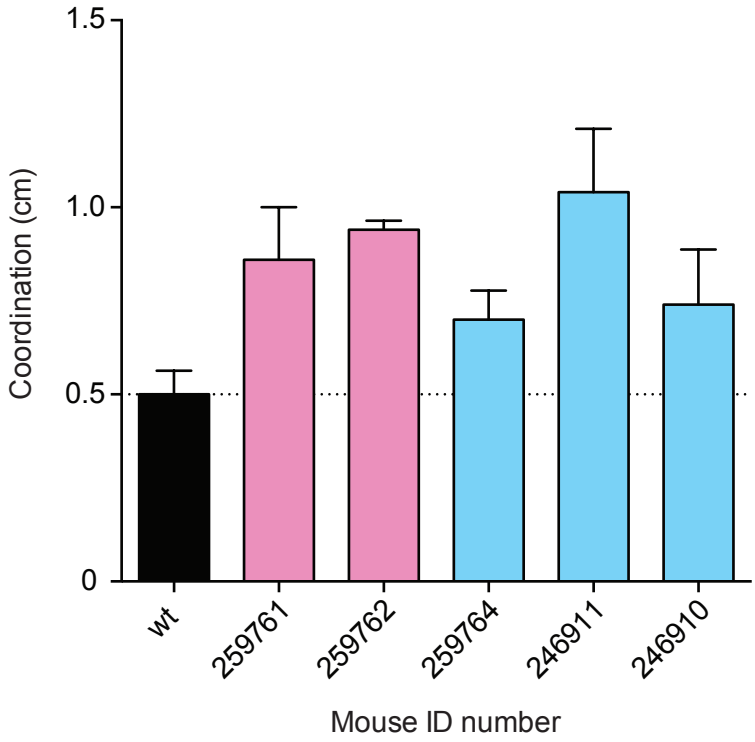

Figure 4-31. Nidogen-1 KO animals display a coordination defect from a young age

The paws of 3 months old nidogen-1 KO mice (2 females, pink and 3 males, blue) were painted, the mice were let to walk on a white stripe of paper and the distance between the front and hind footprint was determined on both sides (coordination, cm). The distance between the front and hind footprints of nidogen-1 KO animals is higher than normal; this is due to severe coordination defects caused by early-onset progressive paralysis.

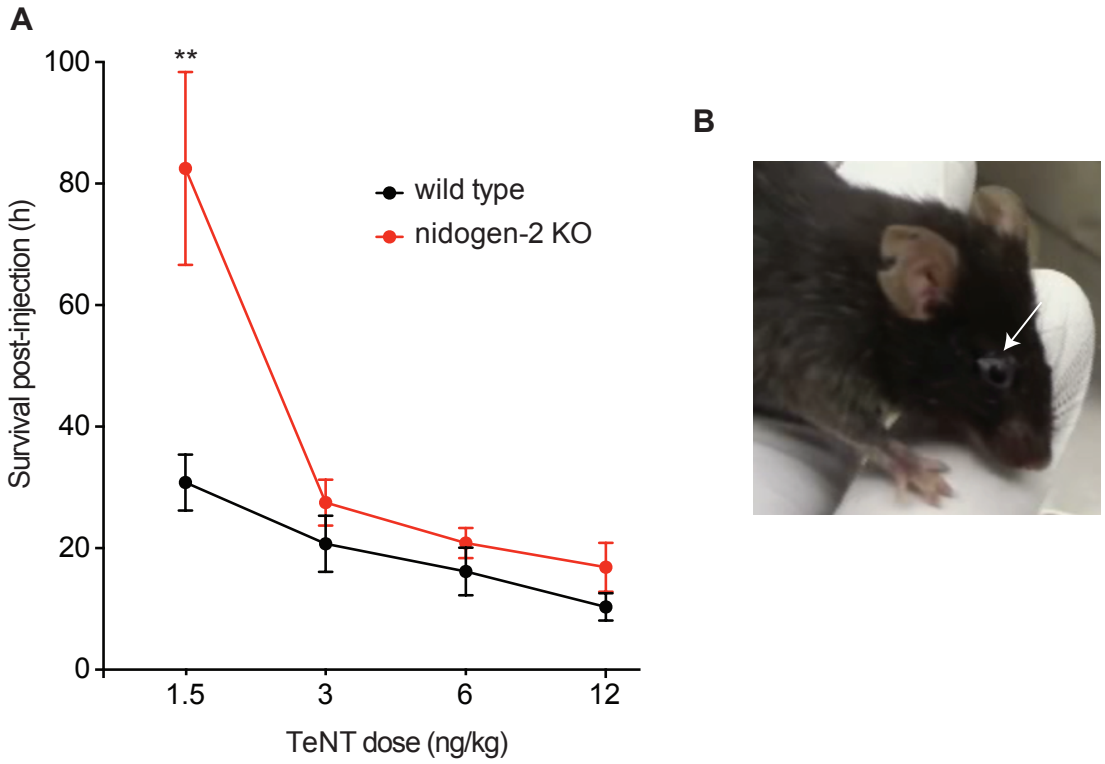

Figure 4-32. Nidogen-2 KO mice are less sensitive to tetanus intoxication

(A) Age and weight matched nidogen-2 KO and wild type mice were injected intraperitoneally with TeNT and monitored for up to 96 h. The time of termination due to loss of righting reflex was plotted against the TeNT dose. Note that generalised tetanus in nidogen-2 KO animals is significantly delayed at lower doses (1.5 ng/kg) compared to wild type controls (n=2 experiments, minimum 2 mice per group; t-test; **, $p<0.01$; error bar: SD). Modified from (Bercsenyi et al., 2014). Reprinted with permission from AAAS.
(B) Nidogen-2 KO mice presented with a grey crescent in their eyes (white arrow), the symptom of *keratoconjuctivitis sicca*, which is a characteristic of botulism.

4.13 Summary

- Both nidogen-1 and -2 are present in primary motor neuron cultures.
- Nidogen-2 is bound and internalised together with H_CT in motor neurons
- The G2 domain of nidogen-1 fits into the 'R' pocket of H_CT, in the same site where the N1 peptide binds.
- Point mutations within the 'R' site decrease H_CT binding to both the N1 and N2 peptides.
- Both nidogen-1 and -2 bind to H_CT directly and this interaction is blocked by the N1 and N2 peptides, respectively.
- Exogenous full-length nidogen-1 enhances both binding and internalisation of H_CT in motor neurons; this effect is completely blocked by the N1 peptide.
- Co-injection of TeNT with soluble nidogen-1 leads to an earlier onset of tetanic paralysis.
- The protein tyrosine phosphatase receptor. LAR colocalises with nidogen-2 and H_CT on the surface of motor neurons. TrkB colocalises with internalised H_CT in motor neurons. The TrkB antibody competes with H_CT binding to its receptor complex.
- Nidogen-2 internalisation is increased by BDNF stimulation, H_CT internalisation and starvation.
- H_CT colocalises with SV2A and this colocalisation is significantly decreased by the addition of exogenous full-length nidogen-1.
- When H_CT is used at a high concentration (40-60 nM), nidogen-1 and -2 KO motor neurons and NMJs show close to normal level of internalisation. But when H_CT concentration is dropped to 10-20 nM, nidogen-2 KO motor neurons bind significantly less H_CT than wild type cells and nidogen-1 and -2 NMJs bind significantly less H_CT than wild type muscles.
- Synaptic vesicle recycling is functional in nidogen-1 and -2 KO NMJs.
- Nidogen double KO animals do not survive until E13,5 and this prevented the experiments on primary motor neurons. I dissected hindbrains from E11,5 embryos and in lack of both nidogens, they do not bind H_CT, apart from a small subset of cells in the developing mesencephalon.

- Nidogen-2 KO animals are less sensitive to tetanus intoxication at lower concentrations (1.5 ng/kg). At higher TeNT concentrations, they display silver-eye syndrome; a characteristic of botulism.

Chapter 5. H_CT is transcytosed in motor neuron cultures together with nidogen-2

During TeNT intoxication, the light chain of TeNT is released in the cytoplasm of inhibitory interneurons, where it cleaves VAMP/synaptobrevin, leading to the silencing of inhibitory inputs on motor neurons. However, TeNT has access to motor neuron endplates only from the periphery. To get into inhibitory interneurons, it must be taken up by motor neurons, undergo axonal retrograde transport, get released in the vicinity of inhibitory synapses.

The trans-synaptic transfer of TeNT between motor neurons and interneurons has been accepted in the field for a long time; however, it has never been proven experimentally. To test this, H_CT must be applied in a compartmentalised culture, where the axonal network is isolated from the cell bodies. Campenot chambers have been available since 1977 (Campenot, 1977), but they are assembled on plastic bottom dishes, making fluorescent imaging problematic (Campenot et al., 2009). The other disadvantage of Campenot chambers is that their preparation is very labour intensive and the success of the chamber assembly relies on the skills of the operator. This in turn leads to high intrinsic variability. Microfluidic dishes are made of polydimethylsiloxane (PDMS), a transparent polymer, which can be covalently attached to glass bottom dishes after plasma cleaning (Park et al., 2006). This approach is less time-consuming, easier to master and yields less faulty/leaking chambers.

G. Menendez (Molecular Neuropathobiology laboratory, Cancer Research UK) established efficient protocols for the design and assembly of microfluidic chambers in our laboratory. There are 4 wells, or reservoirs, which are connected by two vertical channels on each side (16 mm long, 1 mm wide and 150 µm high; Figure 5-1 A). The channels are interconnected by microgrooves, which are shallow and long enough to provide microfluidic isolation between the two channels. Their dimension prevents crossing of freshly plated cells, but allows axons to grow through them. In the initial design, the microgrooves were 800 µm long, 10 µm wide and 3-4 µm high. These conditions provided microfluidic isolation, and allowed the crossing of sensory axons. However, motor neurons were never successfully

cultured in these chambers, since the microgrooves proved too long and motor neuron axons did not reach the other side.

5.1 Microfluidic chamber design and fabrication

I decided to reduce the length of the microgrooves to improve the crossing rate of motor neuron axons. G. Menendez (Molecular Neuropathobiology laboratory, Cancer Research UK) has previously observed, that cells had a tendency to migrate through microgrooves of up to 500 µm in length (Menendez, 2010). To avoid this side effect, I designed the microgrooves to be more shallow, 1-2 µm high, but shorter, only 500 µm in length (Figure 5-1). I prepared the new design using the software Canvas (ADC Systems), under the guidance of G. Menendez. The final design was replicated onto SU9 silicone wafers using photolithography (microLIQUID, Spain). These wafers were then used to make PDMS replicas, which can be mounted on plastic or glass bottom dishes and used as a microfluidic chamber. To avoid any damage to the original wafer, the first PDMS insets were used to create identical epoxy resins and use these as templates for the repetitive chamber preparations. Epoxy resins are more resistant to scratches and damage, than the original SU9 silicone wafer, and they are also easier to replace. I used 50 mm diameter glass bottom dishes for live cell imaging and immunofluorescence applications. PDMS insets were irreversibly attached to the dish using plasma cleaner. Plasma cleaner creates temporarily reactive chemical groups on the surface of the glass and PDMS that can form irreversible bonds if put in contact immediately after treatment.

Before plating motor neurons, I wanted to make sure that the pattern on the silicone wafer was correctly replicated. To check this, I prepared PDMS replicas and imaged them using scanning electron microscopy (SEM; performed by A. Weston, Cancer Research UK, London Research Institute). This analysis confirmed that the microgrooves are 500 µm long (Figure 5-1 B), 10 µm wide and only 1-2 µm deep (Figure 5-1 C). The walls of the microgrooves are not entirely smooth, and this provides a surface that is favourable for growing axons. There is

perfect fluidic isolation between the two channels, if a higher liquid column (volume) is added to the other side (Figure 5-1 D).

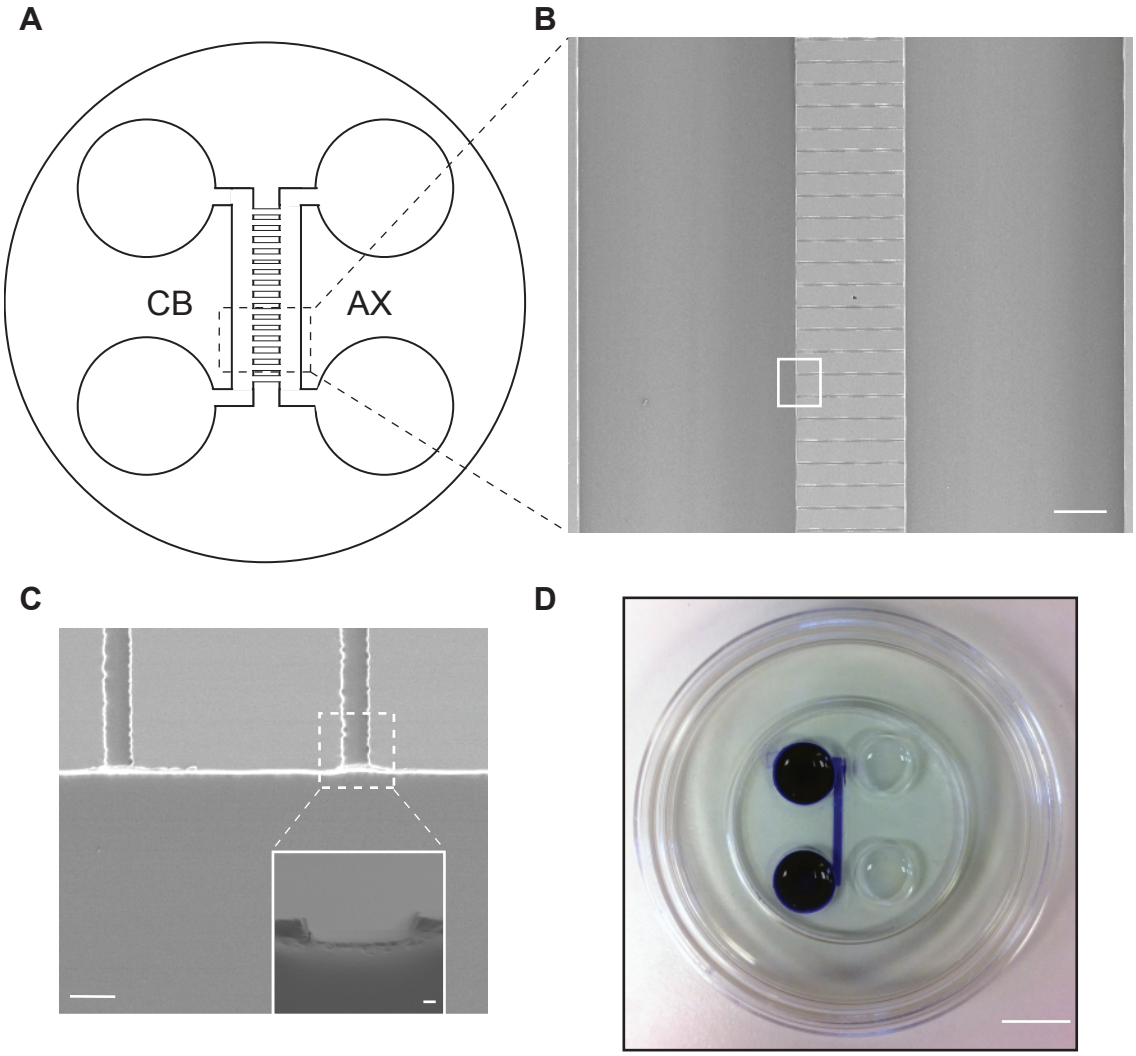

Figure 5-1. Microfluidic chambers with shorter, but shallower microgrooves still provide fluidic isolation

(A) The pattern of two longitudinal channels, and horizontal microgrooves connecting the channels was replicated onto a silicon wafer using photo-litography. This wafer was then used as a master to produce PDMS insets. Four round wells were punched into these insets to create the reservoir wells. **(B)** 500 µm long microgrooves connect the two longitudinal channels. Scale bar: 250 µm. **(C)** High magnification image from the highlighted area in (B). The microgrooves are 10 µm wide, but only 1-2 µm deep to avoid the loss of microfluidic isolation due to the shortening of the grooves. Scale bar: 20 µm on the main panel, 1 µm on the inset. **(D)** The PDMS inset was attached to a glass bottom Willco® dish and the microfluidic isolation was tested by adding 150 µl of PBS+bromophenol blue on the left side, and 200 µl PBS on the right side. The chamber was left for 24 h before imaging. There is microfluidic isolation between the two longitudinal channels. Scale bar: 10 mm.

5.2 Primary motor neuron cultures in microfluidic chambers

Once I have confirmed that the new design was correctly replicated on the PDMS insets and the chambers provided microfluidic isolation despite the decreased length of the microgrooves, I tested their suitability to grow primary motor neurons. Following the irreversible attachment of the PDMS inset to the glass bottom dish, I added PBS containing 0.8% BSA overnight at 37°C to both sides to make the hydrophobic surface produced by plasma cleaning more hydrophilic. The dishes were then coated with L-poly-ornithine/laminin overnight at 37°C, and to make sure that the microgrooves are coated as much as possible, a high volume difference was applied to the two sides and the chambers were tipped on one side to enhance the liquid flow. Freshly dissected primary motor neurons or freshly disaggregated embryonic stem (ES) cell derived motor neurons were loaded into one channel (somatodendritic compartment), using a high density (up to 100,000 cells) in low volume (10 µl) of motor neuron medium (completed with 1 ng/ml BDNF). Pipetting directly into the channel helped to avoid cells attaching in the reservoirs. A higher volume of motor neuron medium (15 µl) was added to the other channel (axonal compartment) to prevent the freshly plated cells from migrating through the microgrooves. Extra motor neuron medium of identical composition was added drop by drop on both axonal and somatodendritic sides once the neurons attached to the glass on the somatodendritic side (2 h at 37°C after plating), with a slightly higher volume on the somatodendritic compartment to aid axonal crossing.

The first axons reached the axonal compartment within 3 d after plating and there was a well-established dense axonal network by DIV 7. The shortening of the microgrooves has improved axon crossing, but the cell density in the somatodendritic compartment (100,000 cells per chamber) made imaging challenging (Figure 5-2). I have decreased the number of cells plated to 50,000 per chamber and this lead to a less dense axonal network, but allowed a better imaging of the somatodendritic compartment (Figure 5-3). All further experiments were performed using this cell density during plating.

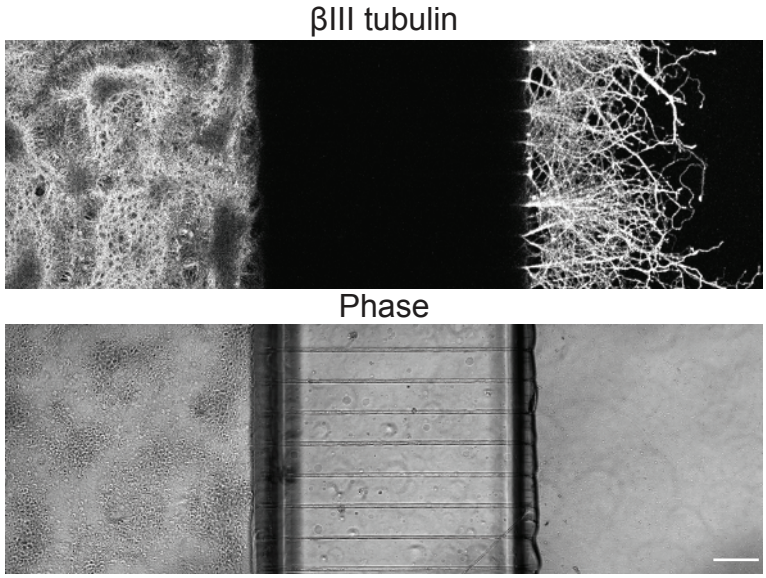

Figure 5-2. Primary motor neurons cross in microfluidic chambers when plated at a high density

Freshly dissected motor neurons (100,000 cell/chamber) were plated into the somatodendritic compartment (left hand side) of microfluidic chambers. The axons crossed and established a dense network by DIV 7 (right hand side). Scale bar: 100 µm.

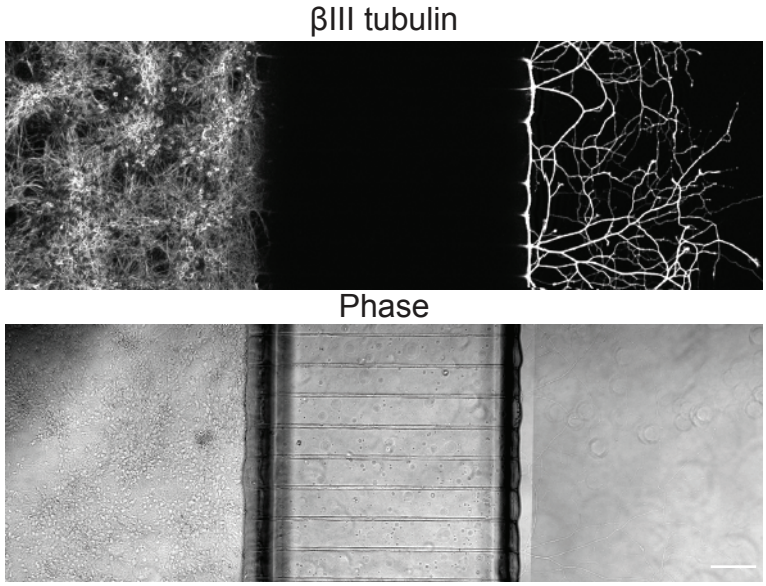

Figure 5-3. Primary motor neurons cross in microfluidic chambers when plated at medium density

Freshly dissected motor neurons (50,000 cell/chamber) were plated into the somatodendritic compartment (left hand side) of microfluidic chambers. The axons crossed and established a less dense, but extended network by DIV 7 (right hand side). Scale bar: 100 µm.

Next, I wanted to test whether only motor neurons were capable of crossing the microgrooves using a mixed ventral horn cell preparation. Unfortunately there is no specific antibody to label the axons of motor neurons, so I turned to murine neural progenitor cells, which express GFP (green fluorescent protein) under the motor neuron specific HB9 promoter. To do this, I differentiated the ES cells into ventral horn neurons, and plated them in the somatodendritic compartment. After 4 d, at the stage of early axonal crossing, I fixed the chambers and stained for βIII tubulin and SMI31. The SMI31 antibody recognises heavily phosphorylated neurofilament, which is most abundant in axons; this makes it an excellent axonal marker. I found that both motor neurons and non-motor neurons' axons crossed the microgrooves (Figure 5-4). This finding was not surprising, since only a proportion of the ES-derived neurons are GFP-positive and GFP-negative neurons grow extensive and long neurite networks. This experiment also showed that several axons coming from different neurons can bundle together in one microgroove.

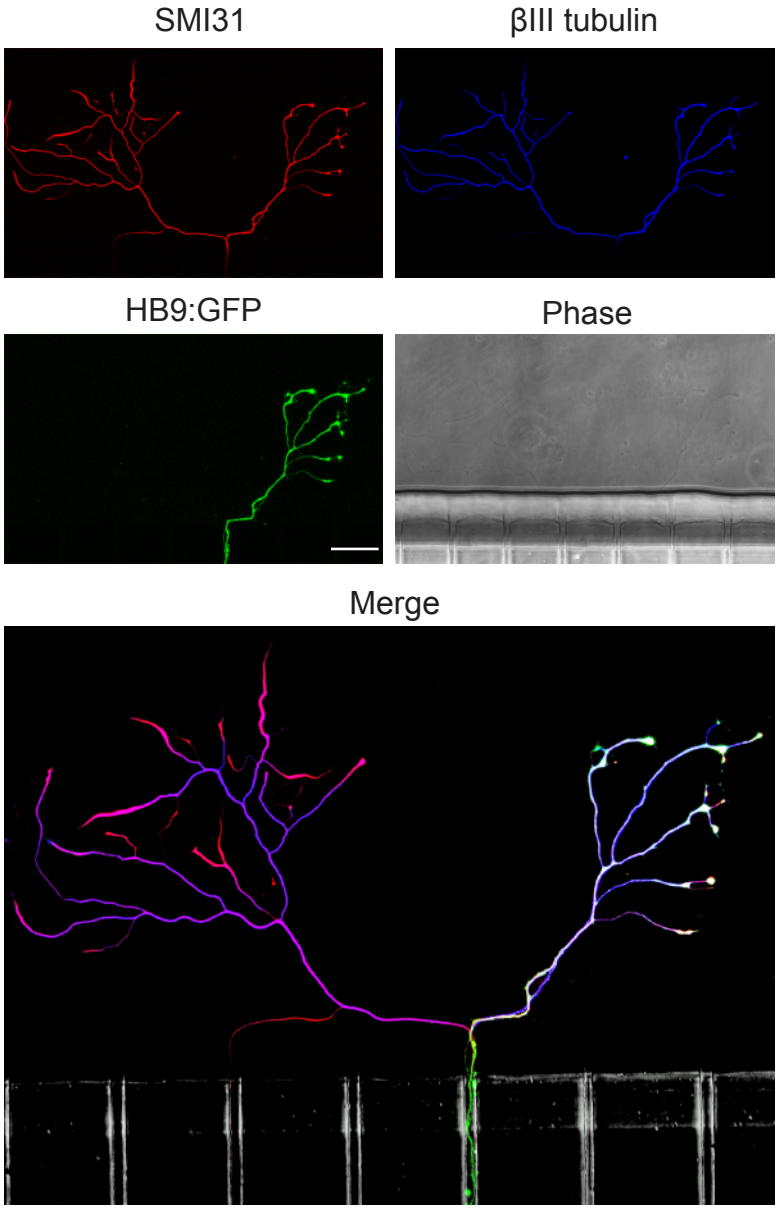

Figure 5-4. Different type of neurons cross in microfluidic chambers

ES derived HB9::GFP (green) neurons were plated in the somatodendritic compartment of microfluidic chambers. The cells were allowed to settle and grow axons to the axonal side (DIV 4) before fixation, permeabilisation and blocking. Both compartments were stained for βIII tubulin (blue) to label the whole neuronal network and SMI 31 (red) to label axons. Note that the antibodies do not stain the axons within the microgrooves due to microfluidic isolation. Scale bar: 50 μm.

5.3 H_CT is taken up at the axonal compartment and transported retrogradely to the somatodendritic compartment

The aim of this approach was to prove that H_CT is transcytosed in primary motor neuron cultures. Before testing this, I needed to optimise its uptake and retrograde transport in microfluidic chambers. I plated primary motor neurons into the somatodendritic compartment and let the axons cross for 7 d. Then I added AlexaFluor555-H_CT in motor neuron medium to the axonal compartment and made sure that the somatodendritic compartment contained a higher volume of medium to avoid diffusion of the probe. The cells were left to internalise and transport H_CT for 2 h at 37°C before washing with HBSS and fixing with 4% PFA for 15 min at room temperature. Both compartments were permeabilised with PBSTr for 10 min at room temperature before blocking with IFBB for 1 h and adding mouse anti-βIII tubulin primary antibody for 1 h at room temperature. Both compartments were washed and goat AlexaFluor647-conjugated anti-mouse secondary antibody was added for 30 min to reveal the neuronal network. The chambers were imaged, paying special attention to the cell bodies of neurons, which had axons on the axonal side. All axons were positive for H_CT, which had been retrogradely transported back to the cell body (Figure 5-5 A). The length of the initial incubation (2h) appeared to be ideal for studying transcytosis and synaptic transfer, because numerous neurons accumulated H_CT, which did not have an apparent axon crossing to the axonal side (Figure 5-5 B). However, this experiment did not formally prove that synaptic transfer had occurred via functional synaptic connections between neurons.

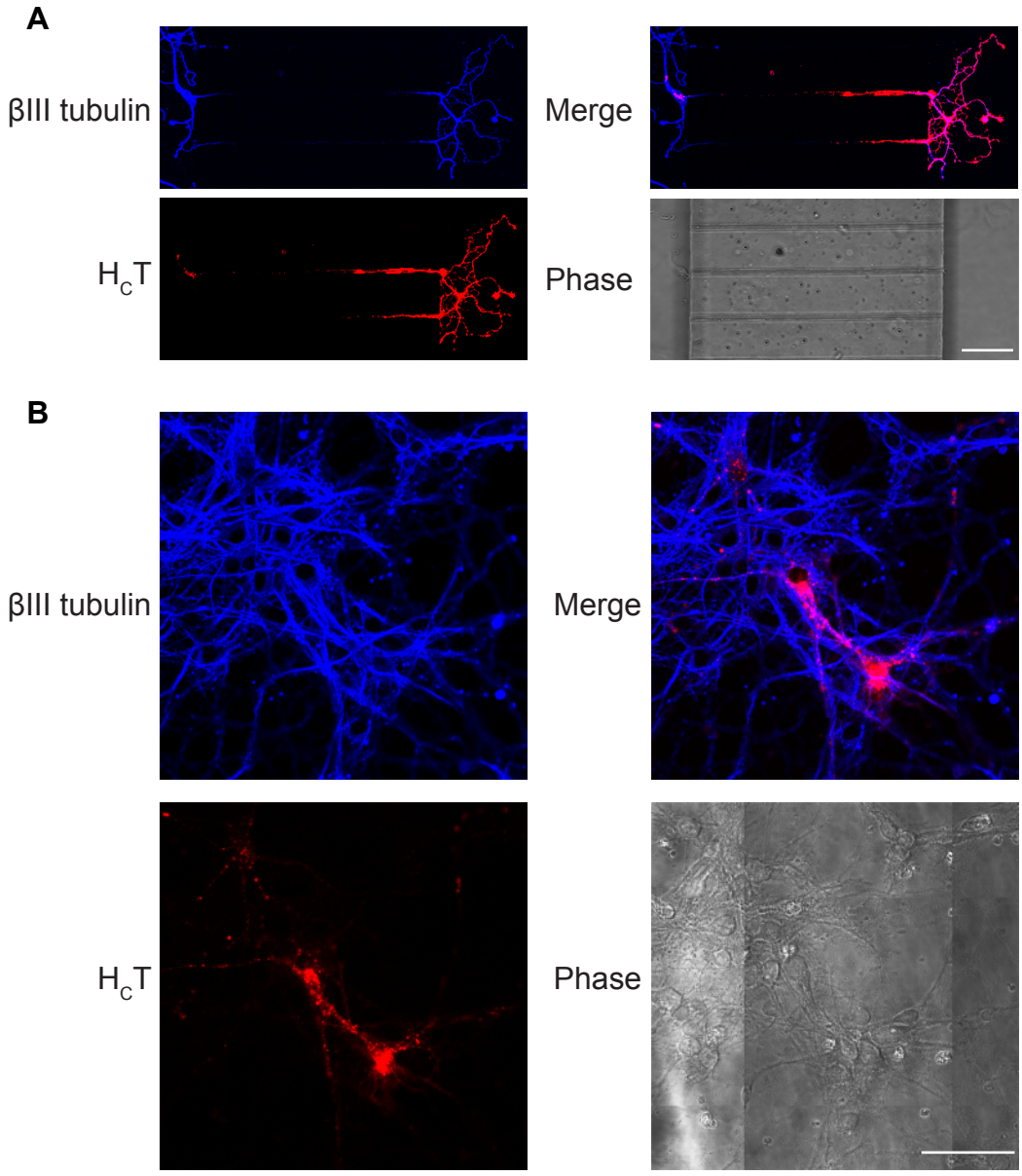

Figure 5-5. H_CT is retrogradely transported in compartmentalised motor neuron cultures

Freshly dissected primary motor neurons were plated into the somatodendritic compartment of microfluidic chambers; axons were allowed to cross for 7 d before adding AlexaFluor555-H_CT to the axonal compartment. **(A)** H_CT (red) bound, internalised and underwent axonal retrograde transport in the axonal compartment. The neuronal network is stained with βIII tubulin (blue). Scale bar: 100 μm. **(B)** H_CT accumulates in cell bodies in the somatodendritic compartment. Note that one of the neurons does not possess an axon extended towards the microgrooves, suggesting that it did not cross to the other side. Scale bar: 50 μm.

5.4 H_CT is transferred between neurons in microfluidic chambers

5.4.1 Cholera toxin subunit B is not, but H_CT is transferred between neurons in the somatodendritic compartment

To prove that H_CT is transcytosed, I turned to a probe, which is a great retrograde tracer but does not get transcytosed in neurons. Cholera toxin subunit B (CTB) is the binding fragment of cholera toxin and binds to the ganglioside GM1 with high affinity (Merritt et al., 1994). It is an excellent retrograde tracer (Wan et al., 1982); it binds to all neurons in primary motor neuron cultures, but never gets transferred between neurons (Schwab et al., 1979). CTB was shown to accumulate in lysosomes after transport (Llewellyn-Smith et al., 1990) in medullary neurons, while other studies conducted on intestinal cells showed that it is transported to the endoplasmic reticulum through the trans-Golgi network (TGN) (Lencer and Tsai, 2003).

I added AlexaFluor555-H_CT and AlexaFluor488-CTB to the axonal compartment of microfluidic chambers and allowed both probes to internalise and get transported for 2 h at 37°C. The chambers were washed extensively and the somatodendritic compartment was stained for βIII tubulin to label the neuronal network as before. Both CTB and H_CT were retrogradely transported, sharing the majority of transport compartments (Figure 5-6; white arrows), this is in agreement with previous experiments performed in our laboratory by M. Terenzio (Schmieg et al., 2014) and G. Menendez (Menendez, 2010). However, despite the overlap between the transport compartments of H_CT and CTB, they are differentially sorted and the probes are directed into different intracellular destinations. G. Menendez showed that CTB accumulates in the TGN in dorsal root ganglia neurons (Menendez, 2010).

The sorting of H_CT in motor neurons has not been studied in detail, but it is expected to be targeted to a transcytotic route together with the neurotrophin receptors, TrkB and $p75^{NTR}$ and get transferred between neurons (Lalli et al., 2003a, Bercsenyi et al., 2013).

In the somatodendritic compartment, I found neurons containing H_CT but not CTB. Since all axons in the axonal compartment were stained with both probes,

this result suggests that these neurons did not have an axon projecting to the axonal compartment. The only way they could have been exposed to H_CT was through synaptic transfer from another neuron, which had an axon extended to the axonal compartment. The two neurons imaged in Figure 5-6 have close contact sites between their arborisation (yellow arrowheads); and one of them contains H_CT but not CTB (secondary contact neuron), while the other contains both (projecting neuron). H_CT must have been released by the projecting neuron and internalised by the secondary contact neuron. This result demonstrated for the first time that H_CT undergoes synaptic transfer between neurons in compartmentalised primary motor neuron cultures.

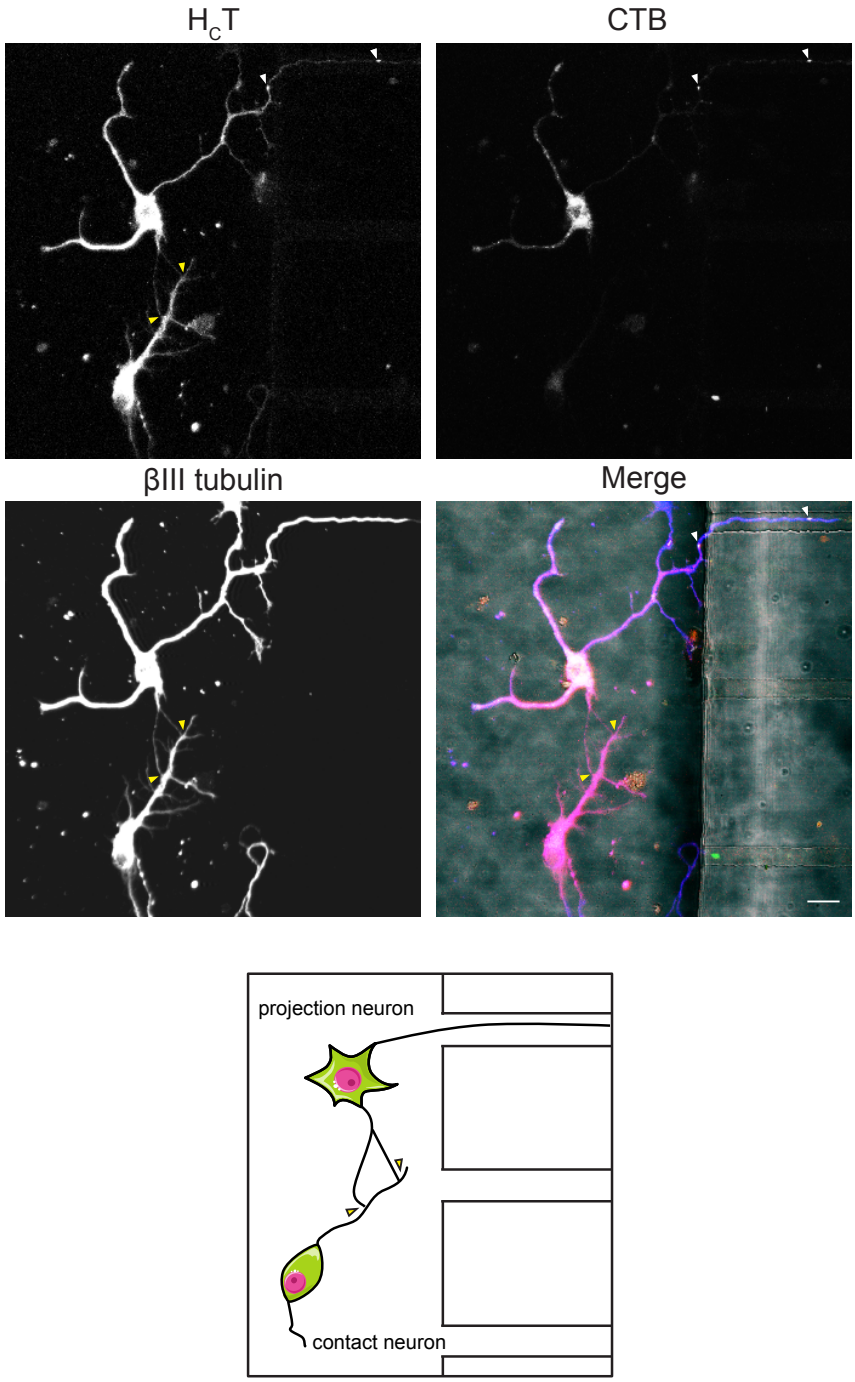

Figure 5-6. H_CT is transcytosed in primary motor neurons

Primary motor neurons were plated in microfluidic chambers and left to grow axons through the microgrooves for 7 days. AlexaFluor555-H_CT (pseudocolored grey, red in merge) and AlexaFluor488-CTB (pseudocolored grey, green in merge) were added to the axonal side simultaneously and left to get internalised and transported for 2 h at 37°C. Both compartments were washed with HBSS before fixing, blocking, permeabilising and staining for βIII tubulin (pseudocolored grey). The white arrowheads show shared transport compartments between H_CT and CTB, while the yellow arrowheads point at possible transcytosis sites (see schematic). Scale bar: 20 µm.

5.4.2 Nidogen-2 is present in the extracellular space in the axonal compartment

The axonal compartment was coated with poly-ornithine and laminin, but was completely free of cells and it was microfluidically isolated from the somatodendritic compartment. Since H_CT was efficiently taken up by the axons in the axonal compartment, I asked whether nidogen-2 was present there. To test this, I did an immunostaining with the nidogen-2 antibody as described earlier. Nidogen-2 was highly concentrated around the leading edge of crossing axons and was present in the extracellular space and on the surface of axons in large quantities (Figure 5-7).

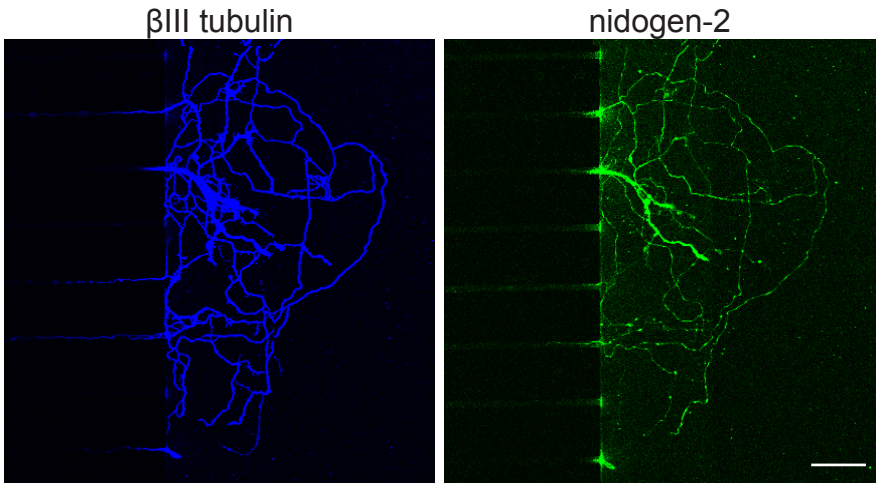

Figure 5-7. Nidogen-2 is present in the axonal compartment in microfluidic chambers

The axonal compartment was fixed, permeabilised and stained for βIII tubulin (blue) and nidogen-2 (green). Scale bar: 100 µm.

5.4.3 H_CT is transcytosed with nidogen-2

Next, I wanted to test whether nidogen-2 is synaptically transferred together with H_CT from motor neurons. This includes the capture at the basal lamina, binding on the cell surface and internalisation, axonal transport, sorting and exocytosis of the transport vesicle through the somatodendritic PM. To test this, I added AlexaFluor555-HA-H_CT and rabbit anti-nidogen-2 antibody to the axonal side of microfluidic chambers and allowed 2 h at 37°C for internalisation, retrograde

transport and transcytosis to occur. Cells were fixed and blocked without permeabilisation. Keeping the PM intact was important to ensure that antibodies can only recognise antigens that are present on the PM. Rat anti-HA primary antibody was added to the somatodendritic compartment, followed by goat AlexaFluor488-conjugated anti-rat to label AlexaFluor555-HA-H_CT, which has been exposed on the PM. Goat AlexaFluor647- conjugated anti-rabbit antibody was added to label exposed nidogen-2 bound by the rabbit anti-nidogen antibody. Both probes underwent exocytosis through the somatodendritic membrane together and this lead to the exposure of the probes (Figure 5-8), indicating that nidogen-2 stays together with H_CT all along its journey inside motor neurons, and maybe even beyond.

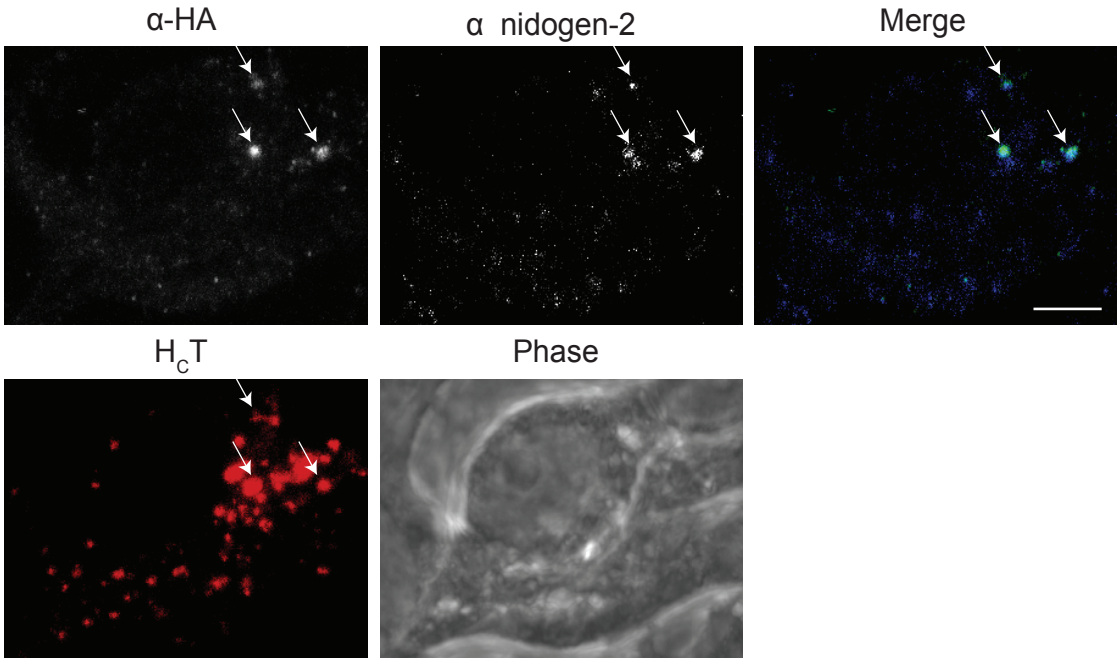

Figure 5-8. H_CT and nidogen-2 are transcytosed together

Primary motor neurons were plated in microfluidic chambers and let to grow axons through the microgrooves for 7 d. AlexaFluor555-HA-H_CT (red) and rabbit anti-nidogen-2 were added simultaneously to axonal side to allow internalisation, axonal transport and transcytosis for 2 h at 37°C. The cells were fixed and blocked without permeabilisation. Rat anti-HA primary antibody was added, followed by goat AlexaFluor488- conjugated anti-rat to label re-presented AlexaFluor555-HA-H_CT on the PM (pseudocolored grey, green on merge) and goat AlexaFluor647- conjugated anti-rabbit antibody to label exposed nidogen-2 (pseudocolored grey, blue on merge). Scale bar: 10 μm.

5.5 Summary

- I designed new microfluidic chambers, with 500 µm long and 1-2 µm deep microgrooves. These chambers provide microfluidic isolation between the somatodendritic and axonal compartment and are suitable for motor neuron culture.
- The axons of different neuronal types present in the ES-cell derived and primary motor neuron cultures cross the microgrooves successfully within 7 days after plating. 50,000 cells per chamber is the ideal cell density to be plated in the somatodendritic compartment for optimal imaging.
- H_CT is taken up at the axonal compartment; it is retrogradely transported and accumulates in the cell body.
- Both H_CT and CTB are taken up and transported together, but their internal sorting is different, since CTB accumulated in the TGN, while H_CT is targeted to the somatodendritic PM, exocytosed and taken up by neighbouring neurons.
- Nidogen-2 is colocalised with H_CT during binding, uptake, transport and re-presentation on the PM in the soma.

Chapter 6. Discussion

6.1 Aims of the Ph.D. project

- Find an inhibitor of tetanus intoxication
- Identify and characterise the protein receptor of TeNT at the NMJ
- Investigate the synaptic transfer of TeNT between motor neurons and interneurons

6.2 The N1 peptide is a potent inhibitor of tetanus intoxication

One of the main aims of this project was to develop an inhibitor, which could serve as a template for therapeutic interventions against tetanus. The N1 peptide emerged from the initial peptide screen and it blocks tetanus intoxication in mice; which makes it an excellent template for a therapeutic agent to block the onset and progression of tetanic paralysis.

6.2.1 *In vitro* binding assays – the N1 peptide emerges as the top candidate

Among the assays used in this study, the fluorescent binding assay is the most artefact-free, since the peptides are bound on the bottom of a plate, and directly labelled AlexaFluor555-H_CT is added after blocking with BSA. The N1 peptide showed the highest signal in these experiments, although the N3 and D peptides were also efficient at binding H_CT (Figure 3-2). The main difference in the *in vitro* pull down assay is that instead of binding on the surface of plate, the peptides are bound on the surface of agarose beads. This favoured those peptides, which were more hydrophobic, and new candidates, such as the D, J and O peptides emerged from this assay (Figure 3-3). However, when tested in an ELISA, all three peptides (D,J,O) appeared to bind to the anti-VSVG antibody directly, which indicated that due to their high hydrophobic features, they were binding to proteins unspecifically. In contrast, the N1 peptide bound specifically to H_CT and not the antibody. When the results were normalised to the values where H_CT was omitted from the assay (Figure 3-4), it became clear that the N1 peptide was the best candidate emerging from the entire screen.

6.2.2 The N peptides block H_CT binding on primary motor neurons

All peptides, which showed binding in any of the assays discussed above, were carried forward in competition assays on primary motor neurons. We identified a peptide within nidogen-2, which was very similar to the N1 peptide (THIYQWRQT), but contained inverted motifs (NQTWSYHID) (Kohfeldt et al., 1998). Both the N1 and N2 peptides blocked H_CT binding and internalisation in primary motor neurons, while the D and O peptides caused aggregation of AlexaFluor555-H_CT and the J and N3 peptides did not have any effect (Figure 3-5). Furthermore, the N1 peptide still had a blocking effect when added to the cells with a 10 min delay, indicating that it might have a higher affinity to H_CT than the protein receptor(s) (Figure 3-11). However, H_CT was present in the motor neuron medium throughout the experiment (45 min in total). We know that H_CT binding is very efficient and occurs very quickly (5-10 min), but the possibility that the N1 peptide added at the 10 min time point blocked binding of the 'late targeting' H_CT pool cannot be excluded and this could have caused the decrease in the internalised pool of H_CT at 45 min. To further test this, H_CT should be added in a 'pulse-chase' experiment, only left on the cells for 10 min, then washed off before the addition of the N1 peptide. If the peptide can still cause a decrease in the total internalised pool of H_CT at 45 min, this effect is likely to be due to interference with receptor internalisation/sorting.

6.2.3 The W is crucial for the interaction between N1 and H_CT

The four core residues of N1 (YQWR) are completely conserved in mammals, while there are numerous single substitutions in the first and last position of the core residues of N2 (TWSY). I performed a peptide array, containing all 20 possible amino acid substitutions in the four key residues in both N1 and N2, to test which positions are the most important for H_CT binding. Due methodological problems in the preparation of these peptide arrays, which make this approach only semi-quantitative, I could not obtain conclusive results (Figure 3-6). To overcome this, I decided to test single alanine mutant peptides for H_CT binding in a fluorescent binding assay and found that mutating the W for A in both peptides completely abolished H_CT binding. Both human peptides (hN1 and hN2) bound H_CT,

albeit less than their mouse counterparts. The N2 peptide had a lower binding ability than the N1 peptide and it was much more sensitive to alanine substitution (Figure 3-7).

Next, we attempted to obtain a crystal structure of the N1 peptide bound to H_CT. I tested the stability of the interaction between the N1 peptide and H_CT in buffers with different pH and found that the interaction between the peptide and H_CT is abolished at pH 5, which is the preferred pH for H_CT crystal formation (Figure 3-8 B). However, the N1 peptide had a far greater binding affinity when compared to the YEW tripeptide, which was previously co-crystallised with H_CT (Jayaraman et al., 2005), indicating that if there were permissive conditions for peptide binding and H_CT crystallisation, there would be a high chance of obtaining co-crystals.

Unfortunately all crystallisation attempts failed to date, therefore we turned to biomolecular modelling. The analysis (performed by G. Zanotti, University of Padova) showed that the majority of the peptide surface is buried in the 'R' pocket of H_CT, predicting that the binding affinity is very high (Figure 3-8 C). The competing potential of the N1 peptide might be due to competition with more than one endogenous receptors. Since it binds into 'R' pocket of H_CT, it most probably blocks all interactions at this site. This might include polysialogangliosides (Stoeckel et al., 1977, Kitamura et al., 1999, Chen et al., 2009) as well as protein receptors (Rummel et al., 2003, Montecucco, 1986).

We tried to determine the binding affinity of the N1 peptide experimentally, but unfortunately we saw no binding on the Octet system and the ITC experiments provided limited information due to technical limitations of this assay. The cellular environment and polysialogangliosides were lacking in both of these experiments, and this might explain the reason why the estimated Kd based on the ITC experiments is 7.5 μM, which is far higher than expected (Figure 3-8 D).

6.2.4 The N1 peptide blocks H_CT binding on the NMJ

To assess the ability of H_CT to bind to the NMJ, I used freshly dissected whole-mount LAL muscles. This preparation is excellent for whole-mount experiments because it consists of only a few cell layers. I allowed 1 h for internalisation and observed that not all NMJs contained H_CT (only 63.6±6.0% of all

NMJs in the muscle are H_CT positive, Figure 3-13). This might be due to multiple reasons:

- A region of the muscle might have folded over and it was not available for H_CT binding.
- These junctions might have taken up H_CT faster than others and the probe was retrogradely transported and cleared from the motor neuron endplate.
- An alternative explanation is that not all NMJs contain determinants for H_CT binding, including the presence of a protein receptor.

By injecting H_CT-HA intramuscularly and sectioning the tissue, we excluded the possibility of antibody penetrance issues and still observed that not all NMJs contain H_CT. This was the case for different time points (30 and 60 min), which makes it unlikely that the empty NMJs transport H_CT faster and suggests that these do not bind H_CT due to the lack of determinant(s) for H_CT binding.

When preincubated with the N1 peptide, H_CT lost its ability to bind to NMJs and the number of H_CT containing NMJs dropped to 14.3±4.7% (Figure 3-13).

6.2.5 The N1 peptide blocks tetanic paralysis *in vivo*

6.2.5.1 Hemidiaphragm assay

TeNT causes paralysis in hemidiaphragm preparations, but the mechanism of its action in this experimental setup is unknown. When the diaphragm is dissected, the phrenic nerve loses its connections with the spinal cord (Simpson, 1977, Simpson, 1984). During tetanus, TeNT is retrogradely transported in motor neuron axons and gets transcytosed into inhibitory interneurons in the spinal cord (Lalli et al., 2003a), but this part of the pathway is not available in this tissue preparation. TeNT is used at a relatively high concentration and this might cause its accumulation in carriers, which undergo pH changes locally, which in turn leads to the release of the L chain and cleavage of its target protein, synaptobrevin, within the motor neuron terminal. By blocking synaptic vesicle release from the phrenic nerve, it causes the paralysis of the muscle; there is no contraction even when a supramaximal stimulus is applied. When TeNT was preincubated with the N1 peptide, it took longer to paralyse the muscle, but the results were not significant

and the N2 peptide appeared to cause the opposite (Figure 3-14). The most probable explanation is that TeNT is mainly using an alternative entry pathway in this assay, and this does not depend on the 'R' site; where the N1 binds, so it does not significantly affect the timeframe of tetanic paralysis.

6.2.5.2 Local tetanus in mice

To test whether the N1 peptide can efficiently block tetanic paralysis *in vivo*, we injected the *triceps surae* muscle of mice with TeNT, which was preincubated with vehicle, control peptide ($N1_{AA}$) or the N1 peptide. TeNT used at a low dose (0.25-2 ng/kg) and injected intramuscularly causes local tetanic paralysis (Samal et al., 1990, Duchen and Tonge, 1973). Since it was injected in the hindlimb, the injected limb got stiff and the mice were not using it to support their weight while walking. The injected leg was lagging behind and this led to a defect in coordination. When mice walk, they place the hind paw where the front paw was located at the previous step. As the injected leg was not positioned properly, we could get a quantitative measurement on the progression of tetanic paralysis. The mice injected with 2 ng/kg TeNT, which was preincubated with the N1 peptide did not present any coordination defects at 25 h, while the other two groups showed a significant impairment (Figure 3-15). At later stages, the injected leg of the control groups got completely paralysed, and the animals refrained from using it to support them while walking. When held by their tail, tetanic mice could not stretch their injected leg outwards, like control animals do, since the *triceps surae* muscle was paralysed. The N1 peptide treated group had a slight impairment in the holding posture, but this was milder than in the other groups (Movie 1).

To gain some understanding on the underlying physiological effect of tetanus intoxication, we performed muscle tension experiments. The *tibialis anterior* muscle was injected with a low dose of TeNT, which was preincubated with vehicle, control peptide or the N1 peptide. After 24 h, when spastic paralysis occurred, the maximal contractile force was determined following supramaximal stimulus. The N1 peptide treated group had less muscle power in the injected than in the non-injected leg, but this difference was not significant, while the other two groups had a significant drop in muscle power (≃90%,Figure 3-16). The N1 treated group retained a significantly bigger percentage of muscle force (43.5±10.5% SEM)

compared to the other two groups (2.4±0.9% SEM for TeNT+DMSO and 0.3±1.4% SEM for TeNT+$N1_{AA}$).

These experiments clearly demonstrated that the N1 peptide protects mice from tetanic paralysis. However, the mechanism of this protective action needed to be elucidated. Based on our predictions, the peptide is likely to bind to the 'R' site of TeNT, where sialic acid was shown to bind. The interruption of this interaction could lead to the blocking action of the N1 peptide. Alternatively, the peptide could block the binding of a protein receptor at the 'R' site, which could potentially be the actual protein it originates from; nidogen-1.

The N1 peptide is a unique blocking agent of tetanus, since no other compound has been identified to date, which could inhibit tetanic paralysis with such efficiency.

If the N1 peptide is able to compete with the receptor even after the binding of TeNT has occurred, it provides a very promising platform for drug development. When patients present with the first line of symptoms (lockjaw) (Centers for Disease, 2012), the agent based on the peptide could be administered systematically and this could prevent the further spread of TeNT to new NMJs. If the innervation circuits of vital muscles, such as the diaphragm can be protected from TeNT, the most common cause of death, respiratory failure can be avoided and this in turn would decrease the high mortality rate. Bone fractures (long bones and the spine) are the consequences of strong muscle spasms, which could also be prevented if the peptide-based new drug blocked TeNT from binding to the NMJs in big skeletal muscles (Centers for Disease, 2012). The second most common cause of death is secondary infection, which occurs during the prolonged hospitalisation. Provided that the novel therapeutic approach involves a compound, which is stable and can stay in the circulation for a long period of time, the hospital stay could be significantly reduced and the chances of contracting infections linked to immobility, cannulas and mechanical ventilation would decrease.

Alternatively, this new approach could be integrated into the current medical intervention protocol (Table 18) and used in combination with Td vaccine (contains inactivated tetanus toxoid and pertussis vaccine) and tetanus immunoglobulin (TIG). This way the patients would not only survive tetanus, but be protected from contracting it again.

Table 18. The current medical protocol for tetanus intoxication (Centers for Disease, 2012)

Vaccination History	Clean, minor wounds		All other wounds	
	Td	TIG	Td	TIG
Unknown or less than 3 doses	Yes	No	Yes	Yes
3 or more doses (last dose less than 5 y ago)	No	No	No	No

6.3 Nidogens are extracellular matrix protein receptors for TeNT

The N1 and N2 peptides originate from nidogen-1 and nidogen-2, respectively. Both nidogens are expressed in primary motor neurons, but nidogen-1 is present in much higher quantities (Figure 4-3). In the initial proteomic analysis of endosomal carriers containing H_CT, nidogen-1, but not -2 was found (Deinhardt et al., 2006b). However, the nidogen-1 antibody only worked for western blotting and not for immunofluorescence, so I relied on the nidogen-2 antibody to perform all immunocytochemistry and immunohistochemistry experiments. I observed cross-reactivity between nidogen-1 and the anti-nidogen-2 antibody in Western blotting, which suggests that to a certain extent, both nidogen isoforms are recognised by this antibody.

6.3.1 Nidogen-2 is taken up together with H_CT in primary motor neurons

By incubating primary motor neurons with H_CT and the anti-nidogen-2 antibody at the same time, I showed that nidogen-2 is taken up together with H_CT in primary motor neurons (Mander's coefficient 66.3±1.1%, Figure 4-4). Furthermore, the proteins interact with each other, since nidogen-2 is immunoprecipitated with H_CT (Figure 4-5). To observe the interaction, the proteins had to be cross-linked prior to immunoprecipitation. Nidogens are heavily glycosylated and H_CT binding to neurons is detergent sensitive. The detergents present in the lysis buffer are likely

to make the interaction between H_CT and nidogens weaker and harder to detect and also disrupt the binding with polysialogangliosides. The cross-linking protocol prevents the disruptive effect of the lysis buffer, by stabilising the interaction. In addition, by allowing internalisation for 5 min, most of the H_CT pool resided in early CCVs. The CCVs concentrate the H_CT-nidogen complex, making them easier to stabilize. Partial hydrolysis of the adducts may occur during preparations of the samples for SDS-PAGE upon incubation at high temperature and alkaline pH, this might be the reason why the main bands on the blot were corresponding to the molecular weight of H_CT (55 kDa) and a heavily glycosylated form of nidogen (250 kDa). The nidogen-2 antibody is cross-reacting with nidogen-1 on western blots, so the observed band might contain nidogen-1 or -2. I looked for the presence of other known proteins, which reside within the signalling endosome (TrkB, sortilin, LAR), but did not detect their presence. However, the immunoprecipitation of H_CT is very challenging, and the proteomic analysis of endosomal carriers has already confirmed the presence of TrkB and $p75^{NTR}$, so I turned to other methods to investigate the identity of the transmembrane protein receptor(s).

6.3.2 Nidogen-1 fits into the 'R' pocket of H_CT

Using biomolecular modelling, we showed that human nidogen-1 fits into the 'R' pocket of H_CT; at the same site, where the N1 peptide binds (Figure 4-6). The residues important for the interaction are listed in Table 19. The common H_CT interacting residues between the N1 peptide and nidogen-1 G2 domain are Q608 and R610, which are conserved between mouse and human nidogen-1 (IYTY**Q**W**R**QT**;** Table 17). Y and W are not predicted to be directly involved in the binding, which is not surprising, given that they are hidden in the intact G2 domain (Figure 4-1 A) and this structure was used in the modelling. The first three residues of the N1 peptide (THI) make hydrogen bonds and polar interactions but these are not conserved between mouse and human. This difference might explain why the hN1 peptide binds H_CT less than N1 (Figure 3-7). Since both the N1 peptide and nidogen-1 bind to the 'R' pocket, they might compete with each other for binding. In turn, this competition might largely contribute to the blocking potential of the N1 peptide *in vivo*.

Unfortunately we could not model the possible interaction between a cleaved form of nidogen-1 (following plasmin cleavage) and H_CT, because no crystal structure was available for the cleavage products of metalloproteases.

The single alanine substitution of Q608 in the mouse peptide (THIY**Q**WRQT) resulted in a significantly decreased binding to H_CT (39.5±2.9% SEM; Figure 3-7), and the Y1229A mutant of H_CT, (Y1229 interacts with Q608, S584 and T582) decreased the binding between H_CT and N1 to a similar extent (40.6±12.2%; Figure 4-7).

The R1226F substitution in H_CT was proven to be the most effective in decreasing the H_CT-N1 interaction (Figure 4-7), which was predicted to bind Q5 in the N1 peptide (corresponding to Q608 in nidogen-1) (Table 15). Furthermore, this H_CT mutant has a much lower toxicity than wild type H_CT (1.4±0.2% SEM) (Rummel, 2006), our data suggests a mechanistic explanation why this residue plays an important role in mediating the entry of H_CT into motor neurons.

To further prove the validity of this model, I showed that both nidogen-1 and -2 bind to H_CT directly and that this binding is blocked when H_CT is preincubated with the N1 and N2 peptides (Figure 4-8).

Table 19. Summary of H_CT-Nidogen-1 or N1 interactions

nidogen-1 (h-G2)		H_CT				N1 (m)	
521	E	N1216					
523	T	G1215					
530	N	A1217					
575	H	N1144					
580	V	N1144					
582	T	I1145	T1146				
584	S	Y1229					
586	T	K1213	Y1229				
604	I				D1214	**T**	1
605	Y				G1233	**H**	2
606	T				K1213	**I**	3
607	Y					Y	4
608	**Q**	Y1229		I1224	R1226	**Q**	5
609	W					W	6
610	**R**	D1214	G1215			R	7
611	Q			D1278	K1143	**Q**	8
612	T					T	9
614	T	N1277					

The residues predicted to be involved in the interaction between the human nidogen-1 G2 domain or mouse N1 peptide and H_CT are shown. The amino acids within the G2 domain and the N1 peptide are in bold and the experimentally tested point mutants of H_CT are highlighted. Q608 and its corresponding amino acid in the N1 peptide, Q5 are highlighted in red, since these are the residues which are involved in binding both in the G2 domain and in the peptide.

6.3.3 Recombinant nidogen-1 increases H_CT binding and internalisation on primary motor neurons and this effect is blocked by the N1 peptide

Nidogens are ECM proteins, and the observation that H_CT entry is dependent on these proteins suggests that there are a certain number of accessible nidogen binding sites for H_CT in the intact ECM. The addition of exogenous soluble nidogens lead to a significant increase in H_CT binding and internalisation, which was completely blocked by the presence of the N1 peptide (Figure 4-9). This is in sharp contrast to the predicted outcome of a similar assay, where the receptor is a transmembrane protein: the soluble domain acts as a scavenger and sequesters the free ligand, leading to a decrease in binding and internalisation (Dong et al., 2006). Nidogen-1 had a dramatic effect (2-3 fold increase), whereas recombinant nidogen-2 only caused a minimal increase in H_CT

binding and internalisation. Due to the unavailability of a nidogen-1 antibody for immunofluorescence, I stained the treated cells with anti-His antibody, which recognises the His-tag on the recombinant protein. It became clear that recombinant nidogen-1 binds to motor neurons (Figure 4-10). When H_CT was preincubated with the N1 peptide, the increase observed in its binding in the presence of recombinant nidogen-1 was diminished, and H_CT binding was still completely blocked (Figure 4-11). This experiment showed that H_CT binding is dependent on the number of nidogen-1 binding sites available. The N1 peptide blocks the interaction between nidogen-1 and H_CT *in situ* and completely abolishes H_CT binding even in the presence of exogenous nidogen-1. However, we still cannot formally exclude the possibility that sialic acid, or another protein receptor bind at this site, and that the N1 peptide would block the interaction between these and H_CT.

6.3.4 Additional nidogen-1 increases TeNT toxicity in mice

Based on the enhancing effect of nidogen-1 on H_CT binding in primary motor neurons cultures, we hypothesised that co-injecting nidogen-1 with TeNT would lead to earlier onset, and/or more severe progression of tetanus. When mice were injected in the *triceps surae* muscle with the mixture of nidogen-1 and TeNT, the onset of tetanic paralysis occurred earlier and the mice progressed faster than the control groups in the early stages of the disease (Figure 4-12). The middle and final stages however, showed a similar timeline to the control groups (Figure 4-13 – the score points are equally spaced), which could be explained if nidogen-1 is required for the binding and subsequent internalisation of TeNT into retrogradely transported signalling endosomes, but cannot influence the speed of transport. Further experiments are required to investigate the mechanism by which exogenous nidogen-1 is facilitating clinical tetanus, but these fell beyond the scope of my PhD.

6.4 The absence of nidogens results in decreased H_CT binding and partially protects mice from tetanus

6.4.1 Nidogen content of the NMJ is the main determinant for H_CT binding

The observation that not all NMJs bind H_CT led us to hypothesise that these junctions lacked a determinant, which was necessary for H_CT binding. To exclude the possibility of lack of access to the site, we injected fluorescently labelled H_CT in the tibialis anterior muscle of wild type mice, with this administration method, the probe spreads from the injection site and reaches all NMJs in the area. We took muscles at different time points to exclude the possibility of identifying false negative NMJs (due to their more efficient uptake and transport of H_CT, these might appear negative at a later time point). However, even at the 30 min time point, about 30% of the NMJs were negative for H_CT, in contrast to other NMJs in their vicinity. The muscles were counterstained for nidogen-2 and we observed that the staining intensity of the nidogen-2 antibody directly correlated to the H_CT content on the NMJs (Figure 4-25). If nidogen-2 was absent, the H_CT did not bind to the NMJ, indicating that nidogen-content is one of the main determinants for H_CT binding.

6.4.2 Nidogen-2 KO neurons bind less H_CT

If nidogens are crucial for TeNT binding at the NMJ and tetanic paralysis, their loss is expected to cause a decrease in H_CT binding and protect mice from tetanus. However, it is not clear, which isoform is more important in these processes, since they have partially overlapping functions and they both bind to H_CT directly, they can probably compensate for each others' loss. Single nidogen KO primary motor neurons internalised H_CT to a similar extent as their wild type counterparts (Figure 4-20, Figure 4-21), however, when the concentration of H_CT was dropped from 40 nM to 10 nM, nidogen-2 KO neurons were less able to bind H_CT than wild type neurons (Figure 4-22).

6.4.3 Nidogen KO NMJs internalise less H_CT

When I tested H_CT internalisation in single nidogen KO LAL muscles, I observed a similar phenomenon as in the primary motor neuron cultures. At a high

concentration (60 nM), H_CT accumulated at the NMJ in all genotypes (Figure 4-26), but it was not capable to enter nidogen-1 and -2 KO NMJs when its concentration was dropped to 20 nM (Figure 4-27). This result is in agreement with our observation in wild type muscles, that nidogen-content is a major determinant for H_CT binding, and it appears that the presence of both isoforms is important.

However, the loss of H_CT binding at the nidogen-1 and -2 KO NMJs might also be due to impairment in the general structure of the NMJ and problems with synaptic vesicle recycling/release. To exclude this possibility, I showed that the binding fragment of BoNT/A, which relies on SV2A for its entry into motor neurons, was internalised in both nidogen-1 and -2 KO NMJs in a similar extent than the wild type NMJ (Figure 4-28). The observed effect of nidogen-1 loss on H_CT uptake at the NMJ was specifically due to the lack of extracellular nidogen-1, since the addition of recombinant nidogen-1 to the medium of LAL muscles restored H_CT binding (Figure 4-29).

6.4.4 Nidogen DKO hindbrains internalise less H_CT

To conclusively demonstrate the importance of nidogens in H_CT binding and uptake, I wanted to test nidogen DKO primary motor neurons and NMJs in the same assays as before. Nidogen DKO mice were reported to be perinatally lethal (Bader et al., 2005), but in our hands, they never reached full gestation. I tried to obtain E13,5 embryos for primary motor neuron dissection, but the double mutants did not reach that age either. I decided to attempt to take hindbrains at E11,5 when nidogen DKO animals were still viable. It was clear that H_CT was not taken up by nidogen DKO hindbrains, however, there was a small region in the developing mesencephalon, where I found H_CT positive cells (Figure 4-30). These cells bind and internalise H_CT in a nidogen-independent way and are positive for βIII tubulin, but their identity and the mechanism through which they internalised H_CT remained unknown.

6.4.5 Mice lacking nidogen-2 are partially protected from tetanus intoxication

Nidogen-1 KO mice presented with severe epileptic seizures and early-onset hindlimb paralysis. Due to these phenotypes, we could not investigate

tetanus intoxication in this strain (Figure 4-31). In contrast, nidogen-2 KO animals were viable and healthy; so we decided to assess their sensitivity to TeNT.

Nidogen-2 KO mice were injected intraperitoneally with different doses of TeNT and the onset and progression of paralysis were closely monitored. When a low dose (1.5 ng/kg) of TeNT was injected into the peritoneal cavity, nidogen-2 KO mice were largely protected from paralysis, most of them survived beyond the humane endpoint of the experiment (Figure 4-32 A). However, when TeNT was injected in higher doses, there was no difference between the groups, although their symptoms were slightly different, and nidogen-2 KO mice appeared to have early breathing problems, which are more common in botulism than in tetanus. Furthermore, these mice developed a grey crescent in their eyes, which is a characteristic symptom of botulism, due to the dryness of the eye (Figure 4-32 B) (Suwan-apichon et al., 2006).

6.5 LAR and TrkB might serve as co-receptors for TeNT

Nidogens reside in the ECM and have no direct contact with the PM. Nidogen-1 was previously shown to interact with β-1 integrins and it serves as a promigratory factor for Schwann cells (Lee et al., 2007). In addition, the nidogen-laminin complex was shown to bind to the protein tyrosine phosphatase receptor, LAR (O'Grady et al., 1998). LAR binds TrkB in a BDNF-dependent manner (Yang et al., 2006) and H_CT binding is increased in the presence of BDNF. Furthermore, H_CT is transported together with $p75^{NTR}$ and TrkB (Terenzio et al., 2014b). Both LAR and TrkB were present in the proteomic screens characterising H_CT containing organelles previously performed in our laboratory (Deinhardt et al., 2006b) and I hypothesised that they might be part of the H_CT binding complex on the PM. Nidogens may therefore serve as a link between H_CT and these proteins (Figure 6-2).

Both LAR and TrkB colocalise with H_CT in primary motor neurons (Figure 4-14, Figure 4-15), furthermore, the incubation of these cells with a polyclonal TrkB antibody inhibits H_CT binding (Figure 4-16). Interestingly when H_CT is pre-bound to the cells, the polyclonal TrkB antibody cannot recognise TrkB anymore. A possible explanation to this phenomenon is that a large protein complex is forming around TrkB during H_CT binding (

Figure 6-1), and this prevents the recognition of the epitope of the antibody. Conversely, when the antibody is already present, the complex cannot form around TrkB and H_CT cannot bind to motor neurons. The possibility, that the TrkB antibody also blocks other H_CT binding sites on the neuronal surface cannot be excluded, even though this is very unlikely, since the antibody is highly specific for TrkB (Figure 4-15 A) and the unbound antibodies were washed away before adding H_CT to the medium.

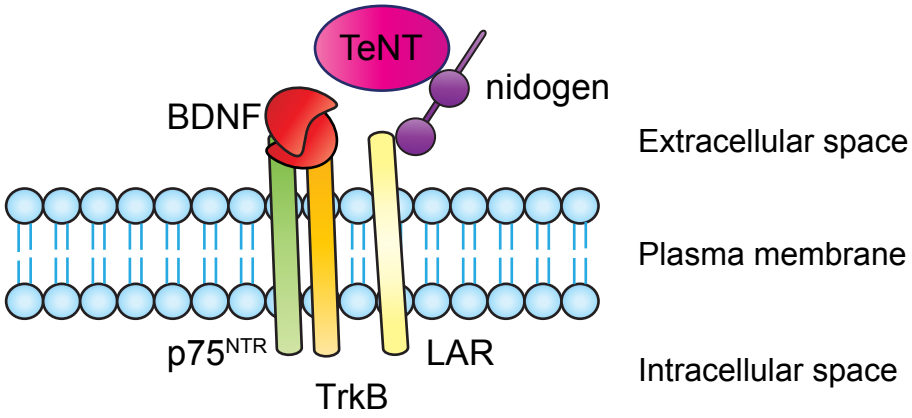

Figure 6-1. The proposed H_CT binding complex
Nidogens form a bridge between TeNT and LAR, which in turn can trigger the formation of TrkB-$p75^{NTR}$ heterodimers. This can happen either in the presence or absence of BDNF.

I tested whether BDNF alone promotes the uptake of nidogen-2 (due to the antibody restrictions) and observed a slight increase in the amount of internalised nidogen-2 in neurons compared to resting conditions. When H_CT is added, there is a similar increase in the level of nidogen-2 internalisation. Although the change in nidogen-2 uptake is lower than expected, this result shows that nidogen-2 uptake is affected by BDNF stimulation (Figure 4-17).

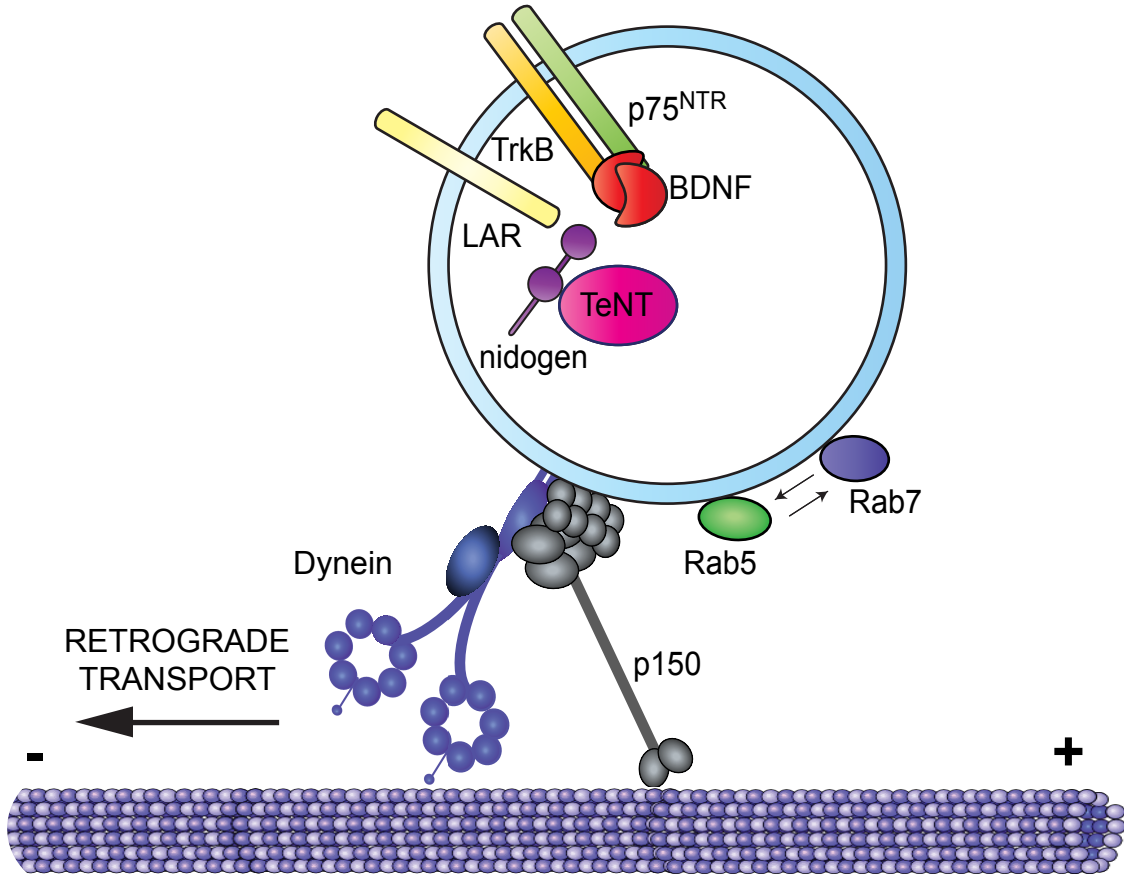

Figure 6-2. The suggested TeNT binding complex in signalling endosomes

Based on the results presented in this thesis, nidogen could serve as a link between TeNT and LAR. LAR in turn binds to TrkB in a BDNF dependent manner, recruiting the TeNT-nidogen complex to signalling endosomes.

When cells were starved in neurobasal medium, there was a robust uptake of nidogen-2 both in neurons and glial cells (Figure 4-17). This result might be due to stress; the cells take up the ECM components to cover their needs for protein synthesis, although this has never been shown before. The relationship between the ECM and starvation has been examined in the context of cancer; these cells rely on the interaction between integrins and the components of the ECM to aid their stress response (Jean et al., 2011). It would be interesting to see whether the robust uptake of nidogen-2 upon starvation has a signalling function, or if it is purely to cover the metabolical needs of neurons and glial cells. If neurotrophins and growth factors are bound to ECM proteins, they might serve as a sink, and

upon starvation the mobilisation of the matrix might be required to obtain the trophic factors stored. Alternatively, this mechanism could serve to loosen up the ECM so the cells can detach and migrate. This is a very important triggering mechanism in metastasis formation in cancer cells (Lu et al., 2012), but it is unlikely to be the reason for the observed robust nidogen uptake in primary motor neuron cultures, since mature motor neurons and their glial support layer are not migratory. By studying this in more detail we could get a more comprehensive view on the role of ECM proteins in the homeostasis of the NMJ. Based on the data presented in this thesis, nidogens are taken up following different signals in an efficient manner, probably participating in neurotrophin signalling, but this aspect of their function has never been studied before.

6.5.1 Recombinant nidogen-1 decreases the colocalisation between H_CT and SV2A

SV2 proteins were previously shown to serve as protein receptors for BoNTs (Dong et al., 2006, Baldwin and Barbieri, 2009, Rummel et al., 2009, Peng et al., 2011) and SV2A was implicated in TeNT binding to central neurons (Yeh et al., 2010). I observed a high colocalisation (45.8±4.7% SEM; Figure 4-19) between SV2A and H_CT after internalisation, but not with SV2C (12±1.6% SEM; Figure 4-18). I hypothesised that the high colocalisation is due to the high concentration of H_CT used in this assay. When mice were injected with a high dose of TeNT, they presented with symptoms of botulism, suggesting that TeNT enters motor neurons through a similar pathway used by BoNTs, and it subsequently blocks local synaptic transmission when applied at a high dose (Matsuda et al., 1982, Habermann et al., 1980). When recombinant nidogen-1 was added together with H_CT to the motor neuron medium, the colocalisation between H_CT and SV2A dropped to 22.2±1.4% (Figure 4-19), which suggests that H_CT prefers to enter neurons via nidogens, if there are enough binding sites available. This is in agreement with the clinical representation of tetanus; at low doses (which are present after bacterial infection and autolysis) TeNT avoids the SV recycling pathway and enters the retrogradely transported signalling endosomes, the latter process is most probably mediated by nidogens.

6.6 H_CT is transcytosed in primary motor neuron cultures

To explain the clinical symptomology of tetanus intoxication, TeNT must be taken up by motor neurons, get retrogradely transported to the motor neuron soma in the spinal cord and get synaptically transferred to inhibitory interneurons. In this thesis, I showed that H_CT is transcytosed in primary motor neuron cultures (Figure 5-6). Furthermore, nidogen-2 is still present at the time of re-presentation on the somatic membrane (Figure 5-8). Before doing this experiment, I observed that nidogen-2 is present in the axonal compartment of microfluidic chambers (Figure 5-7). This result suggests that nidogen-2 is produced and secreted by neurons. Alternatively the growing axon terminal could push its matrix along the microgrooves.

The transcytosis assay on motor neurons was technically not possible before, due to the lack of reliable compartmentalised motor neuron cultures. I overcame this problem by designing microfluidic chambers with shorter, but shallower microgrooves (Figure 5-3). This still maintained the microfluidic isolation between the somatodendritic and axonal compartments, but the shorter distance was permissive for motor neuron axon crossing (Figure 5-1, Figure 5-4).

Since H_CT resides in signalling endosomes, it most probably exploits the transcytotic pathway used by neurotrophins and their receptors (Schwab and Thoenen, 1977, Ascano et al., 2009). The molecular mechanism, by which certain signalling endosomes are sorted to this route, is unknown. To investigate the identity of the molecule, which labels these organelles and targets them for transcytosis, a highly efficient method needs to be established to isolate them in high enough quantities for mass spectrometry analysis. Alternatively, a candidate-based approach could be attempted. Specific Rab proteins might be involved; Rab5 and Rab 7 were shown to be crucial for the initial sorting and the subsequent long-range axonal transport of HCT containing signalling endosomes (Deinhardt et al., 2006b). Rab 11 might be an excellent candidate, as it was recently shown to regulate the transcytosis of beta-site amyloid precursor protein-cleaving enzyme 1 (BACE1) in hippocampal neurons (Buggia-Prevot et al., 2014). To test whether Rab 11 localises to the transcytotic pool of signalling endosomes, a labelled version of

Rab 11 needs to be expressed in neurons, or a high-affinity antibody needs to be purified. Dominant negative and constitutively active versions of the protein need to be overexpressed and their effect on the transcytosed pool of neurotrophin receptors and H_CT should be established.

6.7 The alternative entry hypothesis

The concentration at which H_CT, or TeNT was applied appeared to be crucial in all of the assays described in this thesis. When used at a high concentration, H_CT colocalises with the synaptic vesicle protein, SV2A and enters nidogen-1 and -2 KO motor neurons and NMJs. Furthermore, nidogen-2 KO mice are only protected if TeNT is injected in doses close to the LD_{50} (Gill, 1982), but not higher.

These observations combined with the decreased colocalisation between H_CT and SV2A in the presence of recombinant nidogen-1 lead me to hypothesise that TeNT has two alternative entry routes:

1. **Nidogen-dependent entry into signalling endosomes.**

When TeNT is captured by nidogens localised at the BL of the NMJ, it is presented to the PM receptors, LAR and TrkB. Since the formation of the predicted binding complex is more efficient in the presence of BDNF, additional BDNF is increasing the amount of TeNT entering the neurons. Ligand-bound TrkB then facilitates the internalisation of the complex and the newly formed signalling endosomes recruit Rab5 and Rab7 sequentially, and are sorted to the retrograde axonal transport pathway (Figure 6-2) (Deinhardt et al., 2006b). Once in the motor neuron soma, the signalling endosome containing H_CT is targeted to the transcytosis route and fuses with the PM in close vicinity to inhibitory terminals. The regulation of this process is currently unknown. Trk receptors are transported between the basolateral and apical membranes of neurons, but no specific targeting to inhibitory terminals has been shown to date (Butowt and von Bartheld, 2001, Butowt and von Bartheld, 2003, Ascano et al., 2009). Alternatively, TeNT could be released at random sites on the motor neuron cell body and bind to SV2A

selectively on the PM of inhibitory terminals. It gets internalised into recycling SV, and once the pH in the lumen of these vesicles drops (while the neurotransmitters are reloaded), the L chain is released into the cytosol and cleaves synaptobrevin. This inhibits SV release and silences the inhibitory interneuron. The loss of inhibitory inputs on the motor neuron leads to its over-activation and this causes tetanus.

2. SV2A dependent entry into synaptic vesicle recycling

When nidogens are missing, or TeNT is present at high concentration and all nidogen-binding sites are occupied, it binds to SV2A at the motor neuron endplate. This targets TeNT to the SV recycling pathway (as explained above) and it cleaves synaptobrevin at the presynaptic site of the NMJ. This leads to the silencing of the motor neuron and flaccid paralysis, which are characteristic of botulism.

The similarities between different CNT have been known for a long time, but due to the dramatically different clinical outcome, they were always thought to follow distinct intracellular routes. This study has clearly demonstrated that in the absence of sufficient nidogen-binding sites, or when all nidogen-binding sites are saturated, TeNT is capable of engaging with SV2A, and cause botulism-like symptoms. It was previously shown that TeNT enters synaptic vesicles via binding to SV2 in central neurons, but its colocalisation with SV2A was never investigated prior to this study (Matteoli et al., 1996, Yeh et al., 2010). On the other hand, BoNTA was shown to undergo retrograde axonal transport and retain its activity at distal sites (Antonucci et al., 2008, Restani et al., 2011). Furthermore, BoNT/A undergoes synaptic transfer in the CNS, just like TeNT (Restani et al., 2012b). It would be interesting to test whether BoNTs bind to nidogens and if blocking this interaction can prevent their transport and long-range effects (Figure 6-3).

-

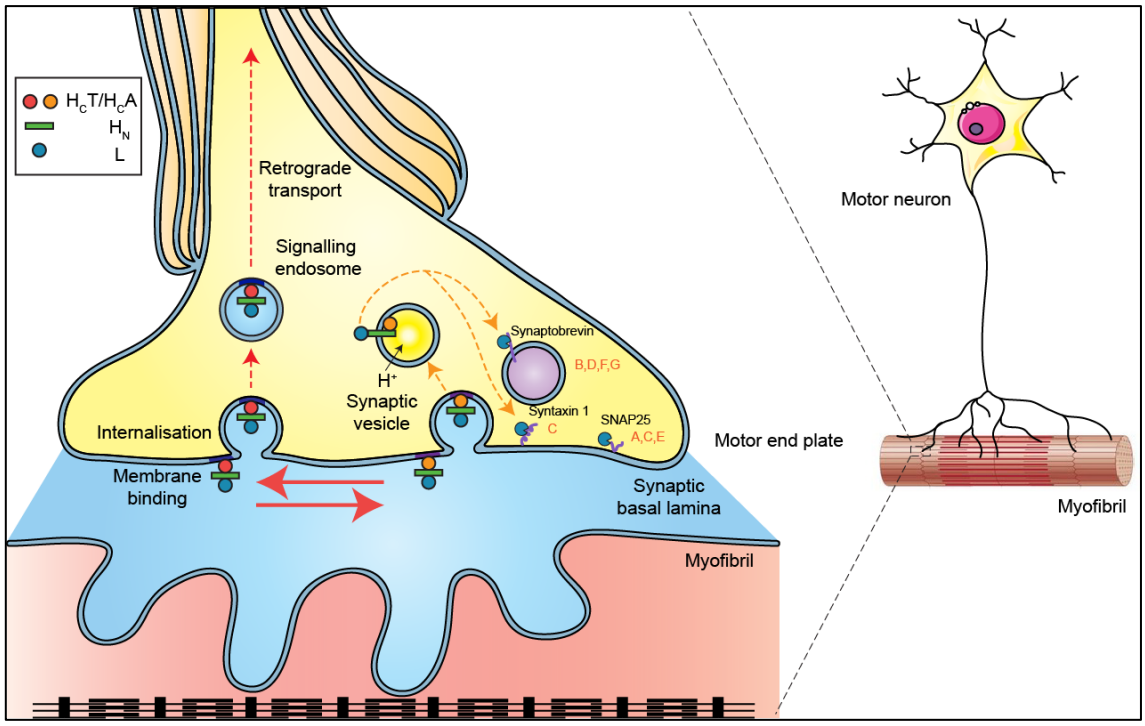

Figure 6-3. Crosstalk between the entry pathway of TeNT and BoNTs in the NMJ

Both TeNT and BoNTs accumulate in the synaptic space of the NMJ. This space is filled with the BL (light blue). In this study we showed that TeNT binds to nidogens and this pathway targets it to the retrograde axonal route. However, it also became clear that TeNT is able to engage with SV2A and can enter SV recycling at the NMJ if there is no nidogen available, or if TeNT is applied at a high dose. BoNT/A was previously shown to enter retrogradely transported carriers in motor neurons, reach the cell body and get transferred to other neurons. I hypothesise that both TeNT and BoNT/A can enter each-others' entry route, and BoNT/A is probably using the same key proteins for its entry into signalling endosomes as TeNT. Reprinted with permission from Elsevier (Schmieg, 2015).

6.8 The emerging importance of BL proteins in synaptic development, health and disease

The ECM fills the extracellular space in our tissues. Despite its abundance and localisation, it was always thought to be a passive component in maintenance and homeostasis; a rigid structure, which keeps the cells in their place and shapes the organs. In the last decade, it became clear, that the ECM, especially its specialised form, the BL does much more than simply keeping the epithelial cells in

line and separating them from the other germ layers (Hughes et al., 2006). Our study is the first of its kind; it shows that a neurotropic virulence factor relies on an ECM protein for its high affinity and neuron specific entry. We have also shown that not all NMJs contain nidogen-2, even if they are in close vicinity (Figure 4-25). The physiological importance of the selective expression of nidogen-2 is unknown; the composition of the BL in individual NMJs has never been examined in detail. It has been documented however, that structural and physiological differences exist among NMJs within the same muscle, which are correlated to the twitch-type of the individual fibers. Fast-twitch fibers have higher quantal contents; the post-synaptic membrane contains more acetylcholine receptor (AChR) and display more folds than the slow-twitch fibers. Different fibers have distinct innervation timeline too; some muscles are 'fast-synapsing' (i.e. TA), while others are 'delayed-synapsing' (i.e. the lateral *gastrocnemius*). However, this has no correlation with the relative abundance of fast- and slow-twitch fibers within the muscle (Pun et al., 2002).

6.8.1 BL in development

6.8.1.1 Agrin

During development, AChR are evenly distributed until the innervating axons reach the muscle. Once the overlying motor endplate is present, its BL gets in direct contact with the myofibril. The neuron secretes agrin (z8 splice isoform), which binds to laminin and accumulates in the synaptic BL (Table 16) (Denzer et al., 1997). Agrin then acts on muscle cells to cluster AChR in the postsynaptic membrane (>10,000 AChR/μm^2 compared to ~10 AChR/μm^2 outside of the postsynaptic site, (Cohen et al., 1997). If the z8 splice isoform of agrin is present, AChR is phosphorylated by transmembrane muscle-specific kinase (MuSK), a protein required for agrin action. However, agrin and MuSK do not bind directly (Glass et al., 1996). Low-density lipoprotein receptor-related protein (LRP4) emerged as a link between agrin and MuSK, which is essential for agrin signalling during post-synaptic differentiation (Kim et al., 2008, Zhang et al., 2008).

Mice lacking agrin die at birth, the AChR clusters are greatly reduced, but not absent; a minority of nerve terminals are opposed to a specialised post-

synaptic membrane, which is enriched in AChR and is still associated with cytoskeletal and BL components (Gautam et al., 1996). When MuSK or LRP-4 is absent, mice show no signs of post-synaptic differentiation (Gautam et al., 1999, Weatherbee et al., 2006).

Furthermore, there is a cross-talk between the Wnt (Wingless-related intergration site) pathway and agrin. Dishevelled (Dvl), a cytosolic effector protein of the Wnt cascade was shown to directly bind to MuSK and regulate its activity (DeChiara et al., 1996, Glass et al., 1997, Luo et al., 2002). Furthermore, Wnt3 collaborates with agrin to induce AChR cluster formation; it is required for the initial cluster formation, which are then enlarged by agrin (Henriquez et al., 2008). The most possible cross-talk between the two pathways is through Rac1, a small GTPase, which is required for the formation of AChR microclusters (Weston et al., 2003, Weston et al., 2000).

6.8.1.2 Rapsyn and Neuregulin

Two further other proteins were implicated in AChR clustering. In rapsyn KO mice, MuSK accumulate at synaptic sites, but this is not followed by AChR clustering (Gautam et al., 1995). Rapsyn is a postsynaptic protein, which binds to AChR (Lin et al., 2001).

Neuronally derived synaptic regulatory factor (neuregulin, NRG-1) is a presynaptic transmembrane protein. Its extracellular domain is released into the BL and is presented to the post-synaptic membrane, where it binds to ErbB tyrosine kinases. NRG-1 increases the amount of AChR at the synaptic site by promoting the expression of AChR genes in the synaptic myofibril nuclei (Won et al., 1999), however, its molecular regulation is still not fully understood (Falls, 2003).

6.8.2 The importance of BL in disease

It is the fine balance between the different components within the BL of the NMJ that are compromised in several diseases, which primarily present with decreased motor function.

Human mutations in COLQ, LAMB2 and AGRN genes (coding for ColQ, laminin β2 and agrin, respectively) cause congenital myasthenic syndromes

(CMSs), which are characterised by muscle weakness and fatigue. Myasthenia gravis (MG) presents with similar symptoms to CMSs, but it is caused by autoantibodies targeting the AChR, MuSK or rapsyn cause the symptoms (Nicholson et al., 1983, Agius et al., 1998, Guptill et al., 2011). There are several different ultrastructure defects in the NMJ in CMSs and MG, such as the reduced size of motor neuron endplate, lower quantal content, encasement of the nerve endings by Schwann cells and shallow synaptic folds on the postsynaptic membrane (Maselli et al., 2012). The latter is more severe in cases, when rapsyn is deficient; this is not surprising, considering that rapsyn is an important regulator of AChR clustering (Burke et al., 2003, Losen et al., 2005, Martinez-Martinez et al., 2007). The strong disruptive effect of the altered composition of synaptic BL on the ultrastructure of the NMJ and the subsequent symptoms of CMSs and MG clearly indicate the importance of this specialised structure in the development and maintenance of the NMJ.

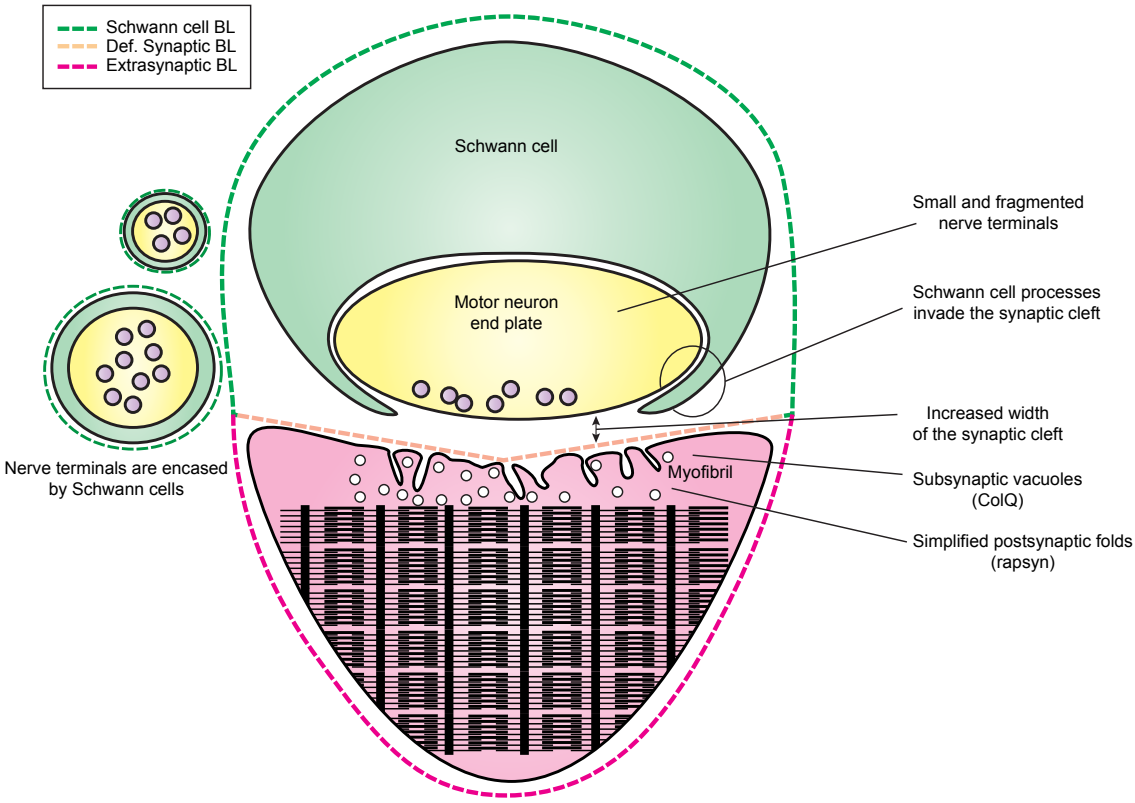

Figure 6-4. NMJ defects in MSCs

Due to the deficiency (lower expression, mislocalisation) of specific synaptic BL components, the nerve terminals become small and fragmented; Schwann cell

processes invade the synaptic cleft, which is increased in diameter. Due to the lack of rapsyn, postsynaptic folds are simple and contain reduced levels of AChR.

It was hypothesised that the NMJs remain immature in spastic quadriplegic cerebral palsy (CP), but it turned out that the only major defect was within the BL; laminin β2 was misplaced between the synaptic and extrasynaptic BL in patients, indicating the importance of this specialised ECM protein in NMJ function. Spastic CP is characterised by stiff muscles, weakness, and poor motor control and the patients have an altered sensitivity to drugs that target the NMJ, further enforcing how crucial the synaptic BL is for drug targeting (Robinson et al., 2013).

The severe progressive paralytic phenotype of the nidogen-1 KO mice was not characterised in detail before, but the epileptic seizures and abnormal posture was reported (Dong et al., 2002). The mechanism by which loss of nidogen-1 causes neuromuscular disruption in Mammals remains unknown, but based on the studies conducted in C. elegans and D. melanogaster it is most likely due to the disruption of the size of the active zones in the NMJs (Kaufmann et al., 2002, Ackley et al., 2005).

6.8.3 The importance of BL in regeneration

6.8.3.1 Central nervous system (CNS)

The poor regenerating capacity of the CNS is well documented, however, if peripheral axons are injured, their potential to regenerate is relatively high. The ECM in the CNS changes upon direct injury, and these changes are detrimental for regeneration (Burnside and Bradbury, 2014). Several ECM components were targeted in an attempt to overcome the negative effect of the ECM after injury, such as Nogo-A (by using inhibiting antibodies, (Bandtlow and Schwab, 2000, Simonen et al., 2003, Zorner and Schwab, 2010, Schwab, 2010) and chondroitin sulphate proteoglycans (chondroitinase-ABC for digesting this ECM component; (Tom et al., 2009). But while the former strategy proved to be highly successful, as it promoted plasticity and improved the motility of spinal cord-injured rats, the latter had no functional benefit despite the increased sprouting (Tom et al., 2009). It became clear, that combination therapy is the way forward, especially since the anti-Nogo-A treatment is time sensitive and is much less effective when started with a delay following injury (Gonzenbach et al., 2012). However, when combined with exercise,

which enhances neurotrophin signalling, especially through BDNF and TrkB (Weishaupt et al., 2012, Houle and Cote, 2013), anti-NogoA treatment can produce excellent results (Gonzenbach et al., 2010, Starkey and Schwab, 2012). Similarly, when combined with treadmill training and additional growth factors, chondroitinase ABC treatment caused functional locomotor improvement in rats (Alluin et al., 2014). Increasing neurotrophin levels through exercise is preferred over administration of exogenous neurotrophins, since they cause many undesired side effects and are very expensive (Perez et al., 2013). By combining these and other strategies, we will be able to turn the ECM from non-permissive to facilitating in regards to axonal regeneration and to promote axonal growth and targeting; these should result in a better outlook for patients with spinal cord injury or stroke.

6.8.3.2 Peripheral Nervous system (PNS)

The ECM in the CNS is non-permissive for regeneration, however, if the synaptic BL of the NMJ remains intact after denervation or destruction of the muscle, it helps to dictate the topology of the NMJs on regenerating cell membranes (Letinsky et al., 1976, McMahan et al., 1978, Sanes et al., 1978). To be able to promote the complete restoration of the NMJ, the BL must not only mark the location, but also provide sufficient trophic support for the survival of the pre/postsynaptic site in absence of the synaptic partner. The best candidates to promote neurite outgrowth and synapse formation are fibroblast growth factor-2 (FGF-2) and BDNF.

BDNF is known to be essential for motor neuron survival, axonal regeneration and to regulate the distribution of postsynaptic AChR (Oppenheim et al., 1992, Yan et al., 1992, Henderson et al., 1993, Wells et al., 1999, Gordon, 2009). When the vibrissal muscles are denervated, BDNF is essential to recover the presynaptic site of the NMJ. BDNF or TrkB heterozygous mice showed a decreased ability to reinnervate the vibrissal muscles, despite manual stimulation, showing that neurotrophin signalling is vital for the beneficial effect of training. The most likely explanation is that BDNF released by the muscle is captured within the ECM and any pro-BDNF present at the time of injury gets cleaved into its mature form upon exercise. Neurons sense the high concentration of BDNF within the empty NMJ and reinnervate it (Sohnchen et al., 2010).

Specialised ECM components at the NMJ might hold the key to explain why the PNS has a greater regenerating capacity, and any candidate ECM proteins, which accumulate neurotrophins, will serve as templates for novel strategies to improve the outlook of patients with CNS injury. Vice versa, engineering growth factors and neurotrophins to bind to ECM proteins with a high affinity, might increase their downstream signalling and lead to a better response to treatment, as it was recently shown in healing of chronic wounds and bone defects (Macri et al., 2007, Martino et al., 2014).

Chapter 7. Concluding remarks and future perspectives

The discovery presented in this thesis, that the protein receptor of TeNT resides within the ECM, is the first of its kind (Bercsenyi et al., 2014). Before reaching the PM, extracellular ligands and neurotropic pathogens must make their way through the ECM, and during this journey, there is a high probability of interaction. By binding to ECM components, these factors could get stuck in the matrix. However, based on recent studies, it appears that the ECM acts as a facilitator of growth factor and neurotrophin signalling, by binding these factors and presenting them to the neural membrane. Although this process is not well studied at the molecular level, it must be tightly regulated and very robust.

I showed in this thesis, that the ECM promotes TeNT binding and uptake into motor neurons (Bercsenyi et al., 2014). Since certain nidogen isoforms are exclusive to the synaptic BL, they do not only serve as an accumulating agent, but also mediate the motor neuron specificity of TeNT.

By interfering with the first step in the capture mechanism of TeNT with a nidogen-specific peptide, N1, I demonstrated that the binding and uptake of TeNT can be blocked and tetanus intoxication can be prevented. This strategy might hold the promise for a long-awaited cure for tetanus in countries where vaccination is not available. To this end, the model of the H_CT-nidogen-1 G2 complex needs to be experimentally verified using a co-crystallisation approach, which in turn might open the way to optimise novel blocking agents for the prevention of tetanus.

A pool of BoNT/A gets retrogradely transported and transcytosed. It is currently not known whether BoNT/A can bind to nidogens or other components of the ECM, and whether this interaction is responsible for its sorting to the transcytosis route. It would also be interesting to test if the N1 peptide can prevent the central effects of BoNT/A, or its interaction with FGFR3.

On the other hand, nerve stimulation should increase the number of SV2A binding sites on the PM for TeNT and if this is the case, it should compensate the blocking effect of the N1 peptide, or the lack of nidogens and restore H_CT binding in primary motor neurons and NMJs.

Furthermore, the composition of the TeNT binding complex needs to be elucidated. LAR and TrkB are both great candidates, but it might be a bigger complex, and an immunoprecipitation followed by mass spectrometry analysis is required to shed light on its components. By obtaining LAR and TrkB deficient motor neurons, the importance of these proteins in the binding and uptake of TeNT could be studied and this might reveal further candidate sites for therapeutic intervention.

Reference List

ACKLEY, B. D., HARRINGTON, R. J., HUDSON, M. L., WILLIAMS, L., KENYON, C. J., CHISHOLM, A. D. & JIN, Y. 2005. The two isoforms of the Caenorhabditis elegans leukocyte-common antigen related receptor tyrosine phosphatase PTP-3 function independently in axon guidance and synapse formation. *J Neurosci,* 25**,** 7517-28.

ACKLEY, B. D., KANG, S. H., CREW, J. R., SUH, C., JIN, Y. & KRAMER, J. M. 2003. The basement membrane components nidogen and type XVIII collagen regulate organization of neuromuscular junctions in Caenorhabditis elegans. *J Neurosci,* 23**,** 3577-87.

AGIUS, M. A., ZHU, S., KIRVAN, C. A., SCHAFER, A. L., LIN, M. Y., FAIRCLOUGH, R. H., OGER, J. J., AZIZ, T. & AARLI, J. A. 1998. Rapsyn antibodies in myasthenia gravis. *Ann N Y Acad Sci,* 841**,** 516-21.

AHNERT-HILGER, G., HOLTJE, M., PAHNER, I., WINTER, S. & BRUNK, I. 2003. Regulation of vesicular neurotransmitter transporters. *Rev Physiol Biochem Pharmacol,* 150**,** 140-60.

AHNERT-HILGER, G., WELLER, U., DAUZENROTH, M. E., HABERMANN, E. & GRATZL, M. 1989. The tetanus toxin light chain inhibits exocytosis. *FEBS Lett,* 242**,** 245-8.

ALLUIN, O., DELIVET-MONGRAIN, H., GAUTHIER, M. K., FEHLINGS, M. G., ROSSIGNOL, S. & KARIMI-ABDOLREZAEE, S. 2014. Examination of the Combined Effects of Chondroitinase ABC, Growth Factors and Locomotor Training following Compressive Spinal Cord Injury on Neuroanatomical Plasticity and Kinematics. *PLoS One,* 9**,** e111072.

ANTONUCCI, F., ROSSI, C., GIANFRANCESCHI, L., ROSSETTO, O. & CALEO, M. 2008. Long-distance retrograde effects of botulinum neurotoxin A. *Journal of Neuroscience,* 28**,** 3689-3696.

ARNOLD, K., BORDOLI, L., KOPP, J. & SCHWEDE, T. 2006. The SWISS-MODEL workspace: a web-based environment for protein structure homology modelling. *Bioinformatics,* 22**,** 195-201.

ASCANO, M., RICHMOND, A., BORDEN, P. & KURUVILLA, R. 2009. Axonal targeting of Trk receptors via transcytosis regulates sensitivity to neurotrophin responses. *J Neurosci,* 29**,** 11674-85.

BADE, S., RUMMEL, A., REISINGER, C., KARNATH, T., AHNERT-HILGER, G., BIGALKE, H. & BINZ, T. 2004. Botulinum neurotoxin type D enables cytosolic delivery of enzymatically active cargo proteins to neurones via unfolded translocation intermediates. *J Neurochem,* 91**,** 1461-72.

BADER, B. L., SMYTH, N., NEDBAL, S., MIOSGE, N., BARANOWSKY, A., MOKKAPATI, S., MURSHED, M. & NISCHT, R. 2005. Compound genetic ablation of nidogen 1 and 2 causes basement membrane defects and perinatal lethality in mice. *Mol Cell Biol,* 25**,** 6846-56.

BALDWIN, M. R. & BARBIERI, J. T. 2007. Association of botulinum neurotoxin serotypes a and B with synaptic vesicle protein complexes. *Biochemistry,* 46**,** 3200-10.

BALDWIN, M. R. & BARBIERI, J. T. 2009. Association of botulinum neurotoxins with synaptic vesicle protein complexes. *Toxicon,* 54**,** 570-4.

BANDTLOW, C. E. & SCHWAB, M. E. 2000. NI-35/250/nogo-a: a neurite growth inhibitor restricting structural plasticity and regeneration of nerve fibers in the adult vertebrate CNS. *Glia,* 29**,** 175-81.

BARBACID, M., LAMBALLE, F., PULIDO, D. & KLEIN, R. 1991. The trk family of tyrosine protein kinase receptors. *Biochim Biophys Acta,* 1072**,** 115-27.

BENOIT, R. M., FREY, D., HILBERT, M., KEVENAAR, J. T., WIESER, M. M., STIRNIMANN, C. U., MCMILLAN, D., CESKA, T., LEBON, F., JAUSSI, R., STEINMETZ, M. O., SCHERTLER, G. F., HOOGENRAAD, C. C., CAPITANI, G. & KAMMERER, R. A. 2014. Structural basis for recognition of synaptic vesicle protein 2C by botulinum neurotoxin A. *Nature,* 505**,** 108-11.

BERCSENYI, K., GIRIBALDI, F. & SCHIAVO, G. 2013. The elusive compass of clostridial neurotoxins: deciding when and where to go? *Curr Top Microbiol Immunol,* 364**,** 91-113.

BERCSENYI, K., SCHMIEG, N., BRYSON, J. B., WALLACE, M., CACCIN, P., GOLDING, M., ZANOTTI, G., GREENSMITH, L., NISCHT, R. & SCHIAVO, G. 2014. Nidogens are therapeutic targets for the prevention of tetanus. *Science,* 346**,** 1118-23.

BHATTACHARYYA, S. D. & SUGIYAMA, H. 1989. Inactivation of botulinum and tetanus toxins by chelators. *Infect Immun,* 57**,** 3053-7.

BIGALKE, H., MULLER, H. & DREYER, F. 1986. Botulinum A neurotoxin unlike tetanus toxin acts via a neuraminidase sensitive structure. *Toxicon,* 24**,** 1065-74.

BILSLAND, L. G., SAHAI, E., KELLY, G., GOLDING, M., GREENSMITH, L. & SCHIAVO, G. 2010. Deficits in axonal transport precede ALS symptoms in vivo. *Proc Natl Acad Sci U S A,* 107**,** 20523-8.

BINZ, T. 2013. Clostridial neurotoxin light chains: devices for SNARE cleavage mediated blockade of neurotransmission. *Curr Top Microbiol Immunol,* 364**,** 139-57.

BINZ, T. & RUMMEL, A. 2009. Cell entry strategy of clostridial neurotoxins. *J Neurochem,* 109**,** 1584-95.

BITTNER, M. A., HABIG, W. H. & HOLZ, R. W. 1989. Isolated light chain of tetanus toxin inhibits exocytosis: studies in digitonin-permeabilized cells. *J Neurochem,* 53**,** 966-8.

BIZZINI, B., STOECKEL, K. & SCHWAB, M. 1977. An antigenic polypeptide fragment isolated from tetanus toxin: chemical characterization, binding to gangliosides and retrograde axonal transport in various neuron systems. *J Neurochem,* 28**,** 529-42.

BLASI, J., CHAPMAN, E. R., LINK, E., BINZ, T., YAMASAKI, S., DE CAMILLI, P., SÜDHOF, T. C., NIEMANN, H. & JAHN, R. 1993a. Botulinum neurotoxin A selectively cleaves the synaptic protein SNAP-25. *Nature,* 365**,** 160-3.

BLASI, J., CHAPMAN, E. R., YAMASAKI, S., BINZ, T., NIEMANN, H. & JAHN, R. 1993b. Botulinum neurotoxin C1 blocks neurotransmitter release by means of cleaving HPC-1/syntaxin. *EMBO J,* 12**,** 4821-8.

BLUM, F. C., CHEN, C., KROKEN, A. R. & BARBIERI, J. T. 2012. Tetanus Toxin and Botulinum Toxin A Utilize Unique Mechanisms To Enter Neurons of the Central Nervous System. *Infection and Immunity,* 80**,** 1662-1669.

BOHNERT, S. & SCHIAVO, G. 2005. Tetanus toxin is transported in a novel neuronal compartment characterized by a specialized pH regulation. *J Biol Chem,* 280**,** 42336-44.

BOSE, K., NISCHT, R., PAGE, A., BADER, B. L., PAULSSON, M. & SMYTH, N. 2006. Loss of nidogen-1 and -2 results in syndactyly and changes in limb development. *J Biol Chem,* 281**,** 39620-9.

BRADFORD, M. M. 1976. A rapid and sensitive method for the quantitation of microgram quantities of protein utilizing the principle of protein-dye binding. *Anal Biochem,* 72**,** 248-54.

BREIDENBACH, M. A. & BRUNGER, A. T. 2004. Substrate recognition strategy for botulinum neurotoxin serotype A. *Nature,* 432**,** 925-9.

BREIDENBACH, M. A. & BRUNGER, A. T. 2005a. 2.3 A crystal structure of tetanus neurotoxin light chain. *Biochemistry,* 44**,** 7450-7.

BREIDENBACH, M. A. & BRUNGER, A. T. 2005b. New insights into clostridial neurotoxin-SNARE interactions. *Trends Mol Med,* 11**,** 377-81.

BRUNGER, A. T. 2007. Version 1.2 of the Crystallography and NMR system. *Nat Protoc,* 2**,** 2728-33.

BUGGIA-PREVOT, V., FERNANDEZ, C. G., RIORDAN, S., VETRIVEL, K. S., ROSEMAN, J., WATERS, J., BINDOKAS, V. P., VASSAR, R. & THINAKARAN, G. 2014. Axonal BACE1 dynamics and targeting in hippocampal neurons: a role for Rab11 GTPase. *Mol Neurodegener,* 9**,** 1.

BURKE, G., COSSINS, J., MAXWELL, S., OWENS, G., VINCENT, A., ROBB, S., NICOLLE, M., HILTON-JONES, D., NEWSOM-DAVIS, J., PALACE, J. & BEESON, D. 2003. Rapsyn mutations in hereditary myasthenia: distinct early- and late-onset phenotypes. *Neurology,* 61**,** 826-8.

BURNS, J. R. & BALDWIN, M. R. 2014. Tetanus Neurotoxin Utilizes Two Sequential Membrane Interactions for Channel Formation. *J Biol Chem*.

BURNSIDE, E. R. & BRADBURY, E. J. 2014. Manipulating the extracellular matrix and its role in brain and spinal cord plasticity and repair. *Neuropathol Appl Neurobiol,* 40**,** 26-59.

BUTOWT, R. & VON BARTHELD, C. S. 2001. Sorting of internalized neurotrophins into an endocytic transcytosis pathway via the Golgi system: Ultrastructural analysis in retinal ganglion cells. *J Neurosci,* 21**,** 8915-30.

BUTOWT, R. & VON BARTHELD, C. S. 2003. Connecting the dots: trafficking of neurotrophins, lectins and diverse pathogens by binding to the neurotrophin receptor p75NTR. *Eur J Neurosci,* 17**,** 673-80.

CALEO, M. & SCHIAVO, G. 2009. Central effects of tetanus and botulinum neurotoxins. *Toxicon,* 54**,** 593-9.

CAMPENOT, R. B. 1977. Local control of neurite development by nerve growth factor. *Proc Natl Acad Sci U S A,* 74**,** 4516-9.

CAMPENOT, R. B., LUND, K. & MOK, S. A. 2009. Production of compartmented cultures of rat sympathetic neurons. *Nat Protoc,* 4**,** 1869-87.

CAROD-ARTAL, F. J. 2014. Tackling chronic migraine: current perspectives. *J Pain Res,* 7**,** 185-94.

CARTER, R. J., LIONE, L. A., HUMBY, T., MANGIARINI, L., MAHAL, A., BATES, G. P., DUNNETT, S. B. & MORTON, A. J. 1999. Characterization of progressive motor deficits in mice transgenic for the human Huntington's disease mutation. *J Neurosci,* 19**,** 3248-57.

CENTERS FOR DISEASE, C. 2012. Epidemiology and Prevention of Vaccine-Preventable Diseases. *The Pink Book,* Tetanus.

CHEN, C., BALDWIN, M. R. & BARBIERI, J. T. 2008. Molecular basis for tetanus toxin coreceptor interactions. *Biochemistry,* 47**,** 7179-86.

CHEN, C., FU, Z., KIM, J. J., BARBIERI, J. T. & BALDWIN, M. R. 2009. Gangliosides as high affinity receptors for tetanus neurotoxin. *J Biol Chem,* 284**,** 26569-77.

CHIU, A. Y. & KO, J. 1994. A novel epitope of entactin is present at the mammalian neuromuscular junction. *J Neurosci,* 14**,** 2809-17.

CHO, H., RAMER, S. E., ITOH, M., KITAS, E., BANNWARTH, W., BURN, P., SAITO, H. & WALSH, C. T. 1992. Catalytic domains of the LAR and CD45 protein tyrosine phosphatases from Escherichia coli expression systems: purification and characterization for specificity and mechanism. *Biochemistry,* 31**,** 133-8.

CLARK, R. A. 2008. Synergistic signaling from extracellular matrix-growth factor complexes. *J Invest Dermatol,* 128**,** 1354-5.

COHEN, I., RIMER, M., LOMO, T. & MCMAHAN, U. J. 1997. Agrin-induced postsynaptic-like apparatus in skeletal muscle fibers in vivo. *Mol Cell Neurosci,* 9**,** 237-53.

COLASANTE, C., ROSSETTO, O., MORBIATO, L., PIRAZZINI, M., MOLGO, J. & MONTECUCCO, C. 2013. Botulinum neurotoxin type A is internalized and translocated from small synaptic vesicles at the neuromuscular junction. *Mol Neurobiol,* 48**,** 120-7.

DAVLETOV, B., BAJOHRS, M. & BINZ, T. 2005. Beyond BOTOX: advantages and limitations of individual botulinum neurotoxins. *Trends Neurosci,* 28**,** 446-452.

DEBANT, A., SERRA-PAGES, C., SEIPEL, K., O'BRIEN, S., TANG, M., PARK, S. H. & STREULI, M. 1996. The multidomain protein Trio binds the LAR transmembrane tyrosine phosphatase, contains a protein kinase domain, and has separate rac-specific and rho-specific guanine nucleotide exchange factor domains. *Proc Natl Acad Sci U S A,* 93**,** 5466-71.

DECHIARA, T. M., BOWEN, D. C., VALENZUELA, D. M., SIMMONS, M. V., POUEYMIROU, W. T., THOMAS, S., KINETZ, E., COMPTON, D. L., ROJAS, E., PARK, J. S., SMITH, C., DISTEFANO, P. S., GLASS, D. J., BURDEN, S. J. & YANCOPOULOS, G. D. 1996. The receptor tyrosine kinase MuSK is required for neuromuscular junction formation in vivo. *Cell,* 85**,** 501-12.

DEINHARDT, K., BERNINGHAUSEN, O., WILLISON, H. J., HOPKINS, C. R. & SCHIAVO, G. 2006a. Tetanus toxin is internalized by a sequential clathrin-dependent mechanism initiated within lipid microdomains and independent of epsin1. *J Cell Biol,* 174**,** 459-71.

DEINHARDT, K., SALINAS, S., VERASTEGUI, C., WATSON, R., WORTH, D., HANRAHAN, S., BUCCI, C. & SCHIAVO, G. 2006b. Rab5 and Rab7 control endocytic sorting along the axonal retrograde transport pathway. *Neuron,* 52**,** 293-305.

DENZER, A. J., BRANDENBERGER, R., GESEMANN, M., CHIQUET, M. & RUEGG, M. A. 1997. Agrin binds to the nerve-muscle basal lamina via laminin. *J Cell Biol,* 137**,** 671-83.

DI SUMMA, P. G., KALBERMATTEN, D. F., RAFFOUL, W., TERENGHI, G. & KINGHAM, P. J. 2013. Extracellular matrix molecules enhance the neurotrophic effect of Schwann cell-like differentiated adipose-derived stem cells and increase cell survival under stress conditions. *Tissue Eng Part A,* 19**,** 368-79.

DOLLY, J. O., WILLIAMS, R. S., BLACK, J. D., TSE, C. K., HAMBLETON, P. & MELLING, J. 1982. Localization of sites for 125I-labelled botulinum neurotoxin at murine neuromuscular junction and its binding to rat brain synaptosomes. *Toxicon,* 20**,** 141-8.

DONG, L., CHEN, Y., LEWIS, M., HSIEH, J. C., REING, J., CHAILLET, J. R., HOWELL, C. Y., MELHEM, M., INOUE, S., KUSZAK, J. R., DEGEEST, K. & CHUNG, A. E. 2002. Neurologic defects and selective disruption of basement membranes in mice lacking entactin-1/nidogen-1. *Lab Invest,* 82**,** 1617-30.

DONG, M., RICHARDS, D. A., GOODNOUGH, M. C., TEPP, W. H., JOHNSON, E. A. & CHAPMAN, E. R. 2003. Synaptotagmins I and II mediate entry of botulinum neurotoxin B into cells. *J Cell Biol,* 162**,** 1293-303.

DONG, M., TEPP, W. H., LIU, H., JOHNSON, E. A. & CHAPMAN, E. R. 2007. Mechanism of botulinum neurotoxin B and G entry into hippocampal neurons. *J Cell Biol,* 179**,** 1511-22.

DONG, M., YEH, F., TEPP, W. H., DEAN, C., JOHNSON, E. A., JANZ, R. & CHAPMAN, E. R. 2006. SV2 is the protein receptor for botulinum neurotoxin A. *Science,* 312**,** 592-6.

DONOVAN, J. J. & MIDDLEBROOK, J. L. 1986. Ion-conducting channels produced by botulinum toxin in planar lipid membranes. *Biochemistry,* 25**,** 2872-6.

DOVER, N., BARASH, J. R., HILL, K. K., XIE, G. & ARNON, S. S. 2014. Molecular characterization of a novel botulinum neurotoxin type H gene. *J Infect Dis,* 209**,** 192-202.

DUCHEN, L. W. & TONGE, D. A. 1973. The effects of tetanus toxin on neuromuscular transmission and on the morphology of motor end-plates in slow and fast skeletal muscle of the mouse. *J Physiol,* 228**,** 157-72.

EMSLEY, P. & COWTAN, K. 2004. Coot: model-building tools for molecular graphics. *Acta Crystallogr D Biol Crystallogr,* 60**,** 2126-32.

ERICKSON, A. C. & COUCHMAN, J. R. 2000. Still more complexity in mammalian basement membranes. *J Histochem Cytochem,* 48**,** 1291-306.

FALLS, D. L. 2003. Neuregulins and the neuromuscular system: 10 years of answers and questions. *J Neurocytol,* 32**,** 619-47.

FIGUEIREDO, D. M., HALLEWELL, R. A., CHEN, L. L., FAIRWEATHER, N. F., DOUGAN, G., SAVITT, J. M., PARKS, D. A. & FISHMAN, P. S. 1997. Delivery of recombinant tetanus-superoxide dismutase proteins to central nervous system neurons by retrograde axonal transport. *Exp Neurol,* 145**,** 546-54.

FISCHER, A. 2013. Synchronized chaperone function of botulinum neurotoxin domains mediates light chain translocation into neurons. *Curr Top Microbiol Immunol,* 364**,** 115-37.

FISCHER, A., GARCIA-RODRIGUEZ, C., GEREN, I., LOU, J., MARKS, J. D., NAKAGAWA, T. & MONTAL, M. 2008. Molecular architecture of botulinum neurotoxin E revealed by single particle electron microscopy. *J Biol Chem,* 283**,** 3997-4003.

FISCHER, A. & MONTAL, M. 2007. Crucial role of the disulfide bridge between botulinum neurotoxin light and heavy chains in protease translocation across membranes. *J Biol Chem,* 282**,** 29604-11.

FISCHER, A., NAKAI, Y., EUBANKS, L. M., CLANCY, C. M., TEPP, W. H., PELLETT, S., DICKERSON, T. J., JOHNSON, E. A., JANDA, K. D. & MONTAL, M. 2009. Bimodal modulation of the botulinum neurotoxin protein-conducting channel. *Proc Natl Acad Sci U S A,* 106**,** 1330-5.

FORD, M. G., MILLS, I. G., PETER, B. J., VALLIS, Y., PRAEFCKE, G. J., EVANS, P. R. & MCMAHON, H. T. 2002. Curvature of clathrin-coated pits driven by epsin. *Nature,* 419**,** 361-6.

FOX, J. W., MAYER, U., NISCHT, R., AUMAILLEY, M., REINHARDT, D., WIEDEMANN, H., MANN, K., TIMPL, R., KRIEG, T., ENGEL, J. & ET AL. 1991. Recombinant nidogen consists of three globular domains and mediates binding of laminin to collagen type IV. *EMBO J,* 10**,** 3137-46.

FOX, M. A., HO, M. S., SMYTH, N. & SANES, J. R. 2008. A synaptic nidogen: developmental regulation and role of nidogen-2 at the neuromuscular junction. *Neural Dev,* 3**,** 24.

GARAY, P. E. J., N.G.; ROSS, J.E.;JAMESON, D. M.; AOKI, R. K., FERNANDEZ-SALAS, E. 2013. BoNT/A Trafficking with FGFR3 in Neuronal Cell Lines Studied with Cross-Correlation RICS. *Biophysical Journal,* 104 (2).

GARCIA, N., TOMAS, M., SANTAFE, M. M., LANUZA, M. A., BESALDUCH, N. & TOMAS, J. 2010. Localization of brain-derived neurotrophic factor, neurotrophin-4, tropomyosin-related kinase b receptor, and p75 NTR receptor by high-resolution immunohistochemistry on the adult mouse neuromuscular junction. *J Peripher Nerv Syst,* 15**,** 40-9.

GARCIA-RODRIGUEZ, C., LEVY, R., ARNDT, J. W., FORSYTH, C. M., RAZAI, A., LOU, J., GEREN, I., STEVENS, R. C. & MARKS, J. D. 2007. Molecular evolution of antibody cross-reactivity for two subtypes of type A botulinum neurotoxin. *Nat Biotechnol,* 25**,** 107-16.

GAUTAM, M., DECHIARA, T. M., GLASS, D. J., YANCOPOULOS, G. D. & SANES, J. R. 1999. Distinct phenotypes of mutant mice lacking agrin, MuSK, or rapsyn. *Brain Res Dev Brain Res,* 114**,** 171-8.

GAUTAM, M., NOAKES, P. G., MOSCOSO, L., RUPP, F., SCHELLER, R. H., MERLIE, J. P. & SANES, J. R. 1996. Defective neuromuscular synaptogenesis in agrin-deficient mutant mice. *Cell,* 85**,** 525-35.

GAUTAM, M., NOAKES, P. G., MUDD, J., NICHOL, M., CHU, G. C., SANES, J. R. & MERLIE, J. P. 1995. Failure of postsynaptic specialization to develop at neuromuscular junctions of rapsyn-deficient mice. *Nature,* 377**,** 232-6.

GERSDORFF, N., OTTO, S., ROEDIGER, M., KRUEGEL, J. & MIOSGE, N. 2007. The absence of one or both nidogens does not alter basement membrane composition in adult murine kidney. *Histol Histopathol,* 22**,** 1077-84.

GIL, C., CHAIB-OUKADOUR, I. & AGUILERA, J. 2003. C-terminal fragment of tetanus toxin heavy chain activates Akt and MEK/ERK signalling pathways in a Trk receptor-dependent manner in cultured cortical neurons. *Biochem J,* 373**,** 613-20.

GIL, C., CHAIB-OUKADOUR, I., BLASI, J. & AGUILERA, J. 2001. HC fragment (C-terminal portion of the heavy chain) of tetanus toxin activates protein kinase C isoforms and phosphoproteins involved in signal transduction. *Biochem J,* 356**,** 97-103.

GIL, C., CHAIB-OUKADOUR, I., PELLICCIONI, P. & AGUILERA, J. 2000. Activation of signal transduction pathways involving trkA, PLCgamma-1, PKC isoforms and ERK-1/2 by tetanus toxin. *FEBS Lett,* 481**,** 177-82.

GIL, C., RUIZ-MEANA, M., ALAVA, M., YAVIN, E. & AGUILERA, J. 1998. Tetanus toxin enhances protein kinase C activity translocation and increases polyphosphoinositide hydrolysis in rat cerebral cortex preparations. *J Neurochem,* 70**,** 1636-43.

GILL, D. M. 1982. Bacterial toxins: a table of lethal amounts. *Microbiol Rev,* 46**,** 86-94.

GLASS, D. J., APEL, E. D., SHAH, S., BOWEN, D. C., DECHIARA, T. M., STITT, T. N., SANES, J. R. & YANCOPOULOS, G. D. 1997. Kinase domain of the muscle-specific receptor tyrosine kinase (MuSK) is sufficient for phosphorylation but not clustering of acetylcholine receptors: required role for the MuSK ectodomain? *Proc Natl Acad Sci U S A,* 94**,** 8848-53.

GLASS, D. J., BOWEN, D. C., STITT, T. N., RADZIEJEWSKI, C., BRUNO, J., RYAN, T. E., GIES, D. R., SHAH, S., MATTSSON, K., BURDEN, S. J., DISTEFANO, P. S., VALENZUELA, D. M., DECHIARA, T. M. & YANCOPOULOS, G. D. 1996. Agrin acts via a MuSK receptor complex. *Cell,* 85**,** 513-23.

GOLDSTEIN, L. S. & YANG, Z. 2000. Microtubule-based transport systems in neurons: the roles of kinesins and dyneins. *Annu Rev Neurosci,* 23**,** 39-71.

GONZENBACH, R. R., GASSER, P., ZORNER, B., HOCHREUTENER, E., DIETZ, V. & SCHWAB, M. E. 2010. Nogo-A antibodies and training reduce muscle spasms in spinal cord-injured rats. *Ann Neurol,* 68**,** 48-57.

GONZENBACH, R. R., ZOERNER, B., SCHNELL, L., WEINMANN, O., MIR, A. K. & SCHWAB, M. E. 2012. Delayed anti-nogo-a antibody application after spinal cord injury shows progressive loss of responsiveness. *J Neurotrauma,* 29**,** 567-78.

GORDON, T. 2009. The role of neurotrophic factors in nerve regeneration. *Neurosurg Focus,* 26**,** E3.

GRAY, K. & ELLIS, V. 2008. Activation of pro-BDNF by the pericellular serine protease plasmin. *FEBS Lett,* 582**,** 907-10.

GUPTA, V. K., YOU, Y., KLISTORNER, A. & GRAHAM, S. L. 2012. Shp-2 regulates the TrkB receptor activity in the retinal ganglion cells under glaucomatous stress. *Biochim Biophys Acta,* 1822**,** 1643-9.

GUPTILL, J. T., SANDERS, D. B. & EVOLI, A. 2011. Anti-MuSK antibody myasthenia gravis: clinical findings and response to treatment in two large cohorts. *Muscle Nerve,* 44**,** 36-40.

HAAPASALO, A., KIM, D. Y., CAREY, B. W., TURUNEN, M. K., PETTINGELL, W. H. & KOVACS, D. M. 2007. Presenilin/gamma-secretase-mediated cleavage regulates association of leukocyte-common antigen-related (LAR) receptor tyrosine phosphatase with beta-catenin. *J Biol Chem,* 282**,** 9063-72.

HABERMANN, E. & DREYER, F. 1986. Clostridial Neurotoxins - Handling and Action at the Cellular and Molecular-Level. *Current Topics in Microbiology and Immunology,* 129**,** 93-179.

HABERMANN, E., DREYER, F. & BIGALKE, H. 1980. Tetanus toxin blocks the neuromuscular transmission in vitro like botulinum A toxin. *Naunyn Schmiedebergs Arch Pharmacol,* 311**,** 33-40.

HAFEZPARAST, M., KLOCKE, R., RUHRBERG, C., MARQUARDT, A., AHMAD-ANNUAR, A., BOWEN, S., LALLI, G., WITHERDEN, A. S., HUMMERICH, H., NICHOLSON, S., MORGAN, P. J., OOZAGEER, R., PRIESTLEY, J. V., AVERILL, S., KING, V. R., BALL, S., PETERS, J., TODA, T., YAMAMOTO, A., HIRAOKA, Y., AUGUSTIN, M., KORTHAUS, D., WATTLER, S., WABNITZ, P., DICKNEITE, C., LAMPEL, S., BOEHME, F., PERAUS, G., POPP, A., RUDELIUS, M., SCHLEGEL, J., FUCHS, H., HRABE DE ANGELIS, M., SCHIAVO, G., SHIMA, D. T., RUSS, A. P., STUMM, G., MARTIN, J. E. & FISHER, E. M. 2003. Mutations in dynein link motor neuron degeneration to defects in retrograde transport. *Science,* 300**,** 808-12.

HALPERN, J. L. & LOFTUS, A. 1993. Characterization of the receptor-binding domain of tetanus toxin. *J Biol Chem,* 268**,** 11188-92.

HALPERN, J. L. & NEALE, E. A. 1995. Neurospecific binding, internalization, and retrograde axonal transport. *Curr Top Microbiol Immunol,* 195**,** 221-41.

HANIU, M., MONTESTRUQUE, S., BURES, E. J., TALVENHEIMO, J., TOSO, R., LEWIS-SANDY, S., WELCHER, A. A. & ROHDE, M. F. 1997. Interactions between brain-derived neurotrophic factor and the TRKB receptor. Identification of two ligand binding domains in soluble TRKB by affinity separation and chemical cross-linking. *J Biol Chem,* 272**,** 25296-303.

HARI, A., DJOHAR, B., SKUTELLA, T. & MONTAZERI, S. 2004. Neurotrophins and extracellular matrix molecules modulate sensory axon outgrowth. *Int J Dev Neurosci,* 22**,** 113-7.

HARPER, C. B., MARTIN, S., NGUYEN, T. H., DANIELS, S. J., LAVIDIS, N. A., POPOFF, M. R., HADZIC, G., MARIANA, A., CHAU, N., MCCLUSKEY, A., ROBINSON, P. J. & MEUNIER, F. A. 2011. Dynamin Inhibition Blocks Botulinum Neurotoxin Type A Endocytosis in Neurons and Delays Botulism. *J Biol Chem,* 286**,** 35966-35976.

HAUCKE, V. 2005. Phosphoinositide regulation of clathrin-mediated endocytosis. *Biochem Soc Trans,* 33**,** 1285-1289.

HAUGSTEN, E. M., ZAKRZEWSKA, M., BRECH, A., PUST, S., OLSNES, S., SANDVIG, K. & WESCHE, J. 2011. Clathrin- and dynamin-independent endocytosis of FGFR3--implications for signalling. *PLoS One,* 6**,** e21708.

HENDERSON, C. E., CAMU, W., METTLING, C., GOUIN, A., POULSEN, K., KARIHALOO, M., RULLAMAS, J., EVANS, T., MCMAHON, S. B., ARMANINI, M. P. & ET AL. 1993. Neurotrophins promote motor neuron survival and are present in embryonic limb bud. *Nature,* 363**,** 266-70.

HENRIQUEZ, J. P., WEBB, A., BENCE, M., BILDSOE, H., SAHORES, M., HUGHES, S. M. & SALINAS, P. C. 2008. Wnt signaling promotes AChR aggregation at the neuromuscular synapse in collaboration with agrin. *Proc Natl Acad Sci U S A,* 105**,** 18812-7.

HERREROS, J., LALLI, G., MONTECUCCO, C. & SCHIAVO, G. 2000a. Tetanus toxin fragment C binds to a protein present in neuronal cell lines and motoneurons. *J Neurochem,* 74**,** 1941-50.

HERREROS, J., LALLI, G. & SCHIAVO, G. 2000b. C-terminal half of tetanus toxin fragment C is sufficient for neuronal binding and interaction with a putative protein receptor. *Biochem J,* 347**,** 199-204.

HERREROS, J., NG, T. & SCHIAVO, G. 2001. Lipid rafts act as specialized domains for tetanus toxin binding and internalization into neurons. *Mol Biol Cell,* 12**,** 2947-60.

HINRICHSEN, L., MEYERHOIZ, A., GROOS, S. & UNGEWICKELL, E. J. 2006. Bending a membrane: How clathrin affects budding. *PNAS,* 103**,** 8715-8720.

HIROKAWA, N., NIWA, S. & TANAKA, Y. 2010. Molecular motors in neurons: transport mechanisms and roles in brain function, development, and disease. *Neuron,* 68**,** 610-38.

HO, M. S., BOSE, K., MOKKAPATI, S., NISCHT, R. & SMYTH, N. 2008. Nidogens-Extracellular matrix linker molecules. *Microsc Res Tech,* 71**,** 387-95.

HOELLER, D., VOLAREVIC, S. & DIKIC, I. 2005. Compartmentalization of growth factor receptor signalling. *Curr Opin Cell Biol,* 17**,** 107-11.

HOLTJE, M., SCHULZE, S., STROTMEIER, J., MAHRHOLD, S., RICHTER, K., BINZ, T., BIGALKE, H., AHNERT-HILGER, G. & RUMMEL, A. 2013. Exchanging the minimal cell binding fragments of tetanus neurotoxin in botulinum neurotoxin A and B impacts their toxicity at the neuromuscular junction and central neurons. *Toxicon,* 75**,** 108-21.

HOPF, M., GOHRING, W., RIES, A., TIMPL, R. & HOHENESTER, E. 2001. Crystal structure and mutational analysis of a perlecan-binding fragment of nidogen-1. *Nat Struct Biol,* 8**,** 634-40.

HOULE, J. D. & COTE, M. P. 2013. Axon regeneration and exercise-dependent plasticity after spinal cord injury. *Ann N Y Acad Sci,* 1279**,** 154-63.

HOWE, C. L. 2005. Modeling the signaling endosome hypothesis: why a drive to the nucleus is better than a (random) walk. *Theor Biol Med Model,* 2**,** 43-57.

HUGHES, B. W., KUSNER, L. L. & KAMINSKI, H. J. 2006. Molecular architecture of the neuromuscular junction. *Muscle Nerve,* 33**,** 445-61.

HYNES, R. O. 2009. The extracellular matrix: not just pretty fibrils. *Science,* 326**,** 1216-9.

IWASAKI, Y., GAY, B., WADA, K. & KOIZUMI, S. 1998. Association of the Src family tyrosine kinase Fyn with TrkB. *J Neurochem,* 71**,** 106-11.

JACKY, B. P., GARAY, P. E., DUPUY, J., NELSON, J. B., CAI, B., MOLINA, Y., WANG, J., STEWARD, L. E., BROIDE, R. S., FRANCIS, J., AOKI, K. R., STEVENS, R. C. & FERNANDEZ-SALAS, E. 2013. Identification of fibroblast growth factor receptor 3 (FGFR3) as a protein receptor for botulinum neurotoxin serotype A (BoNT/A). *PLoS Pathog,* 9**,** e1003369.

JAYARAMAN, S., ESWARAMOORTHY, S., KUMARAN, D. & SWAMINATHAN, S. 2005. Common binding site for disialyllactose and tri-peptide in C-fragment of tetanus neurotoxin. *Proteins,* 61**,** 288-95.

JEAN, C., GRAVELLE, P., FOURNIE, J. J. & LAURENT, G. 2011. Influence of stress on extracellular matrix and integrin biology. *Oncogene,* 30**,** 2697-706.

JOHNSON, K. G., TENNEY, A. P., GHOSE, A., DUCKWORTH, A. M., HIGASHI, M. E., PARFITT, K., MARCU, O., HESLIP, T. R., MARSH, J. L., SCHWARZ, T. L., FLANAGAN, J. G. & VAN VACTOR, D. 2006. The HSPGs Syndecan and Dallylike bind the receptor phosphatase LAR and exert distinct effects on synaptic development. *Neuron,* 49**,** 517-31.

KALLURI, R. 2003. Basement membranes: structure, assembly and role in tumour angiogenesis. *Nat Rev Cancer,* 3**,** 422-33.

KAUFMANN, N., DEPROTO, J., RANJAN, R., WAN, H. & VAN VACTOR, D. 2002. Drosophila liprin-alpha and the receptor phosphatase Dlar control synapse morphogenesis. *Neuron,* 34**,** 27-38.

KELLER, J. E., CAI, F. & NEALE, E. A. 2004. Uptake of botulinum neurotoxin into cultured neurons. *Biochemistry,* 43**,** 526-32.

KIM, N., STIEGLER, A. L., CAMERON, T. O., HALLOCK, P. T., GOMEZ, A. M., HUANG, J. H., HUBBARD, S. R., DUSTIN, M. L. & BURDEN, S. J. 2008. Lrp4 is a receptor for Agrin and forms a complex with MuSK. *Cell,* 135**,** 334-42.

KITAMURA, M., IGIMI, S., FURUKAWA, K. & FURUKAWA, K. 2005. Different response of the knockout mice lacking b-series gangliosides against botulinum and tetanus toxins. *Biochim Biophys Acta,* 1741**,** 1-3.

KITAMURA, M., TAKAMIYA, K., AIZAWA, S. & FURUKAWA, K. 1999. Gangliosides are the binding substances in neural cells for tetanus and botulinum toxins in mice. *Biochim Biophys Acta,* 1441**,** 1-3.

KLEIN, R., NANDURI, V., JING, S. A., LAMBALLE, F., TAPLEY, P., BRYANT, S., CORDON-CARDO, C., JONES, K. R., REICHARDT, L. F. & BARBACID, M. 1991. The trkB tyrosine protein kinase is a receptor for brain-derived neurotrophic factor and neurotrophin-3. *Cell,* 66**,** 395-403.

KOHFELDT, E., SASAKI, T., GOHRING, W. & TIMPL, R. 1998. Nidogen-2: a new basement membrane protein with diverse binding properties. *J Mol Biol,* 282**,** 99-109.

KOHLING, R., NISCHT, R., VASUDEVAN, A., HO, M., WEIERGRABER, M., SCHNEIDER, T. & SMYTH, N. 2006. Nidogen and nidogen-associated basement membrane proteins and neuronal plasticity. *Neurodegener Dis,* 3**,** 56-61.

KORIAZOVA, L. K. & MONTAL, M. 2003. Translocation of botulinum neurotoxin light chain protease through the heavy chain channel. *Nat Struct Biol,* 10**,** 13-8.

KRASZEWSKI, K., MUNDIGL, O., DANIELL, L., VERDERIO, C., MATTEOLI, M. & DE CAMILLI, P. 1995. Synaptic vesicle dynamics in living cultured hippocampal neurons visualized with CY3-conjugated antibodies directed against the lumenal domain of synaptotagmin. *J Neurosci,* 15**,** 4328-42.

KRUEGEL, J. & MIOSGE, N. 2010. Basement membrane components are key players in specialized extracellular matrices. *Cell Mol Life Sci,* 67**,** 2879-95.

KVANSAKUL, M., HOPF, M., RIES, A., TIMPL, R. & HOHENESTER, E. 2001. Structural basis for the high-affinity interaction of nidogen-1 with immunoglobulin-like domain 3 of perlecan. *EMBO J,* 20**,** 5342-6.

KYPTA, R. M., SU, H. & REICHARDT, L. F. 1996. Association between a transmembrane protein tyrosine phosphatase and the cadherin-catenin complex. *J Cell Biol,* 134**,** 1519-29.

LACY, D. B. & STEVENS, R. C. 1999. Sequence homology and structural analysis of the clostridial neurotoxins. *J Mol Biol,* 291**,** 1091-104.

LACY, D. B., TEPP, W., COHEN, A. C., DASGUPTA, B. R. & STEVENS, R. C. 1998. Crystal structure of botulinum neurotoxin type A and implications for toxicity. *Nat Struct Biol,* 5**,** 898-902.

LAEMMLI, U. K. 1970. Cleavage of structural proteins during the assembly of the head of bacteriophage T4. *Nature,* 227**,** 680-5.

LALLI, G., BOHNERT, S., DEINHARDT, K., VERASTEGUI, C. & SCHIAVO, G. 2003a. The journey of tetanus and botulinum neurotoxins in neurons. *Trends Microbiol,* 11**,** 431-7.

LALLI, G., GSCHMEISSNER, S. & SCHIAVO, G. 2003b. Myosin Va and microtubule-based motors are required for fast axonal retrograde transport of tetanus toxin in motor neurons. *J Cell Sci,* 116**,** 4639-50.

LALLI, G., HERREROS, J., OSBORNE, S. L., MONTECUCCO, C., ROSSETTO, O. & SCHIAVO, G. 1999. Functional characterisation of tetanus and botulinum neurotoxins binding domains. *J Cell Sci,* 112 (Pt 16)**,** 2715-24.

LE ROY, C. & WRANA, J. L. 2005. Clathrin- and non-clathrin-mediated endocytic regulation of cell signalling. *Nat Rev Mol Cell Biol,* 6**,** 112-126.

LEE, H. & BENNETT, A. M. 2013. Receptor protein tyrosine phosphatase-receptor tyrosine kinase substrate screen identifies EphA2 as a target for LAR in cell migration. *Mol Cell Biol,* 33**,** 1430-41.

LEE, H. K., SEO, I. A., PARK, H. K., PARK, Y. M., AHN, K. J., YOO, Y. H. & PARK, H. T. 2007. Nidogen is a prosurvival and promigratory factor for adult Schwann cells. *J Neurochem,* 102**,** 686-98.

LENCER, W. I. & TSAI, B. 2003. The intracellular voyage of cholera toxin: going retro. *Trends Biochem Sci,* 28**,** 639-45.

LETINSKY, M. S., FISCHBECK, K. H. & MCMAHAN, U. J. 1976. Precision of reinnervation of original postsynaptic sites in frog muscle after a nerve crush. *J Neurocytol,* 5**,** 691-718.

LIN, W., BURGESS, R. W., DOMINGUEZ, B., PFAFF, S. L., SANES, J. R. & LEE, K. F. 2001. Distinct roles of nerve and muscle in postsynaptic differentiation of the neuromuscular synapse. *Nature,* 410**,** 1057-64.

LLEWELLYN-SMITH, I. J., MINSON, J. B., WRIGHT, A. P. & HODGSON, A. J. 1990. Cholera toxin B-gold, a retrograde tracer that can be used in light and electron microscopic immunocytochemical studies. *J Comp Neurol,* 294**,** 179-91.

LOSEN, M., STASSEN, M. H., MARTINEZ-MARTINEZ, P., MACHIELS, B. M., DUIMEL, H., FREDERIK, P., VELDMAN, H., WOKKE, J. H., SPAANS, F., VINCENT, A. & DE BAETS, M. H. 2005. Increased expression of rapsyn in muscles prevents acetylcholine receptor loss in experimental autoimmune myasthenia gravis. *Brain,* 128**,** 2327-37.

LOUCH, H. A., BUCZKO, E. S., WOODY, M. A., VENABLE, R. M. & VANN, W. F. 2002. Identification of a binding site for ganglioside on the receptor binding domain of tetanus toxin. *Biochemistry,* 41**,** 13644-52.

LU, B., PANG, P. T. & WOO, N. H. 2005. The yin and yang of neurotrophin action. *Nat Rev Neurosci,* 6**,** 603-14.

LU, P., WEAVER, V. M. & WERB, Z. 2012. The extracellular matrix: a dynamic niche in cancer progression. *J Cell Biol,* 196**,** 395-406.

LUO, Z. G., WANG, Q., ZHOU, J. Z., WANG, J., LUO, Z., LIU, M., HE, X., WYNSHAW-BORIS, A., XIONG, W. C., LU, B. & MEI, L. 2002. Regulation of AChR clustering by Dishevelled interacting with MuSK and PAK1. *Neuron,* 35**,** 489-505.

MACRI, L., SILVERSTEIN, D. & CLARK, R. A. F. 2007. Growth factor binding to the pericellular matrix and its importance in tissue engineering. *Adv Drug Deliv Rev.,* 59**,** 1366-1381.

MAHRHOLD, S., RUMMEL, A., BIGALKE, H., DAVLETOV, B. & BINZ, T. 2006. The synaptic vesicle protein 2C mediates the uptake of botulinum neurotoxin A into phrenic nerves. *FEBS Lett,* 580**,** 2011-4.

MANN, K., DEUTZMANN, R., AUMAILLEY, M., TIMPL, R., RAIMONDI, L., YAMADA, Y., PAN, T. C., CONWAY, D. & CHU, M. L. 1989. Amino acid sequence of mouse nidogen, a multidomain basement membrane protein with binding activity for laminin, collagen IV and cells. *EMBO J,* 8**,** 65-72.

MARTINEZ-MARTINEZ, P., LOSEN, M., DUIMEL, H., FREDERIK, P., SPAANS, F., MOLENAAR, P., VINCENT, A. & DE BAETS, M. H. 2007. Overexpression of rapsyn in rat muscle increases acetylcholine receptor levels in chronic experimental autoimmune myasthenia gravis. *Am J Pathol,* 170**,** 644-57.

MARTINO, M. M., BRIQUEZ, P. S., GUC, E., TORTELLI, F., KILARSKI, W. W., METZGER, S., RICE, J. J., KUHN, G. A., MULLER, R., SWARTZ, M. A. & HUBBELL, J. A. 2014. Growth Factors Engineered for Super-Affinity to the Extracellular Matrix Enhance Tissue Healing. *Science,* 343**,** 885-888.

MASELLI, R. A., ARREDONDO, J., FERNS, M. J. & WOLLMANN, R. L. 2012. Synaptic basal lamina-associated congenital myasthenic syndromes. *Ann N Y Acad Sci,* 1275**,** 36-48.

MATSUDA, M., SUGIMOTO, N., OZUTSUMI, K. & HIRAI, T. 1982. Acute botulinum-like intoxication by tetanus neurotoxin in mice. *Biochem Biophys Res Commun,* 104**,** 799-805.

MATTEOLI, M., TAKEI, K., PERIN, M. S., SUDHOF, T. C. & DE CAMILLI, P. 1992. Exo-endocytotic recycling of synaptic vesicles in developing processes of cultured hippocampal neurons. *J Cell Biol,* 117**,** 849-61.

MATTEOLI, M., VERDERIO, C., ROSSETTO, O., IEZZI, N., COCO, S., SCHIAVO, G. & MONTECUCCO, C. 1996. Synaptic vesicle endocytosis mediates the entry of tetanus neurotoxin into hippocampal neurons. *Proc Natl Acad Sci U S A,* 93**,** 13310-5.

MAYER, U., MANN, K., TIMPL, R. & MURPHY, G. 1993. Sites of nidogen cleavage by proteases involved in tissue homeostasis and remodelling. *Eur J Biochem,* 217**,** 877-84.

MAYER, U., ZIMMERMANN, K., MANN, K., REINHARDT, D., TIMPL, R. & NISCHT, R. 1995. Binding properties and protease stability of recombinant human nidogen. *Eur J Biochem,* 227**,** 681-6.

MCMAHAN, U. J., SANES, J. R. & MARSHALL, L. M. 1978. Cholinesterase is associated with the basal lamina at the neuromuscular junction. *Nature,* 271**,** 172-4.

MENENDEZ, G. 2010. Spatio-temporal control of neurotrophin trafficking and signalling in primary neurons cultured inside microfluidic chamber. *PhD thesis,* Imperial College London**,** 194.

MERRITT, E. A., SARFATY, S., VAN DEN AKKER, F., L'HOIR, C., MARTIAL, J. A. & HOL, W. G. 1994. Crystal structure of cholera toxin B-pentamer bound to receptor GM1 pentasaccharide. *Protein Sci,* 3**,** 166-75.

MINICHIELLO, L. 2009. TrkB signalling pathways in LTP and learning. *Nat Rev Neurosci,* 10**,** 850-60.

MIOSGE, N., SASAKI, T. & TIMPL, R. 2002. Evidence of nidogen-2 compensation for nidogen-1 deficiency in transgenic mice. *Matrix Biol,* 21**,** 611-21.

MOCHIDA, S., POULAIN, B., WELLER, U., HABERMANN, E. & TAUC, L. 1989. Light chain of tetanus toxin intracellularly inhibits acetylcholine release at neuro-neuronal synapses, and its internalization is mediated by heavy chain. *FEBS Lett,* 253**,** 47-51.

MOLNAR, T., VOROS, J., SZEDER, B., TAKATS, K., KARDOS, J., KATONA, G. & GRAF, L. 2013. Comparison of complexes formed by a crustacean and a vertebrate trypsin with bovine pancreatic trypsin inhibitor - the key to achieving extreme stability? *FEBS J,* 280**,** 5750-63.

MONTAL, M. 2009. Translocation of botulinum neurotoxin light chain protease by the heavy chain protein-conducting channel. *Toxicon,* 54**,** 565-9.

MONTAL, M. 2010. Botulinum Neurotoxin: A Marvel of Protein Design. *Ann Rev Biochem,* 79**,** 591-617.

MONTECUCCO, C. 1986. How Do Tetanus and Botulinum Toxins Bind to Neuronal Membranes. *Trends Biochem Sci,* 11**,** 314-317.

MONTECUCCO, C., PAPINI, E. & SCHIAVO, G. 1994. Bacterial protein toxins penetrate cells via a four-step mechanism. *FEBS Lett,* 346**,** 92-8.

MONTECUCCO, C., ROSSETTO, O. & SCHIAVO, G. 2004. Presynaptic receptor arrays for clostridial neurotoxins. *Trends Microbiol,* 12**,** 442-446.

MONTECUCCO, C., SCHIAVO, G. & PANTANO, S. 2005. SNARE complexes and neuroexocytosis: how many, how close? *Trends Biochem Sci,* 30**,** 367-72.

MONTESANO, R., ROTH, J., ROBERT, A. & ORCI, L. 1982. Non-coated membrane invaginations are involved in binding and internalization of cholera and tetanus toxins. *Nature,* 296**,** 651-3.

MURSHED, M., SMYTH, N., MIOSGE, N., KAROLAT, J., KRIEG, T., PAULSSON, M. & NISCHT, R. 2000. The absence of nidogen 1 does not affect murine basement membrane formation. *Mol Cell Biol,* 20**,** 7007-12.

MURTHY, V. N. & DE CAMILLI, P. 2003. Cell biology of the presynaptic terminal. *Annu Rev Neurosci,* 26**,** 701-28.

NICHOLSON, G. A., MCLEOD, J. G. & GRIFFITHS, L. R. 1983. Acetylcholine receptor antibody in the diagnosis of myasthenia gravis. *Med J Aust,* 2**,** 334-7.

NIEMANN, H. 1991. Molecular biology of clostridial neurotoxins. *In:* FREER, J. E. A. A. J. H. (ed.) *A Sourcebook of Bacterial Protein Toxins.* London: Academic Press.

NISHIKI, T., KAMATA, Y., NEMOTO, Y., OMORI, A., ITO, T., TAKAHASHI, M. & KOZAKI, S. 1994. Identification of protein receptor for *Clostridium botulinum* type B neurotoxin in rat brain synaptosomes. *J Biol Chem,* 269**,** 10498-503.

NISHIKI, T., TOKUYAMA, Y., KAMATA, Y., NEMOTO, Y., YOSHIDA, A., SATO, K., SEKIGUCHI, M., TAKAHASHI, M. & KOZAKI, S. 1996. The high-affinity binding of Clostridium botulinum type B neurotoxin to synaptotagmin II associated with gangliosides GT1b/GD1a. *FEBS Lett,* 378**,** 253-7.

O'GRADY, P., THAI, T. C. & SAITO, H. 1998. The laminin-nidogen complex is a ligand for a specific splice isoform of the transmembrane protein tyrosine phosphatase LAR. *J Cell Biol,* 141**,** 1675-84.

OBLATT-MONTAL, M., YAMAZAKI, M., NELSON, R. & MONTAL, M. 1995. Formation of ion channels in lipid bilayers by a peptide with the predicted transmembrane sequence of botulinum neurotoxin A. *Protein Sci,* 4**,** 1490-7.

OPPENHEIM, R. W., YIN, Q. W., PREVETTE, D. & YAN, Q. 1992. Brain-derived neurotrophic factor rescues developing avian motoneurons from cell death. *Nature,* 360**,** 755-7.

PARK, J. W., VAHIDI, B., TAYLOR, A. M., RHEE, S. W. & JEON, N. L. 2006. Microfluidic culture platform for neuroscience research. *Nat Protoc,* 1**,** 2128-36.

PENG, L., TEPP, W. H., JOHNSON, E. A. & DONG, M. 2011. Botulinum neurotoxin D uses synaptic vesicle protein SV2 and gangliosides as receptors. *PLoS Pathog,* 7**,** e1002008.

PENNER, R., NEHER, E. & DREYER, F. 1986. Intracellularly injected tetanus toxin inhibits exocytosis in bovine adrenal chromaffin cells. *Nature,* 324**,** 76-8.

PEREZ, M., BENITEZ, S. U., CARTAROZZI, L. P., DEL BEL, E., GUIMARAES, F. S. & OLIVEIRA, A. L. 2013. Neuroprotection and reduction of glial reaction by cannabidiol treatment after sciatic nerve transection in neonatal rats. *Eur J Neurosci,* 38**,** 3424-34.

PIERCE, E. J., DAVISON, M. D., PARTON, R. G., HABIG, W. H. & CRITCHLEY, D. R. 1986. Characterization of tetanus toxin binding to rat brain membranes. Evidence for a high-affinity proteinase-sensitive receptor. *Biochem J,* 236**,** 845-52.

PIRAZZINI, M., BORDIN, F., ROSSETTO, O., SHONE, C. C., BINZ, T. & MONTECUCCO, C. 2013a. The thioredoxin reductase-thioredoxin system is involved in the entry of tetanus and botulinum neurotoxins in the cytosol of nerve terminals. *FEBS Lett,* 587**,** 150-5.

PIRAZZINI, M., HENKE, T., ROSSETTO, O., MAHRHOLD, S., KREZ, N., RUMMEL, A., MONTECUCCO, C. & BINZ, T. 2013b. Neutralisation of specific surface carboxylates speeds up translocation of botulinum neurotoxin type B enzymatic domain. *FEBS Lett,* 587**,** 3831-6.

PIRAZZINI, M., ROSSETTO, O., BERTASIO, C., BORDIN, F., SHONE, C. C., BINZ, T. & MONTECUCCO, C. 2013c. Time course and temperature dependence of the

membrane translocation of tetanus and botulinum neurotoxins C and D in neurons. *Biochem Biophys Res Commun,* 430**,** 38-42.

POT, D. A., WOODFORD, T. A., REMBOUTSIKA, E., HAUN, R. S. & DIXON, J. E. 1991. Cloning, bacterial expression, purification, and characterization of the cytoplasmic domain of rat LAR, a receptor-like protein tyrosine phosphatase. *J Biol Chem,* 266**,** 19688-96.

POULAIN, B., TAUC, L., MAISEY, E. A., WADSWORTH, J. D., MOHAN, P. M. & DOLLY, J. O. 1988. Neurotransmitter release is blocked intracellularly by botulinum neurotoxin, and this requires uptake of both toxin polypeptides by a process mediated by the larger chain. *Proc Natl Acad Sci U S A,* 85**,** 4090-4.

PUHAR, A., JOHNSON, E. A., ROSSETTO, O. & MONTECUCCO, C. 2004. Comparison of the pH-induced conformational change of different clostridial neurotoxins. *Biochem Biophys Res Commun,* 319**,** 66-71.

PUN, S., SIGRIST, M., SANTOS, A. F., RUEGG, M. A., SANES, J. R., JESSELL, T. M., ARBER, S. & CARONI, P. 2002. An intrinsic distinction in neuromuscular junction assembly and maintenance in different skeletal muscles. *Neuron,* 34**,** 357-70.

QUALMANN, B., KOCH, D. & KESSELS, M. M. 2011. Let's go bananas: revisiting the endocytic BAR code. *EMBO J,* 30**,** 3501-15.

RAJAGOPAL, R. & CHAO, M. V. 2006. A role for Fyn in Trk receptor transactivation by G-protein-coupled receptor signaling. *Mol Cell Neurosci,* 33**,** 36-46.

RESTANI, L., ANTONUCCI, F., GIANFRANCESCHI, L., ROSSI, C., ROSSETTO, O. & CALEO, M. 2011. Evidence for anterograde transport and transcytosis of botulinum neurotoxin A (BoNT/A). *J Neurosci,* 31**,** 15650-9.

RESTANI, L., GIRIBALDI, F., MANICH, M., BERCSENYI, K., MENENDEZ, G., ROSSETTO, O., CALEO, M. & SCHIAVO, G. 2012a. Botulinum neurotoxins A and E undergo retrograde axonal transport in primary motor neurons. *PLoS Pathog,* 8**,** e1003087.

RESTANI, L., NOVELLI, E., BOTTARI, D., LEONE, P., BARONE, I., GALLI-RESTA, L., STRETTOI, E. & CALEO, M. 2012b. Botulinum Neurotoxin A Impairs Neurotransmission Following Retrograde Transynaptic Transport. *Traffic,* 13**,** 1083-1089.

RICKMAN, C., MEUNIER, F. A., BINZ, T. & DAVLETOV, B. 2004. High affinity interaction of syntaxin and SNAP-25 on the plasma membrane is abolished by botulinum toxin E. *J Biol Chem,* 279**,** 644-51.

RINALDI, S., BRENNAN, K. M., GOODYEAR, C. S., O'LEARY, C., SCHIAVO, G., CROCKER, P. R. & WILLISON, H. J. 2009. Analysis of lectin binding to glycolipid complexes using combinatorial glycoarrays. *Glycobiology,* 19**,** 789-796.

ROBINSON, K. G., MENDONCA, J. L., MILITAR, J. L., THEROUX, M. C., DABNEY, K. W., SHAH, S. A., MILLER, F. & AKINS, R. E. 2013. Disruption of basal lamina components in neuromotor synapses of children with spastic quadriplegic cerebral palsy. *PLoS One,* 8**,** e70288.

ROSSETTO, O., PIRAZZINI, M. & MONTECUCCO, C. 2014. Botulinum neurotoxins: genetic, structural and mechanistic insights. *Nat Rev Microbiol,* 12**,** 535-49.

ROUX, S., SAINT CLOMENT, C., CURIE, T., GIRARD, E., MENA, F. J., BARBIER, J., OSTA, R., MOLGO, J. & BRULET, P. 2006. Brain-derived neurotrophic factor facilitates in vivo internalization of tetanus neurotoxin C-terminal fragment fusion proteins in mature mouse motor nerve terminals. *Eur J Neurosci,* 24**,** 1546-54.

ROZANOVA, V. D. 1964. On the sensitivity, resistance and tolerance of rats of various ages to tetanus toxin. *Bulletin of Experimental Biology and Medicine,* 54**,** 1341-1346.

RUMMEL, A. 2006. Characterisation of the cell binding domain of Clostridial Neurotoxins. *PhD thesis,* University of Hannover**,** 76.

RUMMEL, A., BADE, S., ALVES, J., BIGALKE, H. & BINZ, T. 2003. Two carbohydrate binding sites in the H(CC)-domain of tetanus neurotoxin are required for toxicity. *J Mol Biol,* 326**,** 835-47.

RUMMEL, A., EICHNER, T., WEIL, T., KARNATH, T., GUTCAITS, A., MAHRHOLD, S., SANDHOFF, K., PROIA, R. L., ACHARYA, K. R., BIGALKE, H. & BINZ, T. 2007. Identification of the protein receptor binding site of botulinum neurotoxins B and G proves the double-receptor concept. *Proc Natl Acad Sci U S A,* 104**,** 359-64.

RUMMEL, A., HAFNER, K., MAHRHOLD, S., DARASHCHONAK, N., HOLT, M., JAHN, R., BEERMANN, S., KARNATH, T., BIGALKE, H. & BINZ, T. 2009. Botulinum neurotoxins C, E and F bind gangliosides via a conserved binding site prior to stimulation-dependent uptake with botulinum neurotoxin F utilising the three isoforms of SV2 as second receptor. *J Neurochem,* 110**,** 1942-1954.

RUMMEL, A., KARNATH, T., HENKE, T., BIGALKE, H. & BINZ, T. 2004a. Synaptotagmins I and II act as nerve cell receptors for botulinum neurotoxin G. *J Biol Chem,* 279**,** 30865-70.

RUMMEL, A., MAHRHOLD, S., BIGALKE, H. & BINZ, T. 2004b. The H_{CC}-domain of botulinum neurotoxins A and B exhibits a singular ganglioside binding site displaying serotype specific carbohydrate interaction. *Mol Microbiol,* 51**,** 631-43.

SALINAS, S., BILSLAND, L. G., HENAFF, D., WESTON, A. E., KERIEL, A., SCHIAVO, G. & KREMER, E. J. 2009. CAR-associated vesicular transport of an adenovirus in motor neuron axons. *PLoS Pathog,* 5**,** e1000442.

SAMAL, K. K., LATH, J. R., SAHU, C. S. & MISHRA, S. C. 1990. Tetanus with local palsy. *J Assoc Physicians India,* 38**,** 873-5.

SANES, J. R., MARSHALL, L. M. & MCMAHAN, U. J. 1978. Reinnervation of muscle fiber basal lamina after removal of myofibers. Differentiation of regenerating axons at original synaptic sites. *J Cell Biol,* 78**,** 176-98.

SANFORD, M. 2014. OnabotulinumtoxinA (Botox): A Review of its Use in the Treatment of Urinary Incontinence in Patients with Multiple Sclerosis or Subcervical Spinal Cord Injury. *Drugs,* 74**,** 1659-72.

SCHECTERSON, L. C. & BOTHWELL, M. 2010. Neurotrophin receptors: Old friends with new partners. *Dev Neurobiol,* 70**,** 332-8.

SCHIAVO, G., BENFENATI, F., POULAIN, B., ROSSETTO, O., POLVERINO DE LAURETO, P., DASGUPTA, B. R. & MONTECUCCO, C. 1992. Tetanus and botulinum-B neurotoxins block neurotransmitter release by proteolytic cleavage of synaptobrevin. *Nature,* 359**,** 832-5.

SCHIAVO, G., MATTEOLI, M. & MONTECUCCO, C. 2000. Neurotoxins affecting neuroexocytosis. *Physiol Rev,* 80**,** 717-66.

SCHIAVO, G., PAPINI, E., GENNA, G. & MONTECUCCO, C. 1990a. An intact interchain disulfide bond is required for the neurotoxicity of tetanus toxin. *Infect Immun,* 58**,** 4136-41.

SCHIAVO, G., POULAIN, B., ROSSETTO, O., BENFENATI, F., TAUC, L. & MONTECUCCO, C. 1992a. Tetanus toxin is a zinc protein and its inhibition of neurotransmitter release and protease activity depend on zinc. *Embo J,* 11**,** 3577-83.

SCHIAVO, G., ROSSETTO, O., SANTUCCI, A., DASGUPTA, B. R. & MONTECUCCO, C. 1992b. Botulinum neurotoxins are zinc proteins. *J Biol Chem,* 267**,** 23479-83.

SCHIAVO, G., SANTUCCI, A., DASGUPTA, B. R., MEHTA, P. P., JONTES, J., BENFENATI, F., WILSON, M. C. & MONTECUCCO, C. 1993. Botulinum neurotoxins serotypes A and E cleave SNAP-25 at distinct COOH-terminal peptide bonds. *FEBS Lett,* 335**,** 99-103.

SCHIAVO, G., SHONE, C. C., BENNETT, M. K., SCHELLER, R. H. & MONTECUCCO, C. 1995. Botulinum neurotoxin type C cleaves a single Lys-Ala bond within the carboxyl-terminal region of syntaxins. *J Biol Chem,* 270**,** 10566-70.

SCHIAVO, G., SHONE, C. C., ROSSETTO, O., ALEXANDER, F. C. & MONTECUCCO, C. 1993a. Botulinum neurotoxin serotype F is a zinc endopeptidase specific for VAMP/synaptobrevin. *J Biol Chem,* 268**,** 11516-9.

SCHMIEG, N., MENENDEZ, G., SCHIAVO, G. & TERENZIO, M. 2014. Signalling endosomes in axonal transport: travel updates on the molecular highway. *Semin Cell Dev Biol,* 27**,** 32-43.

SCHMIEG, N. BERCSENYI, K.; SCHIAVO, G 2015. Uptake and transport of Clostridial Neurotoxins
The comprehensive sourcebook of bacterial protein toxins, 4th Edition. In press

SCHMITT, A., DREYER, F. & JOHN, C. 1981. At least three sequential steps are involved in the tetanus toxin-induced block of neuromuscular transmission. *Naunyn Schmiedebergs Arch Pharmacol,* 317**,** 326-30.

SCHWAB, M. & THOENEN, H. 1977. Selective trans-synaptic migration of tetanus toxin after retrograde axonal transport in peripheral sympathetic nerves: a comparison with nerve growth factor. *Brain Res,* 122**,** 459-74.

SCHWAB, M. E. 2010. Functions of Nogo proteins and their receptors in the nervous system. *Nat Rev Neurosci,* 11**,** 799-811.

SCHWAB, M. E., SUDA, K. & THOENEN, H. 1979. Selective retrograde transsynaptic transfer of a protein, tetanus toxin, subsequent to its retrograde axonal transport. *J Cell Biol,* 82**,** 798-810.

SCHWAB, M. E. & THOENEN, H. 1976. Electron microscopic evidence for a transsynaptic migration of tetanus toxin in spinal cord motoneurons: an autoradiographic and morphometric study. *Brain Res,* 105**,** 213-27.

SCHYMEINSKY, J., NEDBAL, S., MIOSGE, N., POSCHL, E., RAO, C., BEIER, D. R., SKARNES, W. C., TIMPL, R. & BADER, B. L. 2002. Gene structure and functional analysis of the mouse nidogen-2 gene: nidogen-2 is not essential for basement membrane formation in mice. *Mol Cell Biol,* 22**,** 6820-30.

SERRA-PAGES, C., MEDLEY, Q. G., TANG, M., HART, A. & STREULI, M. 1998. Liprins, a family of LAR transmembrane protein-tyrosine phosphatase-interacting proteins. *J Biol Chem,* 273**,** 15611-20.

SHERIDAN, R. E. 1998. Gating and permeability of ion channels produced by botulinum toxin types A and E in PC12 cell membranes. *Toxicon,* 36**,** 703-17.

SHONE, C. C., HAMBLETON, P. & MELLING, J. 1987. A 50-kDa fragment from the NH2-terminus of the heavy subunit of *Clostridium botulinum* type A neurotoxin forms channels in lipid vesicles. *Eur J Biochem,* 167**,** 175-80.

SIMONEN, M., PEDERSEN, V., WEINMANN, O., SCHNELL, L., BUSS, A., LEDERMANN, B., CHRIST, F., SANSIG, G., VAN DER PUTTEN, H. & SCHWAB, M. E. 2003. Systemic deletion of the myelin-associated outgrowth inhibitor Nogo-A improves regenerative and plastic responses after spinal cord injury. *Neuron,* 38**,** 201-11.

SIMPSON, L. L. 1977. The effects of acute and chronic botulinum toxin treatment on receptor number, receptor distribution and tissue sensitivity in rat diaphragm. *J Pharmacol Exp Ther,* 200**,** 343-51.

SIMPSON, L. L. 1984. The binding fragment from tetanus toxin antagonizes the neuromuscular blocking actions of botulinum toxin. *J Pharmacol Exp Ther,* 229**,** 182-7.

SIMPSON, L. L. 2000. Identification of the characteristics that underlie botulinum toxin potency: implications for designing novel drugs. *Biochimie,* 82**,** 943-53.

SIMPSON, L. L., COFFIELD, J. A. & BAKRY, N. 1994. Inhibition of vacuolar adenosine triphosphatase antagonizes the effects of clostridial neurotoxins but not phospholipase A2 neurotoxins. *J Pharmacol Exp Ther,* 269**,** 256-62.

SOHNCHEN, J., GROSHEVA, M., KIRYAKOVA, S., HUBBERS, C. U., SINIS, N., SKOURAS, E., ANKERNE, J., KAIDOGLOU, K., FRIES, J. W., IRINTCHEV, A., DUNLOP, S. A. & ANGELOV, D. N. 2010. Recovery of whisking function after manual stimulation of denervated vibrissal muscles requires brain-derived neurotrophic factor and its receptor tyrosine kinase B. *Neuroscience,* 170**,** 372-80.

STARKEY, M. L. & SCHWAB, M. E. 2012. Anti-Nogo-A and training: can one plus one equal three? *Exp Neurol,* 235**,** 53-61.

STEVENS, R. C., EVENSON, M. L., TEPP, W. & DASGUPTA, B. R. 1991. Crystallization and preliminary X-ray analysis of botulinum neurotoxin type A. *J Mol Biol,* 222**,** 877-80.

STÖCKEL, K., SCHWAB, M. & THOENEN, H. 1975. Comparison between the retrograde axonal transport of nerve growth factor and tetanus toxin in motor, sensory and adrenergic neurons. *Brain Res,* 99**,** 1-16.

STOECKEL, K., SCHWAB, M. & THOENEN, H. 1977. Role of gangliosides in the uptake and retrograde axonal transport of cholera and tetanus toxin as compared to nerve growth factor and wheat germ agglutinin. *Brain Res,* 132**,** 273-85.

STREULI, M., KRUEGER, N. X., ARINIELLO, P. D., TANG, M., MUNRO, J. M., BLATTLER, W. A., ADLER, D. A., DISTECHE, C. M. & SAITO, H. 1992. Expression of the receptor-linked protein tyrosine phosphatase LAR: proteolytic cleavage and shedding of the CAM-like extracellular region. *EMBO J,* 11**,** 897-907.

STROTMEIER, J., LEE, K., VOLKER, A. K., MAHRHOLD, S., ZONG, Y., ZEISER, J., ZHOU, J., PICH, A., BIGALKE, H., BINZ, T., RUMMEL, A. & JIN, R. 2010. Botulinum neurotoxin serotype D attacks neurons via two carbohydrate-binding sites in a ganglioside-dependent manner. *Biochem J,* 431**,** 207-16.

STURA, E. A., LE ROUX, L., GUITOT, K., GARCIA, S., BREGANT, S., BEAU, F., VERA, L., COLLET, G., PTCHELKINE, D., BAKIRCI, H. & DIVE, V. 2012. Structural framework for covalent inhibition of Clostridium botulinum neurotoxin A by targeting Cys165. *J Biol Chem,* 287**,** 33607-14.

SUN, S., SURESH, S., LIU, H., TEPP, W. H., JOHNSON, E. A., EDWARDSON, J. M. & CHAPMAN, E. R. 2011. Receptor binding enables botulinum neurotoxin B to sense low pH for translocation channel assembly. *Cell Host Microbe,* 10**,** 237-47.

SUN, S., TEPP, W. H., JOHNSON, E. A. & CHAPMAN, E. R. 2012. Botulinum neurotoxins B and E translocate at different rates and exhibit divergent responses to GT1b and low pH. *Biochemistry,* 51**,** 5655-62.

SUWAN-APICHON, O., RIZEN, M., RANGSIN, R., HERRETES, S., REYES, J. M., LEKHANONT, K. & CHUCK, R. S. 2006. Botulinum toxin B-induced mouse model of keratoconjunctivitis sicca. *Invest Ophthalmol Vis Sci,* 47**,** 133-9.

SWAMINATHAN, S. 2011. Molecular structures and functional relationships in clostridial neurotoxins. *FEBS J,* 278**,** 4467-85.

TENG, H. K., TENG, K. K., LEE, R., WRIGHT, S., TEVAR, S., ALMEIDA, R. D., KERMANI, P., TORKIN, R., CHEN, Z. Y., LEE, F. S., KRAEMER, R. T., NYKJAER, A. & HEMPSTEAD, B. L. 2005. ProBDNF induces neuronal apoptosis via activation of a receptor complex of p75NTR and sortilin. *J Neurosci,* 25**,** 5455-63.

TENG, K. K., FELICE, S., KIM, T. & HEMPSTEAD, B. L. 2010. Understanding proneurotrophin actions: Recent advances and challenges. *Dev Neurobiol,* 70**,** 350-9.

TERENZIO, M., GOLDING, M., RUSSELL, M. R., WICHER, K. B., ROSEWELL, I., SPENCER-DENE, B., ISH-HOROWICZ, D. & SCHIAVO, G. 2014a. Bicaudal-D1 regulates the intracellular sorting and signalling of neurotrophin receptors. *EMBO J,* 33**,** 1582-98.

TERENZIO, M., GOLDING, M. & SCHIAVO, G. 2014b. siRNA screen of ES cell-derived motor neurons identifies novel regulators of tetanus toxin and neurotrophin receptor trafficking. *Front Cell Neurosci,* 8**,** 140.

THAILAND, N. P. 2006. Preliminary investigation of botulism food poisoning outbreak from home-canned bamboo shoots. *WESR,* 37**,** 3.

TOM, V. J., KADAKIA, R., SANTI, L. & HOULE, J. D. 2009. Administration of chondroitinase ABC rostral or caudal to a spinal cord injury site promotes anatomical but not functional plasticity. *J Neurotrauma,* 26**,** 2323-33.

TSUJIKAWA, K., ICHIJO, T., MORIYAMA, K., TADOTSU, N., SAKAMOTO, K., SAKANE, N., FUKADA, S., FURUKAWA, T., SAITO, H. & YAMAMOTO, H. 2002. Regulation of Lck and Fyn tyrosine kinase activities by transmembrane protein tyrosine phosphatase leukocyte common antigen-related molecule. *Mol Cancer Res,* 1**,** 155-63.

TSUJIKAWA, K., KAWAKAMI, N., UCHINO, Y., ICHIJO, T., FURUKAWA, T., SAITO, H. & YAMAMOTO, H. 2001. Distinct functions of the two protein tyrosine phosphatase domains of LAR (leukocyte common antigen-related) on tyrosine dephosphorylation of insulin receptor. *Mol Endocrinol,* 15**,** 271-80.

UNICEF 2000. Maternal and Neonatal Tetanus Elimination by 2005.

VALE, R. D. 2003. The molecular motor toolbox for intracellular transport. *Cell,* 112**,** 467-80.

VANDELAER, J., BIRMINGHAM, M., GASSE, F., KURIAN, M., SHAW, C. & GARNIER, S. 2003. Tetanus in developing countries: an update on the Maternal and Neonatal Tetanus Elimination Initiative. *Vaccine,* 21**,** 3442-5.

WADE, A., THOMAS, C., KALMAR, B., TERENZIO, M., GARIN, J., GREENSMITH, L. & SCHIAVO, G. 2012. Activated leukocyte cell adhesion molecule modulates neurotrophin signaling. *J Neurochem,* 121**,** 575-86.

WAN, X. C., TROJANOWSKI, J. Q. & GONATAS, J. O. 1982. Cholera toxin and wheat germ agglutinin conjugates as neuroanatomical probes: their uptake and clearance, transganglionic and retrograde transport and sensitivity. *Brain Res,* 243**,** 215-24.

WANG, D., KRILICH, J., PELLETT, S., BAUDYS, J., TEPP, W. H., BARR, J. R., JOHNSON, E. A. & KALB, S. R. 2013. Comparison of the catalytic properties of the botulinum neurotoxin subtypes A1 and A5. *Biochim Biophys Acta,* 1834**,** 2722-8.

WEATHERBEE, S. D., ANDERSON, K. V. & NISWANDER, L. A. 2006. LDL-receptor-related protein 4 is crucial for formation of the neuromuscular junction. *Development,* 133**,** 4993-5000.

WEISHAUPT, N., BLESCH, A. & FOUAD, K. 2012. BDNF: the career of a multifaceted neurotrophin in spinal cord injury. *Exp Neurol,* 238**,** 254-64.

WELLER, U., DAUZENROTH, M. E., GANSEL, M. & DREYER, F. 1991. Cooperative action of the light chain of tetanus toxin and the heavy chain of botulinum toxin type A on the transmitter release of mammalian motor endplates. *Neurosci Lett,* 122**,** 132-4.

WELLS, C. L. & WILKINS, T. D. 1996. Clostridia: Sporeforming Anaerobic Bacilli. *In:* BARON, S. (ed.) *Medical Microbiology.* 4th ed. Galveston (TX).

WELLS, D. G., MCKECHNIE, B. A., KELKAR, S. & FALLON, J. R. 1999. Neurotrophins regulate agrin-induced postsynaptic differentiation. *Proc Natl Acad Sci U S A,* 96**,** 1112-7.

WESTON, C., GORDON, C., TERESSA, G., HOD, E., REN, X. D. & PRIVES, J. 2003. Cooperative regulation by Rac and Rho of agrin-induced acetylcholine receptor clustering in muscle cells. *J Biol Chem,* 278**,** 6450-5.

WESTON, C., YEE, B., HOD, E. & PRIVES, J. 2000. Agrin-induced acetylcholine receptor clustering is mediated by the small guanosine triphosphatases Rac and Cdc42. *J Cell Biol,* 150**,** 205-12.

WHITEMARSH, R. C., TEPP, W. H., BRADSHAW, M., LIN, G., PIER, C. L., SCHERF, J. M., JOHNSON, E. A. & PELLETT, S. 2013. Characterization of botulinum neurotoxin A subtypes 1 through 5 by investigation of activities in mice, in neuronal cell cultures, and in vitro. *Infect Immun,* 81**,** 3894-902.

WHO 2014. Global Immunization Data. http://www.who.int/.

WILLIAMSON, L. C., BATEMAN, K. E., CLIFFORD, J. C. & NEALE, E. A. 1999. Neuronal sensitivity to tetanus toxin requires gangliosides. *J Biol Chem,* 274**,** 25173-80.

WILLIAMSON, L. C. & NEALE, E. A. 1994. Bafilomycin A1 inhibits the action of tetanus toxin in spinal cord neurons in cell culture. *J Neurochem,* 63**,** 2342-5.

WILLS, Z., BATEMAN, J., KOREY, C. A., COMER, A. & VAN VACTOR, D. 1999. The tyrosine kinase Abl and its substrate enabled collaborate with the receptor phosphatase Dlar to control motor axon guidance. *Neuron,* 22**,** 301-12.

WON, S., SI, J., COLLEDGE, M., RAVICHANDRAN, K. S., FROEHNER, S. C. & MEI, L. 1999. Neuregulin-increased expression of acetylcholine receptor epsilon-subunit gene requires ErbB interaction with Shc. *J Neurochem,* 73**,** 2358-68.

YAMASAKI, S., BAUMEISTER, A., BINZ, T., BLASI, J., LINK, E., CORNILLE, F., ROQUES, B., FYKSE, E. M., SUDHOF, T. C., JAHN, R. & ET AL. 1994. Cleavage of members of the synaptobrevin/VAMP family by types D and F botulinal neurotoxins and tetanus toxin. *J Biol Chem,* 269**,** 12764-72.

YAN, Q., ELLIOTT, J. & SNIDER, W. D. 1992. Brain-derived neurotrophic factor rescues spinal motor neurons from axotomy-induced cell death. *Nature,* 360**,** 753-5.

YANG, T., MASSA, S. M. & LONGO, F. M. 2006. LAR protein tyrosine phosphatase receptor associates with TrkB and modulates neurotrophic signaling pathways. *J Neurobiol,* 66**,** 1420-36.

YANG, T., YIN, W., DEREVYANNY, V. D., MOORE, L. A. & LONGO, F. M. 2005. Identification of an ectodomain within the LAR protein tyrosine phosphatase receptor that binds homophilically and activates signalling pathways promoting neurite outgrowth. *Eur J Neurosci,* 22**,** 2159-70.

YEH, F. L., DONG, M., YAO, J., TEPP, W. H., LIN, G., JOHNSON, E. A. & CHAPMAN, E. R. 2010. SV2 mediates entry of tetanus neurotoxin into central neurons. *PLoS Pathog,* 6**,** e1001207.

YOWLER, B. C., KENSINGER, R. D. & SCHENGRUND, C. L. 2002. Botulinum neurotoxin A activity is dependent upon the presence of specific gangliosides in neuroblastoma cells expressing synaptotagmin I. *J Biol Chem,* 277**,** 32815-9.

ZHANG, B., LUO, S., WANG, Q., SUZUKI, T., XIONG, W. C. & MEI, L. 2008. LRP4 serves as a coreceptor of agrin. *Neuron,* 60**,** 285-97.

ZORNER, B. & SCHWAB, M. E. 2010. Anti-Nogo on the go: from animal models to a clinical trial. *Ann N Y Acad Sci,* 1198 Suppl 1**,** E22-34.